

# **FUEL ASSEMBLY SHAKER TEST**

**for Determining Loads on a  
PWR Assembly under  
Surrogate Normal Conditions of Truck Transport**

**Fuel Cycle Research & Development**

*Prepared for  
U.S. Department of Energy  
Used Fuel Disposition Campaign*

*Paul McConnell,  
Gregg Flores, Robert Wauneka, Greg Koenig,  
Doug Ammerman, John Bignell,  
Sylvia Saltzstein, Ken Sorenson*

*Sandia National Laboratories*

*SAND2013-5210P, Rev. 0.1  
FCRD-UFD-2013-000190  
June 30, 2013 (revised December 1, 2013)*







*Sandia National Laboratories is a multi-program laboratory managed and operated by Sandia Corporation, a wholly owned subsidiary of Lockheed Martin Corporation, for the U.S. Department of Energy's National Nuclear Security Administration under contract DE-AC04-94AL85000.*

#### **DISCLAIMER**

This information was prepared as an account of work sponsored by an agency of the U.S. Government. Neither the U.S. Government nor any agency thereof, nor any of their employees, makes any warranty, expressed or implied, or assumes any legal liability or responsibility for the accuracy, completeness, or usefulness, of any information, apparatus, product, or process disclosed, or represents that its use would not infringe privately owned rights. References herein to any specific commercial product, process, or service by trade name, trade mark, manufacturer, or otherwise, does not necessarily constitute or imply its endorsement, recommendation, or favoring by the U.S. Government or any agency thereof. The views and opinions of authors expressed herein do not necessarily state or reflect those of the U.S. Government or any agency thereof.



Revision 2  
 12/20/2012

## APPENDIX E FCT DOCUMENT COVER SHEET <sup>1</sup>

Name/Title of Deliverable/Milestone/Revision No. "Fuel Assembly Shaker Test for Determining Loads on a PWR Assembly under Normal Conditions of Transport" FCRD-UFD-2013-000190

Work Package Title and Number FT-13SN081304

Work Package WBS Number M2FT-13SN0813041

Responsible Work Package Manager Paul McConnell   
 (Name/Signature)

Date Submitted June 28, 2013

Quality Rigor Level for Deliverable/Milestone <sup>2</sup>	<input checked="" type="checkbox"/> QRL-3	<input type="checkbox"/> QRL-2	<input type="checkbox"/> QRL-1 Nuclear Data	<input type="checkbox"/> Lab/Participant QA Program (no additional FCT QA requirements)
--	---	--------------------------------	--	---

This deliverable was prepared in accordance with Sandia National Laboratories  
 (Participant/National Laboratory Name)

QA program which meets the requirements of  
 DOE Order 414.1     NQA-1-2000     Other

**This Deliverable was subjected to:**

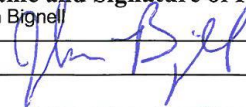
Technical Review

**Technical Review (TR)**

**Review Documentation Provided**

- Signed TR Report or,  
 Signed TR Concurrence Sheet or,  
 Signature of TR Reviewer(s) below

**Name and Signature of Reviewers**

John Bignell  


Peer Review

**Peer Review (PR)**

**Review Documentation Provided**

- Signed PR Report or,  
 Signed PR Concurrence Sheet or,  
 Signature of PR Reviewer(s) below

**NOTE 1:** Appendix E should be filled out and submitted with the deliverable. Or, if the PICS:NE system permits, completely enter all applicable information in the PICS:NE Deliverable Form. The requirement is to ensure that all applicable information is entered either in the PICS:NE system or by using the FCT Document Cover Sheet.

**NOTE 2:** In some cases there may be a milestone where an item is being fabricated, maintenance is being performed on a facility, or a document is being issued through a formal document control process where it specifically calls out a formal review of the document. In these cases, documentation (e.g., inspection report, maintenance request, work planning package documentation or the documented review of the issued document through the document control process) of the completion of the activity, along with the Document Cover Sheet, is sufficient to demonstrate achieving the milestone. If QRL 1, 2, or 3 is not assigned, then the Lab / Participant QA Program (no additional FCT QA requirements) box must be checked, and the work is understood to be performed and any deliverable developed in conformance with the respective National Laboratory / Participant, DOE or NNSA-approved QA Program.

## SUMMARY

The United States current plan of long-term storage and deferred transportation of used nuclear fuel (UNF) at its nuclear power plants and independent spent fuel storage installations, along with the trend of nuclear power plants using reactor fuel for a longer time, creates unanswered questions concerning the ability of this aged, high-burnup fuel to withstand stresses and strains seen during normal conditions of transport from its current location to a future consolidated storage facility or permanent repository.

Sandia National Laboratories conducted tests using surrogate instrumented rods in a  $17 \times 17$  pressurized water reactor (PWR) fuel assembly to capture the response to the loadings that would be experienced during normal conditions of transport along a 700-mile truck journey.

The instrumented assembly was placed within a basket fabricated for the tests which was then placed upon a shaker and subjected to shock and vibration loadings derived from two previous 700-mile over-the-road truck tests.

Due to cost, availability, and worker exposure concerns, an aged, high-burnup assembly could not be used. Therefore, most of the rods in the assembly were surrogate rods selected to have similar mass and stiffness as Zircaloy-4 rods filled with  $\text{UO}_2$  fuel. Copper alloy tubes filled with lead rods closely meet the stiffness and weight criteria for simulating Zircaloy-4/ $\text{UO}_2$ -pellet rods. The surrogate copper/lead rods were used for all but three positions within the assembly. The remaining three, which were instrumented for the tests, used lead-filled Zircaloy-4 tubes.

The test results can be used to support an assessment of the ability of aged, high-burnup cladding to withstand normal transport loads by comparing the strength of the aged, high-burnup cladding (outside the scope of this report, but being collected within separate effects testing in other Department of Energy (DOE) Used Fuel Disposition Campaign programs) to the experimentally measured strains imposed on the cladding during normal transport measured in this test. However, compromises made in constructing the surrogate test assembly (e.g., no pellet—clad interaction) will have to be addressed to definitively conclude that high-burnup UNF can indeed withstand normal conditions of transport.



## **ACKNOWLEDGEMENTS**

The authors acknowledge John Orchard and Ned Larson of the US Department of Energy; Gordon Bjorkman of the US Nuclear Regulatory Commission; Justin Coleman and Steve Marschman of Idaho National Laboratory; Harold Adkins, Brady Hanson, and Nicholas Klymyshyn of Pacific Northwest National Laboratory; and Melissa C de Baca, Jerome Cap, Ron Coleman, Remi Dingreville, and Sam Durbin, all of Sandia National Laboratories, for their invaluable technical support and encouragement.



## CONTENTS

SUMMARY .....	iv
ACKNOWLEDGEMENTS .....	vi
<b>1. INTRODUCTION .....</b>	<b>1</b>
1.1 Purpose .....	1
1.2 Background .....	3
1.3 Goals .....	3
<b>2. TEST OVERVIEW .....</b>	<b>5</b>
2.1 Objectives of test .....	5
2.1.1 Basis of test .....	6
2.1.2 General Description of Test .....	9
2.2 Test Procedures .....	14
2.2.1 Unirradiated Fuel Assembly .....	14
2.2.2 Instrumentation .....	15
2.3 Test Parameters .....	16
2.3.1 Instrumentation Plan .....	21
2.3.2 Test Unit Preparation .....	26
2.3.3 Test Set-up .....	26
2.3.4 Perform Test .....	26
2.3.5 Post Test Activities .....	26
<b>3. TEST INPUT SPECIFICATIONS .....</b>	<b>27</b>
3.1 Introduction .....	27
3.2 Instrumentation .....	27
3.3 Random Vibration Test Specifications .....	28
3.4 Shock – Decayed Sine Specifications and Time Histories .....	29
3.5 Derivation of Test Specifications .....	40
3.5.1 Derivation of Random Vibration Test Specification .....	41
3.5.2 Derivation of Shock Test Specification .....	42
<b>4. TEST RESULTS .....</b>	<b>45</b>
4.1 Test Sequence .....	45
4.2 Test Data .....	46
4.3 Data Reduction .....	47
4.4 Discussion of Results .....	47
4.4.1 Magnitude of Strains .....	47
4.4.2 Shock Test #1 .....	49
4.4.3 Random Vibration Test #5 .....	51
4.4.4 Fracture Mechanics Analysis Based on Stresses from Test Data and Analyses .....	52
4.4.5 Comparison of Test Data with PNNL Analyses .....	54
4.4.6 Post-test Examination of Zircaloy Rods and Spacer Grids .....	111

5. CONCLUSIONS AND RECOMMENDATIONS .....	115
6. REFERENCES .....	117
7. BIBLIOGRAPHY RELATED TO ASSEMBLY SHAKER TEST .....	118
APPENDIX A SUPPLEMENTAL FIGURES .....	122

## FIGURES

Figure 1.	Surrogate PWR assembly with instrumented rods within the basket.....	1
Figure 2.	Basket-containing assembly with instrumented surrogate fuel rods placed upon a shaker to simulate vibrational and shock loading associated with a normal 700-mile truck journey. ....	2
Figure 3.	Used nuclear fuel transportation, transportation vibration spectra (which results in loads applied to cladding), and material property data (e.g., cladding). ....	2
Figure 4.	Fuel assembly: Lead-filled copper and lead-filled Zircaloy-4 tubes were used as surrogates to aged, irradiated fuel. ....	5
Figure 5.	Basket containing assembly on shaker.....	10
Figure 6.	Location of Zircaloy rods (3) instrumented for the shaker tests within the assembly.....	11
Figure 7.	Copper tube containing a lead rod used as a surrogate Zircaloy/UO <sub>2</sub> rod. ....	12
Figure 8.	Basket dimensions. The assembly within the basket and the expander head used on the shaker are shown. ....	13
Figure 9.	Instrumentation on top-middle Zircaloy-4 rod and spacer grid.....	13
Figure 10.	Position of instrumentation on assembly and basket.....	15
Figure 11.	Instrumentation on top-middle and top-side Zircaloy-4 rod and spacer grid. ....	17
Figure 12.	Technical data used to select copper tubes as surrogate tubes based on Zircaloy-4 tube dimensions.....	18
Figure 13.	Shock data from the 56,000 lbs. (25,401 kg) truck cask transportation report [4a]. ....	19
Figure 14.	Shock data from the 44,000 lbs (19,958 kg) truck cask transportation report [4b]. ....	20
Figure 15.	Data derived from the truck cask transportation report used as input to the shaker.....	21
Figure 16.	PWR assembly showing spans between spacer grids. ....	22
Figure 17.	Fuel Reactor Assembly on Shaker Table. ....	28
Figure 18.	Cross Section of Fuel Reactor Assembly. ....	28
Figure 19.	Recommended Random Vibration Test Specification. ....	29
Figure 20.	Recommended Shock Test Specification. ....	30
Figure 21.	Initial Realization of Decayed Sine.....	32
Figure 22.	Second Realization of Decayed Sine. ....	34
Figure 23.	Third Realization of Decayed Sine. ....	36
Figure 24.	Fourth Realization of Decayed Sine.....	38
Figure 25.	Fifth Realization of Decayed Sine. ....	40
Figure 26.	Recommended Test Specification and Underlying ASDs. ....	42
Figure 27.	Recommended Test Specification and Underlying Shock Spectra. ....	43
Figure 28.	Range of Frequencies.....	43
Figure 29.	Elastic portion of stress—strain curve for Zircaloy-4, unirradiated, 100°F; low burnup, 250°F; and high burnup, 250°F.....	49

Figure 30.	Micro-strains, Top-middle Rod, Span 1 calculated by PNNL finite element analysis of shaker shock test .....	55
Figure 31.	Shock Test #1. All Strain Gauges. Micro-strain v. time.....	60
Figure 32.	Shock Test #1. All Strain Gauges. Micro-strain v. time. Expanded time scale 1.1 to 1.3 seconds. ....	60
Figure 33.	Shock Test #1. Top-middle Rod, Span 1. Micro-strain v. time.....	61
Figure 34.	Shock Test #1. Top-middle Rod, Span 1. Micro-strain v. time. Expanded time scale 1.1 to 1.3 seconds. ....	61
Figure 35.	Shock Test #1. Top-middle Rod, Span 5. Micro-strain v. time.....	62
Figure 36.	Shock Test #1. Top-middle Rod, Span 5. Micro-strain v. time. Expanded time scale 1.1 to 1.3 seconds. ....	62
Figure 37.	Shock Test #1. Top-middle Rod, Span 10. Micro-strain v. time.....	63
Figure 38.	Shock Test #1. Top-middle Rod, Span 10. Micro-strain v. time. Expanded time scale 1.1 to 1.3 seconds. ....	63
Figure 39.	Shock Test #1. Top-side Rod, Span 1. Micro-strain v. time. ....	64
Figure 40.	Shock Test #1. Top-side Rod, Span 1. Micro-strain v. time. Expanded time scale 1.1 to 1.3 seconds. ....	64
Figure 41.	Shock Test #1. Top-side Rod, Span 10. Micro-strain v. time. ....	65
Figure 42.	Shock Test #1. Top-side Rod, Span 10. Micro-strain v. time. Expanded time scale 1.1 to 1.3 seconds. ....	65
Figure 43.	Shock Test #1. Bottom-side Rod, Span 1. Micro-strain v. time. ....	66
Figure 44.	Shock Test #1. Bottom-side Rod, Span 1. Micro-strain v. time. Expanded time scale 1.1 to 1.3 seconds. ....	66
Figure 45.	Shock Test #1. Bottom-side Rod, Span 5. Micro-strain v. time.....	67
Figure 46.	Shock Test #1. Bottom-side Rod, Span 5. Micro-strain v. time. Expanded time scale 1.1 to 1.3 seconds. ....	67
Figure 47.	Shock Test #1. Top-middle Spacer Grids and Rod, Span 1. Acceleration.....	68
Figure 48.	Shock Test #1. Top-middle Spacer Grids and Rod, Span 1. Acceleration, Expanded time scale 1.1 to 1.3 seconds. ....	68
Figure 49.	Shock Test #1. Top-middle Spacer Grids and Rod, Span 5. Acceleration.....	69
Figure 50.	Shock Test #1. Top-middle Spacer Grids and Rod, Span 5. Acceleration, Expanded time scale 1.1 to 1.3 seconds. ....	69
Figure 51.	Shock Test #1. Top-side Spacer Grids and Rod, Span 10. Acceleration. ....	70
Figure 52.	Shock Test #1. Top-side Spacer Grids and Rod, Span 10. Acceleration, Expanded time scale 1.1 to 1.3 seconds. ....	70
Figure 53.	Shock Test #1. Control Rod Acceleration v. time. Acceleration.....	71
Figure 54.	Shock Test #1. Control Rod Acceleration v. time. Expanded time scale 1.1 to 1.3 seconds. ....	71
Figure 55.	Shock Test #1. Basket Acceleration v. time.....	72

Figure 56.	Shock Test #1. Basket Acceleration $v.$ time. Expanded time scale 1.1 to 1.3 seconds. ....	72
Figure 57.	Shock Test #1. Input (Control) Acceleration $v.$ time and Triaxial Acceleration $v.$ time on Basket Mounting Plate. ....	73
Figure 58.	Shock Test #1. Input (Control) Acceleration $v.$ time and Triaxial Acceleration $v.$ time on Basket Mounting Plate. Expanded time scale 1.1 to 1.3 seconds. ....	73
Figure 59.	Shock Test #1. Shaker Input (Control) Acceleration, Vertical Acceleration on Basket Mounting Plate, Basket Accelerations (top end, mid-span, bottom end), Control Rod accelerations (top and bottom ends), and Assembly Spacer Grids (top and bottom ends) $v.$ time. Expanded time scale 1 to 4 seconds. ....	74
Figure 60.	Shock Test #1. Fast Fourier Transformation. Top-middle Rod, Span 1. ....	74
Figure 61.	Shock Test #1. Fast Fourier Transformation. Top-middle Rod, Span 5. ....	75
Figure 62.	Shock Test #1. Fast Fourier Transformation. Top-middle Rod, Span 10. ....	75
Figure 63.	Shock Test #1. Fast Fourier Transformation. Top-side Rod, Span 1. ....	76
Figure 64.	Shock Test #1. Fast Fourier Transformation. Top-side Rod, Span 10. ....	76
Figure 65.	Shock Test #1. Fast Fourier Transformation. Bottom-side Rod, Span 1. ....	77
Figure 66.	Shock Test #1. Fast Fourier Transformation. Bottom-side Rod, Span 5. ....	77
Figure 67.	Vibration Test #5. All Strain Gauges. Micro-strain $v.$ time. ....	78
Figure 69.	Vibration Test #5. Top-middle Rod, Span 1. Micro-strain $v.$ time. ....	79
Figure 71.	Vibration Test #5. Top-middle rod, Span 5. Micro-strain $v.$ time. ....	80
Figure 73.	Vibration Test #5. Top-middle Rod, Span 10. Micro-strain $v.$ time. ....	81
Figure 75.	Comparison of Top-middle Rod, Span 10 $\mu\epsilon$ $v.$ time for Shock Test #1 and Random Vibration Test #5. ....	82
Figure 76.	Vibration Test #5. Top-side Rod, Span 1. Micro-strain $v.$ time. ....	83
Figure 78.	Vibration Test #5. Top-side Rod, Span 10. Micro-strain $v.$ time. ....	84
Figure 80.	Vibration Test #5. Bottom-side Rod, Span 1. Micro-strain $v.$ time. ....	85
Figure 82.	Vibration Test #5. Bottom-side Rod, Span 5. Micro-strain $v.$ time. ....	86
Figure 84.	Vibration Test #5. Top-middle Spacer Grids and Rod, Span 1. Acceleration. ....	87
Figure 85.	Vibration Test #5. Top-middle Spacer Grids and Rod, Span 1. Acceleration. Expanded time scale 17.8 to 18 seconds. ....	87
Figure 86.	Vibration Test #5. Top-middle Spacer Grids and Rod, Span 5. Accelerations $v.$ time. ....	88
Figure 87.	Vibration Test #5. Top-middle Spacer Grids and Rod, Span 5. Acceleration. Expanded time scale 17.8 to 18 seconds. ....	88
Figure 88.	Vibration Test #5. Top-side Spacer Grids and Rod, Span 10. Accelerations $v.$ time. ....	89
Figure 89.	Vibration Test #5. Top-side Spacer Grids and Rod, Span 10. Acceleration. Expanded time scale 17.8 to 18 seconds. ....	89
Figure 90.	Vibration Test #5. Control Rod Acceleration $v.$ time. ....	90
Figure 91.	Vibration Test #5. Control Rod Acceleration $v.$ time. Expanded time scale 17.8 to 18 seconds. ....	90

Figure 92.	Vibration Test #5. Basket Accelerations v. time.....	91
Figure 93.	Vibration Test #5. Basket Accelerations v. time. Expanded time scale 17.8 to 18 seconds.....	91
Figure 94.	Vibration Test #5. Input (Control) Acceleration v. time and Triaxial Accelerations v. time on Basket Mounting Plate.....	92
Figure 95.	Vibration Test #5. Input (Control) Acceleration v. time and Triaxial Accelerations v. time on Basket Mounting Plate. Expanded time scale 17.8 to 18 seconds.....	92
Figure 96.	Vibration Test #5. Top-middle Rod, Span 1. Ratio of micro-strains to baseplate vertical acceleration (Channel 23) v. Hz.....	93
Figure 97.	Vibration Test #5. Top-middle rod, Span 5. Ratio of micro-strain to baseplate vertical acceleration (Channel 23) v. Hz.....	93
Figure 98.	Vibration Test #5. Top-middle Rod, Span 10. Ratio of micro-strains to baseplate vertical acceleration (Channel 23) v. Hz.....	94
Figure 99.	Vibration Test #5. Top-side Rod, Span 1. Ratio of micro-strains to baseplate vertical acceleration (Channel 23) v. Hz.....	94
Figure 100.	Vibration Test #5. Top-side Rod, Span 10. Ratio of micro-strains to baseplate vertical acceleration (Channel 23) v. Hz.....	95
Figure 101.	Vibration Test #5. Bottom-side Rod, Span 1. Ratio of micro-strains to baseplate vertical acceleration (Channel 23) v. Hz.....	95
Figure 102.	Vibration Test #5. Bottom-side Rod, Span 5. Ratio of micro-strains to baseplate vertical acceleration (Channel 23) v. Hz.....	96
Figure 103.	Vibration Test #5. Top-middle spacer grids and rod, Span 5. Ratio of assembly accelerations to baseplate vertical acceleration v. Hz.....	96
Figure 104.	Vibration Test #5. Top-side spacer grids and rod, Span 10. Ratio of assembly accelerations to baseplate vertical acceleration v. Hz.....	97
Figure 105.	Vibration Test #5. Control rod. Ratio of control rod accelerations to baseplate vertical acceleration v. Hz.....	97
Figure 106.	Vibration Test #5. Basket. Ratio of basket acceleration to baseplate vertical acceleration v. Hz.....	98
Figure 107.	Vibration Test #5. Input (control) Accelerometer and Triaxial Basket Mounting Plate accelerometers. Ratio of accelerations to baseplate vertical acceleration (Channel 23) v. Hz.....	98
Figure 108.	Vibration Test #5. Control Rod. Acceleration Power Spectral Density v. Hz.....	99
Figure 109.	Vibration Test #5. Basket Acceleration Power Spectral Density v. Hz.....	99
Figure 110.	Vibration Test #5. Input (Control) and Triaxial Baseplate Acceleration Power Spectral Density v. Hz.....	100
Figure 111.	Vibration Test #5. Target Data Input to Shaker Control System v. Input (Control) (Channel 1) Acceleration Power Spectral Density v. Hz.....	100
Figure 112.	Vibration Test #5. Top-middle Rod, Span 1 Micro-strain Power Spectral Density v. Hz.....	101

Figure 113.	Vibration Test #5. Top-middle Rod, Span 5 Micro-strain Power Spectral Density v. Hz. ....	101
Figure 114.	Vibration Test #5. Top-middle Rod, Span 10 Micro-strain Power Spectral Density v. Hz. ....	102
Figure 115.	Vibration Test #5. Top-side Rod, Span 1 Micro-strain Power Spectral Density v. Hz. ....	102
Figure 116.	Vibration Test #5. Top-side Rod, Span 10 Micro-strain Power Spectral Density v. Hz. ....	103
Figure 117.	Vibration Test #5. Bottom-side Rod, Span 1 Micro-strain Power Spectral Density v. Hz. ....	103
Figure 118.	Vibration Test #5. Bottom-side Rod, Span 5 Micro-strain Power Spectral Density v. Hz. ....	104
Figure 119.	Target Data Input to Shaker Control System v. Peak Accelerations for Shock Tests #1, #2, and #5 v. Hz. ....	104
Figure 120.	Shock Test #1. Input (Control, Channel 1) and Basket Accelerations Fast Fourier Transformation. ....	105
Figure 121.	Shock Test #1. Input (Control, Channel 1) and Control Rod Accelerations Fast Fourier Transformation. ....	105
Figure 122.	Shock Test #1. Input (Control, Channel 1) and Baseplate Triaxial Accelerations Fast Fourier Transformation. ....	106
Figure 123.	Shock Test #1. Input (Control, Channel 1) and Top-middle Spacer Grids and Rod, Span 5 Accelerations Fast Fourier Transformation. ....	106
Figure 124.	Shock Test #1. Input (Control, Channel 1) and Top-side Spacer Grids and Rod, Span 10 Accelerations Fast Fourier Transformation. ....	107
Figure 125.	Shock Test #1. Input (Control, Channel 1) and Top-side Spacer Grids, Span 10 Accelerations Fast Fourier Transformation. ....	107
Figure 126.	Shock Test #1 Shock Response Spectra. Top-middle Rod and Spacer Grids, Span 1, Accelerometers. ....	108
Figure 127.	Shock Test #1 Shock Response Spectra Top-middle Rod and Spacer Grids, Span 5, Accelerometers. ....	108
Figure 128.	Shock Test #1 Shock Response Spectra Top-side Rod and Spacer Grids, Span 10, Accelerometers. ....	109
Figure 129.	Shock Test #1 Shock Response Spectra Control Rod Accelerometers. ....	109
Figure 130.	Shock Test #1 Shock Response Spectra Basket Accelerometers. ....	110
Figure 131.	Shock Test #1 Shock Response Spectra INPUT/CONTROL and Triaxial Baseplate Accelerometers. ....	110
Figure 132.	The bottom of the top-middle Zircaloy-4 rod at the bottom end of the assembly. ....	111
Figure 133.	The inner side of the top basket plate. ....	112
Figure 134.	The top of the assembly, bottom end, showing top-middle Zircaloy-4 rod and adjacent spacer grid. ....	113

Figure 135.	The top of the top-middle Zircaloy-4 rod at the bottom end of the assembly (with strain gauge attached). The box brackets the region of the rod that was within the spacer grid (partially shown on the right). The arrow points to a region of circumferential wear on the rod presumably caused by the spacer-grid springs during testing. The estimated depth of the wear is approximately 0.001 inch (0.025mm).....	114
Figure 136.	Observers of the assembly shaker tests, April 30, 2013. Left to right: Harold Adkins, PNNL; Sylvia Saltzstein, SNL; Brady Hanson, PNNL; and Ken Sorenson, Greg Koenig, Robert Wauneka, Paul McConnell, John Bignell, SNL. ....	116
Figure A-1.	Bottom, isometric, side, and top views of basket mounting plate.....	124
Figure A-2.	Basket for shaker test. ....	125
Figure A-3.	Bottom plate of basket showing mounting plates. ....	126
Figure A-4.	Assembly within basket. ....	126
Figure A-5.	Assembly in the basket.....	127
Figure A-6.	End view of basket/assembly on shaker.....	127
Figure A-7.	Position of triaxial accelerometers mounting block on middle basket mounting plate.....	128
Figure A-8.	Location of INPUT/CONTROL accelerometer on shaker.....	129
Figure A-9.	Micro-Measurements Strain Gauge Data Sheet. ....	130
Figure A-10.	Model 2250A/AM1-10 Accelerometer Data Sheet.....	131
Figure A-11.	Dimensions of the NAC-LWT PWR basket simulated to contain the assembly on the shaker. ....	133

## TABLES

Table 1. Constraints and compromises for the assembly shaker test.....	7
Table 2. Truck (56,000 lbs [25,401 kg]) vibration data [4a] .....	19
Table 3. Truck (44,000 lbs. [19,958 kg]) vibration data [4b] .....	20
Table 4. Spans Between Spacer Grids .....	22
Table 5. Instrumentation Nomenclature and Locations on Test Unit .....	23
Table 6. Input Accelerometers.....	27
Table 7. Response Accelerometers and Strain Gauges.....	27
Table 8. Vibration Breakpoints.....	29
Table 9. Reference Shock Breakpoints.....	30
Table 10. Initial Realization of Decayed Sine Parameters .....	31
Table 11. Second Realization of Decayed Sine Parameters .....	32
Table 12. Third Realization of Decayed Sine Parameters .....	35
Table 13. Fourth Realization of Decayed Sine Parameters .....	37
Table 14. Fifth Realization of Decayed Sine Parameters .....	39
Table 15. Input to Cargo (g) – Vertical Axis 99% Level of 0 to Peak Amplitude .....	41
Table 16. Shaker Test Sequence .....	46
Table 17. Estimated applied stress intensities at the tip of circumferential flaws in the cladding of a fuel rod subjected to stresses experimentally measured .....	54
Table 18. Summary of Maximum Micro-strains Measured on Zircaloy Fuel Rods during Shock Test #1 .....	56
Table 19. Summary of Maximum Micro-Strains, Average Micro-Strains, $\mu\epsilon_{RMS}$ , and Average Peak Micro-Strains, $\mu\epsilon_{peak}$ , Measured on Zircaloy Fuel Rods during Random Vibration Test #5 .....	57
Table 20. Average Accelerations, $g_{RMS}$ , and Average Peak Accelerations, $g_{peak}$ , Measured during Random Vibration Test #5.....	58
Table 21. Maximum Micro-Strains, Each Strain Gauge, Duplicative Tests.....	59





## 1. INTRODUCTION

Long-term storage and subsequent transportation of high-burnup used nuclear fuel (UNF) is an issue requiring quantitative knowledge of UNF material properties and its response to mechanical loadings during transport. The fuel clad is the first line of defense for containment of the used nuclear fuel; therefore, it is important to understand if cladding can maintain its integrity during normal conditions of transportation.<sup>1</sup>

### 1.1 Purpose

This test program was designed to better understand fuel rod response to *normal* conditions of truck transport (NCT) loadings as defined by 10CFR 71.71 in order to estimate the ability of aged, used nuclear fuel to withstand these conditions. The experimental work was focused on testing a  $17 \times 17$  PWR assembly containing instrumented surrogate fuel rods (Figure 1) placed upon a shaker (Figure 2) to simulate vibrational and shock loading associated with a normal 700-mile truck journey.

The data from the tests described herein shall also be compared to data to be generated in other DOE Used Nuclear Fuel Disposition Campaign separate effects testing activities to obtain mechanical properties of high-burnup and aged UNF. Comparing the strains applied to fuel cladding during NCT to the strength of UNF enables an assessment of the ability of the cladding to withstand post-storage transportation environments (Figure 3).



Figure 1. Surrogate PWR assembly with instrumented rods within the basket.

---

1. Degradation of cladding has been identified as a high priority technical data gap by the Department of Energy and the Nuclear Regulatory Commission among other domestic and international entities.



Figure 2. Basket-containing assembly with instrumented surrogate fuel rods placed upon a shaker to simulate vibrational and shock loading associated with a normal 700-mile truck journey.

The data from these tests shall also be coupled with data describing the mechanical properties of aged high-burnup fuel to validate models used to predict the behavior of aged, high-burnup fuel under normal conditions of transport.

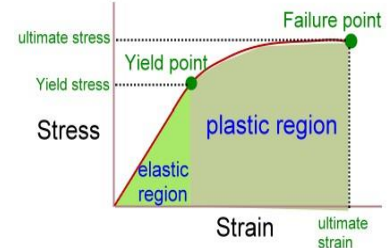
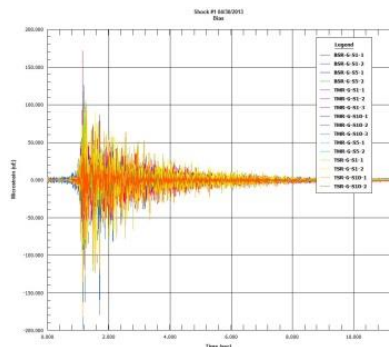


Figure 3. Used nuclear fuel transportation, transportation vibration spectra (which results in loads applied to cladding), and material property data (e.g., cladding).

## 1.2 Background

The normal conditions of transport are those defined within the United States Nuclear Regulatory Commission (US NRC) regulations in 10 Code of Federal Regulations (CFR) Part 71 [1] and the International Atomic Energy Agency SSR-6 regulations [2].

Specifically, the regulations require packages for transporting UNF to meet conditions defined in 10 CFR Part 71.71 during normal transport. The effect of “vibration normally incident to transport” must be determined for a package design (§71.71(c)(5)). The NRC also provides guidance in §2.5.6.5 *Vibration* in the “Standard Review Plan for Transportation Packages for Radioactive Material,” US NRC NUREG-1609 [3], which also cites NUREG/CR-0128 and NUREG/CR-1277 [4-5]. These documents include information on shock loadings and random vibration.

Fuel manufacturers, cask vendors, and regulators have concluded (based on analyses using vibration and shock data from NUREG/CR-0128) that unirradiated fuel rods and rods irradiated to relatively low-burnup levels (e.g., < 45GWd/MTU) can withstand the loads imposed upon them by normal conditions of transport. Numerous shipments of low-burnup UNF have confirmed the integrity of the rods to normal conditions of transport.

However, fuel is being irradiated to higher burnup levels and planned to be stored for longer periods of time. Both of these conditions—high burnup levels and aging during storage—may lead to cladding degradation to such an extent that it may not withstand NCT loads. Little data exists to justify the technical basis for asserting that aged, high-burnup fuel can withstand normal conditions of transport.

## 1.3 Goals

The data needed to help predict if aged, high-burnup fuel can withstand normal conditions of transport falls in two categories: 1) the loads imposed directly on rods during NCT (the scope of this report); and 2) the material properties of aged, high-burnup cladding (outside the scope of this report). Fuel rods subjected to high burnups *may* be sufficiently embrittled such that loads applied to the rods during normal transport *could* result in rod failure.

Zircaloy-4 cladding burned to high levels will likely experience an increase in yield strength with a significant decrease in ductility. Brittle fracture of high-burnup Zircaloy-4 could occur at applied stresses approaching the yield strength of the material. High-burnup Zircaloy-4 may also be below the ductile-to-brittle transition temperature at temperatures associated with long-term dry storage and subsequent transport of used fuel. This implies that the alloy will be at its “lower shelf” and susceptible to brittle fracture. Unirradiated and low-burnup (to a to-be-determined burnup level) Zircaloy-4 likely exhibits ductility at stress levels beyond the yield strength and is less susceptible to brittle fracture.

The margin of safety between the applied loads on fuel rods and the material properties of the high-burnup rods has not been quantified. So, a relevant question is, “Is the stress applied to the fuel during normal conditions of transport less than the yield strength of the fuel rods?<sup>2</sup>” This can be represented as:

---

2. In terms of fracture mechanics, the question can be restated: Is the applied stress intensity,  $K_I$ , at the tip of a crack in the cladding less than the fracture toughness,  $K_{Ic}$ , of the Zircaloy-4? The applied stress intensity is a function of the applied stress

Are the stresses and strains applied to the fuel during normal conditions of transport less than the yield strength of the fuel rods?

The goal of this test program is to expand understanding of UNF loading environments and subsequent response of UNF to these environments. Given a quantitative understanding of fuel rod response, the material properties of high-burnup degraded fuel can be coupled with realistic loadings to analytically estimate degraded fuel response to these transport conditions.

---

and crack size; fracture toughness is a material property somewhat analogous to the yield strength. Section 4.4.4 presents a fracture mechanics assessment for Zircaloy-4.

## 2. TEST OVERVIEW

This section describes the plan for testing of  $17 \times 17$  PWR assembly (Figure 4) containing surrogate fuel rods placed upon a shaker to simulate vibrational and shock loading associated with a normal transport of an assembly within a truck cask on a trailer. This test series was performed by implementing plans and procedures identified herein.

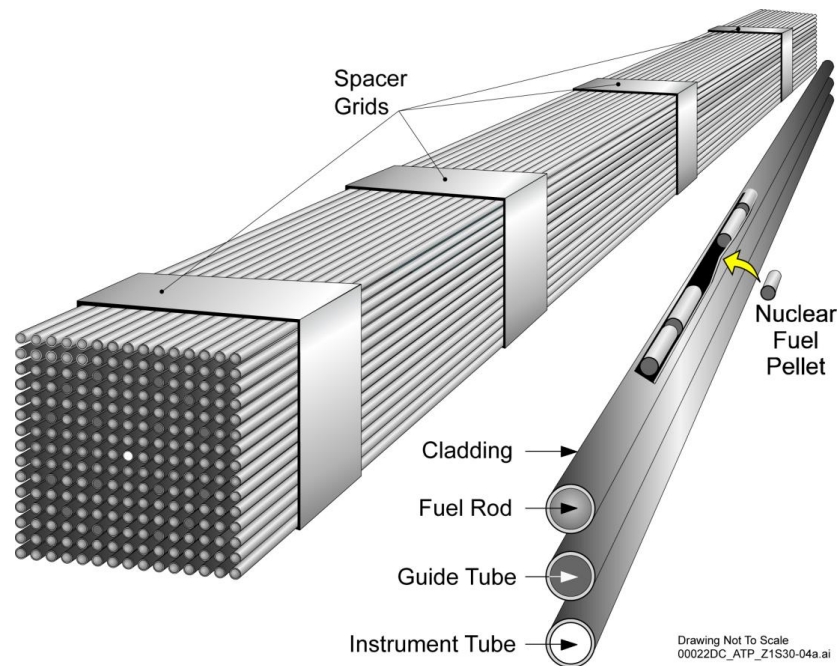


Figure 4. Fuel assembly: Lead-filled copper and lead-filled Zircaloy-4 tubes were used as surrogates to aged, irradiated fuel<sup>3</sup>.

This test provides data approximating the mechanical loads to which fuel rods are subjected during normal truck transport conditions. The integrity of the fuel rod cladding is a function of its 1) material properties – yield and tensile strength, elastic modulus, fatigue strength, fracture toughness – all of which may degrade with high burnup and long aging times - and 2) the mechanical loads to which the cladding may be subjected.

This test addresses the latter – the mechanical loads applied to the cladding during normal transport conditions.

### 2.1 Objectives of test

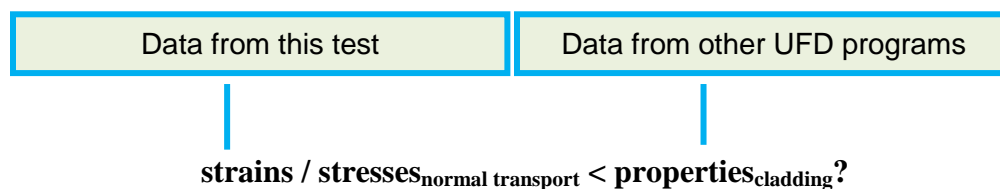
The objectives of this test program were to:

3. Fuel “rods” consist of a zirconium-alloy “tubes” filled with  $\text{UO}_2$  pellets. In this test program, copper tubes and Zircaloy-4 tubes (hollow) were filled with lead rods (solid) to make surrogate fuel “rods” for the assembly. The term “rod” is used herein to describe 1) these surrogates, 2) the lead rods, and 3) actual fuel rods. The term “tube” is used when describing the copper or Zircaloy-4 tubes without their lead rods.

- Simulate over-the-road shock and vibration loadings on a full-scale surrogate fuel assembly by applying the loadings directly to fuel cladding.
- Instrument the cladding to capture accelerations and strains imposed by the mechanical loadings resulting from the normal condition of transport vibrations and shocks.
- Provide a data<sup>4</sup> – applied stress<sub>normal transport</sub> - related to the issue of the margin of safety to understand if there is an immediate concern about the ability for aged, used fuel to withstand normal conditions of transport.

In related work, UFD test programs at DOE national laboratories shall measure properties of high burnup cladding, (e.g., yield strength<sub>cladding</sub>).

The two can then be compared to answer the question:



The test results will allow for an analytic assessment of the ability of aged, high burnup cladding to withstand normal transport loads by comparing the strength of the aged, high burnup cladding to the stresses imposed on the cladding during normal transport. The data will also allow for a fracture mechanics-based failure assessment by relating the applied stress intensity associated with a hypothetical crack in cladding to the fracture toughness of Zircaloy-4.

The data from the assembly shaker test (fuel rod accelerations and applied strains) shall be also used to validate finite element models of fuel assemblies being developed at Pacific Northwest National Laboratory (PNNL). The validated models can be used to predict the loads on fuel rods for other basket configurations and transport environments, particularly rail.

### 2.1.1 Basis of test

The *ideal test* would be to place an *irradiated fuel assembly* in an *actual cask* and do *over-the-road/rail tests* to measure the vibrational and shock response directly on the rods to the transport conditions. But, performing such a test with an irradiated assembly would be costly and instrumenting high-burnup cladding is not possible due to high personnel radiation exposures.

An alternative solution is to use an *unirradiated assembly* in an *actual cask*. However, no rail casks are available, only truck casks with internal contamination because they have all been in reactor pools.

Due to these conditions, the test plan took the practical alternative to place an unirradiated fuel assembly using a surrogate rod material on a shaker and subject the assembly to vibrations and shocks simulating normal transport via a truck cask.

---

4. The stress on the rods is converted from the experimentally-measured strains.

As such compromises were required in the test design. Table 1 identifies components of an ideal test, constraints to these components, and the compromises made to develop the final test configuration.

Table 1. Constraints and compromises for the assembly shaker test

Issue	Ideal Experimental Design	Constraint	Compromise Solution for Test	Comments
1	Use actual cask	<ul style="list-style-type: none"> <li>• Available truck cask lease costly</li> <li>• Available truck casks contaminated</li> <li>• Rail casks unavailable</li> </ul>	<ul style="list-style-type: none"> <li>• Perform test without a cask</li> <li>• Simulate truck transport with a shaker</li> </ul>	Applicable shock/vibration data available from NUREG/CR-0128
2	Use actual PWR assembly	<ul style="list-style-type: none"> <li>• Use of an irradiated assembly causes worker exposure and many test facilities will not accept rad material</li> <li>• Use of an unirradiated assembly with UO<sub>2</sub> pellets not feasible - cost</li> </ul>	PWR assembly was available without full complement of zirconium alloy rods	The possibility of obtaining a fully loaded assembly from a vendor explored
3	Use zirconium alloy rods	Limited number of Zircaloy-4 rods available	<ul style="list-style-type: none"> <li>• Use copper alloy tubes for most assembly locations</li> <li>• Use Zircaloy-4 rods for those rods to be instrumented</li> </ul>	Among many materials evaluated for surrogates for Zircaloy-4 and UO <sub>2</sub> , copper and lead had best combination of material
4	Use UO <sub>2</sub> pellets in rods	UO <sub>2</sub> pellets unavailable	Use lead rods as surrogate	

Table 1. (cont.)

Issue	Ideal Experimental Design	Constraint	Compromise Solution for Test	Comments
5	Rods have same material properties as used in an actual assembly	See 3 and 4	<ul style="list-style-type: none"> <li>• Surrogate copper/lead rods possess properties similar to Zircaloy/<math>UO_2</math> rods</li> <li>• Adjust wall thickness of copper tubes so that <math>EI_{Cu} \approx EI_{Zircaloy-4}</math></li> <li>• Adjust amount of lead in tubes so total assembly weight is that of an actual assembly</li> </ul>	properties (elastic modulus and density, respectively), availability, and cost
6	Assembly is in an actual basket which is within a cask	<ul style="list-style-type: none"> <li>• See 1</li> <li>• Actual basket unavailable</li> </ul>	Construct a basket to contain assembly	See 7, 10
7	Basket within a truck cask has some freedom of motion	Experimentally unviable to allow basket to move shaker due to shaker control constraints	Attach basket to shaker to prevent motion	See 10
8	Assembly in basket has freedom of motion	None	Fuel assembly allowed same freedom of motion as an assembly within an actual NAC-LWT PWR basket	Within the basket, the assembly has 0.45 in. (1.14 cm) clearance at the top and 0.225 in. (0.57 cm) along the sides

Table 1. (cont.)

Issue	Ideal Experimental Design	Constraint	Compromise Solution for Test	Comments
9	Assembly subjected to actual truck transport environment	See 1	Derive inputs for shaker from truck vibration/shock data [4a, 4b]	<ul style="list-style-type: none"> <li>• Vibration data and shaker inputs ranged from 3 Hz to 2,000 Hz</li> <li>• Shock data ranges from 0.5 Hz to 420 Hz. Shaker inputs for shock ranged from 3 Hz to 600 Hz</li> </ul>
10	Basket/ assembly within an actual truck cask	See 1	<ul style="list-style-type: none"> <li>• Basket constructed to conform to material (aluminum), weight, and internal dimensions of NAC-LWT PWR basket (see 7 and 8)</li> <li>• Basket affixed to shaker</li> </ul>	
11	Instrument assembly and basket (accelerometers and strain gauges)	Number of instruments limited by cost and availability (accelerometers) and data collection limitations (strain gauges)	<ul style="list-style-type: none"> <li>• Apply expert judgment and analyses [7] to define location of instruments</li> <li>• Used 16 strain gauges and 25 accelerometers</li> </ul>	All rods are expected to respond in a similar manner (per analyses)

### 2.1.2 General Description of Test

These tests were conducted to capture the response of a surrogate 17×17 PWR fuel assembly to the loadings that would be experienced during a 700-mile truck journey. Specifically, the acceleration of the rods and strains imposed upon the cladding - in its representative

configuration (i.e., *in-an-assembly-within-a-basket-within-a cask-tied-to-a-transport-conveyance*) to actual loadings imposed during normal conditions of transport. The assembly was placed upon a shaker and subjected to loadings derived from over-the-road *truck* tests (Figure 5).

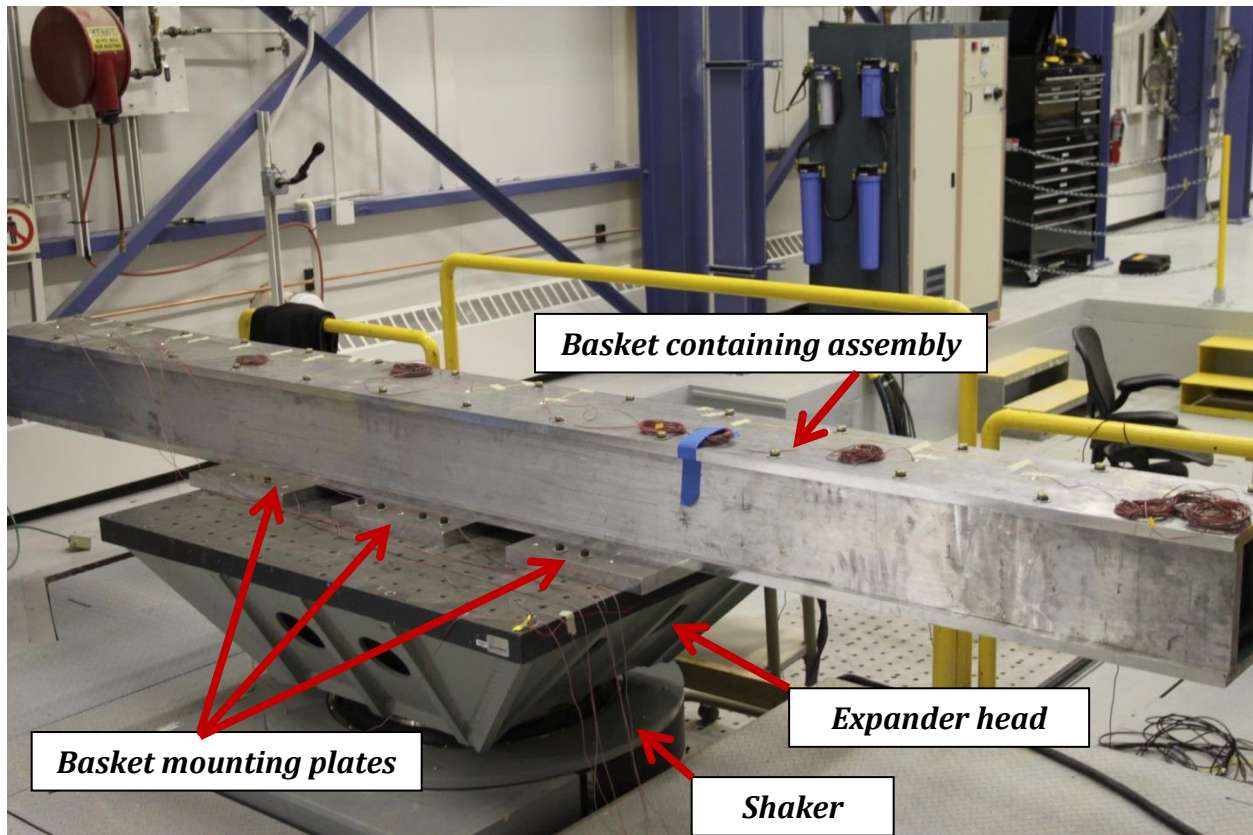


Figure 5. Basket containing assembly on shaker.

NOTE: A 60 in × 48 in (1.5 m × 1.2m) expander head is shown mounted to the cylindrical shaker. Basket is mounted to the expander head.

Most of the rods used for the tests were not actual zirconium-alloy/UO<sub>2</sub>-pellet rods. Surrogate rods were selected that had similar mass, stiffness, and natural frequency as the actual irradiated rods. Copper alloy (ASTM B 88, copper alloy C12200<sup>5</sup>) tubes filled with lead rods approximately meet the criteria for simulating Zircaloy-4/UO<sub>2</sub>-pellet rods. They were used for all but three positions within the assembly; unirradiated Zircaloy-4/lead rods were used for the assembly positions that were selected to be instrumented for the test: the top-center rod position, a top-side position, and a bottom-side position.

Figure 6 shows three views of the locations of the Zircaloy rods within the assembly.

---

5. Copper Development Association, Inc. Alloy No. 122 [www.copper.org/resources/properties/144\\_8/144\\_8.html](http://www.copper.org/resources/properties/144_8/144_8.html).

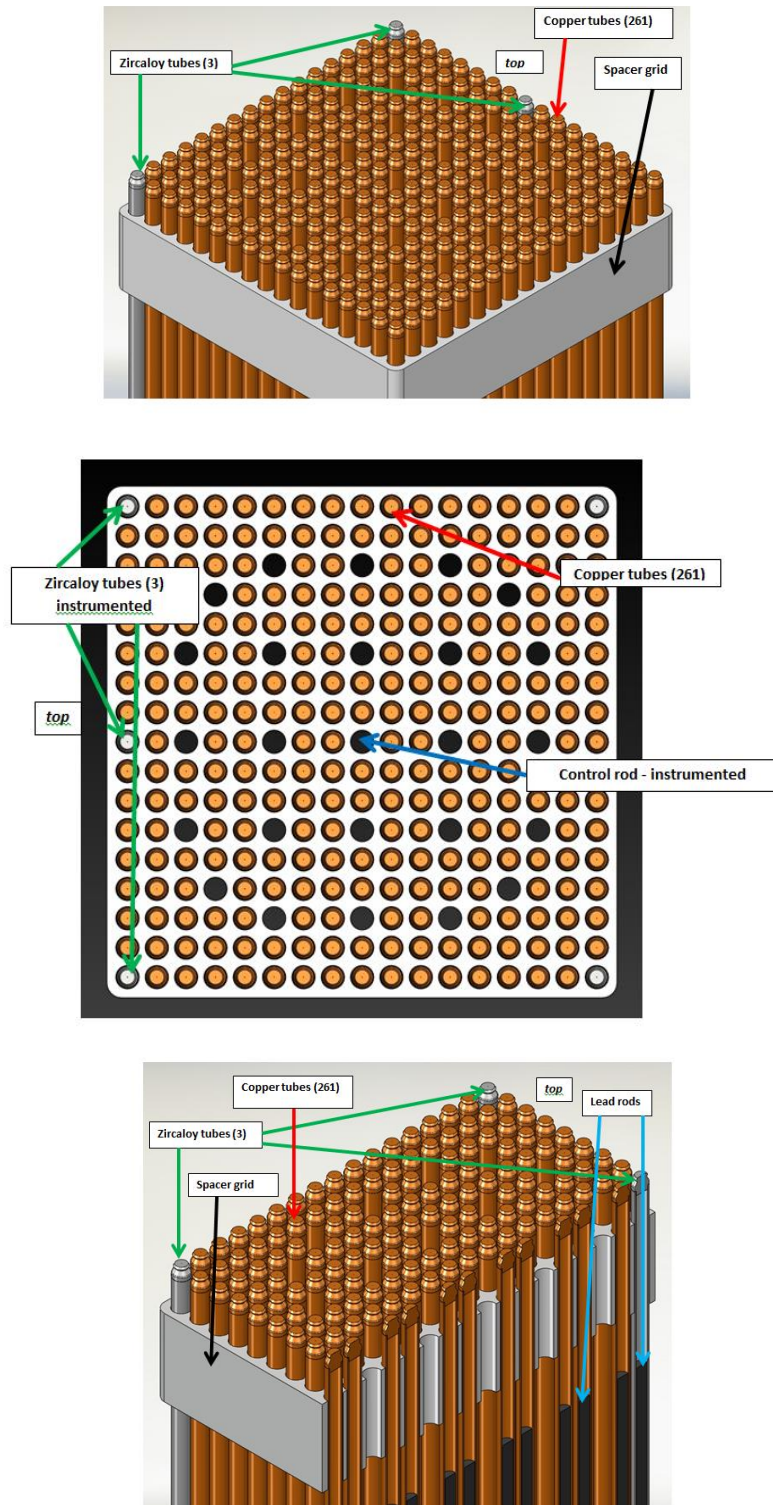


Figure 6. Location of Zircaloy rods (3) instrumented for the shaker tests within the assembly.

Figure 7 shows a lead rod inserted in to a copper tube used as a surrogate Zircaloy/ $\text{UO}_2$  rod.



Copper tube outer diameter (OD), in. (mm)	0.375 (9.525)
Copper tube inner diameter (ID), in. (mm)	0.312 (7.925)
Copper tube wall thickness, in. (mm)	0.0315 (0.8)
Radial Clearance between copper and lead, in. (mm)	0.016 (0.41)
Lead rod OD, in. (mm)	0.28 (7.11) <sup>6</sup>

Figure 7. Copper tube containing a lead rod used as a surrogate Zircaloy/ $\text{UO}_2$  rod.

The assembly was placed within a basket constructed for the test with nominal dimensions of the NAC-LWT cask PWR (single) assembly basket (Figure 8). The NAC-LWT basket weighs 840 lbs. (381 kg) and has an interior cross-section of 8.88 in.  $\times$  8.88 in. (22.6 cm  $\times$  22.6 cm). The test basket weighed approximately the same as the NAC-LWT PWR basket (837 lbs. [380 kg]) and had the same cross-sectional and length dimensions (161.5 in. [410.2 cm]).

---

6. Zircaloy-4 tubes have an O.D. of 0.379 in. (9.5 mm) and a wall (clad) thickness of 0.0225 in. (0.572 mm).  $\text{UO}_2$  fuel pellets have a diameter of 0.322 in. (8.19 mm). The dimensions of the copper tube and lead were selected primarily so the weight of the copper/lead rods would closely match that of a Zircaloy-4/ $\text{UO}_2$  rod.

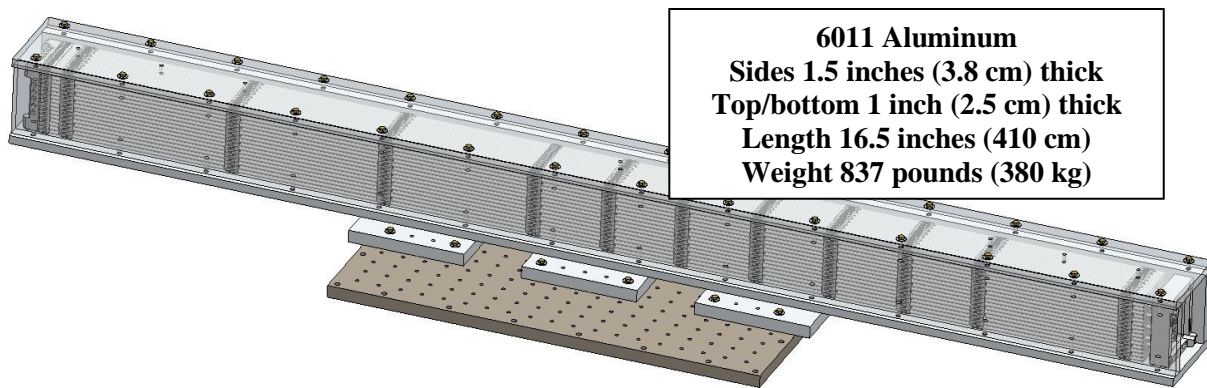


Figure 8. Basket dimensions. The assembly within the basket and the expander head used on the shaker are shown.

Finite-element modeling provided information on which rods within the assembly should be instrumented and on which locations on those rods the instrumentation for measuring strains and accelerations should be placed. Figure 9 shows accelerometers and a strain gauge on a region of one of the Zircaloy-4 rods. Finite-element modeling after the shaker tests are conducted will allow an estimate of the response all the rods experienced during the simulated road tests based on the surrogate rods test data.

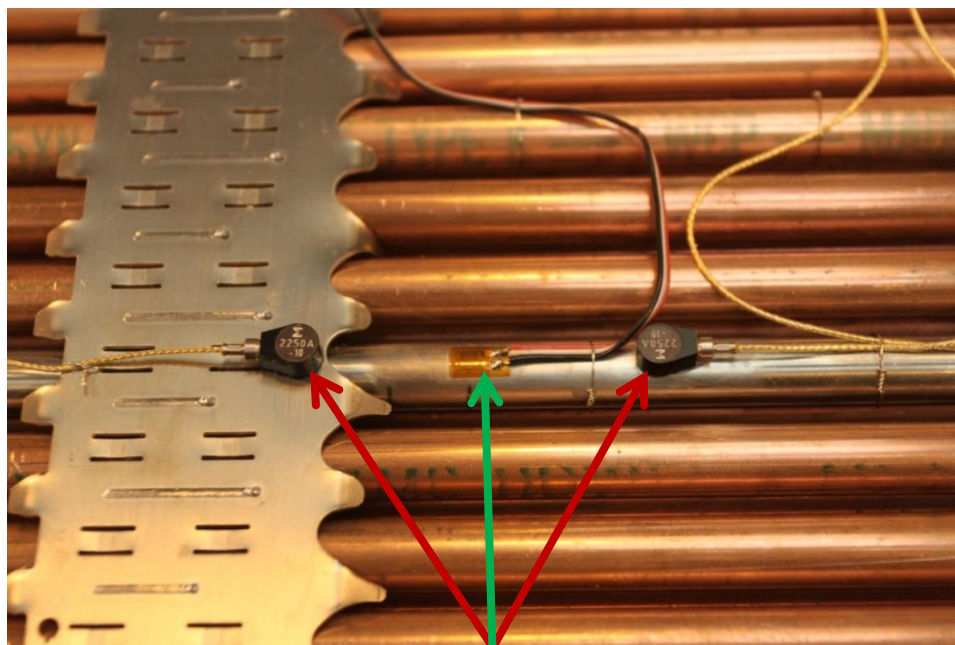


Figure 9. Instrumentation on top-middle Zircaloy-4 rod and spacer grid.  
NOTE: Red arrows point to accelerometer; green to strain gauge.

## 2.2 Test Procedures

This test procedure:

- Defines instrumentation requirements,
- Defines pretest and posttest inspection and construction tasks,
- Describes steps required to perform the shaker tests,
- Identifies applicable supporting and controlling documents, and
- Defines information, documentation, and data required to document the tests.

This procedure, in conjunction with the SNL Job Safety Analysis, Work Control – Level of Rigor, NEPA Review Information, Accept Work, and the Quality Assurance Program Plan documents, comprised the planning package for the test program.

### 2.2.1 Unirradiated Fuel Assembly

The availability of an actual fuel assembly, either PWR or boiling water reactor (BWR), was the most important requirement for the tests and, fortuitously, Sandia had procured PWR and BWR fuel assemblies and Zircaloy rods for an unrelated test program. A PWR assembly was selected for the shaker tests because PWR fuel is more common than BWR fuel in the US. Another reason is PWR rods are more flexible and exhibit greater deflection during over-the-road conditions that could contribute higher strains applied to the rods than BWR rods; therefore, the strains seen on PWR rods may bound those of BWR rods. A full complement of Zircaloy-4 rods was unavailable for the shaker tests, however, so only three were used for the tests.

Ideally, irradiated, high-burnup, aged fuel rods would be used for the tests, but due to cost, availability, and work dose concerns, their use was not an option for the tests. Instead, the tests required a surrogate material for the fuel and cladding.<sup>7</sup> The over-the-road shaker test simulations tests were conducted with unirradiated clad pins (Zircaloy-4 and copper tubing) filled with lead to represent the mass of the fuel.

The ideal surrogate rod for testing would have the same mass and flexibility as an irradiated rod. Unirradiated fuel has a gap between the fuel pellets and the cladding, but as they become irradiated, fuel pellets swell and close the gap; thus, unirradiated fuel rods are not an exact surrogate for irradiated rods. A solid rod of some metal may be appropriate, but a survey indicated that the cost is prohibitive in the lengths necessary to match that of the PWR rods (e.g., 13-foot [4-m] molybdenum rods). So, a decision was made to disregard the issue of pellet—clad interaction for the rods to be used for the test<sup>8</sup>, and instead, use tubes in which a rod was inserted with a gap between the tubes and the solid rods (similar to the case of unirradiated Zircaloy rods and fuel pellets). It was necessary to attempt to match the properties of surrogate rods with those of irradiated rods, although differences in the rod response can be quantified by numerical analysis posttest. The properties of zirconium alloy rods were used to select a surrogate rod of appropriate stiffness and mass.

---

7. The cost is significant – approximately \$100k for a 17 × 17 PWR assembly with Zircaloy rods (without UO<sub>2</sub> pellets).

8. A related DOE program is currently addressing the pellet—clad interaction issue. Once the analysis is benchmarked to data from this test, effects of the pellet—clad interaction from related tests can be incorporated into the analyses.

## 2.2.2 Instrumentation

### 2.2.2.1 Placement of the Instruments on the Test Unit

Strain gauges were placed on the cladding to obtain the maximum peak strains to which the cladding is subjected during normal transport. Accelerometers were placed at strategic locations on the shaker, basket, assembly spacer grids, and selected rods (Figure 10). The tests employed 16 strain gauges and 25 accelerometers.

Modeling an assembly identified the optimum locations for the instrumentation [7], with Zircaloy-4 rods placed at the top, middle rod location; a top, side location; and the bottom, side location below the top, side Zircaloy-4 rod. Instrumentation was placed at various locations on these three rods at the midpoint between spacer grid supports and adjacent to the spacer grids to provide a representative profile of the loading on the rods. Section 2.3.2 provides the detailed instrumentation plan.

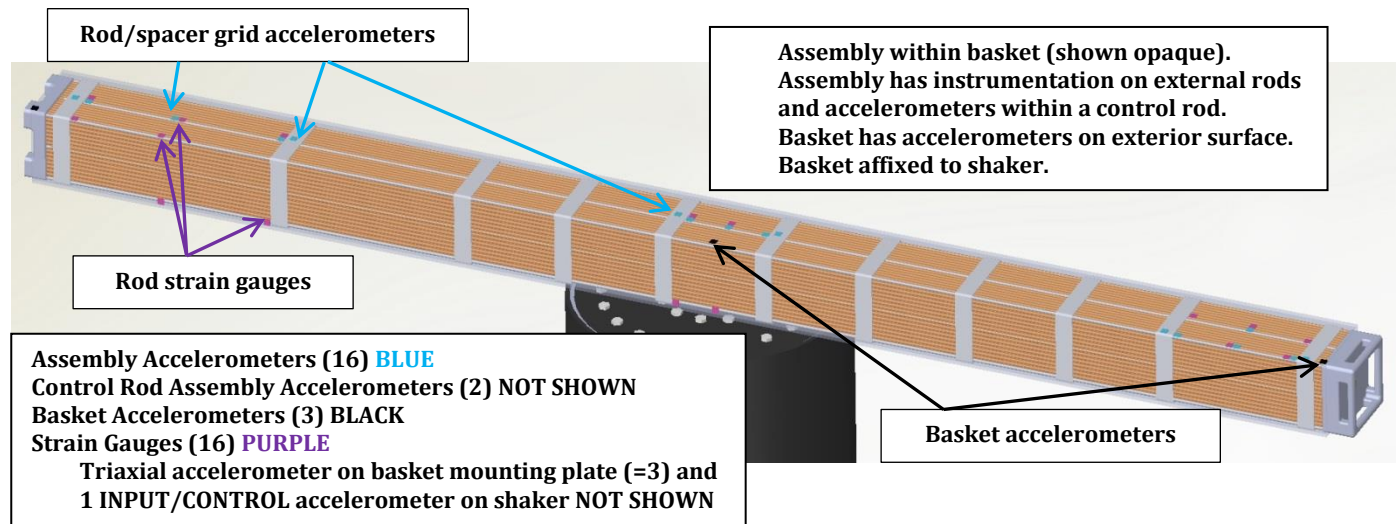


Figure 10. Position of instrumentation on assembly and basket.  
 NOTE: Arrows show example instrument locations.

### 2.2.2.2 Shaker Used for Tests

The shaker used for the tests was a MB Dynamics C220 base-isolated electrodynamic shaker system located in the Sandia Experimental Environmental Simulation Organization's Vibration and Acoustics Laboratory (Building 6560). This shaker is used to test large-scale test structures. It has a 4-ft shaker head diameter. A 4-ft by 5-ft expander head was mounted onto the shaker head. Capabilities of the shaker include: 10-2,000 Hz sine/random, 30,000 lbs. force, 86 g peak, 45 in./sec velocity, and 2-in. peak-to-peak displacement.

### **2.2.2.3 Data Reduction and Analysis**

The voltage output versus time for each accelerometer and strain gauge was recorded for each shock and vibration test. The output voltages were converted to acceleration or micro-strain per the calibration factor for each accelerometer or strain gauge.

The test results will be assessed relative to known or estimated properties of cladding to judge the effect of the normal transport conditions on the integrity of the cladding. Yield strength and elastic modulus are cladding properties of interest available for unirradiated and irradiated conditions, with fracture toughness and cladding fatigue strength also relevant.

PNNL refined and modified a LS-DYNA structural model of a detailed  $17 \times 17$  assembly to include specific details for the test assembly and basket and utilized accelerations imposed during the actual shaker testing [6].

## **2.3 Test Parameters**

This test procedure:

- Defines instrumentation requirements,
- Identifies individuals involved in this program and defines their responsibilities,
- Defines pretest and posttest inspection and construction tasks,
- Describes steps required to perform the shaker tests,
- Identifies applicable supporting and controlling documents, and
- Defines information, documentation, and data required to document the tests.

The instrumented fuel assembly within its surrogate basket was securely affixed upon the shaker. Using the inputs from the analyses of the vibration and shock data from Section 3, the shaker imparted loads to the basket/assembly while the shaker data acquisition system recorded the responses from the accelerometers and the strain gauges attached to the test unit.

The vibration facility in Excitation Equipment Building 6560 Area III at Sandia provided controllable simulation of vibration, acceleration, and shock environments. A shaker within this facility was used for the tests.

Additional figures in the Appendix provide more test details.

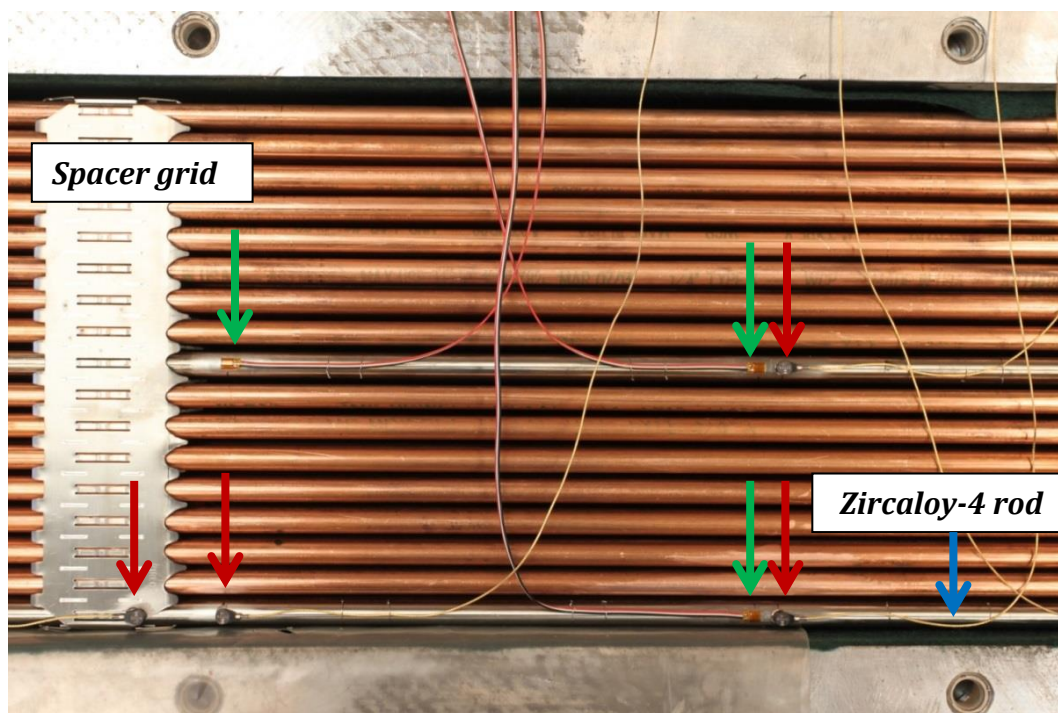


Figure 11. Instrumentation on top-middle and top-side Zircaloy-4 rod and spacer grid.  
NOTE: Red arrows point to accelerometer; green to strain gauge.

Figure 12 provides the material property data evaluated in selecting the copper/lead surrogate rod for the shaker tests. A SOLIDWORKS™ simulation predicted a bending response difference of less than 5% between the copper-lead rod and Zircaloy-lead rods.

The combined Modulus/Moment of Inertia properties were checked to assess the combined stiffness of each rod:

- $EI_{Cu} = 8.71 \text{ K-in}^2$
- $EI_{Zirc} = 5.53 \text{ K-in}^2$

The conclusion is that copper tubing is slightly stiffer than Zircaloy.

Although the material surrogates do not mimic the true material properties exactly, they are the best as far as availability, constructability, and cost.  $UO_2$  and lead share very similar densities but  $UO_2$  is considerably stiffer than lead. Zircaloy is 30% less dense than copper but Zircaloy has stiffness similar to copper. An actual assembly weighs approximately 1,404 lbs. (637 kg). The experimental assembly weighed approximately 1,446 lbs. (656 kg). The difference in weight between the actual and experimental assemblies is 42 lbs. (19 kg – a 3% difference). Although the stiffness of actual and the experimental surrogate rods were not the same (mostly due to properties of the  $UO_2$  v. lead), the weights of the two rods were nearly exact - *weight is considered the most important parameter to simulate*. Thus, dynamic response of the test assembly is expected to closely represent that of a real fuel assembly. Also, analysis benchmarked to this data will be used with data from used fuel bend tests obtained from a related DOE program.

Zirc and Surrogate Material Properties (Based on equivalent thickness and variable EI)									
Zirc		Aluminum		Brass		Carbon Steel		Copper	
E <sub>Zirc</sub> (GPa)	99	E <sub>Al</sub> (GPa)	70	E <sub>Brass</sub> (GPa)	110	E <sub>SS</sub> (GPa)	205	E <sub>Cu</sub> (GPa)	115
E <sub>Zirc</sub> (ksi)	14359	E <sub>Al</sub> (ksi)	10153	E <sub>Brass</sub> (ksi)	15954	E <sub>SS</sub> (ksi)	29733	E <sub>Cu</sub> (ksi)	16679
ρ <sub>Zirc</sub> (g/cm <sup>3</sup> )	6.55	ρ <sub>Al</sub> (g/cm <sup>3</sup> )	2.7	ρ <sub>Brass</sub> (g/cm <sup>3</sup> )	8.5	ρ <sub>SS</sub> (g/cm <sup>3</sup> )	7.85	ρ <sub>Cu</sub> (g/cm <sup>3</sup> )	8.94
ρ <sub>Zirc</sub> (g/in <sup>3</sup> )	107	ρ <sub>Al</sub> (g/in <sup>3</sup> )	44	ρ <sub>Brass</sub> (g/in <sup>3</sup> )	139	ρ <sub>SS</sub> (g/in <sup>3</sup> )	129	ρ <sub>Cu</sub> (g/in <sup>3</sup> )	147
h (in)	151.79	h (in)	144	h (in)	151.79	h (in)	151.79	h (in)	151.79
Vol <sub>Zirc</sub> (in <sup>3</sup> )	3.77	Vol <sub>Al</sub> (in <sup>3</sup> )	5.38	Vol <sub>Brass</sub> (in <sup>3</sup> )	5.67	Vol <sub>SS</sub> (in <sup>3</sup> )	5.67	Vol <sub>Cu</sub> (in <sup>3</sup> )	5.67
Mass (g)	404.80	Mass (g)	238.19	Mass (g)	790.42	Mass (g)	729.98	Mass (g)	831.34
t (in)	0.0225	t (in)	0.03500	t (in)	0.03500	t (in)	0.03500	t (in)	0.03500
D <sub>Zirc</sub> (in)	0.374	D <sub>Al</sub> (in)	0.375	D <sub>Brass</sub> (in)	0.375	D <sub>SS</sub> (in)	0.375	D <sub>Cu</sub> (in)	0.375
d <sub>Zirc</sub> (in)	0.329	d <sub>Al</sub> (in)	0.305	d <sub>Brass</sub> (in)	0.305	d <sub>SS</sub> (in)	0.305	d <sub>Cu</sub> (in)	0.305
EI (k*in <sup>2</sup> )	5.532	EI (k*in <sup>2</sup> )	5.543	EI (k*in <sup>2</sup> )	8.710	EI (k*in <sup>2</sup> )	16.232	EI (k*in <sup>2</sup> )	8.710
Zirc Rod (lbs)	0.891	Al Rod (lbs)	0.525	Brass Rod (lbs)	1.739	CS Rod (lbs)	1.606	Cu Rod (lbs)	1.829



Moment of Inertia = I  $\frac{\pi(D^4 - d^4)}{64}$

Figure 12. Technical data used to select copper tubes as surrogate tubes based on Zircaloy-4 tube dimensions.

Input for the shaker table was taken from U.S. Nuclear Regulatory Commission, “Shock and Vibration Environments for a Large Shipping Container During Truck Transport (Part II),” NUREG/CR-0128 and Cliff F. Magnuson, “Shock and Vibration Environments for Large Shipping Container during Truck Transport (Part I),” SAND77-1110, September 1977 [4a, 4b] (referenced in NUREG-1609, “Standard Review Plan for Transportation Packages for Radioactive Material” Section 2.5.6.5 Vibration [3]). Key details from this report are:

- Vibration and shock data obtained were measured by accelerometers attached to the exterior of two truck casks over a 700-mile (1,127-km) journey.
- One cask weighed 56,000 lbs. (25,401 kg) [4a] and the second weighed 44,000 lbs. (19,958 kg) [4b].
- Speeds ranged from 0 to 55 mph (0 to 88.5 km/hr).

Figures 13 and 14 and Tables 2 and 3 show data from this report.

Using the most conservative data from the two reports [4a, 4b], the shaker table simulated the vibration and shock experienced by the cask during transport.

Accelerometers placed along the length of the Zircaloy rods measured shock and vibration. Accelerometers were also on the basket and shaker. Strain gauges placed along the length of the rods measured strain. The stresses on the fuel rods were estimated posttest based on the strain gauge readings.

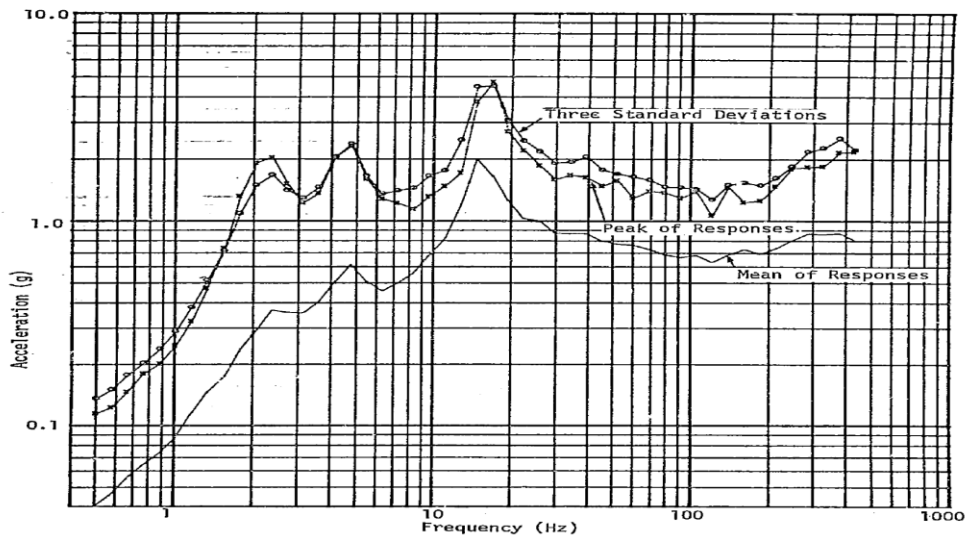


Figure 5. Superimposed Shock Response Spectra, 3% Damping, Vertical Axis

22

Figure 13. Shock data from the 56,000 lbs. (25,401 kg) truck cask transportation report [4a].

Table 2. Truck (56,000 lbs [25,401 kg]) vibration data [4a]

Truck Vibration 249 100N (56,000-Pound) Cargo

Frequency Band (Hz)	Input to Cargo (g); 99% Level of Zero-to-Peak Amplitude		
	Longitudinal Axis	Transverse Axis	Vertical Axis
0-5	0.27	0.10	0.52
5-10	0.14	0.07	0.27
10-20	0.19	0.19	0.37
20-40	0.10	0.07	0.19
40-80	0.10	0.10	0.37
80-120	0.07	0.10	0.37
120-180	0.07	0.10	0.52
180-240	0.05	0.10	0.52
240-350	0.07	0.14	0.52
350-500	0.05	0.07	0.37
500-700	0.05	0.02	0.10
700-1000	0.05	0.02	0.10
1000-1400	0.14	0.05	0.10
1400-1900	0.03	0.02	0.10

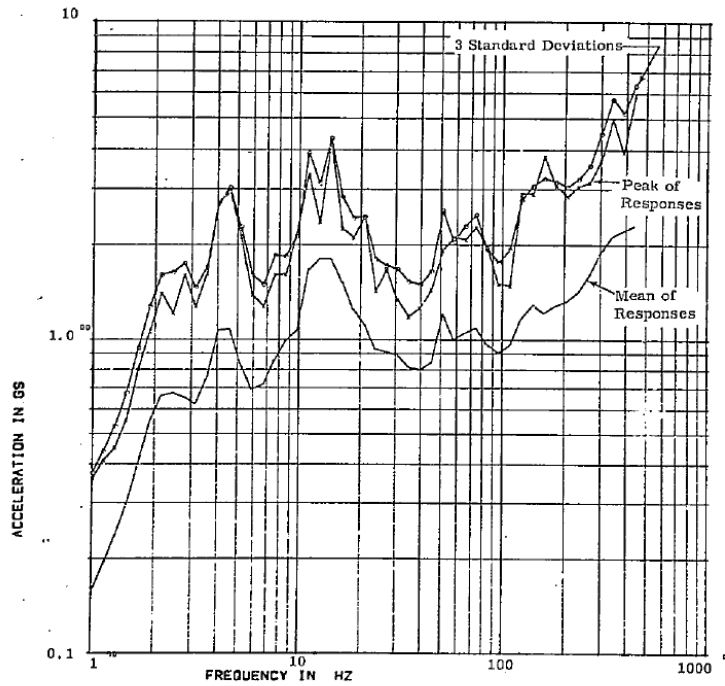


Figure 6. Superimposed Shock Response Spectra--3% Damping--  
Vertical Axis

Figure 14. Shock data from the 44,000 lbs (19,958 kg) truck cask transportation report [4b].

Table 3. Truck (44,000 lbs. [19,958 kg]) vibration data [4b]

Truck Vibration  
195 700 N (44,000 Pound) Cargo

Frequency Band - Hz	Input to Cargo (g) 99% Level of 0 to Peak Amplitude		
	Longitudinal Axis	Transverse Axis	Vertical Axis
0-5	0.14	0.14	0.27
5-10	0.19	0.19	0.19
10-20	0.27	0.27	0.27
20-40	0.10	0.27	0.27
40-80	0.14	0.14	0.52
80-120	0.07	0.10	0.52
120-180	0.07	0.10	0.52
180-240	0.05	0.10	0.52
240-350	0.05	0.10	0.52
350-500	0.05	0.05	0.14
500-700	0.04	0.04	0.07
700-1000	0.03	0.07	0.07
1000-1400	0.01	0.04	0.05
1400-1900	0.01	0.05	0.05

Figure 15 presents data derived from the vibration and shock measured on the truck cask and serve as inputs to the shaker. These curves were developed to provide the input to the shaker for

the vibration and shock tests. Section 3 describes in detail the methodology for deriving these curves.

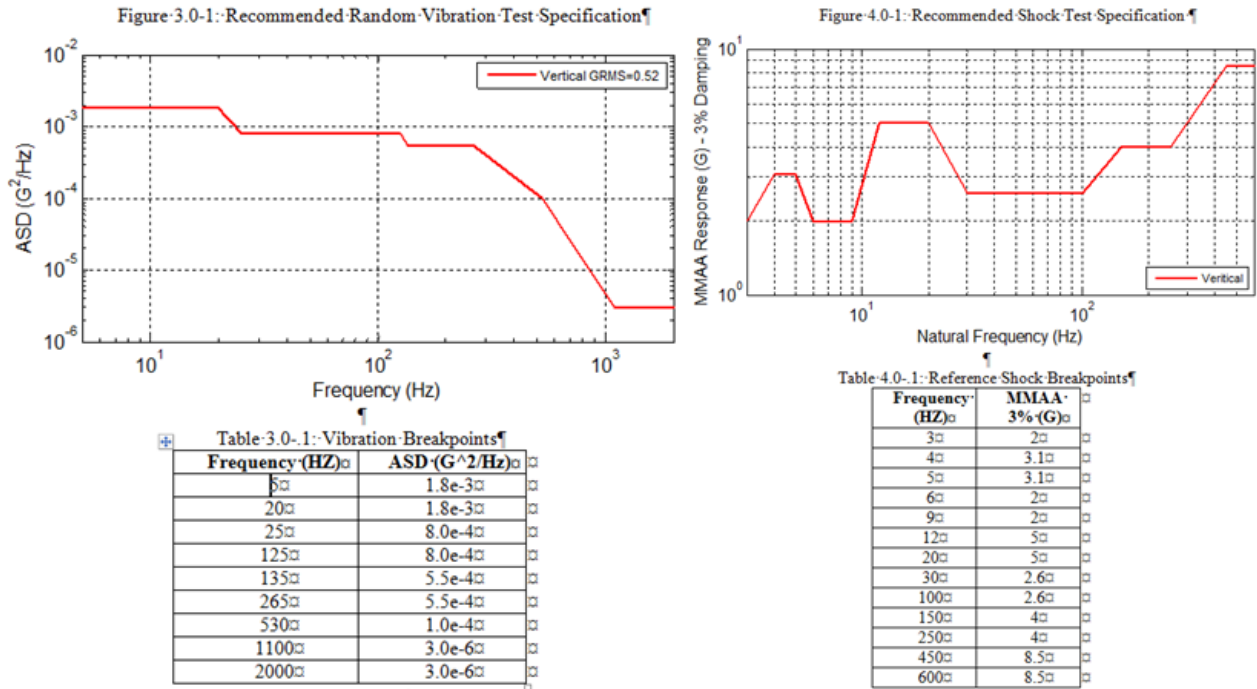


Figure 15. Data derived from the truck cask transportation report used as input to the shaker.

### 2.3.1 Instrumentation Plan

The location of the instruments, accelerometers, and strain gauges was informed by PNNL analyses [7] and expert judgment at Sandia. Eighteen accelerometers were placed on the rods and spacer grids, with an additional seven larger accelerometers on the basket and shaker.

#### 2.3.1.1 Spans between Spacer Grids

Table 4 lists the spans between the spacer grids –for each of the ten spans, which were denoted from left to right (bottom-nozzle end to top-nozzle end of the assembly) as S1 – S10.

Table 4. Spans Between Spacer Grids

Span 1 = 22.973 inch (58.35 cm)
Span 2 = 21.142 inch (53.70 cm)
Span 3 = 20.650 inch (52.45 cm)
Span 4 = 10.315 inch (26.20 cm)
Span 5 = 10.197 inch (25.90 cm)
Span 6 = 10.413 inch (26.45 cm)
Span 7 = 10.158 inch (25.80 cm)
Span 8 = 10.334 inch (26.25 cm)
Span 9 = 10.217 inch (25.95 cm)
Span 10 = 20.354 inch (51.70 cm)

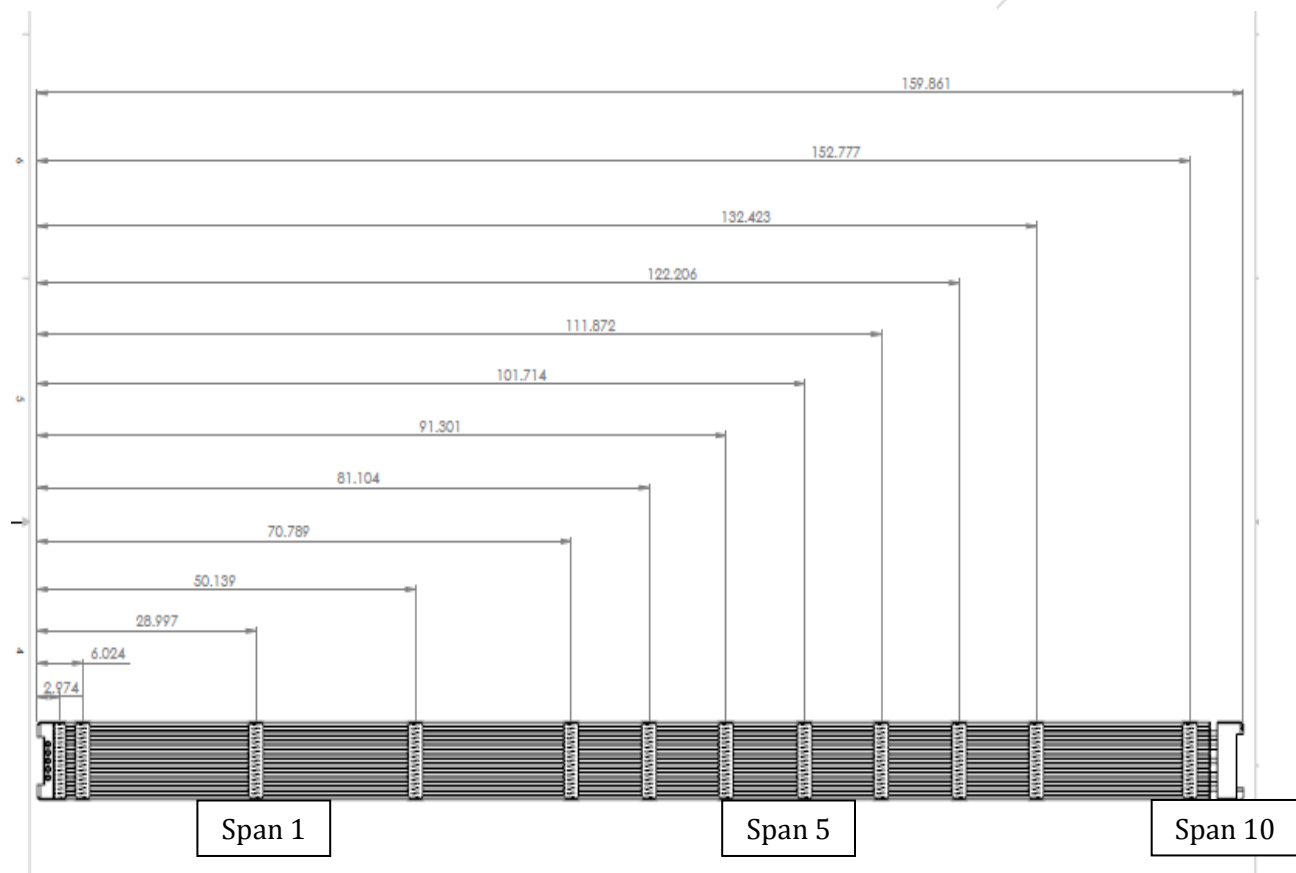


Figure 16. PWR assembly showing spans between spacer grids.

NOTE: Bottom-nozzle end of assembly is at the left. Spans 1 to 10 go from left to right, bottom-nozzle end to top-nozzle end of assembly.

### 2.3.1.2 Instrumentation Nomenclature, Locations, and Data Acquisition Channels

Table 5 documents the instrumentation nomenclature and locations used on the test unit.

Table 5. Instrumentation Nomenclature and Locations on Test Unit

Instrumentation Nomenclature	Serial #	Channel	Cal. Factor	Location (in.) from bottom nozzle
<b>Top-Middle Rod (TMR) Top-Middle Spacer Grids (TMSG)</b>				
<b>Model 2250A-10 Accelerometers</b>			<b>mV/g</b>	
(Malfunction after Test #7) TMSG-A-S1-1	17209	2	10.06	6.5
(Malfunction after Test #7) TMR-A-S1-2	17210	3	9.963	8.375
TMR-A-S1-3	17211	4	10.01	17.0
(Malfunction during Test #5) TMR-A-S1-4	17218	5	9.859	26.375
TMSG-A-S1-5	17219	6	9.955	28.25
TMSG-A-S5-1	17220	7	9.903	81.6875
TMR-A-S5-2	17221	8	10.02	83.5
TMR-A-S5-3	17222	9	9.984	85.875
TMR-A-S5-4	16825	10	9.926	89.6875
TMSG-A-S5-5	16917	11	9.977	90.5625
(Malfunction for all tests) TMR-A-S10-1	17203	12	9.913	143.0

NOTE: "A" denotes accelerometer; "S1, S5, and S10" denote the spans on the assembly.

Table 5. (cont.)

Instrumentation Nomenclature	Serial #	Channel	Cal. Factor	Location (in.) from bottom nozzle
<b>CEA-03-062UW-350 Strain Gauges</b>			<b>Gauge Factor</b>	
TMR-G-S1-1		33	2.150	7.3125
TMR-G-S1-2		34	2.150	17.3125
TMR-G-S1-3		35	2.150	27.3125
TMR-G-S5-1		36	2.150	82.5
TMR-G-S5-2		37	2.150	86.1875
TMR-G-S10-1		38	2.150	134.1875
TMR-G-S10-2		39	2.150	142.625
TMR-G-S10-3		40	2.150	151.25
<b>Top-Side Rod (TSR)</b>				
<b>Top-Side Spacer Grids (TSSG)</b>				
<b>Model 2250A-10 Accelerometers</b>			<b>mV/g</b>	
TSSG-A-S10-1	16916	13	10.00	132.9375
TSR-A-S10-2	16918	14	9.984	134.1875
TSR-A-S10-3	16919	15	9.839	143.0
TSR-A-S10-4	16920	16	9.809	149.9375
TSSG-A-S10-5	17202	17	9.818	152.3125
<b>CEA-03-062UW-350 Strain Gauges</b>			<b>Gauge Factor</b>	
TSR-G-S1-1		41	2.150	7.3125
TSR-G-S1-2		42	2.150	17.3125
TSR-G-S10-1		43	2.150	142.625
TSR-G-S10-2		44	2.150	151.25

NOTE: "G" denotes strain gauge.

Table 5. (cont.)

Instrumentation Nomenclature	Serial #	Channel	Cal. Factor	Location (in.) from bottom nozzle
<b>Bottom-Side Rod (BSR)</b>				
<b>CEA-03-062UW-350 Strain Gauges</b>			<b>Gauge Factor</b>	
BSR-G-S1-1		45	2.150	17.3125
BSR-G-S1-2		46	2.150	27.3125
BSR-G-S5-1		47	2.150	82.5
BSR-G-S5-2		48	2.150	86.1875
<b>Center Control Rod (CR)</b>				
<b>Model 2250A-10 Accelerometers</b>			<b>mV/g</b>	
CR-A-S1-1 (Bottom Nozzle)	17204	18	10.03	2.0
CR-A-S10-1 (Top Nozzle)	16923	19	10.22	155.375
<b>Basket</b>				
<b>Model 2221D Accelerometers</b>			<b>mV/g</b>	<b>Location</b>
B-A-S1-1	ED06	20		0.75" bottom end basket -1.25" side
B-A-S5-1	DR47	21		81" from top end of basket × 1.25" from side
B-A-S10-1	EL32	22		0.75" from top end of basket × 1.25" from side
<b>Shaker and Baseplate</b>				
Baseplate SH-A-X (vertical)	ER02	23		
Baseplate SH-A-Y (lateral)	ED07	24		7.75" bottom side edge baseplate × 3" edge baseplate
Baseplate SH-A-Z (longitudinal)	ET31	25		
Shaker INPUT/CONTROL shaker A-1	DR54	1		3.5" top-end center base plate × 0.875" edge baseplate

### 2.3.2 Test Unit Preparation

The basket and assembly test unit was prepared as follows:

1. Construct basket by bolting four plates of 6061 aluminum per dimensions indicated in Figure 14. Provide cutouts of instrumentation wires. Line inner wall of basket with felt (0.040 in. [1 mm] thick).
2. Construct basket mounting plates from three pieces of 6061 aluminum 16 in. × 22 in. × 1.5 in. (40.6 cm × 55.9 cm × 3.8 cm). Bolt mounting plates to basket.
3. Insert lead rods into the surrogate copper tubes and the Zircaloy tubes.
4. Insert all rods into the assembly.
5. Attach strain gauges and accelerometers onto the rods and spacer grids selected for instrumentation.
6. Place assembly into basket.
7. Complete instrumentation installation forms.

### 2.3.3 Test Set-up

The basket and assembly test unit were prepared using the following instructions:

1. Mount basket/assembly unit onto shaker. Bolt basket mounting plates to shaker.
2. Attach accelerometers to the basket and shaker.
3. Attach instrumentation to the shaker facility recording equipment. Calibrate instrumentation.
4. Photograph shaker and test unit.

### 2.3.4 Perform Test

The group prepared the basket and assembly test unit using the following instructions:

1. Apply vibration input to the shaker
  - A. Random vibration
  - B. Sine sweep.
2. Apply shock input to the shaker.

### 2.3.5 Post Test Activities

1. Disassemble test unit.
2. Collect test data for posttest analyses.

### 3. TEST INPUT SPECIFICATIONS<sup>9</sup>

#### 3.1 Introduction

The Environments Engineering Group was asked to derive a set of set of random vibration and shock test specifications for a laboratory test of a reactor fuel assembly. These specifications were derived from the vibration and shocks presented in References [4a, 4b]. The purpose of the laboratory test is to measure loads during normal highway transportation. This memo presents test specifications for the vertical axis only as it is believed that is the direction that will affect the loading.

The instrumentation has not yet been optimized and is subject to change. Section 2 presents the instrumentation. Section 3 presents the random vibration specification. Section 4 presents the decayed sine specifications.

#### 3.2 Instrumentation

The placement of instrumentation is designed to obtain the peak strain and has not been optimized. Therefore it is subject to change after further discussion with the model group. The accelerometers are used to get insight into what the structure is doing.

Table 6 presents the input accelerometers and their locations. Table 7 presents the response accelerometer and strain gauge locations. The first few node shapes will determine where on the tube sections the strain gauges are placed. Figure 17 shows the fuel reactor assembly on the shaker table and the input and response locations. Figure 18 shows a cross section of the fuel reactor assembly and the location of tubes 1 to 5.

Table 6. Input Accelerometers

Type	Location
Limit Accelerometers	Right Fixture End
	Left Fixture End
Control	Fixture Midpoint

Table 7. Response Accelerometers and Strain Gauges

Location	Tube 1	Tube 2	Tube 3	Tube 4	Tube 5
End Spacer	A		A	A	
End Tube Section	A, S				
Mid-span Spacer	A		A	A	
Mid-span Tube Section	A, S				

NOTE: A – denotes accelerometer; S – denotes strain gauge.

9. Section 3 was prepared as a letter report by Melissa C de Baca and Jerome Cap, Sandia National Laboratories, March 20, 2013. Minor editing has been made for consistency and numbering of figures and tables.

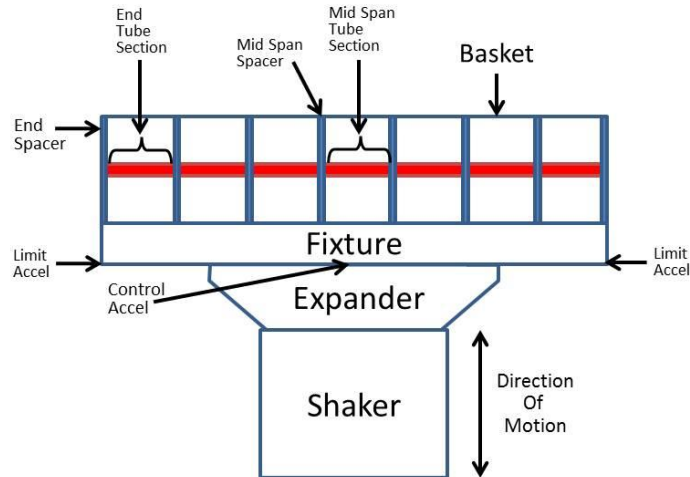


Figure 17. Fuel Reactor Assembly on Shaker Table.

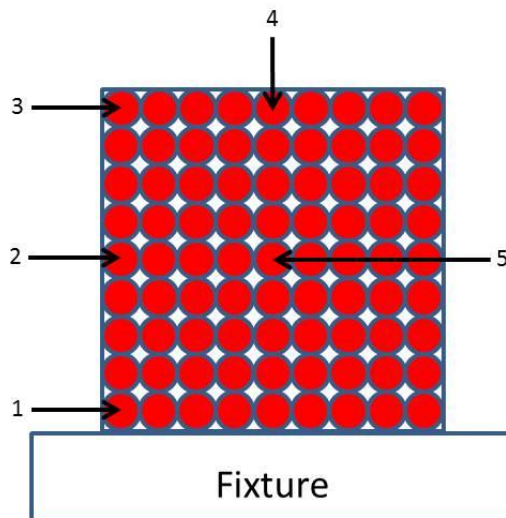


Figure 18. Cross Section of Fuel Reactor Assembly.

### 3.3 Random Vibration Test Specifications

Figure 19 shows the recommend random vibration test specification to be applied at the midpoint of the fixture. Table 8 presents the corresponding breakpoints. The test should be run for a duration of one minute or long enough to obtain good data. Section 3.5 shows the derivation of this test specification.

Because the necessary shape of the limit channels is unknown, they will be a scaled version of the control channel applied at the left and right ends of the fixture. The scaling will be determined at the time of the test.

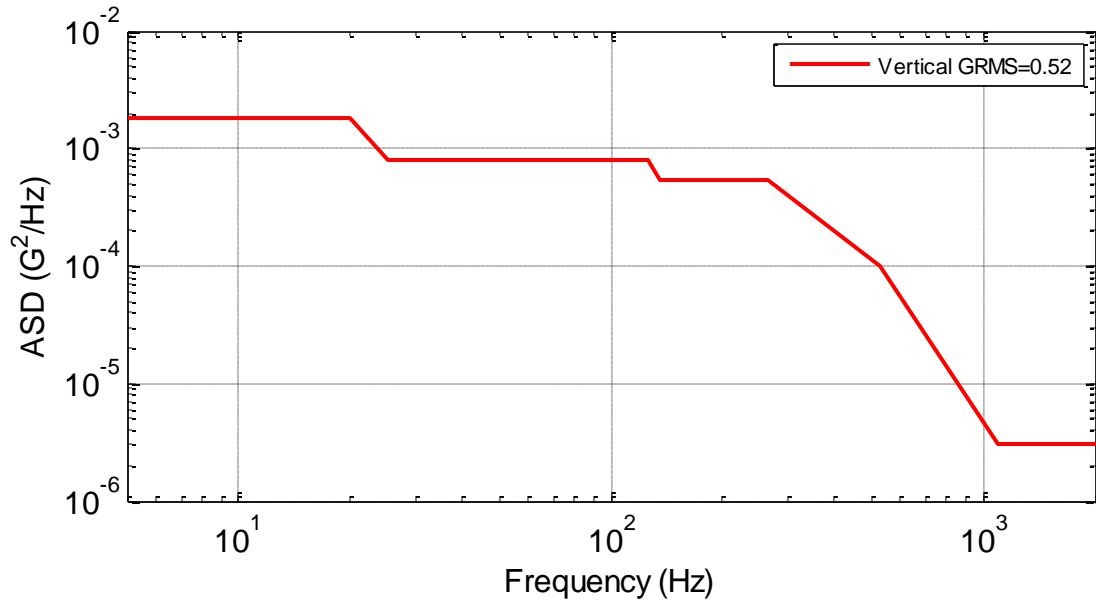


Figure 19. Recommended Random Vibration Test Specification.

Table 8. Vibration Breakpoints

Frequency (HZ)	ASD (G <sup>2</sup> /Hz)
5	1.8e-3
20	1.8e-3
25	8.0e-4
125	8.0e-4
135	5.5e-4
265	5.5e-4
530	1.0e-4
1,100	3.0e-6
2,000	3.0e-6

### 3.4 Shock – Decayed Sine Specifications and Time Histories

Figure 20 shows the recommended shock test specification. Table 9 lists the corresponding breakpoints.

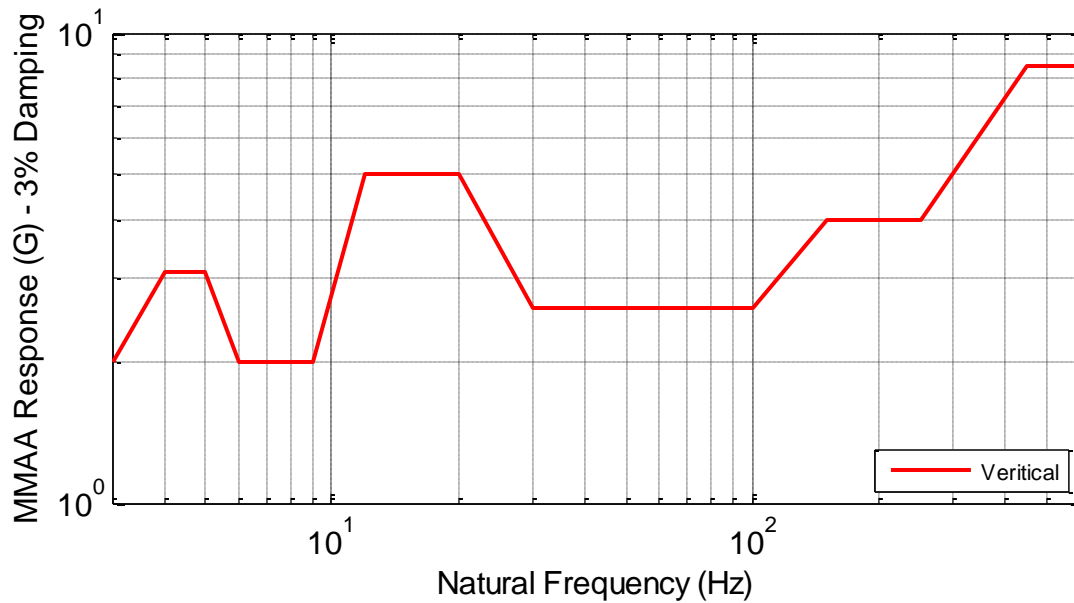


Figure 20. Recommended Shock Test Specification.

Table 9. Reference Shock Breakpoints

Frequency (HZ)	MMAA 3% (G)
3	2
4	3.1
5	3.1
6	2
9	2
12	5
20	5
30	2.6
100	2.6
150	4
250	4
450	8.5
600	8.5

Tables 10 to 14 list the parameters for the five decayed sine realizations and show the SRS parameters, the acceleration parameters, and the decayed sine parameters. Figures 21 to 25 show the reference shock spectra compared against the corresponding decayed sine shock spectra, and the corresponding accelerations, velocities, and displacements.

Table 10. Initial Realization of Decayed Sine Parameters

<b>SRS Parameters</b>							
<b>fmin</b>	<b>fmax</b>	<b>pts/oct</b>	<b>Damp</b>	<b>SRS Type</b>			
3.00	600.00	8.00	0.03	MMAA			
<b>Acceleration History Parameters</b>							
<b>Sample Rate</b>		<b>Frame Size</b>		<b>Gravity Constant</b>		<b>Ptype</b>	
5,120		32,768		386.00		1	
<b>Value</b>		<b>Acceleration (G)</b>		<b>Velocity (in./sec)</b>		<b>Displacement (in.)</b>	
<b>Min</b>		-2.54		-11.86		-0.3894	
<b>Max</b>		2.25		12.20		0.4633	
<b>Res</b>		0.04		-0.30		-0.0029	
<b>Decayed Sine Parameters</b>							
<b>Frequency (Hz)</b>	<b>Accel (G)</b>	<b>Decay Rate</b>	<b>Delay</b>	<b>Frequency (Hz)</b>	<b>Accel (G)</b>	<b>Decay Rate</b>	<b>Delay</b>
3.3	-0.308	0.0228	0.0000	75.9	0.076	0.0010	0.0000
3.9	0.297	0.0192	0.0000	82.7	-0.053	0.0009	0.0000
4.6	-0.243	0.0162	0.0000	90.2	0.086	0.0008	0.0000
5.5	0.156	0.0137	0.0000	98.3	-0.039	0.0008	0.0000
6.5	-0.080	0.0115	0.0000	107.1	0.066	0.0007	0.0000
7.7	0.091	0.0097	0.0000	116.8	-0.067	0.0006	0.0000
9.1	-0.127	0.0082	0.0000	127.3	0.102	0.0006	0.0000
10.8	0.267	0.0069	0.0000	138.7	-0.120	0.0005	0.0000
12.8	-0.328	0.0058	0.0000	151.2	0.117	0.0005	0.0000
15.2	0.300	0.0049	0.0000	164.8	-0.096	0.0005	0.0000
18.1	-0.300	0.0041	0.0000	179.6	0.104	0.0004	0.0000
21.4	0.176	0.0035	0.0000	195.8	-0.094	0.0004	0.0000
24.8	-0.160	0.0030	0.0000	213.4	0.124	0.0003	0.0000
27.0	0.122	0.0028	0.0000	232.6	-0.101	0.0003	0.0000
29.4	-0.056	0.0025	0.0000	253.5	0.111	0.0003	0.0000
32.1	0.049	0.0023	0.0000	276.3	-0.123	0.0003	0.0000
35.0	-0.055	0.0021	0.0000	301.2	0.200	0.0002	0.0000
38.1	0.051	0.0020	0.0000	328.3	-0.157	0.0002	0.0000
41.5	-0.018	0.0018	0.0000	357.8	0.177	0.0002	0.0000
45.3	0.041	0.0016	0.0000	390.0	-0.255	0.0002	0.0000
49.3	-0.065	0.0015	0.0000	425.1	0.275	0.0002	0.0000
53.8	0.052	0.0014	0.0000	463.3	-0.284	0.0002	0.0000
58.6	-0.075	0.0013	0.0000	505.0	0.238	0.0001	0.0000
63.9	0.071	0.0012	0.0000	550.5	-0.236	0.0001	0.0000
69.6	-0.076	0.0011	0.0000	600.0	0.371	0.0001	0.0000
				1.1	0.099	0.9500	-0.1459

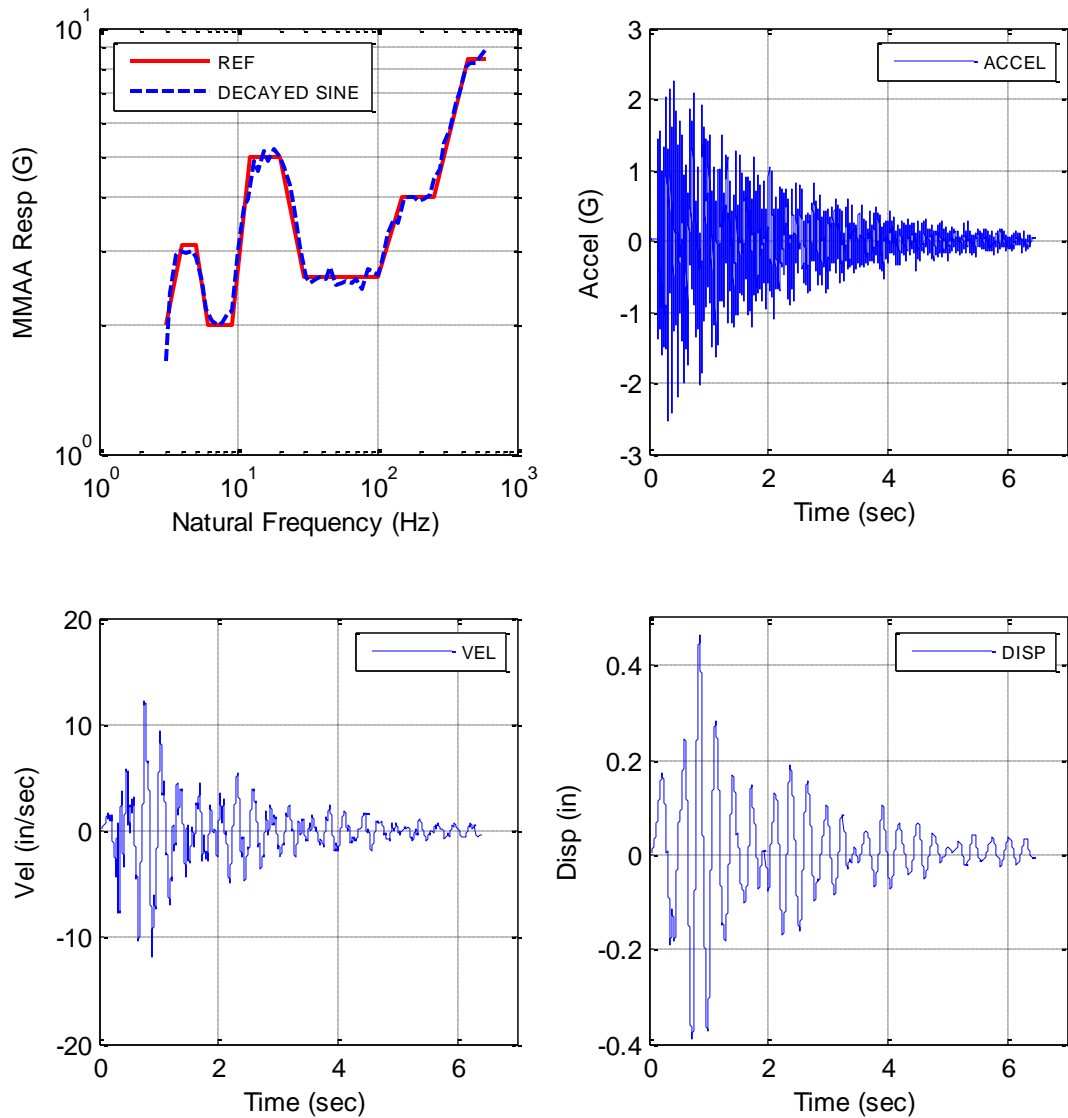


Figure 21. Initial Realization of Decayed Sine.

Table 11. Second Realization of Decayed Sine Parameters

SRS Parameters				
fmin	fmax	pts/oct	Damp	SRS Type
3.00	600.00	8.00	0.03	MMAA
Acceleration History Parameters				
Sample Rate	Frame Size	Gravity Constant	Ptype	
5,120	32,768	386.00	1	
Value	Acceleration (G)	Velocity (in./sec)	Displacement (in.)	
Min	-2.17	-9.50	-0.3534	
Max	2.35	12.05	0.4211	
Res	0.02	-0.10	0.0155	

Decayed Sine Parameters							
Frequency (Hz)	Accel (G)	Decay Rate	Delay	Frequency (Hz)	Accel (G)	Decay Rate	Delay
3.3	-0.275	0.0228	0.0000	76.2	0.079	0.0010	0.0000
3.9	0.287	0.0191	0.0000	83.8	-0.083	0.0009	0.0000
4.5	-0.292	0.0166	0.0000	90.6	0.039	0.0008	0.0000
5.6	0.145	0.0133	0.0000	96.0	-0.077	0.0008	0.0000
6.5	-0.078	0.0115	0.0000	106.9	0.070	0.0007	0.0000
7.8	0.075	0.0095	0.0000	117.7	-0.101	0.0006	0.0000
9.0	-0.062	0.0083	0.0000	127.5	0.074	0.0006	0.0000
10.4	0.224	0.0071	0.0000	137.9	-0.116	0.0005	0.0000
12.8	-0.300	0.0058	0.0000	154.7	0.136	0.0005	0.0000
15.1	0.300	0.0050	0.0000	167.7	-0.101	0.0004	0.0000
18.7	-0.266	0.0040	0.0000	183.0	0.154	0.0004	0.0000
22.1	0.220	0.0034	0.0000	194.7	-0.076	0.0004	0.0000
24.8	-0.174	0.0030	0.0000	214.6	0.109	0.0003	0.0000
26.5	0.116	0.0028	0.0000	237.3	-0.109	0.0003	0.0000
28.7	-0.076	0.0026	0.0000	259.4	0.108	0.0003	0.0000
32.2	0.064	0.0023	0.0000	279.0	-0.086	0.0003	0.0000
34.6	-0.064	0.0022	0.0000	296.9	0.185	0.0003	0.0000
39.0	0.050	0.0019	0.0000	331.2	-0.114	0.0002	0.0000
42.6	-0.053	0.0018	0.0000	350.2	0.205	0.0002	0.0000
44.8	0.049	0.0017	0.0000	388.5	-0.256	0.0002	0.0000
50.1	-0.056	0.0015	0.0000	429.2	0.285	0.0002	0.0000
54.9	0.056	0.0014	0.0000	474.2	-0.291	0.0002	0.0000
59.0	-0.069	0.0013	0.0000	513.6	0.249	0.0001	0.0000
65.2	0.070	0.0011	0.0000	550.5	-0.189	0.0001	0.0000
71.3	-0.052	0.0010	0.0000	574.7	0.281	0.0001	0.0000
				1.1	0.102	0.9500	-0.1458

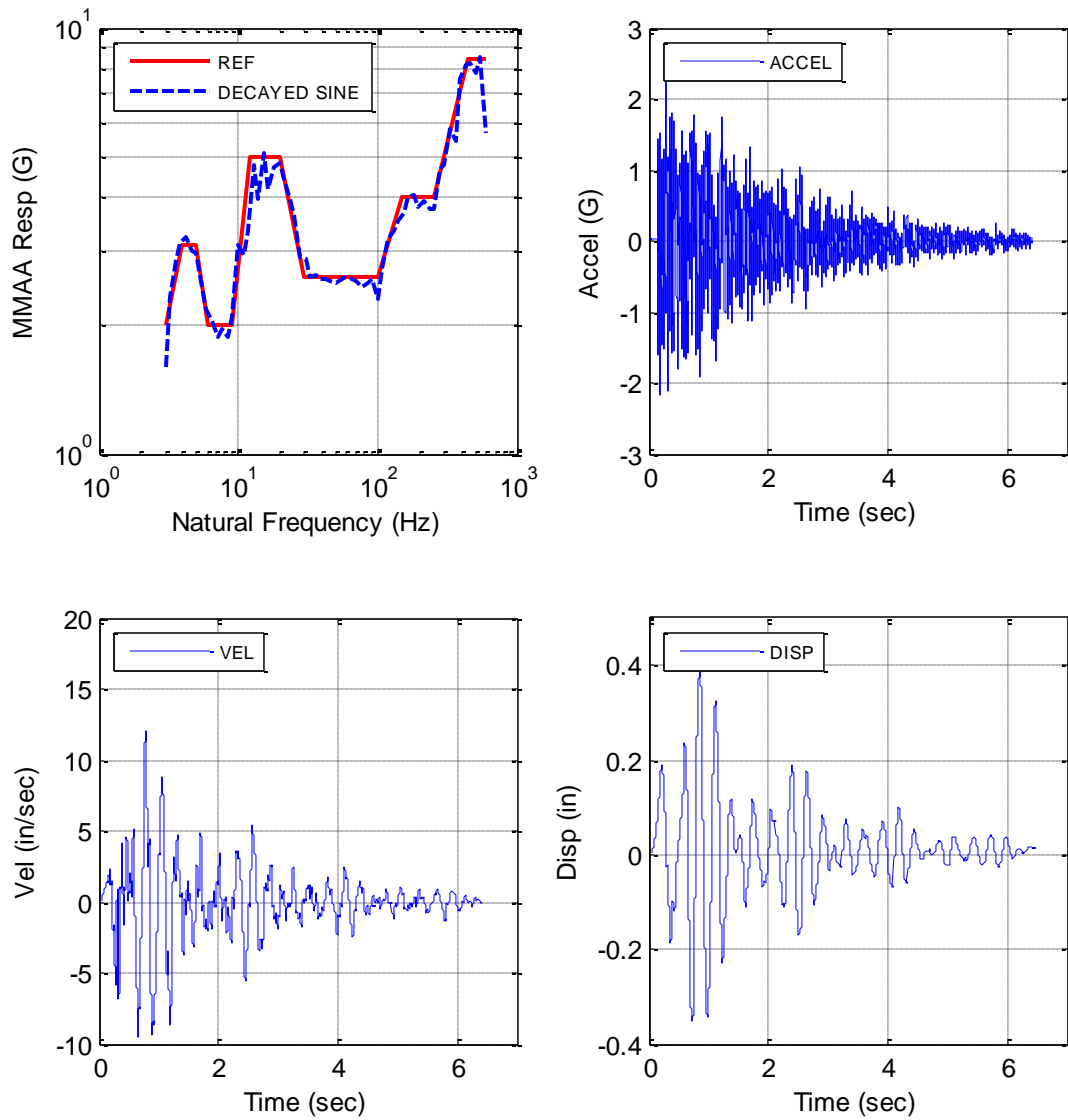


Figure 22. Second Realization of Decayed Sine.

Table 12. Third Realization of Decayed Sine Parameters

<b>SRS Parameters</b>							
<b>fmin</b>	<b>fmax</b>	<b>pts/oct</b>	<b>Damp</b>	<b>SRS Type</b>			
3.00	600.00	8.00	0.03	MMAA			
<b>Acceleration History Parameters</b>							
<b>Sample Rate</b>	<b>Frame Size</b>	<b>Gravity Constant</b>		<b>Ptype</b>			
5,120	32,768	386.00		1			
<b>Value</b>	<b>Accel (G)</b>	<b>Velocity (in./sec)</b>		<b>Disp (in.)</b>			
<b>Min</b>	-2.57	-10.50		-0.4529			
<b>Max</b>	2.50	12.37		0.4690			
<b>Res</b>	-0.04	0.15		0.0265			
<b>Decayed Sine Parameters</b>							
<b>Frequency (Hz)</b>	<b>Accel (G)</b>	<b>Decay Rate</b>	<b>Delay</b>	<b>Frequency (Hz)</b>	<b>Accel (G)</b>	<b>Decay Rate</b>	<b>Delay</b>
3.3	-0.287	0.0229	0.0000	76.8	0.077	0.0010	0.0000
4.1	0.332	0.0183	0.0000	81.9	-0.051	0.0009	0.0000
4.8	-0.237	0.0154	0.0000	92.1	0.054	0.0008	0.0000
5.7	0.127	0.0131	0.0000	100.0	-0.043	0.0007	0.0000
6.4	-0.108	0.0116	0.0000	106.6	0.057	0.0007	0.0000
7.7	0.032	0.0097	0.0000	116.8	-0.097	0.0006	0.0000
8.9	-0.111	0.0084	0.0000	128.7	0.119	0.0006	0.0000
11.2	0.287	0.0067	0.0000	141.2	-0.136	0.0005	0.0000
13.4	-0.300	0.0056	0.0000	152.2	0.149	0.0005	0.0000
15.9	0.199	0.0047	0.0000	165.6	-0.071	0.0005	0.0000
18.2	-0.280	0.0041	0.0000	178.2	0.109	0.0004	0.0000
21.7	0.228	0.0034	0.0000	195.5	-0.126	0.0004	0.0000
24.1	-0.149	0.0031	0.0000	215.9	0.099	0.0003	0.0000
27.6	0.082	0.0027	0.0000	237.4	-0.136	0.0003	0.0000
29.4	-0.043	0.0025	0.0000	256.6	0.104	0.0003	0.0000
31.6	0.002	0.0024	0.0000	269.7	-0.069	0.0003	0.0000
35.7	-0.045	0.0021	0.0000	304.2	0.182	0.0002	0.0000
38.6	0.056	0.0019	0.0000	327.5	-0.170	0.0002	0.0000
42.4	-0.058	0.0018	0.0000	357.0	0.200	0.0002	0.0000
44.8	0.051	0.0017	0.0000	382.6	-0.238	0.0002	0.0000
49.8	-0.018	0.0015	0.0000	432.4	0.305	0.0002	0.0000
54.3	0.090	0.0014	0.0000	459.6	-0.189	0.0002	0.0000
57.5	-0.055	0.0013	0.0000	498.9	0.265	0.0001	0.0000
63.6	0.068	0.0012	0.0000	546.5	-0.229	0.0001	0.0000
68.9	-0.099	0.0011	0.0000	574.7	0.308	0.0001	0.0000
				1.1	0.104	0.9500	-0.1466

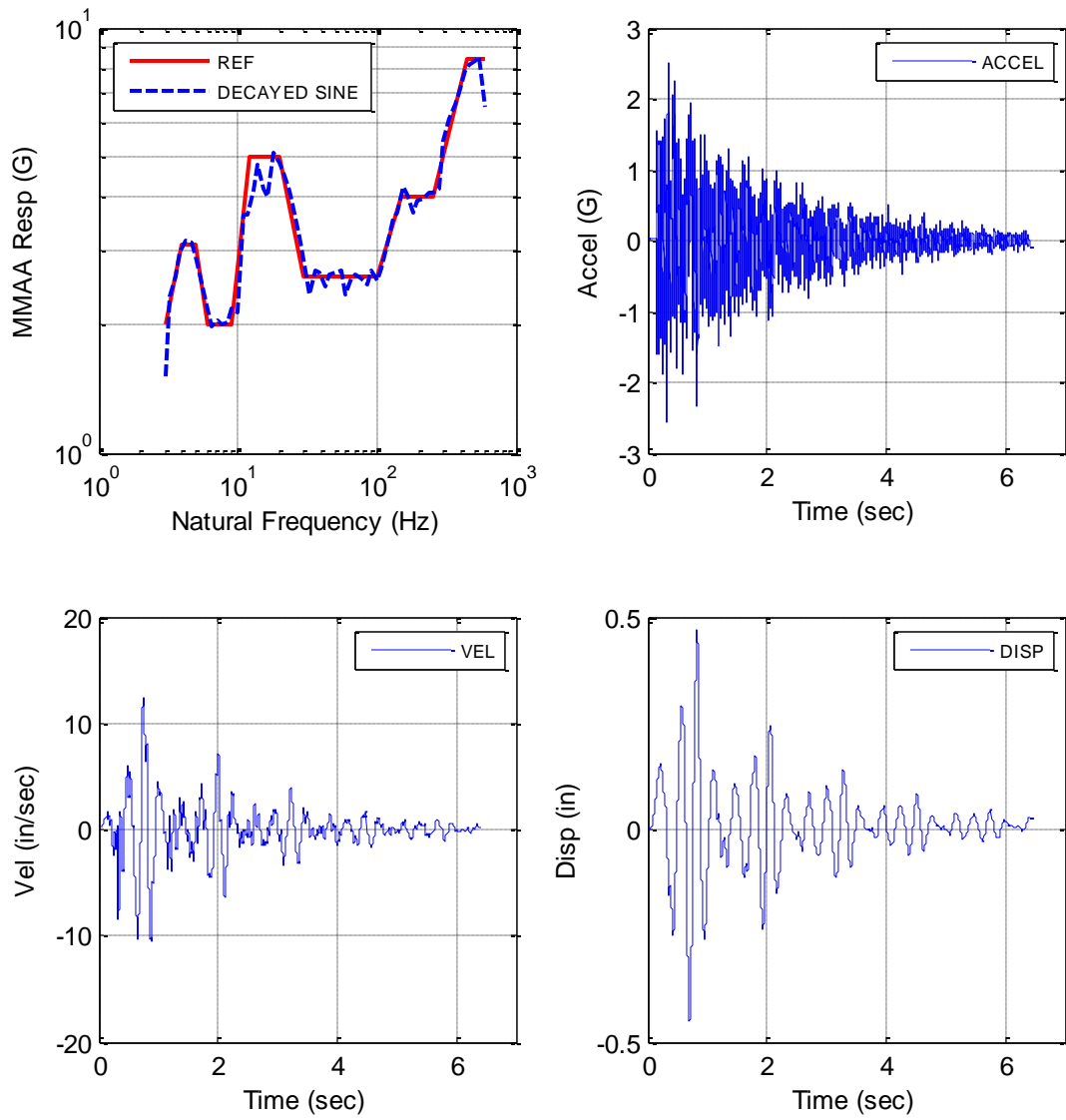


Figure 23. Third Realization of Decayed Sine.

Table 13. Fourth Realization of Decayed Sine Parameters

<b>SRS Parameters</b>							
<b>fmin</b>	<b>fmax</b>	<b>pts/oct</b>	<b>Damp</b>	<b>SRS Type</b>			
3.00	600.00	8.00	0.03	MMAA			
<b>Acceleration History Parameters</b>							
<b>Sample Rate</b>	<b>Frame Size</b>	<b>Gravity Constant</b>		<b>Ptype</b>			
5,120	32,768	386.00		1			
<b>Value</b>	<b>Accel (G)</b>	<b>Velocity (in./sec)</b>		<b>Disp (in.)</b>			
<b>Min</b>	-2.62	-10.73		-0.4000			
<b>Max</b>	2.07	11.06		0.4339			
<b>Res</b>	0.05	-0.18		-0.0047			
<b>Decayed Sine Parameters</b>							
<b>Frequency (Hz)</b>	<b>Accel (G)</b>	<b>Decay Rate</b>	<b>Delay</b>	<b>Frequency (Hz)</b>	<b>Accel (G)</b>	<b>Decay Rate</b>	<b>Delay</b>
3.3	-0.312	0.0226	0.0000	76.2	0.081	0.0010	0.0000
3.9	0.277	0.0191	0.0000	82.9	-0.064	0.0009	0.0000
4.6	-0.253	0.0163	0.0000	89.5	0.066	0.0008	0.0000
5.4	0.158	0.0138	0.0000	98.0	-0.032	0.0008	0.0000
6.5	-0.083	0.0115	0.0000	107.2	0.084	0.0007	0.0000
7.8	0.120	0.0095	0.0000	114.3	-0.070	0.0007	0.0000
9.6	-0.154	0.0078	0.0000	129.9	0.069	0.0006	0.0000
11.1	0.246	0.0067	0.0000	135.7	-0.126	0.0005	0.0000
12.7	-0.335	0.0059	0.0000	150.8	0.146	0.0005	0.0000
15.8	0.279	0.0047	0.0000	167.7	-0.120	0.0004	0.0000
17.4	-0.253	0.0043	0.0000	178.8	0.130	0.0004	0.0000
20.5	0.268	0.0036	0.0000	197.1	-0.127	0.0004	0.0000
24.0	-0.134	0.0031	0.0000	217.1	0.115	0.0003	0.0000
26.5	0.098	0.0028	0.0000	237.4	-0.052	0.0003	0.0000
29.2	-0.047	0.0026	0.0000	259.4	0.125	0.0003	0.0000
31.8	0.046	0.0023	0.0000	272.2	-0.097	0.0003	0.0000
34.1	-0.049	0.0022	0.0000	297.7	0.141	0.0003	0.0000
38.2	0.049	0.0020	0.0000	335.3	-0.189	0.0002	0.0000
40.7	-0.070	0.0018	0.0000	359.9	0.211	0.0002	0.0000
44.5	0.052	0.0017	0.0000	390.4	-0.238	0.0002	0.0000
49.7	-0.081	0.0015	0.0000	428.0	0.243	0.0002	0.0000
54.8	0.081	0.0014	0.0000	471.4	-0.257	0.0002	0.0000
60.1	-0.072	0.0012	0.0000	506.3	0.211	0.0001	0.0000
64.2	0.076	0.0012	0.0000	542.5	-0.238	0.0001	0.0000
71.5	-0.065	0.0010	0.0000	574.7	0.315	0.0001	0.0000
				1.1	0.113	0.9500	-0.1447

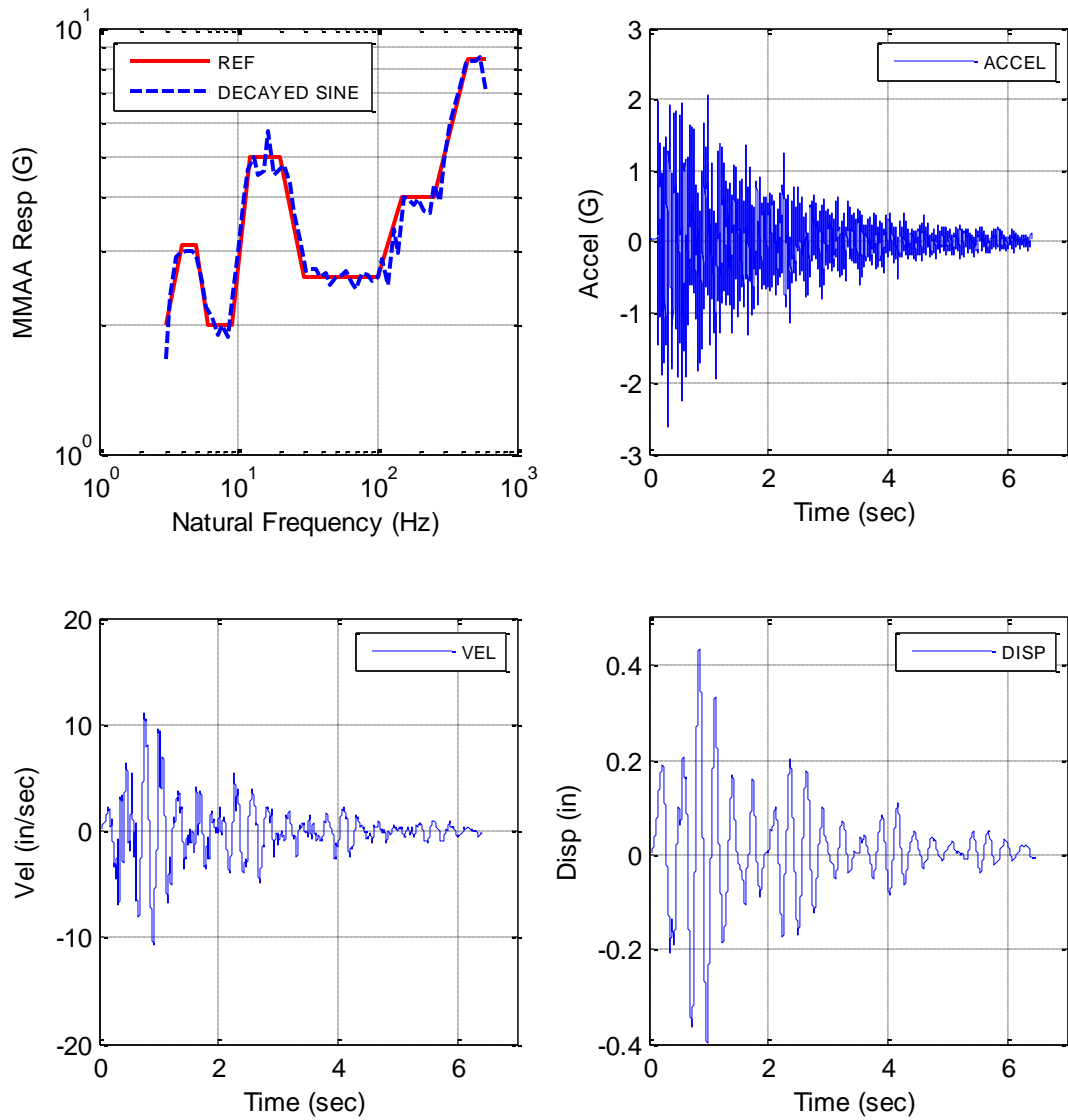


Figure 24. Fourth Realization of Decayed Sine.

Table 14. Fifth Realization of Decayed Sine Parameters

<b>SRS Parameters</b>							
<b>fmin</b>	<b>fmax</b>	<b>pts/oct</b>	<b>Damp</b>	<b>SRS Type</b>			
3.00	600.00	8.00	0.03	MMAA			
<b>Acceleration History Parameters</b>							
<b>Sample Rate</b>	<b>Frame Size</b>	<b>Gravity Constant</b>		<b>Ptype</b>			
5,120	32,768	386.00		1			
Value	Acceleration (G)	Velocity (in/sec)		Displacement (in)			
<b>Min</b>	-2.24	-11.26		-0.4353			
<b>Max</b>	2.05	11.50		0.4461			
<b>Res</b>	0.01	-0.06		0.0235			
<b>Decayed Sine Parameters</b>							
<b>Frequency (Hz)</b>	<b>Accel (G)</b>	<b>Decay Rate</b>	<b>Delay</b>	<b>Frequency (Hz)</b>	<b>Accel (G)</b>	<b>Decay Rate</b>	<b>Delay</b>
3.3	-0.304	0.0229	0.0000	75.5	0.090	0.0010	0.0000
4.1	0.338	0.0183	0.0000	83.2	-0.075	0.0009	0.0000
4.7	-0.243	0.0160	0.0000	90.1	0.050	0.0008	0.0000
5.6	0.130	0.0134	0.0000	96.1	-0.069	0.0008	0.0000
6.6	-0.071	0.0112	0.0000	105.7	0.078	0.0007	0.0000
7.6	0.101	0.0098	0.0000	118.9	-0.069	0.0006	0.0000
9.2	-0.130	0.0081	0.0000	124.2	0.111	0.0006	0.0000
10.9	0.235	0.0068	0.0000	141.4	-0.122	0.0005	0.0000
12.4	-0.300	0.0060	0.0000	148.0	0.117	0.0005	0.0000
15.4	0.262	0.0049	0.0000	166.4	-0.128	0.0004	0.0000
18.5	-0.274	0.0040	0.0000	179.8	0.053	0.0004	0.0000
21.3	0.226	0.0035	0.0000	193.1	-0.128	0.0004	0.0000
25.1	-0.193	0.0030	0.0000	214.4	0.093	0.0003	0.0000
27.3	0.126	0.0027	0.0000	228.3	-0.074	0.0003	0.0000
29.2	-0.032	0.0026	0.0000	256.0	0.122	0.0003	0.0000
32.0	0.078	0.0023	0.0000	278.0	-0.079	0.0003	0.0000
34.8	-0.062	0.0021	0.0000	294.5	0.170	0.0003	0.0000
38.7	0.047	0.0019	0.0000	321.1	-0.182	0.0002	0.0000
42.1	-0.037	0.0018	0.0000	351.7	0.198	0.0002	0.0000
45.1	0.043	0.0017	0.0000	380.7	-0.238	0.0002	0.0000
49.9	-0.072	0.0015	0.0000	424.1	0.284	0.0002	0.0000
55.1	0.086	0.0014	0.0000	471.7	-0.267	0.0002	0.0000
59.5	-0.042	0.0013	0.0000	508.6	0.186	0.0001	0.0000
64.6	0.064	0.0012	0.0000	551.6	-0.144	0.0001	0.0000
68.3	-0.049	0.0011	0.0000	574.7	0.299	0.0001	0.0000
				1.1	0.087	0.9500	-0.1465

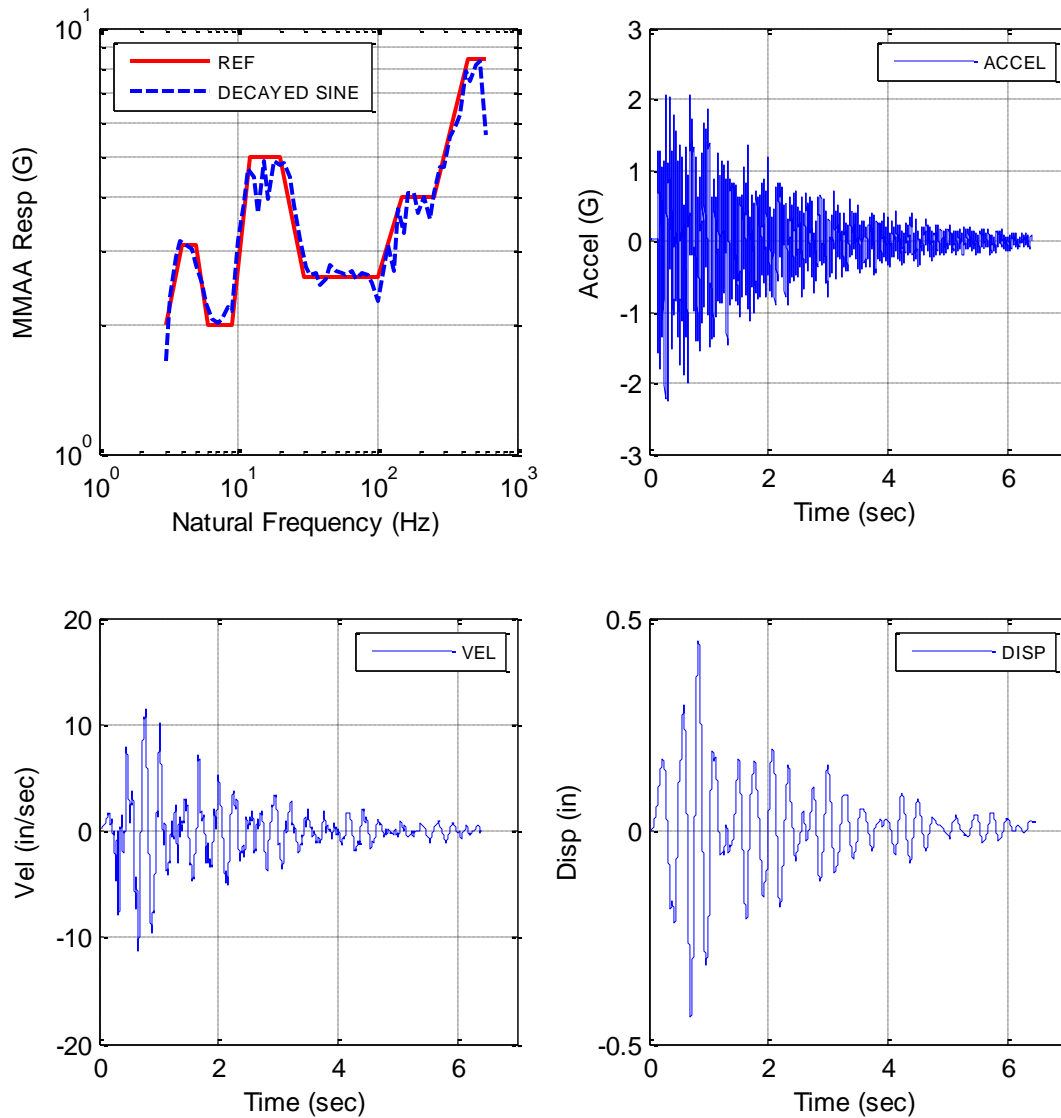


Figure 25. Fifth Realization of Decayed Sine.

### 3.5 Derivation of Test Specifications

The initial plan of the customer was to have a reactor fuel assembly in a large truck cast with the fuel rods instrumented within the cast to measure loads during normal highway transport. The cask was to be placed upon a trailer in a horizontal position for the test. However, they were unable to procure a cask and had to resort to simulating the field environment using the large electrodynamic shakers in Building 6560.

The only shock and vibration data available to derive the laboratory test specifications were from two field tests performed in the late 1970s in which large shipping containers were

transported by truck [4a, 4b]. Section 3.5.1 describes the derivation of the random vibration test specification. Section 3.5.2 describes the derivation of the shock test specification.

### 3.5.1 Derivation of Random Vibration Test Specification

The actual weight of the fuel reactor assembly falls between 44,000 lbs. and 56,000 lbs. Therefore, it was decided that enveloping the response data from both configurations would be conservative. Due to the age of the documents, the vibration test were presented in the form of VIBRAN spectra, which are defined as the 99% level of 0 to peak amplitudes for a series of sequential bandpass filtered versions of the raw data. Table 15 shows the VIBRAN spectra for the vertical axis.

Table 15. Input to Cargo (g) – Vertical Axis 99% Level of 0 to Peak Amplitude

Frequency Band	44,000 lbs. [1]	56,000 lbs. [2]
0 – 5	0.27	0.52
5 – 10	0.19	0.27
10 – 20	0.27	0.37
20 – 40	0.27	0.19
40 – 80	0.52	0.37
80 – 120	0.52	0.37
120 – 180	0.52	0.52
180 – 240	0.52	0.52
240 – 350	0.52	0.52
350 – 500	0.14	0.37
500 – 700	0.07	0.10
700 – 1,000	0.07	0.10
1,000 – 1,400	0.05	0.10
1,400 – 1,900	0.05	0.10

However, in order to use this information, it was first necessary to convert the data into Acceleration Spectral Densities (ASDs). The process for doing this is shown in equation 1, where ZPA is the zero to peak amplitude value taken from the VIBRAN spectra and FR is the corresponding frequency bandwidth.

$$ASD = (ZPA \div 3)^2 \div (FR(2) - FR(1)) \quad \{\text{Eq. 1}\}$$

However, the resulting raw ASDs contain vertical steps at the boundaries of the frequency bands and this cannot be replicated with modern shaker control systems. Therefore, during the process of enveloping the raw ASDs from each data source, ramps were introduced into the resulting composite ASD test specification. Figure 26 shows the recommended test specification and the underlying ASDs.

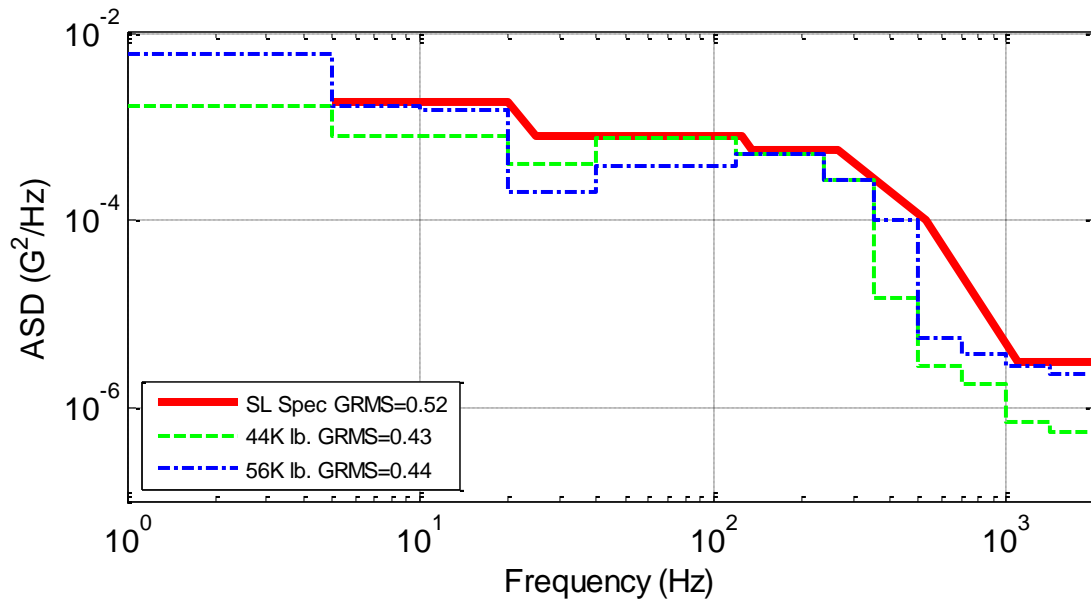


Figure 26. Recommended Test Specification and Underlying ASDs.

### 3.5.2 Derivation of Shock Test Specification

As the Shock Response Spectra (SRS), displayed graphically for the 44,000-lbs. cargo and the 56,000-lbs. cargo in References 4a and 4b, had to be digitized to obtain electronic data before being used. There were three SRS displayed; the  $3\sigma$ , the peak of responses, and the mean of responses. Due to the quality of the plot it was decided to extract the envelope from the three SRS when digitizing.

A straight-line segment SRS shock test specification was created that enveloped the 44,000-lbs. and 56,000 lbs. SRS. Figure 27 shows the recommended test specification and the underlying SRS.

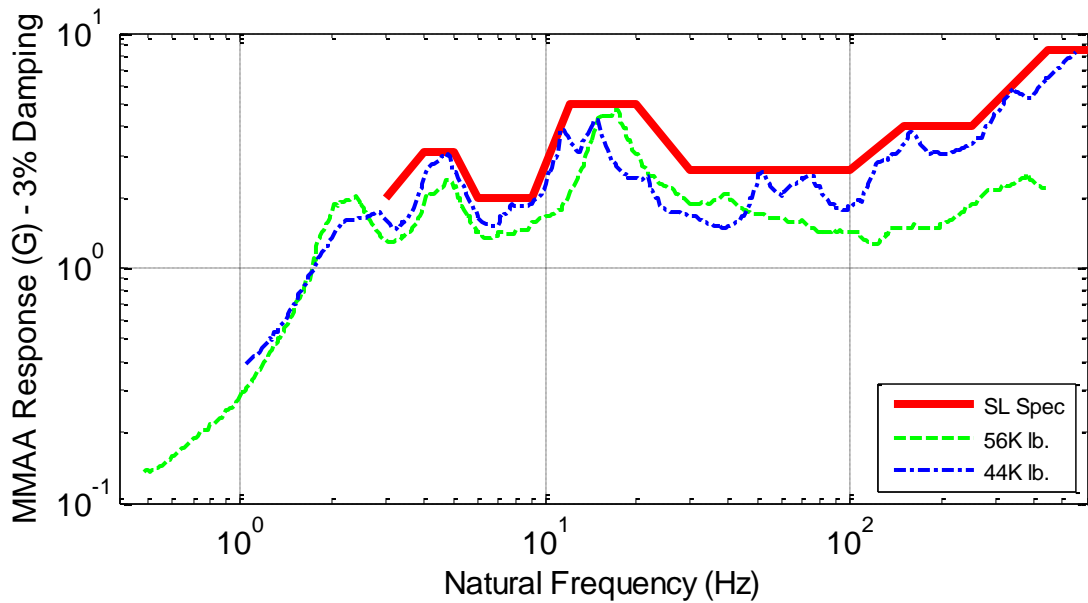


Figure 27. Recommended Test Specification and Underlying Shock Spectra.

In order to implement a test using SRS, one must first generate an acceleration waveform with an SRS that approximates the desired SRS within an acceptable tolerance band. The most common waveform type is composed of a sum of decayed sinusoids having different frequencies and decay rates. However, as there are unlimited waveforms with a similar SRS to the desired SRS, the group decided to generate five unique realizations.

The tonal frequencies for the first realization were defined to have a spacing of 4 tones/octave below 24 Hz and 8 tones/octave above 24 Hz. “Jitter” was added to the first set of tonal frequencies to obtain the remaining four unique transients. Figure 28 shows the range a given tonal frequency was allowed to vary. The frequencies were allowed to vary a maximum of 80% from the midpoint (i.e.,  $F_1$ ) in the positive and negative direction (i.e.,  $F_{1low}$  and  $F_{1high}$ ). A uniform random distribution was used to determine the amount each frequency varied within its specified range.

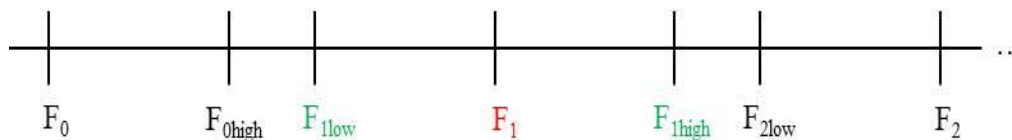


Figure 28. Range of Frequencies.



## 4. TEST RESULTS

### 4.1 Test Sequence

A total of 11 valid tests of the basket/assembly unit were performed on the shaker April 30 and May 1, 2013. Table 16 lists the test sequence. Each shock test ran for 10.8 seconds and each random vibration test ran for a few minutes although only 23 seconds of data representative of the vibration spectrum are shown in the figures in this report.

Frequencies input for the shock tests # (refer to Table 16) were limited to a lower bound of 4 Hz. At frequencies between 3.2 to 3.9 Hz, a very high frequency response of input/control accelerometer (Channel 1) occurred due to bottoming of the shaker, which caused an uncontrollable accelerometer-feedback loop to the shaker. The bottoming of the shaker was a result of the high deflections of the shaker at the low frequencies. This effect was corrected by limiting the lower frequency for the shock spectra to 4 Hz.<sup>10</sup>

Malfunctions occurred during testing for some of the accelerometers, including accelerometer TMR-A-S10-1 (Channel 12), which was inoperative for all tests, accelerometer TMR-A-S1-4 (Channel 5) which malfunctioned during Test #5, and accelerometers TMSG-A-S1-1 and TMR-A-S1-2 (Channels 2 and 3), which malfunctioned after Test #7.

- 
10. The low frequency response of the fuel assembly involves low-order modes of the assembly vibrating as a unit. The lowest order (the one with the lowest natural frequency) is the assembly bending like a simply supported beam. The maximum strain in a simply supported beam undergoing free vibration occurs at the top and bottom of the beam at its mid-span. This strain is calculated by the expression:

$$\varepsilon = \frac{48\Delta c}{5L^2}$$

where:

$\varepsilon$  = strain

$\Delta$  = deflection at mid-span

$c$  = distance from the neutral axis to the top or bottom of the beam (half the beam depth in this case)

$L$  = length of the beam

The fuel rods in an assembly are held in position by the spacer grids, and the frictional force at these junctions is insufficient for each of the rods to not slide when the assembly bends. Therefore, the strain in the rods is due to them following the shape of the deflected assembly. In the case of this test, the maximum deflection possible for the assembly is limited by the clearance between the assembly and the top of the basket (0.25 in), the length of the assembly is 159.86 in., and  $c$  is half the fuel tube diameter (0.187 in.). These parameters lead to a maximum strain in the rod of 18  $\mu\epsilon$ . This strain level is insignificant, so vibration of the assembly in this low-frequency mode is not important to the overall results.

Table 16. Shaker Test Sequence

Test		Comments	
<b>04/30/13: #1</b>	<b>Random Vibration #1</b>	<b>High amplitude spikes at high Hz</b>	
<b>#2</b>	Random Vibration #2		
<b>#3</b>	Random Vibration #3		
<b>#4</b>	Sine sweep: 5 – 1,100 Hz	Shaker shutdown at 1,100 Hz	
<b>#5</b>	Shock #1	Frequencies to 4 Hz	Decayed sine realization 1
<b>#6</b>	Random Vibration #4	High amplitude spikes at high Hz	
<b>05/01/13: #7</b>	<b>Random Vibration #5</b>		
<b>#8</b>	Shock #2		Decayed sine realization 2
<b>#9</b>	Shock #3		Decayed sine realization 3
<b>#10</b>	Shock #4		Decayed sine realization 4
<b>#11</b>	Shock #5		Decayed sine realization 5
<b>#12</b>	Random Vibration #6	High amplitude spikes at high Hz	
<b>.csv data:</b>	<b>Random Vibration</b>	<b>Shock</b>	
	12,800 samples/second	6,400 samples/second	Time-history data
	1 sample = 1/12,800 s	1 sample = 1/6,400 s	
	Units = $\mu\epsilon$	Units = g	

## 4.2 Test Data

Table 16 shows that each of the five shock tests corresponded to a different decayed sine realization for the same shock spectrum (Section 3.4). The six random vibration tests are all duplicates of the same vibration spectrum (Section 3.3). Shock Test #1 and Random Vibration Test #5 were arbitrarily selected for data reduction for this report. Table 21 shows a comparison of maximum micro-strains for duplicative tests and is discussed in Section 4.4.3.3.

The sampling rate was 6,400 samples/sec for the shock tests, so each time-history datum represents 1/6,400 seconds of shock data. The sampling rate for the random vibration tests was 12,800 samples/sec—each datum represents 1/12,800 seconds of vibration data.

The units for accelerometer Channels 1 to 25 are “g” (gravitation force, positive and negative<sup>11</sup>). The units for strain gauge Channels 33 to 48 are  $\pm$  micro-strain ( $\mu$ -in./in. or  $\mu$ -m/m).

11. The accelerometers were zeroed in a one  $g_{\text{earth}}$  field so that the actual acceleration the test unit was subjected to was the measured acceleration plus one  $g_{\text{earth}}$ .

## 4.3 Data Reduction

The data reduction of the time-history records was performed using a Sandia-developed code, K2<sup>12</sup>, which employs Stearns and David<sup>13</sup> digital data processing algorithms.

There were six duplicative random vibration tests and five shock tests conducted for this test program.

This test report highlights results from one of the random vibration tests and one of the shock tests. The results from these tests should be typical of any of the other random vibration and shock tests.

Due to the enormous amount of data collected, the raw data used to derive the tables and plots of the test results is not included in this report. Separate electronic SAND reports will be issued that provide all of the raw time-history (TH) test data ( $\mu\epsilon$  v. time and g v. time) for the eleven tests.

## 4.4 Discussion of Results

### 4.4.1 Magnitude of Strains

Tables 18 to 21 present micro-strain and acceleration data recorded for each instrument.

There was very little difference between strains measured on the rods due to shock loadings or vibration loads.

The maximum strain on a fuel rod measured during three shock shaker tests listed in Table 21 was 213  $\mu\text{in./in.}$  ( $\mu\text{m/m}$ ), which was at the mid-span of Span 10 of the top-middle rod during Shock Test #2. Span 10 is one of the longer spans located at the top-nozzle end of the assembly.

For Shock Tests #1, #2, and #5 the absolute value of the average maximum micro-strain for all the strain gauges was 99  $\mu\text{in./in.}$  ( $\mu\text{m/m}$ ).

The maximum strain on a fuel rod measured during three vibration tests listed in Table 21 was 207  $\mu\text{in./in.}$  ( $\mu\text{m/m}$ ) which was again at the mid-span of Span 10 of the top-middle rod during Random Vibration Test #4. For Random Vibration Tests #4, #5, and #6 the absolute value of the average maximum micro-strain for all the strain gauges was 91  $\mu\text{in./in.}$  ( $\mu\text{m/m}$ )

---

12. FAMTEK Professional Services, Inc., K2 Data Analysis Software, Version K2 Release 1.1.5 (Build 9), designed for Sandia National Laboratories, August 14, 2011.

13. Samuel D. Stearns and Ruth A. David, "Signal Processing Algorithms," Prentice-Hall, Inc., 1988.

The maximum strain measured for the six tests analyzed was 213  $\mu\text{in./in.}$  ( $\mu\text{m/m}$ ).

The average maximum strain was 112  $\mu\text{in./in.}$  ( $\mu\text{m/m}$ ) for Shock Test #1 and 100  $\mu\text{in./in.}$  ( $\mu\text{m/m}$ ) for the Random Vibration Test #5.

*The magnitude of these strains is very low in terms of the strength of Zircaloy-4.*

The stresses corresponding to the maximum experimentally measured strains are approximately 3 ksi (20.6 MPa) as shown in Figure 29, which is a plot of the elastic portion of the stress-strain curves for unirradiated and low-burnup and high-burnup Zircaloy-4. The figure indicates just how low the magnitude of the strains and corresponding stresses were on the rods relative to the elastic limit of unirradiated and irradiated Zircaloy-4. Even with considering the axial stress offset due to internal pressure in irradiated Zircaloy-4 rods, estimated to be approximately 6 ksi (41 MPa), the applied stresses to the rod would be still low relative to the yield strength.

The results suggest that failure of the rods during NCT is unlikely due to a strain- or stress-based failure mechanism. The applied strains on the rods and the corresponding applied stresses may be too low relative to the strength of the cladding to cause failure in the absence of cracks. Further work is underway in other DOE programs to assess Zircaloy-4 performance based on inelastic, brittle fracture material property conditions.

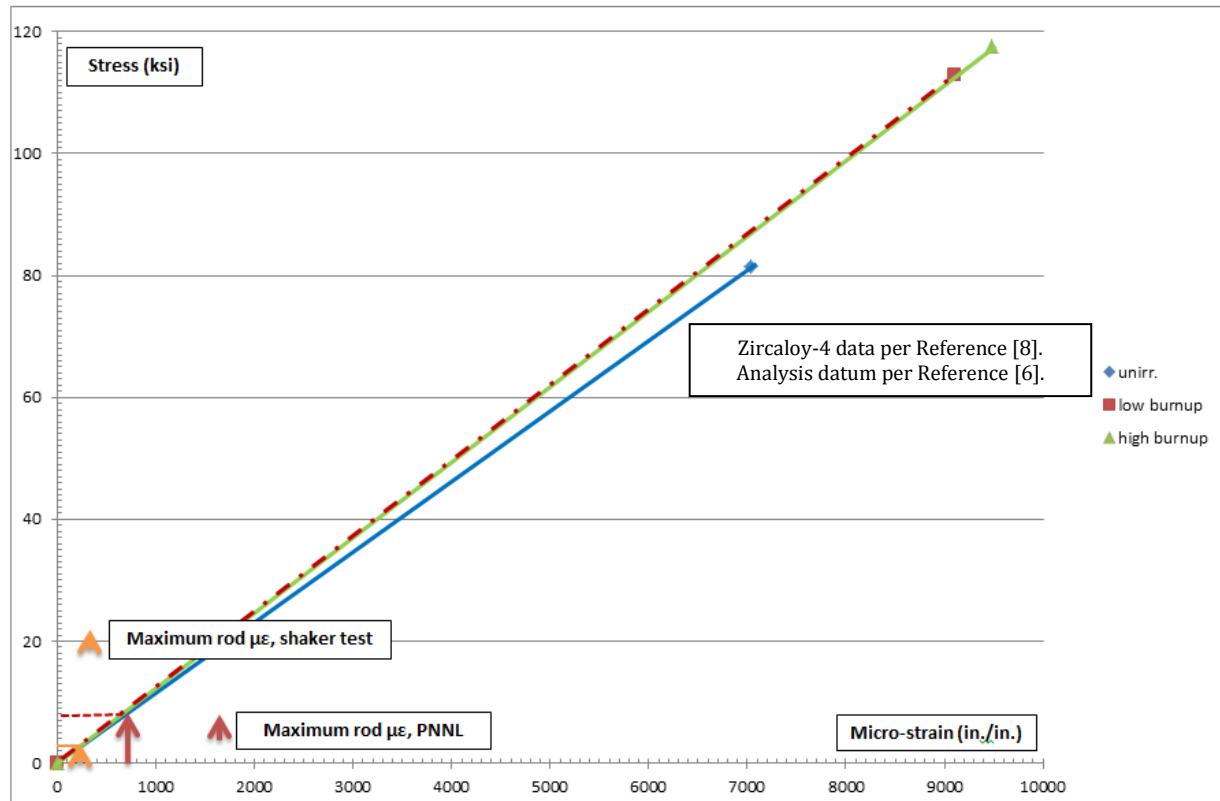


Figure 29. Elastic portion of stress—strain curve for Zircaloy-4, unirradiated, 100°F; low burnup, 250°F; and high burnup, 250°F.<sup>14</sup>

#### 4.4.2 Shock Test #1

Shock Test #1 time-history data were analyzed to generate plots of the strain gauge and acceleration measurements.

##### 4.4.2.1 Strains for Shock Test #1

Figures 31 to 46 show the strains measured on the rods in units of  $\mu\epsilon$  v. time for each position at which a strain gauge was placed. The plots identify the rod and its span and the locations on a given span (adjacent to a spacer grid or at the mid-span between spacer grids). For all locations there is one figure that shows the entire shock test time history (10.8 seconds) and another that shows a short window in time (1.1 to 1.3 seconds) that encompasses the maximum strain.

Table 18 compares strains on the rods at the various strain gauge locations for Shock Test #1.

The maximum strain measured during Shock Test #1 was 199  $\mu\text{in./in.}$  ( $\mu\text{m/m}$ ) at the mid-span of Span 10 (top-nozzle end of assembly) on the top-middle rod. The lowest maximum strain was 54  $\mu\text{in./in.}$  ( $\mu\text{m/m}$ ) on the top-side rod, Span 1, adjacent to a spacer grid. The difference

<sup>14</sup> The definition used for this figure of “low burnup” is Zircaloy-4 with a hydrogen concentration of 300 ppm subjected to a fluence of  $5.00\text{E}+25$   $\text{n/m}^2$ . “High burnup” corresponds to a hydrogen concentration of 600 ppm subjected to a fluence of  $1.00\text{E}+26$   $\text{n/m}^2$ . [per. corr. Ken Geelhood, PNNL, May 2013].

between the highest and lowest maximum strains is insignificant in terms of the effect on the behavior of a Zircaloy-4 rod as can be discerned from Figure 29.

The average maximum strains measured at all locations for Shock Test #1 were 112  $\mu\text{in./in.}$  ( $\mu\text{m/m}$ ). Of the three rods instrumented, the top-middle rod exhibited the highest average maximum strains: 124  $\mu\text{in./in.}$  ( $\mu\text{m/m}$ ). Span 10 exhibited the highest average maximum strains, 125  $\mu\text{in./in.}$  ( $\mu\text{m/m}$ ), and the mid-span location strains averaged higher than the locations adjacent to spacer grids, 118  $\mu\text{in./in.}$  ( $\mu\text{m/m}$ ).

Figures 60 to 66 show the fast Fourier transformations of the strain  $v.$  time data for Shock Test #1 in units of  $\mu\epsilon/\text{Hz}$   $v.$  Hz. Note that the rods responded primarily at the lower frequencies below approximately 75 Hz.

#### **4.4.2.2 Accelerations for Shock Test #1**

Figures 47 to 59 show all of the accelerations on the rods, spacer grids, control rod, basket, basket baseplate, and shaker in units of  $g$   $v.$  time. The plots indicate the accelerometer and its location. For all locations there is one figure that shows the entire time history and another that shows a short window in time that encompasses the maximum strain.

Peak accelerations on the top-side rod, Span 10, exceeded 40  $g$  (Figures 51 and 52).

Figures 55 and 56 show that the ends of the basket exhibited higher  $g$  than the acceleration at the mid-span of the basket indicating motion of the basket ends relative to the mid-span.

Figures 57 and 58 indicate that the vertical acceleration on the basket mounting plate closely matched the INPUT/CONTROL accelerations on the shaker (the lateral and longitudinal accelerations on the basket mounting plate were, as expected, very low).

Figure 59 compares the accelerations for a three-second span of time for Shock Test #1 of the shaker INPUT/CONTROL, to the basket mounting plate, the basket, the control rod, and a spacer grid at each end of the assembly. All maximum accelerations at these locations exceeded the INPUT/CONTROL acceleration (note the table adjacent to Figure 59). Only the acceleration at the mid-span of the basket was similar to that of the INPUT/CONTROL. The two ends of the basket had nearly identical maximum accelerations. The maximum acceleration at the bottom end of the control rod exceeded that at the top end. Similarly, the bottom-end assembly spacer grid maximum acceleration exceeded that of the top-end spacer grid.

Figure 119 “Target Data Input to Shaker Control System  $v.$  Peak Accelerations” shows the target data input (Section 3, Figure 21) and the shaker control system peak accelerations for Shock Tests #1, #2, and #5 in units of  $g_{\text{peak}}$   $v.$  log Hz. Figure 119 indicates that the desired input to the shaker for Shock Tests #1, #2, and #5 (peak accelerations  $v.$  log Hz as derived from the truck cask data) were matched by the shock accelerations measured during the tests. In addition, the figure shows that the accelerations from one test to another were nearly identical.

Figures 120 to 125 show the fast Fourier transformations of the Shock Test #1 acceleration data in units of  $g/\text{Hz}$   $v.$  Hz. Note the peaks below 50 Hz and at approximately 400 Hz.

The shock response spectra for the accelerometers for Shock Test #1 are shown in Figures 126 to 131 in units of  $g_{\text{peak}}$   $v.$  log Hz with maximum peak accelerations occurring between 400 Hz and 500 Hz.

### 4.4.3 Random Vibration Test #5

#### 4.4.3.1 Strains for Random Vibration Test #5

Figures 67 to 83 show all of the strains on the rods for Random Vibration Test #5 in units of  $\mu\epsilon$  v. time for each position at which a strain gauge was placed: the rod, the spans, and locations on a given span. For all locations there is one figure that shows the entire time history analyzed (23 seconds) and another that shows a short window in time that encompasses the maximum strain (17.8 to 18 seconds).

Figure 75 is a comparison of Top-middle Rod, Span 10  $\mu\epsilon$  v. time for Shock Test #1 and Random Vibration Test #5.

Table 20 compares maximum, average strains<sup>15</sup>,  $\mu\epsilon_{RMS}$ , and average peak strains,  $\mu\epsilon_{peak}$ , on the rods, at the various strain gauge locations for Random Vibration Test #5. The average maximum strain for all the gauges was 100  $\mu\text{in./in.}$  ( $\mu\text{m/m}$ ). The average strains recorded for all the locations for the 23 seconds analyzed was 20  $\mu\text{in./in.}$  ( $\mu\text{m/m}$ ) and the average peak strain was 24  $\mu\text{in./in.}$  ( $\mu\text{m/m}$ ). The difference between any of these strain values is insignificant in terms of the effect on the response of a Zircaloy-4 rod.

The maximum strain measured during Random Vibration Test #5 was 183  $\mu\text{in./in.}$  ( $\mu\text{m/m}$ ) at the mid-span of Span 10 (top-nozzle end of assembly) on the top-middle rod – the same location as for Shock Test #1. The lowest maximum strain was 60  $\mu\text{in./in.}$  ( $\mu\text{m/m}$ ) on the top-side rod, Span 1, adjacent to a spacer grid—again the same location as for Shock Test #1.

The average maximum strain measured at all locations for Random Vibration Test #5 was 100  $\mu\text{in./in.}$  ( $\mu\text{m/m}$ ). Of the three rods instrumented, the top-side rod exhibited the highest average maximum strains: 114  $\mu\text{in./in.}$  ( $\mu\text{m/m}$ ). Span 10 had the highest average maximum strains, 124  $\mu\text{in./in.}$  ( $\mu\text{m/m}$ ), and the mid-span locations had strains averaging higher than the locations adjacent to spacer grids, 112  $\mu\text{in./in.}$  ( $\mu\text{m/m}$ ).

Figures 96 to 102 show the ratios of micro-strains to the basket mounting baseplate vertical acceleration (Channel 23) for Random Vibration Test #5 in units of  $\mu\epsilon/g_{\text{vertical baseplate}}$  v. Hz. Note that the peak ratios on the rods occurred at low frequencies, while secondary peaks consistently occurred around 400 Hz to 500 Hz and between 1,500 Hz and 2,000 Hz.

Figures 112 to 118 show the micro-strain power spectral densities in units of  $\mu\epsilon^2/\text{Hz}$  v. log Hz. These figures indicate that the power spectral densities peaked between 30 Hz and 50 Hz.

#### 4.4.3.2 Accelerations for Random Vibration Test #5

Figures 84 to 95 show all of the accelerations on the rods, spacer grids, control rod, basket, basket mounting baseplate, and shaker in units of g v. time. The accelerometer and its location are indicated in the plots. For all locations there is one figure that shows the entire time history and another that shows a short window in time that encompasses the maximum strain.

Table 20 shows average accelerations,  $g_{RMS}$ , and average peak accelerations,  $g_{peak}$ , measured during Random Vibration Test #5.

The average peak accelerations for the input/control accelerometer on the shaker expander head were 0.7 g. The vertical accelerometer on the basket baseplate, the ends of the control rod,

---

15. For a uniform sine wave, the RMS value is 70.7% of the amplitude.

and the mid-span of the top of the basket were similar and only slightly greater than that of the input/control location: 1.4 g, 1 g and 1.3 g, and 1.3 g, respectively. The ends of the basket exhibited average peak accelerations of 2.7 g and 2.4 g which indicate that the ends of the basket moved relative to the mid-span of the basket. That motion was in phase as shown in Figure 93. The mid-span location of Span10 of the top-side rod was 6.5 g while the mid-span location of Span 5 of the top-middle rod was 5.7 g indicating motion of the rods within the assembly during the tests relative to the input acceleration.

Figures 103 to 107 show the ratios of assembly accelerations to baseplate vertical acceleration for Random Vibration Test #5 in units of  $g/g_{\text{vertical baseplate}} \nu. \text{ Hz}$ . Note the response of the assembly at frequency of approximately 400 Hz and between 1,500 Hz to 2,000 Hz.

Figures 108 to 110 show acceleration power spectral densities in units of  $g^2/\text{Hz} \nu. \log \text{ Hz}$ .

Figure 108, the acceleration power spectral densities for the control rod, shows response at frequencies between 20 Hz to 30 Hz, 80 Hz, and peaks at approximately 400 Hz. The basket acceleration power spectral densities, Figure 109, similarly showed high response at 400 Hz, but there was also response at a frequency of approximately at 700 Hz. The baseplate response, Figure 110, was highest at approximately 700 Hz although there was significant response at 400 Hz.

Figure 111 shows the target data input (Section 3) and the shaker input/control system peak acceleration (Channel 1)  $\nu. \log \text{ Hz}$ . This figure confirms that the input to the shaker and hence the test unit matched the desired target frequencies established per the analysis described in Section 3.

#### **4.4.3.3 Comparison of Duplicative Test Data**

Table 21 compares the maximum strains measured at all locations for Shock Tests #1, #2, and #5 and Random Vibration Tests #4, #5, and #6 (refer to Table 16). This comparison confirms that test results were nearly identical from test to test. This test report primarily has data for Shock Test #1 and Random Vibration Tests #5. For example, the absolute values of the maximum micro-strains measured by the strain gauge denoted TMR-G-S10-2 for Shock Tests #1, #2, and #5 were 198  $\mu\epsilon$ , 213  $\mu\epsilon$ , and 184  $\mu\epsilon$ ; the absolute values of the maximum micro-strains measured by the strain gauge denoted TMR-G-S10-2 for Random Vibration Tests #4, #5, and #6 were 207  $\mu\epsilon$ , 183  $\mu\epsilon$ , and 172  $\mu\epsilon$ .

#### **4.4.4 Fracture Mechanics Analysis Based on Stresses from Test Data and Analyses**

The strain data measured during the tests, for shock and vibration loadings, suggest that the axial strains on the rod—and the corresponding applied stresses—are very low in relation to the elastic limit of unirradiated Zircaloy-4 and the estimated elastic limits for low-burnup and high-burnup Zircaloy-4.<sup>16</sup> This suggests that cladding will not fail during NCT via strain- or stress-based failure criteria (Figure 29).

---

16. The definition of “low burnup” is Zircaloy-4 with a hydrogen concentration of 300 ppm subjected to a fluence of  $5.00\text{E}+25 \text{ n/m}^2$ . “High burnup” corresponds to a hydrogen concentration of 600 ppm subjected to a fluence of  $1.00\text{E}+26 \text{ n/m}^2$ . [per. corr. Ken Geelhood, PNNL, May 2013].

Irradiation of Zircaloy-4 increases the yield strength of the material with little effect on the elastic modulus. The ductility of high-burnup Zircaloy-4 cladding is no doubt degraded meaning that once the yield limit is reached in high-burnup cladding, there will be little or no plasticity—brittle fracture could occur at the yield limit or below. However, the stresses derived from the strains (and associated stresses) measured in the shaker tests are so low that there is a large margin between the applied stresses and the Zircaloy-4 yield strength.

Cladding could fail via a fracture mechanics-based criterion, however. Brittle fracture can occur at any stress below the yield limit in cladding containing damage or flaws, or that develops flaws under fatigue loading. Limited data, some derived from models, suggests a degradation of the fracture toughness of high-burnup Zircaloy-4. In the presence of a crack in the cladding of sufficient size, fracture could occur at relatively low stresses.

An evaluation of the stresses required to cause fracture in the presence of cracks in high-burnup cladding of various sizes has been made. These evaluations required an estimate of the fracture toughness,  $K_{Ic}$ , of high-burnup Zircaloy-4. Data for the fracture toughness of Zircaloys is discussed in References [8] and [9]. Reference [9] summarizes the data:

“The data for irradiated Zircaloy-2 (Zr-2) and Zircaloy-4 (Zr-4) materials shows the lowest room temperature  $K_{Ic}$  values to be in the range of 12 MPa- $\sqrt{m}$  to 15 MPa- $\sqrt{m}$  for hydrogen concentrations of the order of 1000 ppm. Such low values, however, are typical of beta-quenched material, which has different microstructural characteristics than fuel cladding. A more typical lower-bound value of  $K_{Ic}$  for end-of-life burnup at 20°C with relatively high hydrogen concentration ( $\approx 750$  ppm) is in the range of 18-20 MPa- $\sqrt{m}$ . The corresponding  $K_{Ic}$  value for temperatures above 280°C is 30 MPa- $\sqrt{m}$ . These  $K_{Ic}$  values are to be contrasted with 50 MPa- $\sqrt{m}$  and higher for moderately irradiated materials with low hydrogen concentrations. The fracture toughness data reviewed in the foregoing supports the following conservative criteria, recommended herein for application to normally discharged fuel with prototypical burnup and hydrogen contents.

- (a)  $K_{Ic} = 18$  MPa- $\sqrt{m}$  for  $T < 100^\circ\text{C}$ ,  $100 < H < 500$  ppm
- (b)  $K_{Ic} = 50$  MPa- $\sqrt{m}$  for  $T > 280^\circ\text{C}$ ,  $H < 100$  ppm
- (c)  $K_{Ic} = 30$  MPa- $\sqrt{m}$  for  $T > 280^\circ\text{C}$ ,  $100 < H < 500$  ppm
- (d)  $K_{Ic} = 20$  MPa- $\sqrt{m}$  for  $T > 280^\circ\text{C}$ ,  $500 < H < 750$  ppm
- (e)  $K_{Ic} = 12$  MPa- $\sqrt{m}$  for any temperature,  $H > 1,000$  ppm.”

The lowest values above most likely correspond to the Zircaloy lower shelf behavior as determined by the ductile-to-brittle transition temperature.

In order to calculate the stress or crack size required to cause fracture of the cladding, equations relating the applied stress intensity,  $K_I$ , the crack size, and the applied stress are used. When the applied stress intensity,  $K_I$ , exceeds the fracture toughness,  $K_{Ic}$ , fracture at the crack tip occurs. A circumferential crack is the most likely to cause fracture in the presence of axial, bending stresses such as those experienced by cladding. Reference [10] suggests using a part-through crack in a flat plate solution for a crack in a pipe or a tube (Reference [11] provides expressions for a circumferential crack in a tube).

The expressions used for the calculations from Reference [10] were:

$$K_I = Y\sigma_b\sqrt{(\pi a)}, \text{ where } Y = 1, \sigma_b = \text{applied bending stress}$$

and the more detailed expression in Reference [10], Section A.2.2.1 (the first expression results in somewhat higher values of  $K_I$ ).

The Zircaloy-4 rods have a wall thickness,  $t$ , of 0.0225 inches (0.57 mm). Semi-elliptical circumferential surface cracks with  $a/2c = 1/6$  were assumed, where “ $a$ ” is the crack depth at the deepest point and “ $2c$ ” is the length of the crack. The assumed applied stress was 3 ksi (20.6 MPa) which corresponded to the maximum strain measured during the shaker tests. The calculations also assumed through-wall flaws of varying depth,  $a/t = 0.1, 0.25, \text{ and } 0.5$ .

Table 17 presents results of the applied stress intensities for the maximum applied stresses tests for a range of crack sizes.

Table 17. Estimated applied stress intensities at the tip of circumferential flaws in the cladding of a fuel rod subjected to stresses experimentally measured

Crack depth/Zircaloy-rod wall thickness, $a/t$	Applied stress, (MPa)	Applied stress intensity, $K_I$ , at crack tip, (MPa- $\sqrt{m}$ )
0.10	20.6	0.2 - 0.3
0.25	20.6	0.4 - 0.4
0.50	20.6	0.5 - 0.6

The calculated applied stress intensities are low relative to even a lower bound fracture toughness for Zircaloy-4 of 12 MPa- $\sqrt{m}$  and crack depths up to half the clad wall thickness; the fracture toughness of Zircaloy-4 significantly exceeds the applied stress intensities calculated for the stress levels measured for the shaker tests.

The resulting implication is that the margin against failure in the presence of a crack on the fuel cladding due to a fracture mechanics-based failure mechanism may be acceptable for the stresses measured by the shaker tests that simulate those expected during normal conditions of transport. The measured strains are very low; it would take a significant preexisting flaw in cladding, and/or significantly degraded fracture toughness, and/or large numbers of cycles under these strains for these strains to be of real concern. This issue should be more thoroughly examined, however, particularly by means of generating additional fracture toughness data on high-burnup Zircaloy-4 and assessments of the sizes of potential cracks in cladding.

#### 4.4.5 Comparison of Test Data with PNNL Analyses

Figure 30 shows the strains analytically calculated for shock test conditions at the top-middle rod, Span 1, below the spacer grids and at the mid-span (denoted A, B, and C). These locations approximately correspond to the locations of strain gauges TMR-G-S1-1, TMR-G-S1-3, and TMR-G-S1-2, respectively.

The finite element analyses predicted strains generally over 200  $\mu\text{in./in.}$  ( $\mu\text{m/m}$ ) with values peaking at over 700  $\mu\text{in./in.}$  ( $\mu\text{m/m}$ ), whereas the experimental data had a maximum strain 171  $\mu\text{in./in.}$  ( $\mu\text{m/m}$ ) (Table 18). However, the differences in the experimentally measured strains and the analytically calculated strains would be minimal in terms of the behavior of a Zircaloy rod subjected to such low strain values (Figure 29): these strains are very low compared with the

elastic limit of the Zircaloy-4. The PNNL analyses are deemed a very close prediction of the shaker test results and the response of the assembly to those tests.<sup>17</sup>

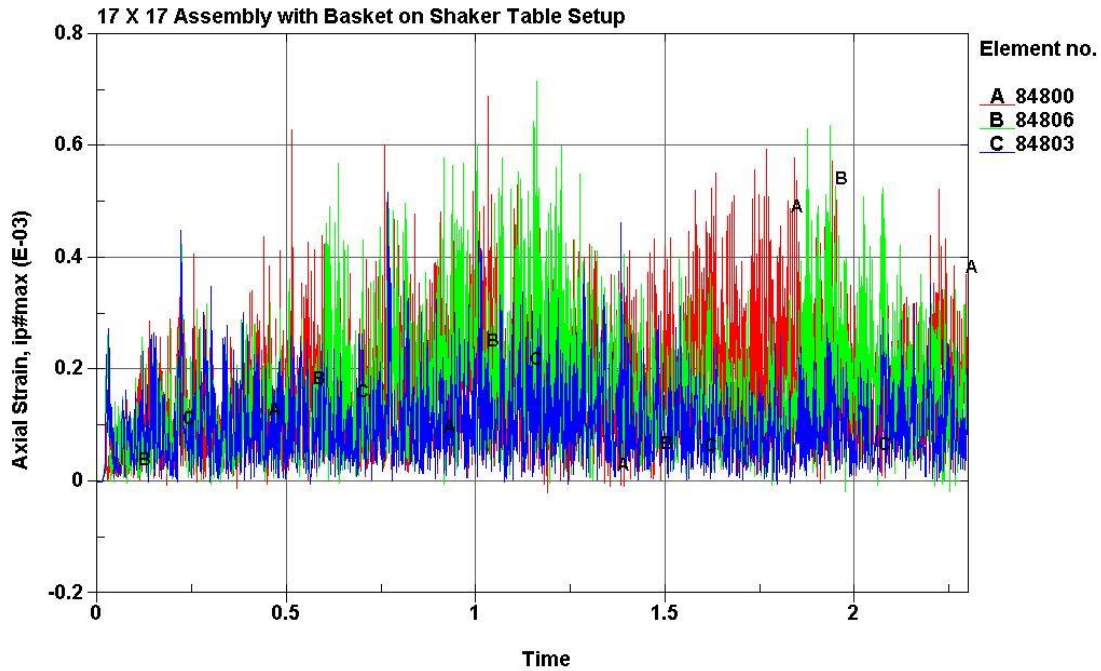


Figure 30. Micro-strains, Top-middle Rod, Span 1 calculated by PNNL finite element analysis of shaker shock test<sup>18</sup>

---

17. A double integration of the acceleration for Shock Test #1 at the mid-span of Span 1 of the top-middle rod (accelerometer TMR-A-S1-3), which was concomitant with the relatively high peak strain measured during Shock Test #1 (131  $\mu\epsilon$  per strain gauge TMR-G-S1-2), was calculated via the K2 code to get an estimate of the rod deflection at the mid-span to confirm that these low strain magnitudes are reasonable (the time range of the acceleration double integrated was 1.146 to 1.16 seconds of shock test #1.). The deflection calculated via the double integration was then converted to the stress. The strain was then calculated for a beam with fixed end conditions and simply supported end conditions. The corresponding micro-strains derived from this deflection were 690  $\mu\epsilon$  for the fixed end conditions and 410  $\mu\epsilon$  for the simply supported condition. The magnitude of these derived micro-strains is very similar to the magnitude of the strains measured (131  $\mu\epsilon$  for TMR-G-S1-2 – Table 19) and analytically calculated. This provides additional confidence that the measured strain values are valid for the test configuration used for the shaker tests.

18. Figure courtesy of Nick Klymyshyn, PNNL.

Table 18. Summary of Maximum Micro-strains Measured on Zircaloy Fuel Rods during Shock Test #1

<b>Shock Test #1 - Micro-strains</b>				
<b>Strain Gauge ID</b>	<b>Rod Location</b>	<b>Span</b>	<b>Position on Span</b>	<b>Maximum (<math>\mu\epsilon</math>)</b>
TMR-G-S1-1	Top-middle rod	Bottom-end (S1)	Adjacent to spacer grid	90
TMR-G-S1-2	Top-middle rod	Bottom-end (S1)	Mid-span	131
TMR-G-S1-3	Top-middle rod	Bottom-end (S1)	Adjacent to spacer grid	171
TMR-G-S5-1	Top-middle rod	Mid-assembly (S5)	Adjacent to spacer grid	104
TMR-G-S5-2	Top-middle rod	Mid-assembly (S5)	Mid-span	97
TMR-G-S10-1	Top-middle rod	Top-end (S10)	Adjacent to spacer grid	127
<b>TMR-G-S10-2</b>	<b>Top-middle rod</b>	<b>Top-end (S10)</b>	<b>Mid-span</b>	<b>199</b>
TMR-G-S10-3	Top-middle rod	Top-end (S10)	Adjacent to spacer grid	70
<b>TSR-G-S1-1</b>	<b>Top-side rod</b>	<b>Bottom-end (S1)</b>	<b>Adjacent to spacer grid</b>	<b>54</b>
TSR-G-S1-2	Top-side rod	Bottom-end (S1)	Mid-span	107
TSR-G-S10-1	Top-side rod	Top-end (S10)	Mid-span	117
TSR-G-S10-2	Top-side rod	Top-end (S10)	Adjacent to spacer grid	113
BSR-G-S1-1	Bottom-side rod	Bottom-end (S1)	Mid-span	62
BSR-G-S1-2	Bottom-side rod	Bottom-end (S1)	Adjacent to spacer grid	121
BSR-G-S5-1	Bottom-side rod	Mid-assembly (S5)	Adjacent to spacer grid	110
BSR-G-S5-2	Bottom-side rod	Mid-assembly (S5)	Mid-span	115
<b>All Strain Gauges Averages</b>				<b>112</b>
<b>Top-middle Rod Averages</b>				<b>124</b>
Top-side Rod Averages				98
Bottom-side Rod Averages				102
Span 1 Averages				105
Span 5 Averages				107
<b>Span 10 Averages</b>				<b>125</b>
<b>Mid span Averages</b>				<b>118</b>
Adjacent to Spacer Grid Averages				107

Table 19. Summary of Maximum Micro-Strains, Average Micro-Strains,  $\mu\epsilon_{RMS}$ , and Average Peak Micro-Strains,  $\mu\epsilon_{peak}$ , Measured on Zircaloy Fuel Rods during Random Vibration Test #5

<b>Random Vibration Test #5 - Micro-Strains</b>						
<b>Strain Gauge ID</b>	<b>Rod Location</b>	<b>Span</b>	<b>Position on Span</b>	<b>Maximum (<math>\mu\epsilon</math>)</b>	<b>Average (<math>\mu\epsilon_{RMS}</math>)</b>	<b>Average (<math>\mu\epsilon_{peak}</math>)</b>
TMR-G-S1-1	Top-middle rod	Bottom-end (S1)	Adjacent to spacer grid	70	19	27
TMR-G-S1-2	Top-middle rod	Bottom-end (S1)	Mid-span	75	21	30
TMR-G-S1-3	Top-middle rod	Bottom-end (S1)	Adjacent to spacer grid	81	19	27
TMR-G-S5-1	Top-middle rod	Mid-assembly (S5)	Adjacent to spacer grid	145	15	21
TMR-G-S5-2	Top-middle rod	Mid-assembly (S5)	Mid-span	80	19	27
TMR-G-S10-1	Top-middle rod	Top-end (S10)	Adjacent to spacer grid	98	14	20
<b>TMR-G-S10-2</b>	<b>Top-middle rod</b>	<b>Top-end (S10)</b>	<b>Mid-span</b>	<b>183</b>	<b>42</b>	<b>59</b>
TMR-G-S10-3	Top-middle rod	Top-end (S10)	Adjacent to spacer grid	74	16	23
<b>TSR-G-S1-1</b>	<b>Top-side rod</b>	<b>Bottom-end (S1)</b>	<b>Adjacent to spacer grid</b>	<b>60</b>	13	18
TSR-G-S1-2	Top-side rod	Bottom-end (S1)	Mid-span	128	26	37
TSR-G-S10-1	Top-side rod	Top-end (S10)	Mid-span	153	41	58
TSR-G-S10-2	Top-side rod	Top-end (S10)	Adjacent to spacer grid	113	15	21
BSR-G-S1-1	Bottom-side rod	Bottom-end (S1)	Mid-span	74	17	24
BSR-G-S1-2	Bottom-side rod	Bottom-end (S1)	Adjacent to spacer grid	71	19	27
<b>BSR-G-S5-1</b>	<b>Bottom-side rod</b>	<b>Mid-assembly (S5)</b>	<b>Adjacent to spacer grid</b>	106	<b>11</b>	<b>16</b>
BSR-G-S5-2	Bottom-side rod	Mid-assembly (S5)	Mid-span	92	13	18
<b>All Strain Gauges Averages</b>				<b>100</b>	<b>20</b>	<b>28</b>
Top-middle Rod Averages				101	21	30
<b>Top-side Rod Averages</b>				<b>114</b>	<b>24</b>	<b>34</b>
Bottom-side Rod Averages				86	15	21
Span 1 Averages				80	19	27
Span 5 Averages				106	15	21
<b>Span 10 Averages</b>				<b>124</b>	<b>26</b>	<b>37</b>
<b>Mid-span Averages</b>				<b>112</b>	<b>26</b>	<b>37</b>
Adjacent to Spacer Grid Averages				91	16	23

Table 20. Average Accelerations,  $g_{RMS}$ , and Average Peak Accelerations,  $g_{peak}$ , Measured during Random Vibration Test #5

Random Vibration Test #5 - Average Accelerations					
Accelerometer ID	Location	Span	Position on Span	Average ( $g_{RMS}$ )	Average ( $g_{peak}$ )
Input/ CONTROL	SHAKER			0.5	0.7
TMSG-A-S1-1	Top-middle spacer grid	1	On spacer grid	1.3	1.8
TMR-A-S1-2	Top-middle rod	1	Adjacent to spacer grid	2.0	2.8
TMR-A-S1-3	Top-middle rod	1	Mid-span	2.0	2.8
TMR-A-S1-4	Top-middle rod	1	Adjacent to spacer grid	0.3	0.4
TMSG-A-S1-5	Top-middle spacer grid	1	On spacer grid	0.7	1.0
TMSG-A-S5-1	Top-middle rod	5	On spacer grid	1.2	1.7
TMR-A-S5-2	Top-middle rod	5	Adjacent to spacer grid	3.7	5.2
TMR-A-S5-3	Top-middle rod	5	Mid-span	4.0	5.7
TMR-A-S5-4	Top-middle rod	5	Adjacent to spacer grid	3.9	5.5
TMSG-A-S5-5	Top-middle rod	5	On spacer grid	0.6	0.8
TSSG-A-S10-1	Top-side spacer grid	10	On spacer grid	0.6	0.8
TSR-A-S10-2	Top-side rod	10	Adjacent to spacer grid	3.8	5.4
TSR-A-S10-3	Top-side rod	10	Mid-span	4.3	6.1
TSR-A-S10-4	Top-side rod	10	Adjacent to spacer grid	4.6	6.5
TSSG-A-S10-5	Top-side spacer grid	10	On spacer grid	1.0	1.4
CR-A-S1-1	Control rod, bottom end	1	On control rod	0.7	1.0
CR-A-S10-1	Control rod, top end	10	On control rod	0.9	1.3
B-A-S1-1	Basket, bottom end	≈ 1	On top edge of basket	1.9	2.7
B-A-S5-1	Basket, mid-span	≈ 5	On top edge of basket	0.9	1.3
B-A-S10-1	Basket, top end	≈ 10	On top edge of basket	1.7	2.4
SH-A-1X (vertical)	Shaker plate, mid-span	≈ 5	Mid-span	1.0	1.4
SH-A-1Y (lateral)	Shaker plate, mid-span	≈ 5	Mid-span	0.08	0.1
SH-A-1Z (longitudinal)	Shaker plate, mid-span	≈ 5	Mid-span	0.09	0.1

Table 21. Maximum Micro-Strains, Each Strain Gauge, Duplicative Tests

Test Strain Gauge ↓	Vibration #4		Vibration #5		Vibration #6		Shock #1		Shock #2		Shock #5	
	Max	Min	Max	Min	Max	Min	Max	Min	Max	Min	Max	Min
TMR-G-S1-1	69	-60	70	-59	65	-56	90	-46	91	-49	64	-43
TMR-G-S1-2	69	-74	67	-75	64	-77	48	-130	56	-119	63	-119
TMR-G-S1-3	73	-64	81	-65	71	-57	172	-53	138	-84	148	-75
TMR-G-S5-1	156	-66	145	-57	145	-61	104	-64	90	-83	114	-61
TMR-G-S5-2	61	-82	70	-80	64	-97	75	-97	99	-88	89	-119
TMR-G-S10-1	90	-55	98	-48	83	-47	127	-66	91	-62	107	-77
TMR-G-S10-2	138	<b>-207</b>	131	-183	121	-172	126	-199	169	<b>-213</b>	101	-184
TMR-G-S10-3	74	-89	67	-74	62	-76	53	-70	69	-71	42	-80
TSR-G-S1-1	55	-41	60	<b>-40</b>	70	-45	53	-36	71	-42	85	-67
TSR-G-S1-2	97	-122	89	-128	93	-105	107	-110	114	-139	134	-150
TSR-G-S10-1	110	-143	113	-153	101	-146	118	-181	130	-153	149	-198
TSR-G-S10-2	45	-113	42	-113	45	-106	<b>35</b>	-112	42	-119	45	-115
BSR-G-S1-1	67	-69	74	-61	46	-67	55	-62	74	-70	61	-81
BSR-G-S1-2	68	-72	71	-58	62	-56	121	-60	116	-74	85	-75
BSR-G-S5-1	65	-108	106	-94	70	-97	71	-111	56	-102	60	-120
BSR-G-S5-2	94	-98	90	-92	94	-105	97	-115	88	-111	94	-91

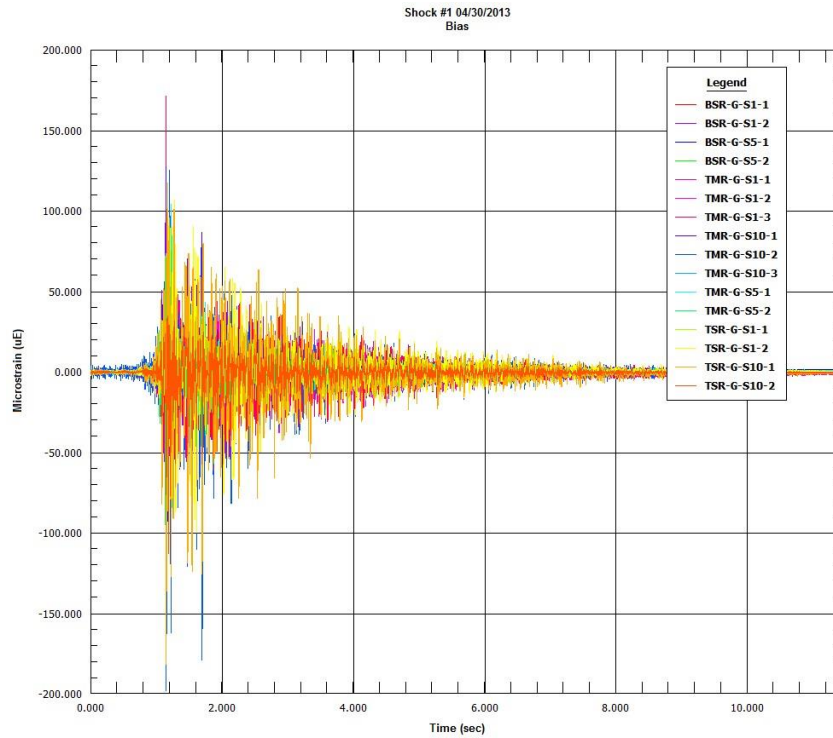


Figure 31. Shock Test #1. All Strain Gauges. Micro-strain v. time.

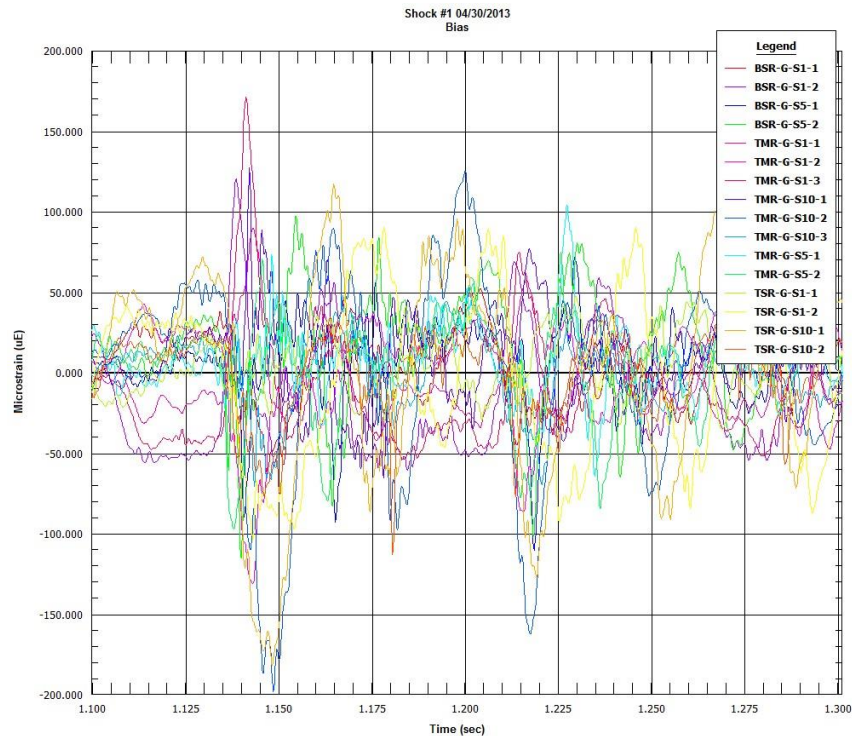


Figure 32. Shock Test #1. All Strain Gauges. Micro-strain v. time. Expanded time scale 1.1 to 1.3 seconds.

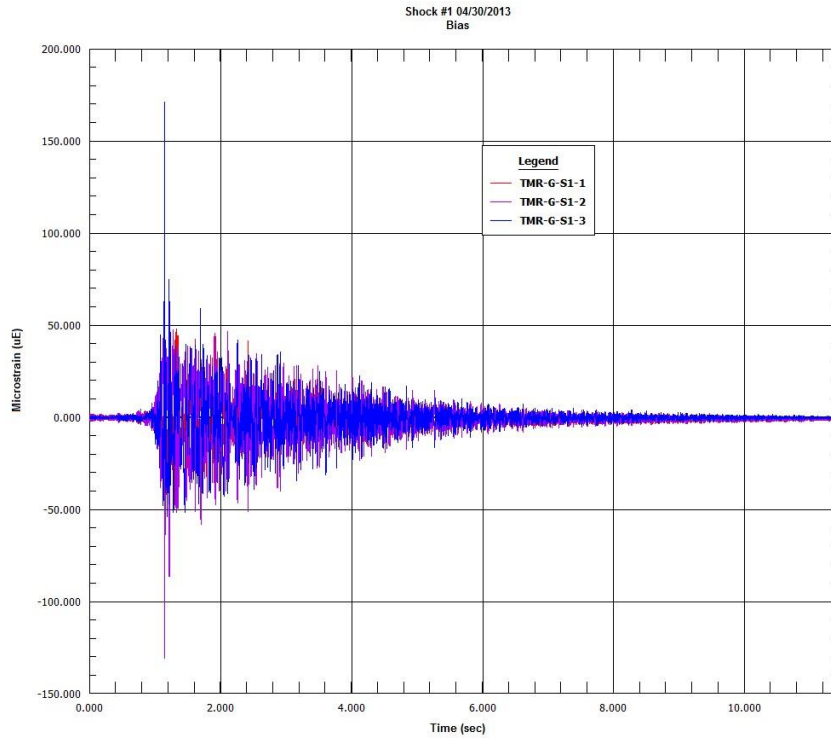


Figure 33. Shock Test #1. Top-middle Rod, Span 1. Micro-strain v. time.

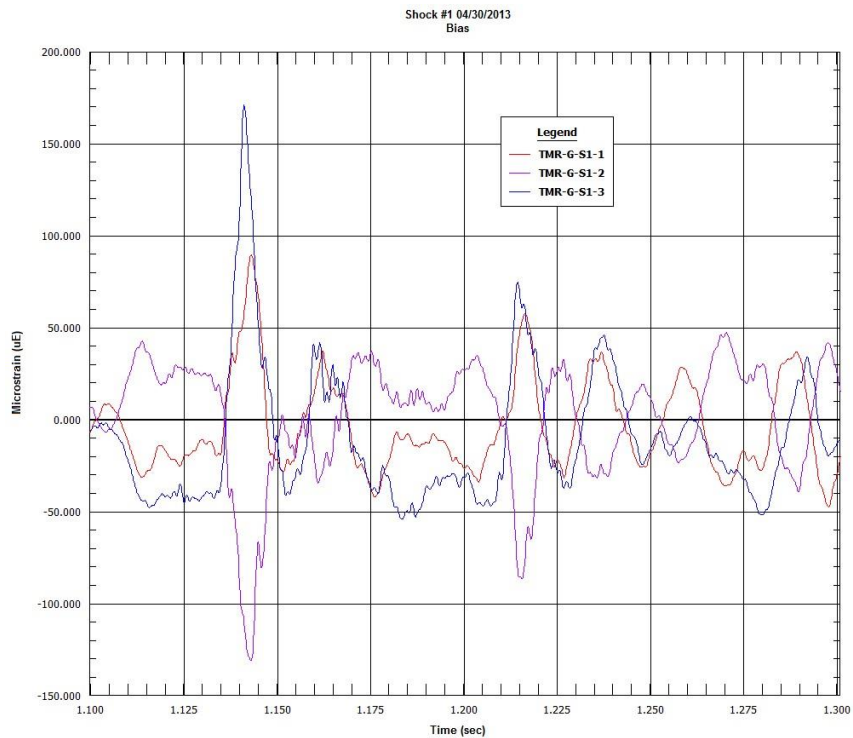


Figure 34. Shock Test #1. Top-middle Rod, Span 1. Micro-strain v. time. Expanded time scale 1.1 to 1.3 seconds.

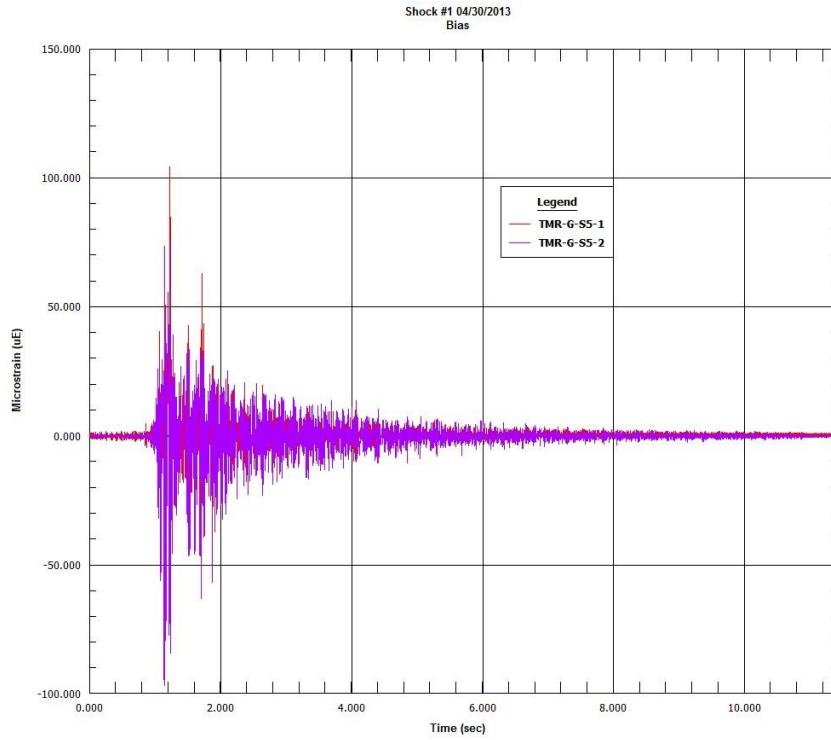


Figure 35. Shock Test #1. Top-middle Rod, Span 5. Micro-strain v. time.

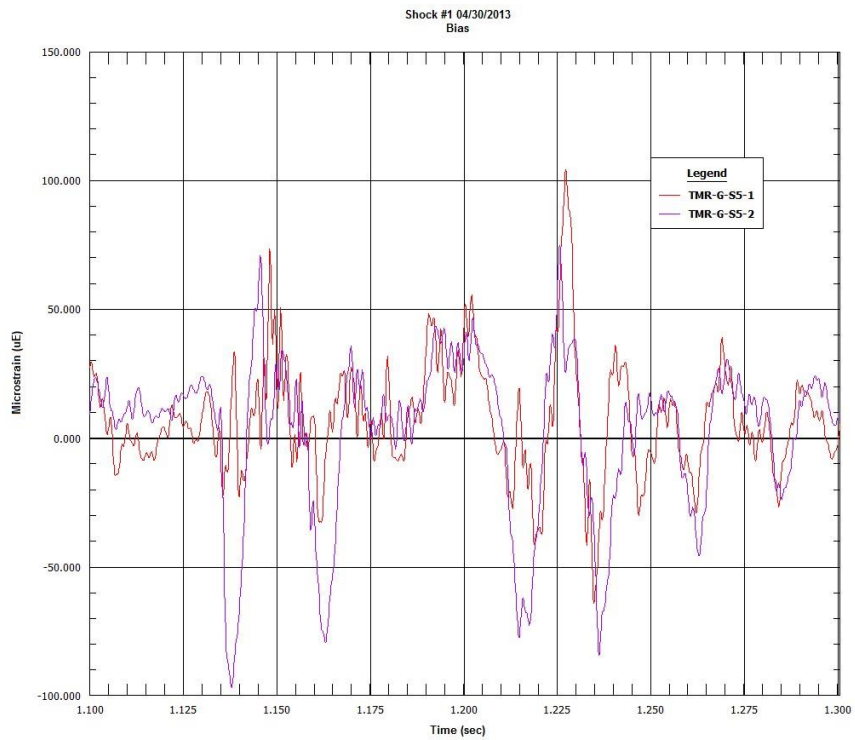


Figure 36. Shock Test #1. Top-middle Rod, Span 5. Micro-strain v. time. Expanded time scale 1.1 to 1.3 seconds.

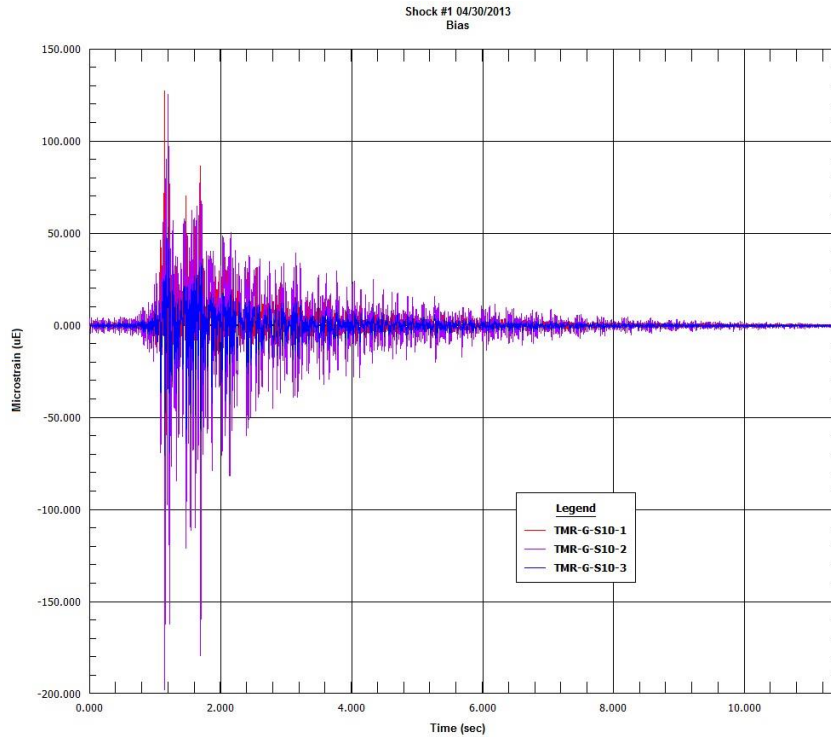


Figure 37. Shock Test #1. Top-middle Rod, Span 10. Micro-strain v. time.

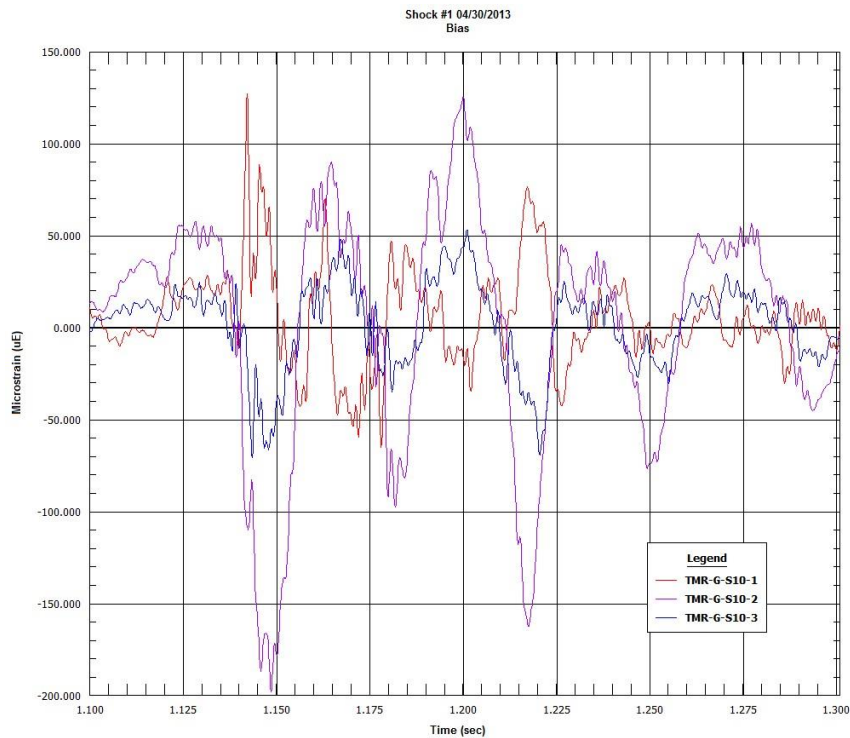


Figure 38. Shock Test #1. Top-middle Rod, Span 10. Micro-strain v. time. Expanded time scale 1.1 to 1.3 seconds.

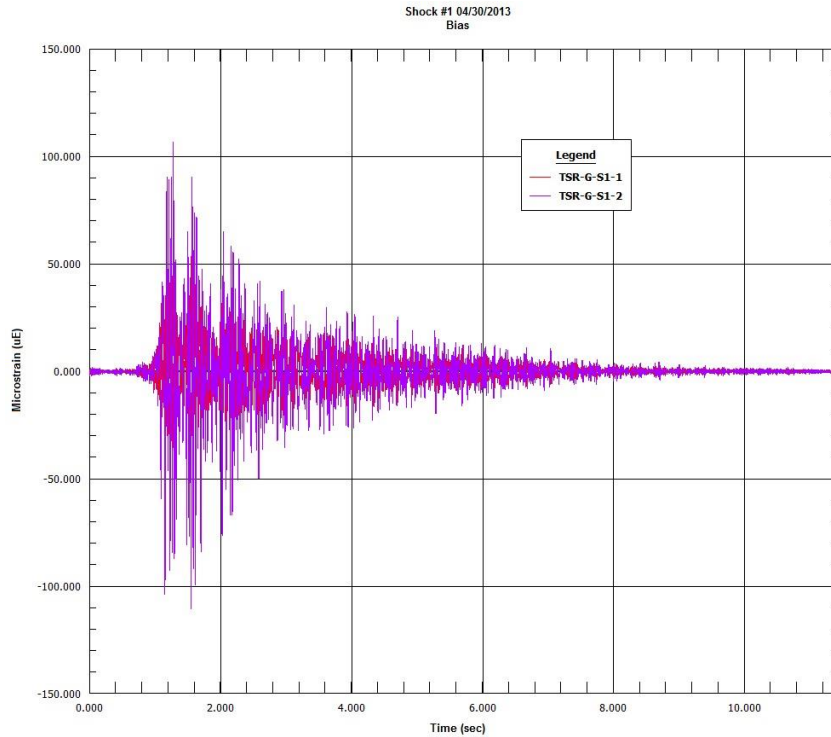


Figure 39. Shock Test #1. Top-side Rod, Span 1. Micro-strain v. time.

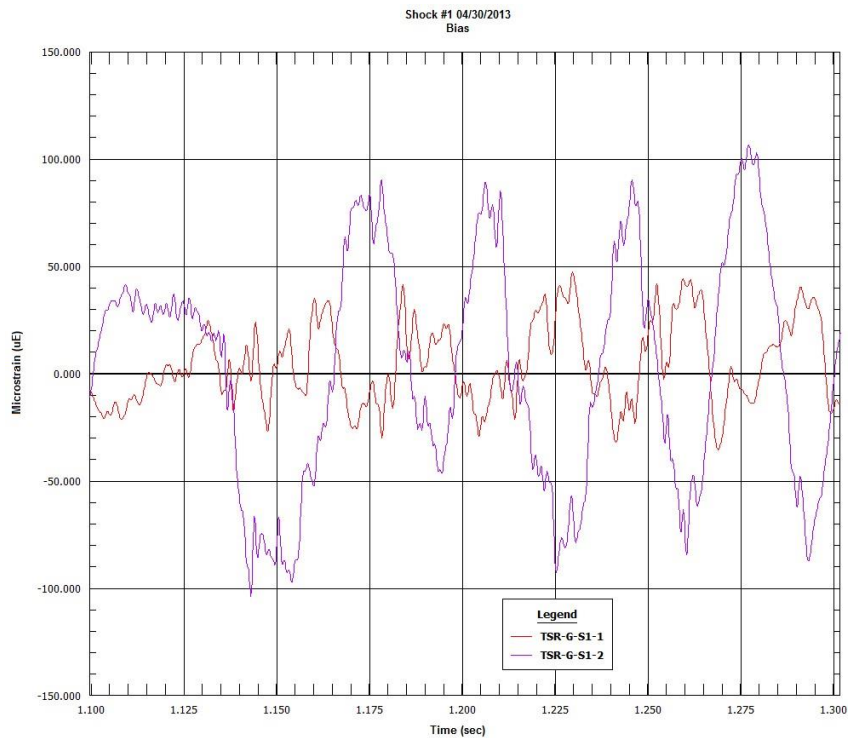


Figure 40. Shock Test #1. Top-side Rod, Span 1. Micro-strain v. time. Expanded time scale 1.1 to 1.3 seconds.

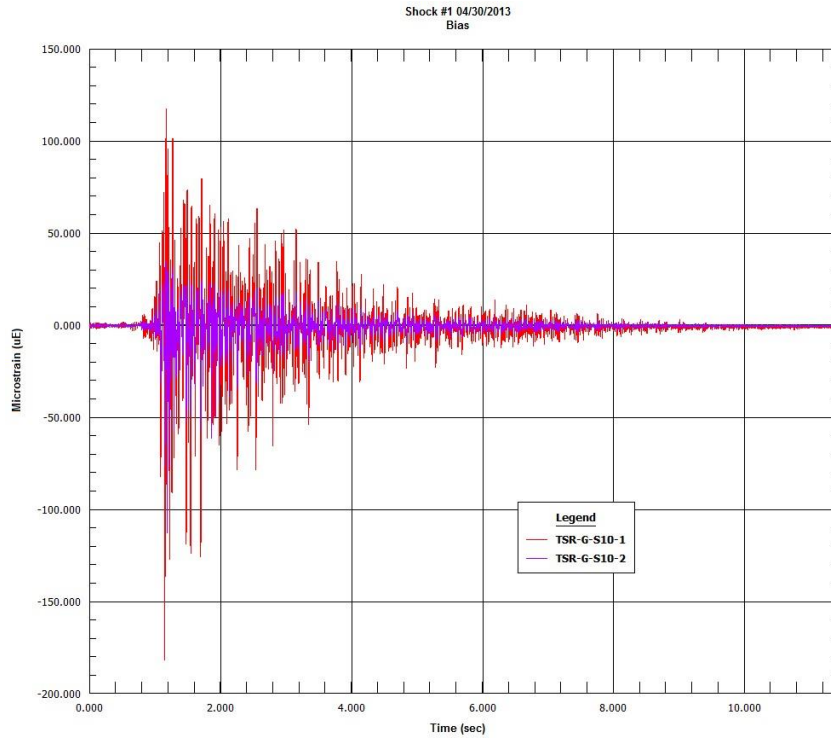


Figure 41. Shock Test #1. Top-side Rod, Span 10. Micro-strain v. time.

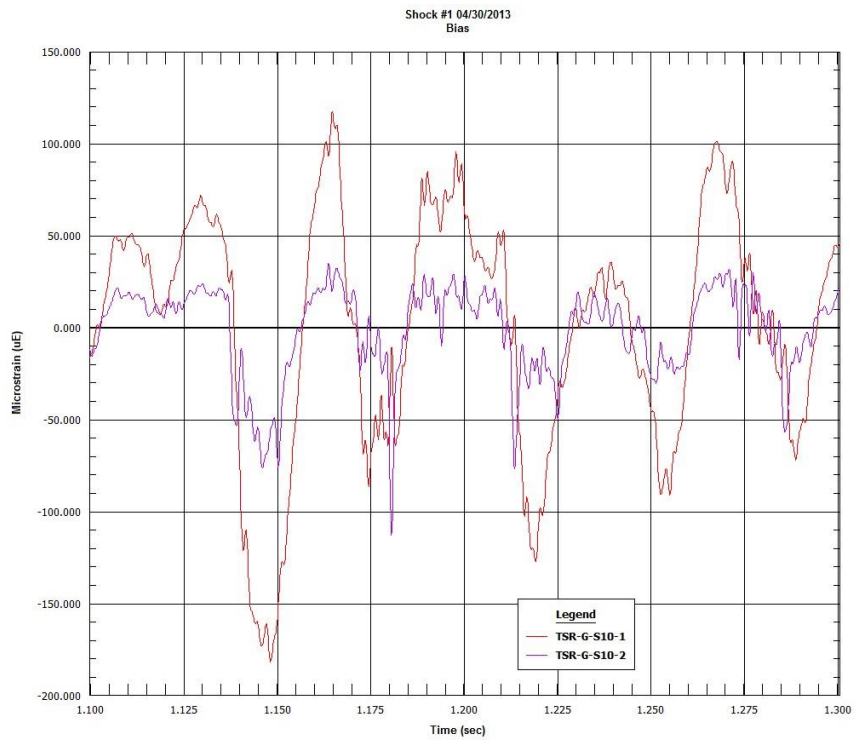


Figure 42. Shock Test #1. Top-side Rod, Span 10. Micro-strain v. time. Expanded time scale 1.1 to 1.3 seconds.

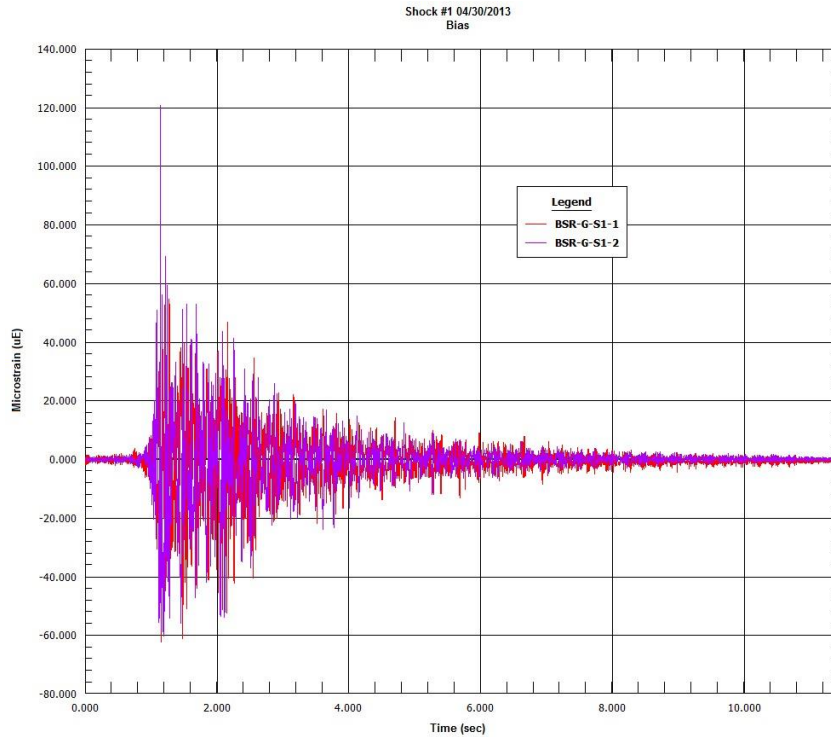


Figure 43. Shock Test #1. Bottom-side Rod, Span 1. Micro-strain v. time.

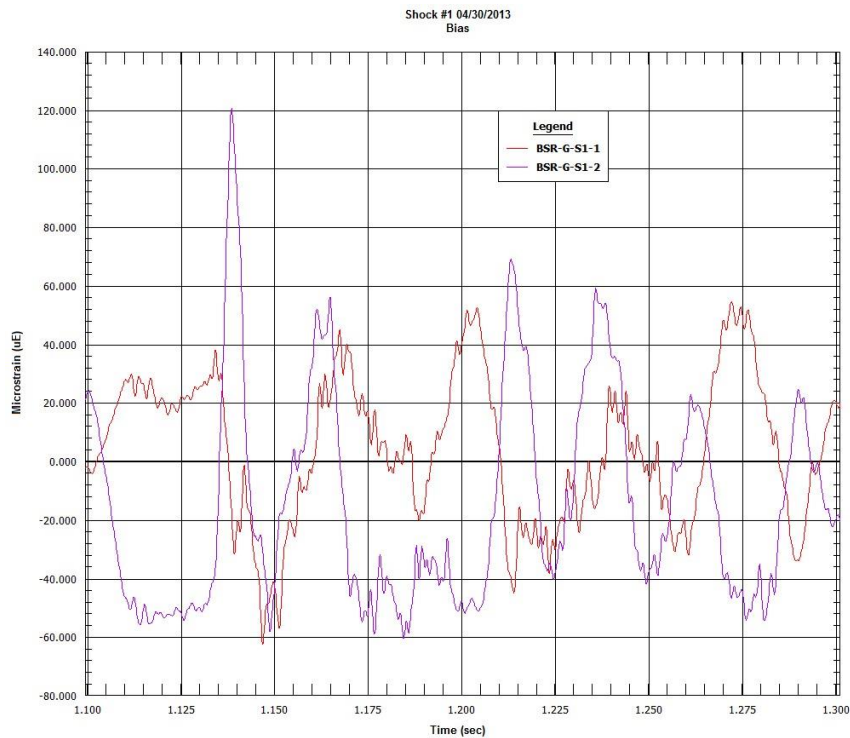


Figure 44. Shock Test #1. Bottom-side Rod, Span 1. Micro-strain v. time. Expanded time scale 1.1 to 1.3 seconds.

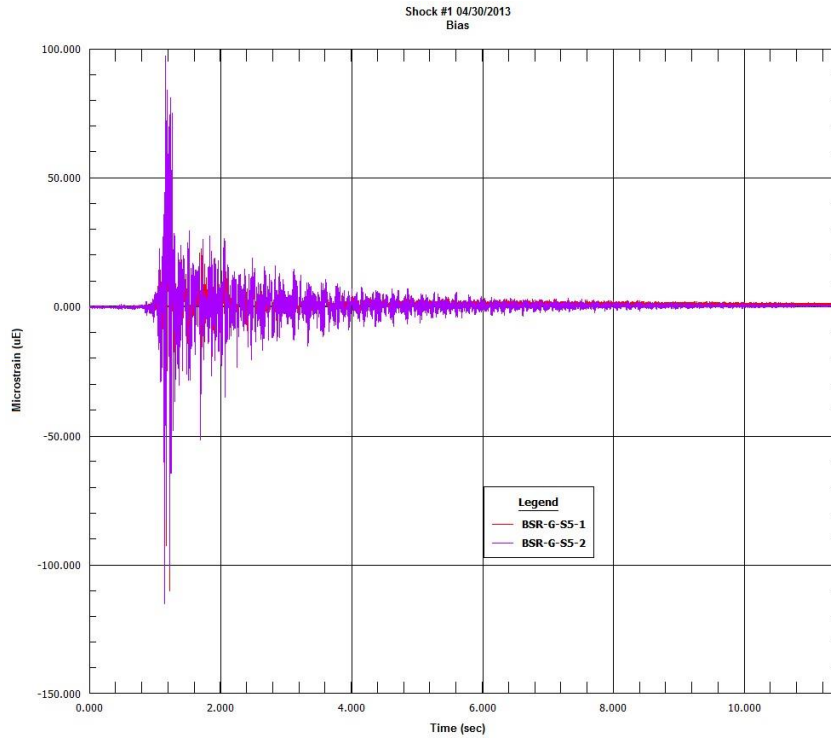


Figure 45. Shock Test #1. Bottom-side Rod, Span 5. Micro-strain v. time.

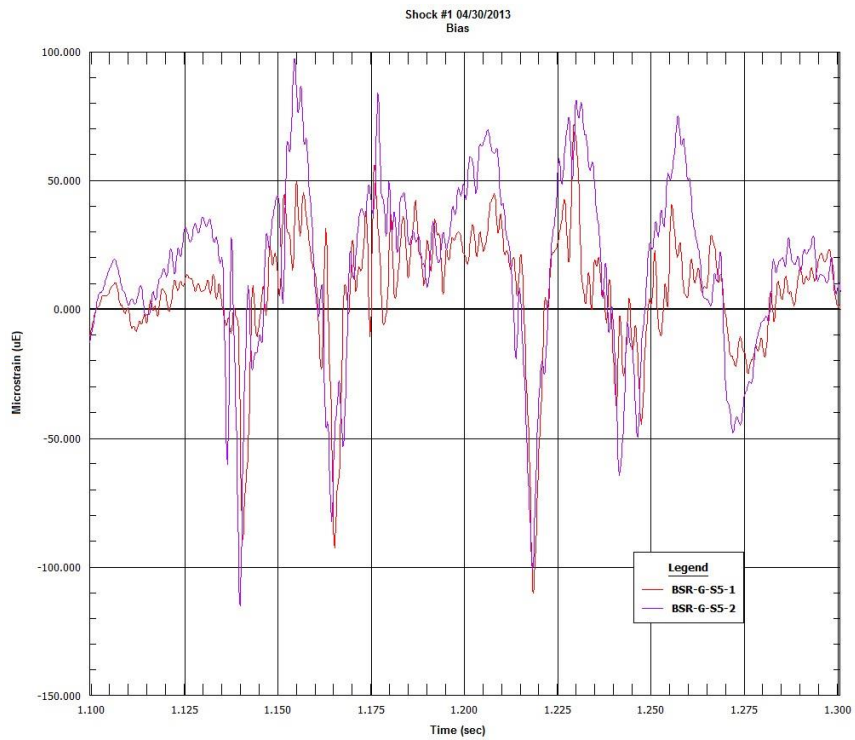


Figure 46. Shock Test #1. Bottom-side Rod, Span 5. Micro-strain v. time. Expanded time scale 1.1 to 1.3 seconds.

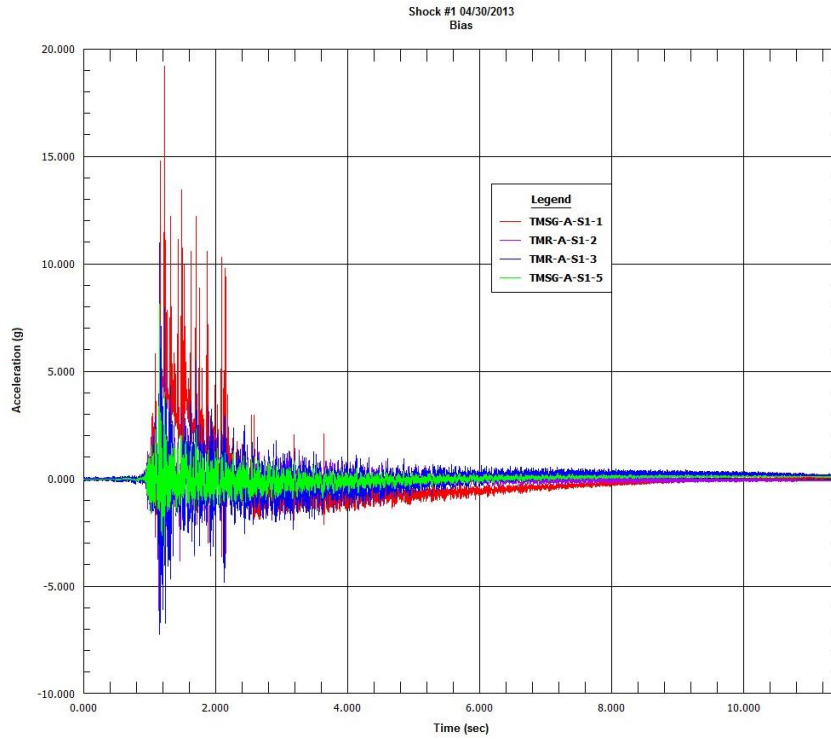


Figure 47. Shock Test #1. Top-middle Spacer Grids and Rod, Span 1. Acceleration.

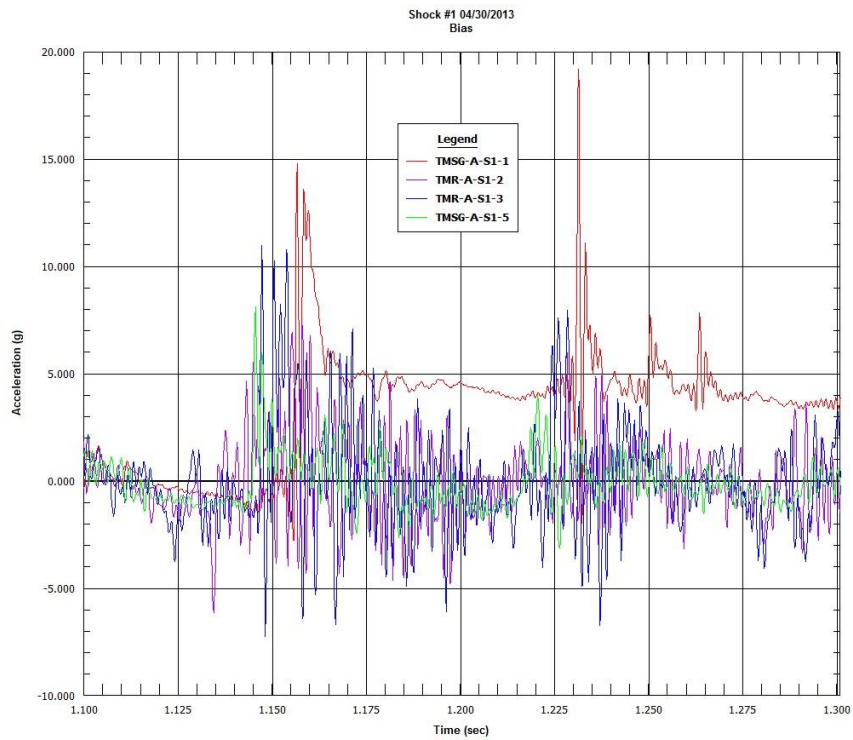


Figure 48. Shock Test #1. Top-middle Spacer Grids and Rod, Span 1. Acceleration, Expanded time scale 1.1 to 1.3 seconds.

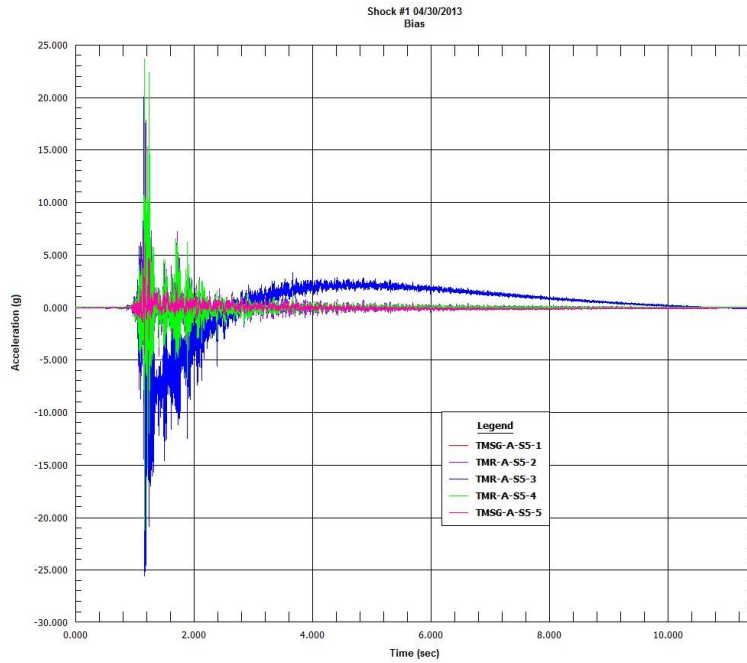


Figure 49. Shock Test #1. Top-middle Spacer Grids and Rod, Span 5. Acceleration.  
NOTE: Malfunction of TMR-A-S5-3.

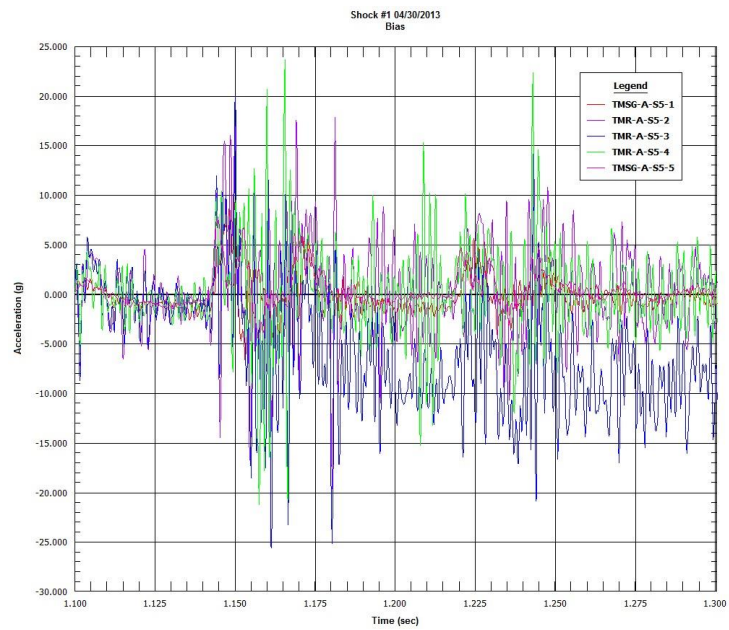


Figure 50. Shock Test #1. Top-middle Spacer Grids and Rod, Span 5. Acceleration,  
Expanded time scale 1.1 to 1.3 seconds.  
NOTE: Malfunction of TMR-A-S5-3.

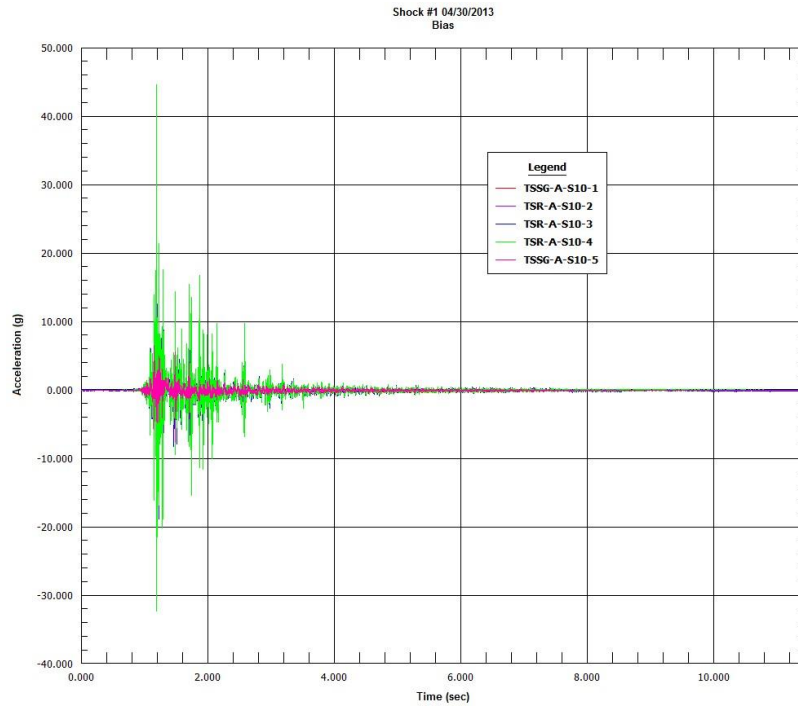


Figure 51. Shock Test #1. Top-side Spacer Grids and Rod, Span 10. Acceleration.

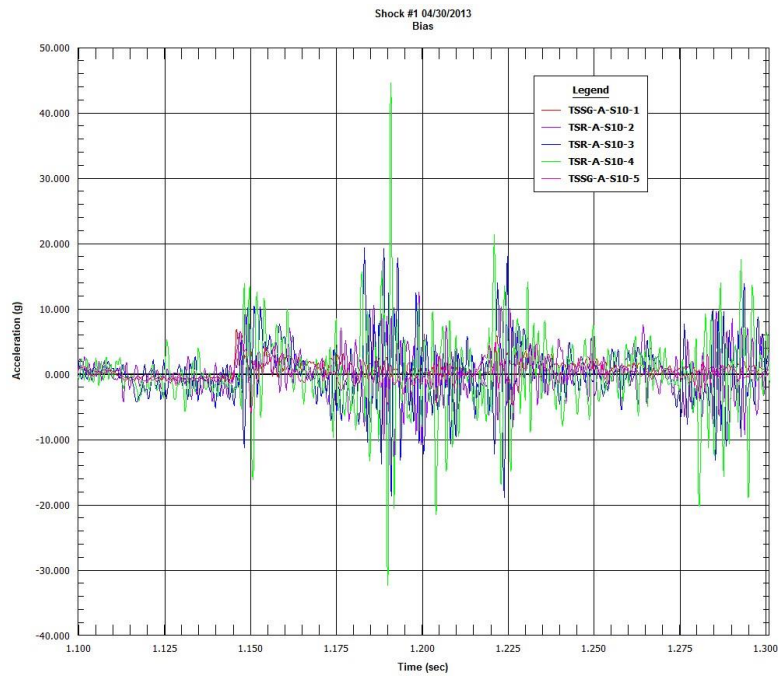


Figure 52. Shock Test #1. Top-side Spacer Grids and Rod, Span 10. Acceleration, Expanded time scale 1.1 to 1.3 seconds.

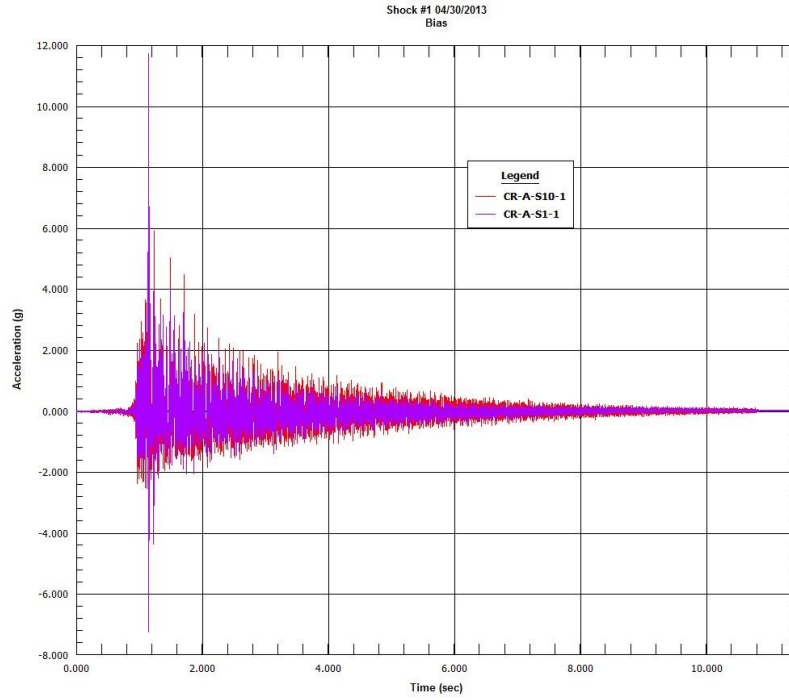


Figure 53. Shock Test #1. Control Rod Acceleration v. time. Acceleration.

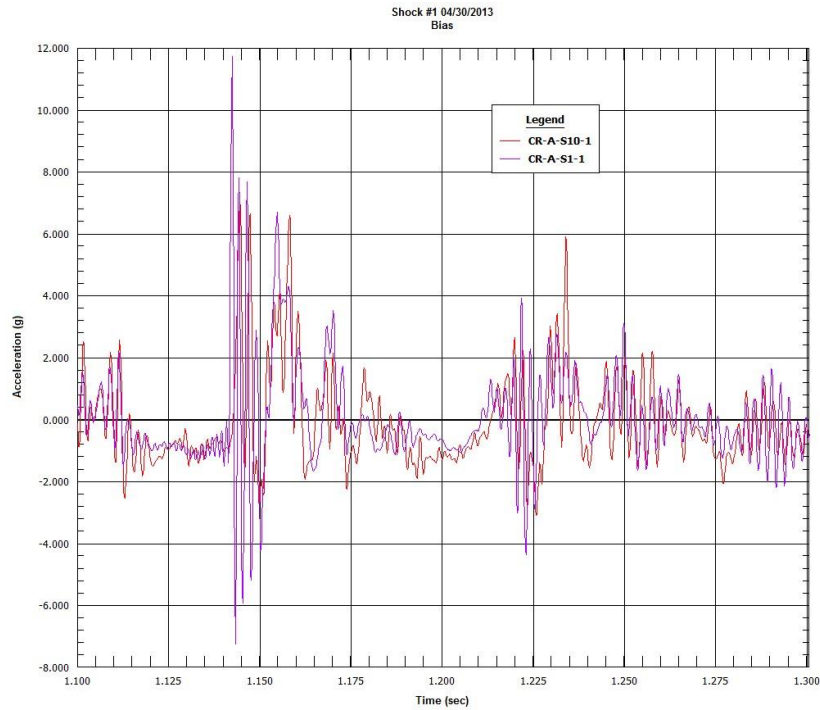


Figure 54. Shock Test #1. Control Rod Acceleration v. time. Expanded time scale 1.1 to 1.3 seconds.

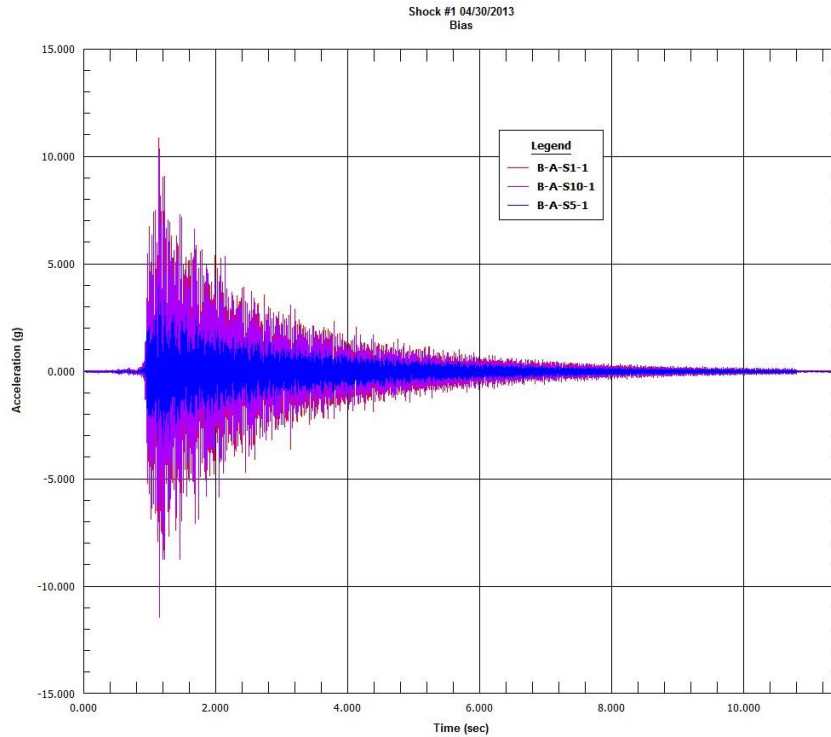


Figure 55. Shock Test #1. Basket Acceleration v. time.

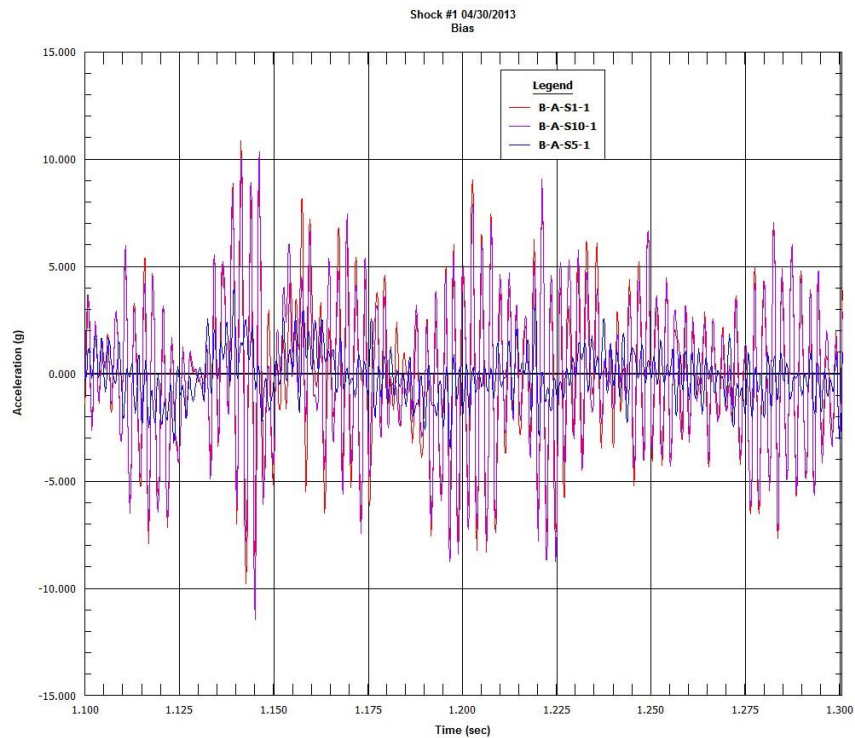


Figure 56. Shock Test #1. Basket Acceleration v. time. Expanded time scale 1.1 to 1.3 seconds.

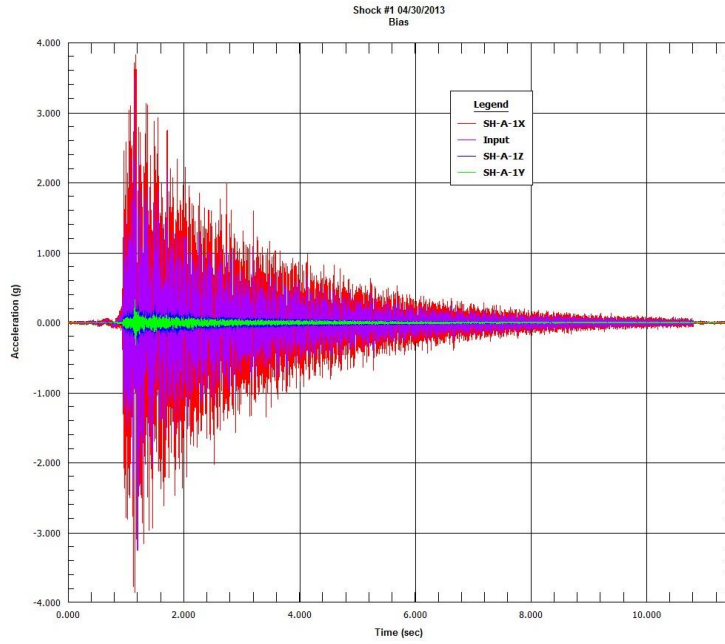


Figure 57. Shock Test #1. Input (Control) Acceleration v. time and Triaxial Acceleration v. time on Basket Mounting Plate.

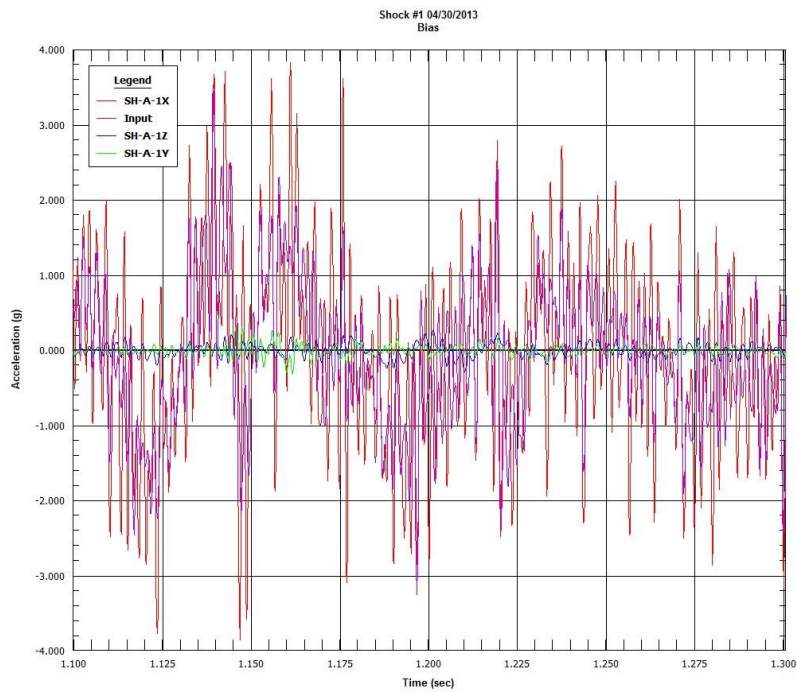


Figure 58. Shock Test #1. Input (Control) Acceleration v. time and Triaxial Acceleration v. time on Basket Mounting Plate. Expanded time scale 1.1 to 1.3 seconds.

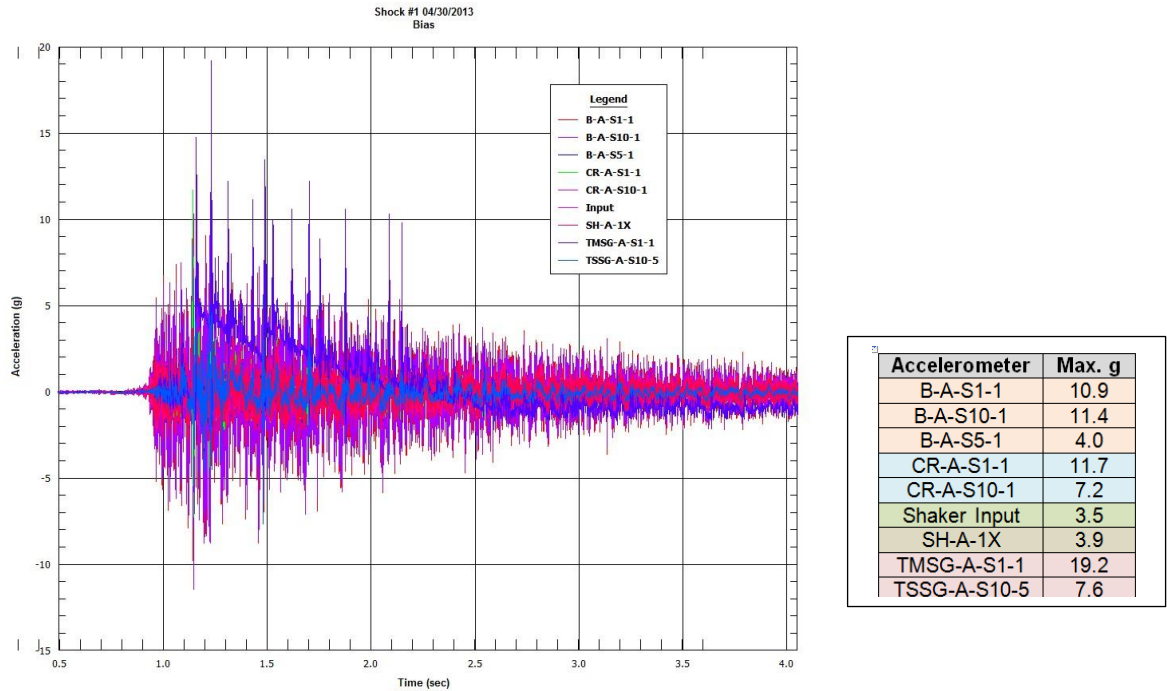


Figure 59. Shock Test #1. Shaker Input (Control) Acceleration, Vertical Acceleration on Basket Mounting Plate, Basket Accelerations (top end, mid-span, bottom end), Control Rod accelerations (top and bottom ends), and Assembly Spacer Grids (top and bottom ends) v. time. Expanded time scale 1 to 4 seconds.

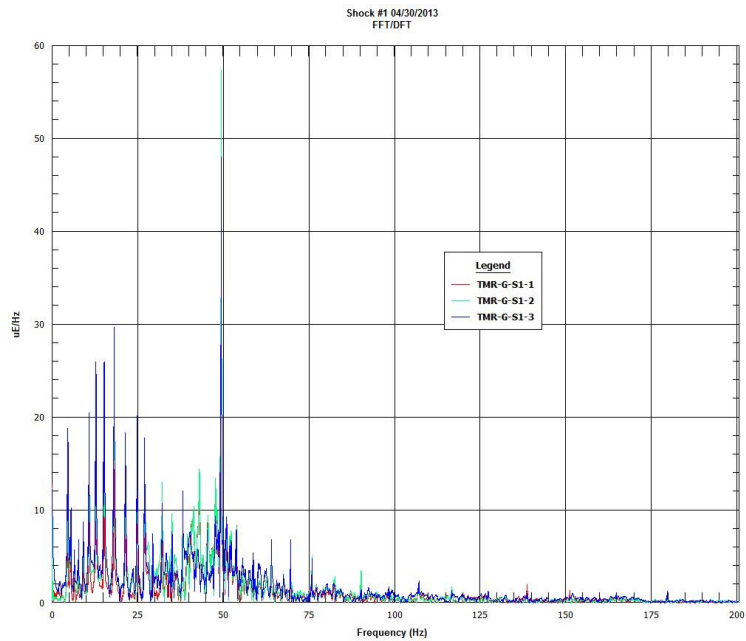


Figure 60. Shock Test #1. Fast Fourier Transformation. Top-middle Rod, Span 1.

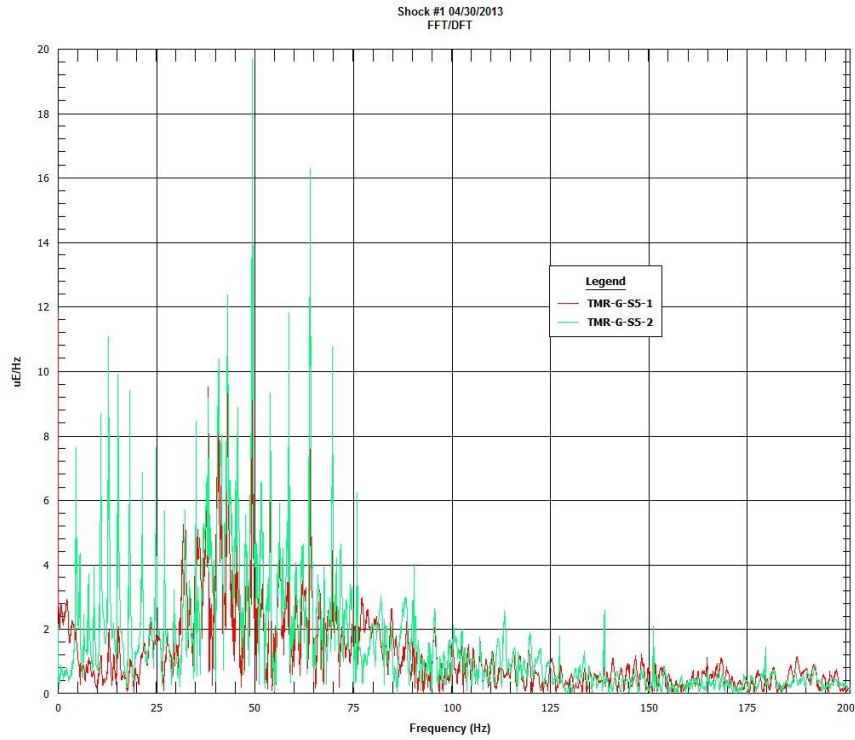


Figure 61. Shock Test #1. Fast Fourier Transformation. Top-middle Rod, Span 5.

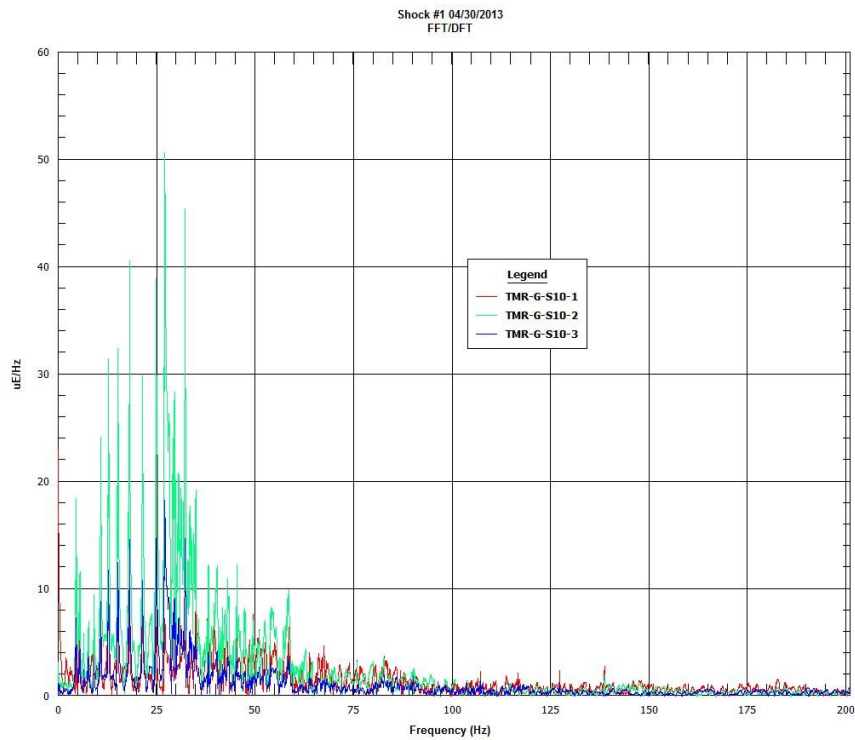


Figure 62. Shock Test #1. Fast Fourier Transformation. Top-middle Rod, Span 10.

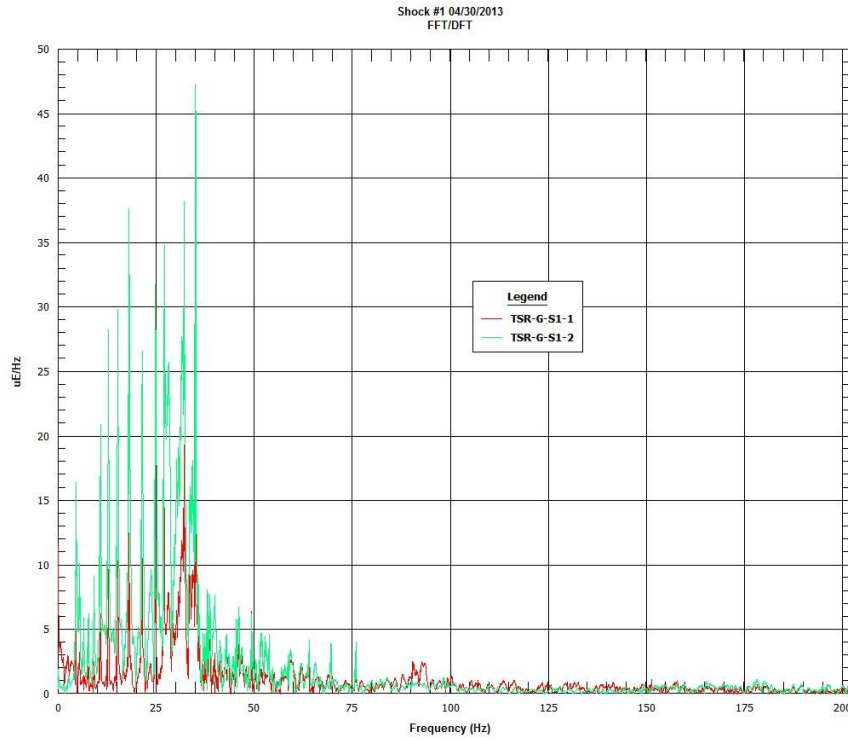


Figure 63. Shock Test #1. Fast Fourier Transformation. Top-side Rod, Span 1.

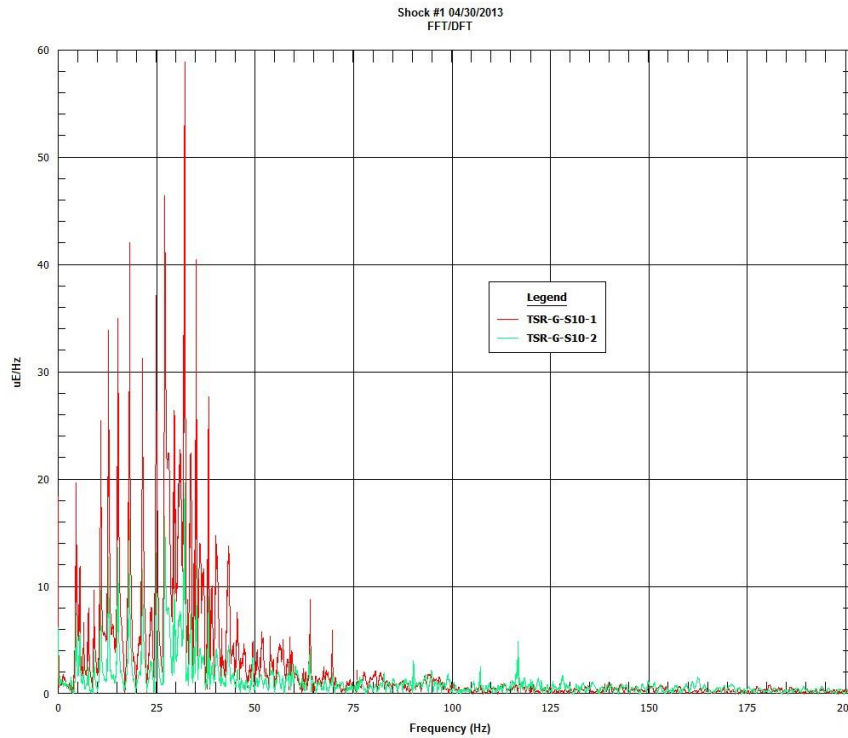


Figure 64. Shock Test #1. Fast Fourier Transformation. Top-side Rod, Span 10.

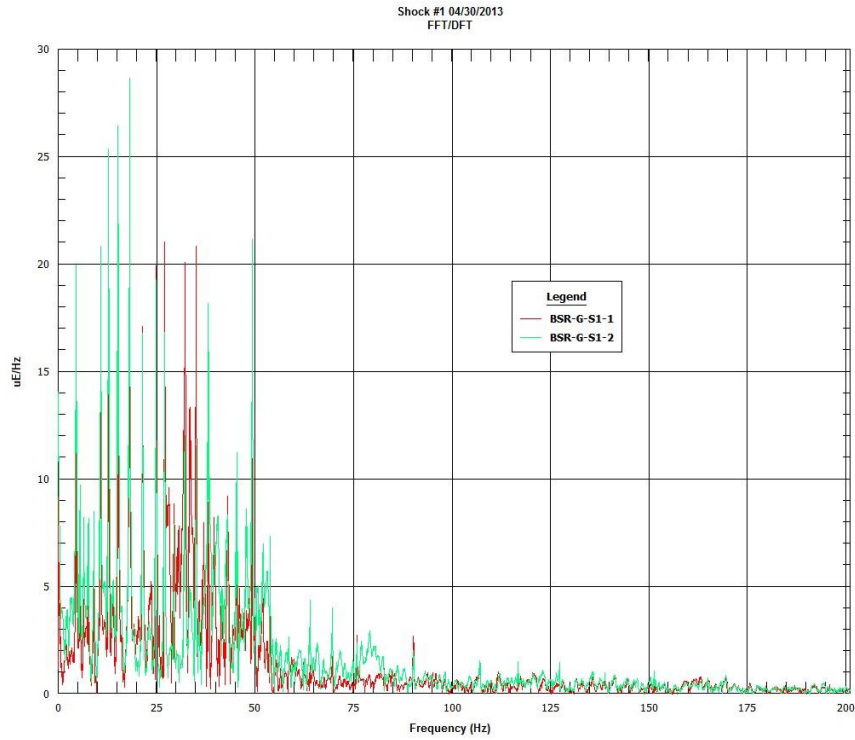


Figure 65. Shock Test #1. Fast Fourier Transformation. Bottom-side Rod, Span 1.

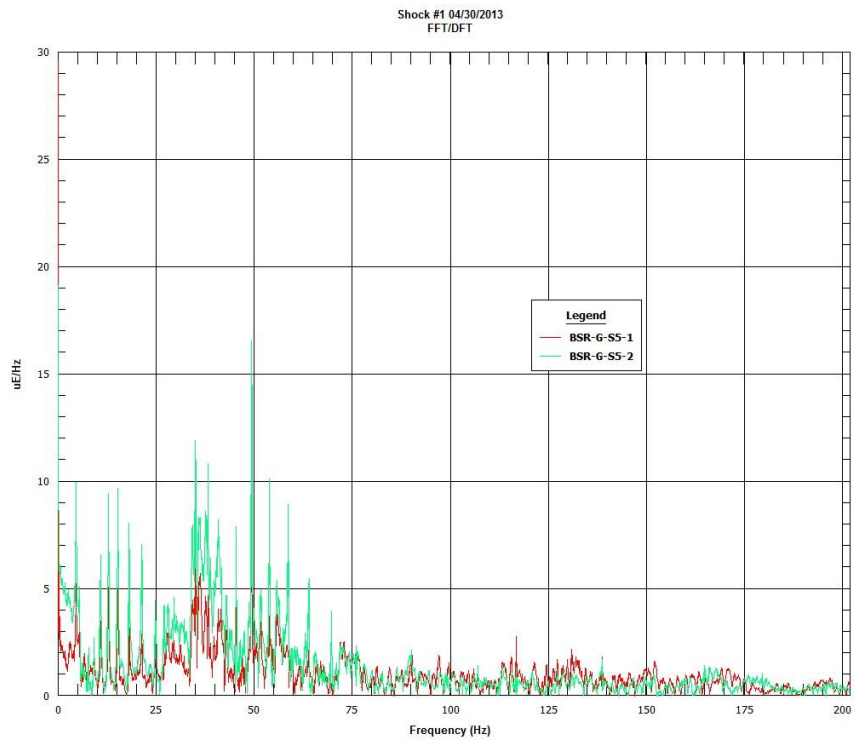


Figure 66. Shock Test #1. Fast Fourier Transformation. Bottom-side Rod, Span 5.

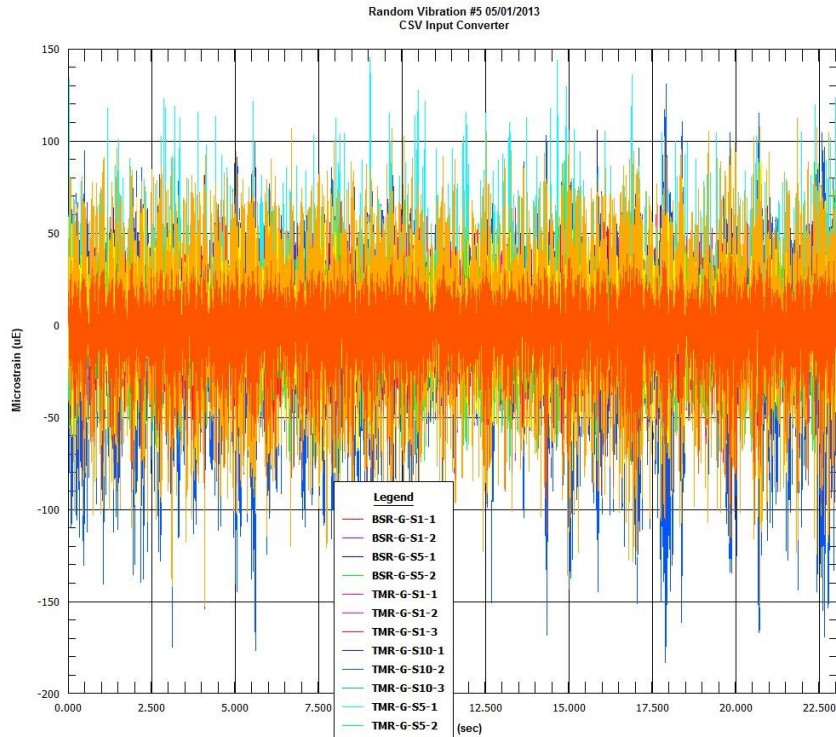


Figure 67. Vibration Test #5. All Strain Gauges. Micro-strain v. time.

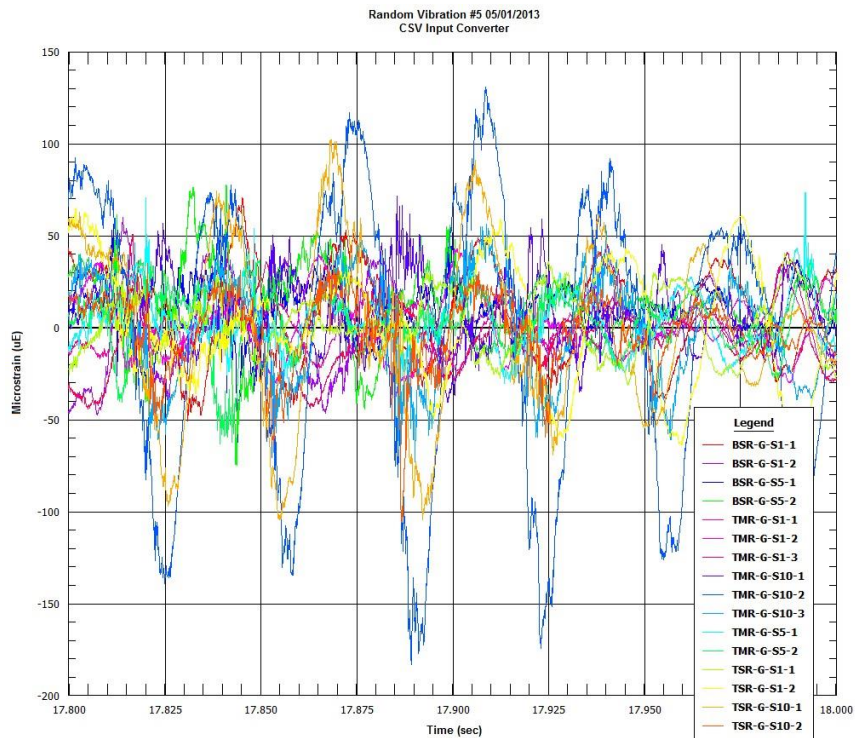


Figure 68. Vibration Test #5. All Strain Gauges. Micro-strain v. time. Expanded time scale 17.8 to 18 seconds.

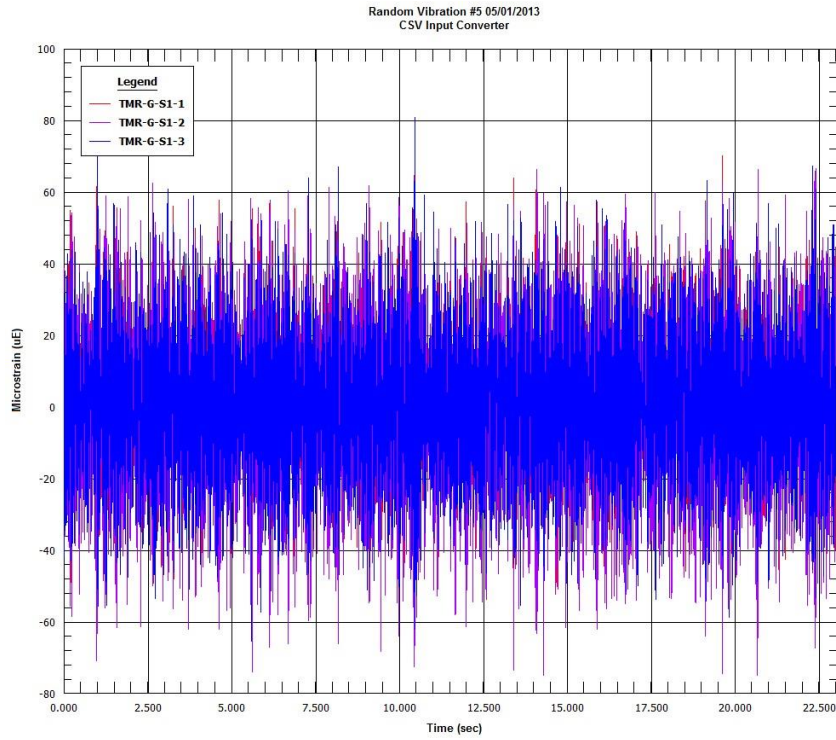


Figure 69. Vibration Test #5. Top-middle Rod, Span 1. Micro-strain v. time.

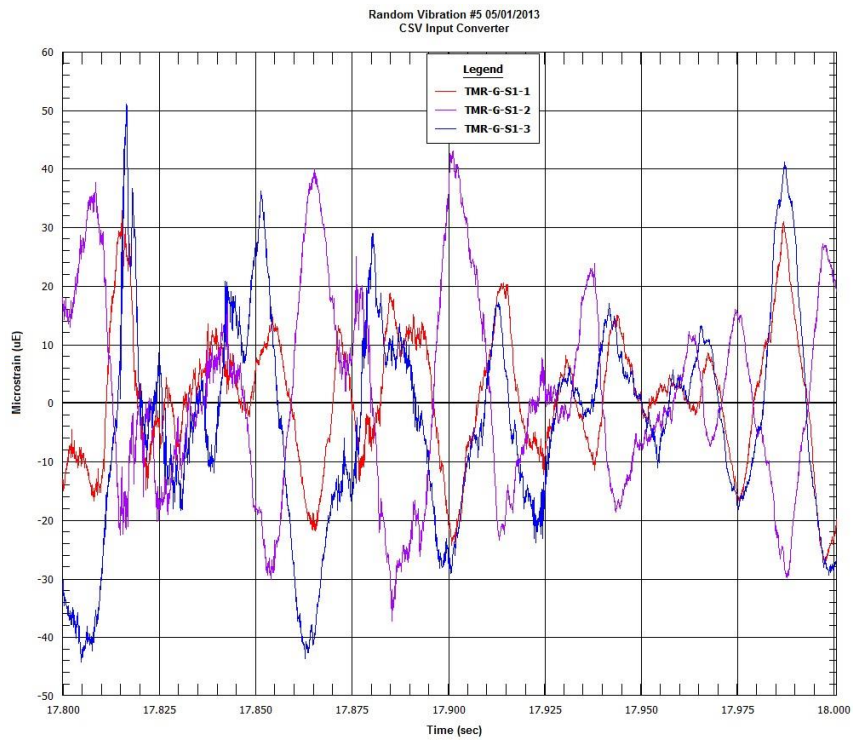


Figure 70. Vibration Test #5. Top-middle Rod, Span 1. Micro-strain v. time. Expanded time scale 17.8 to 18 seconds.

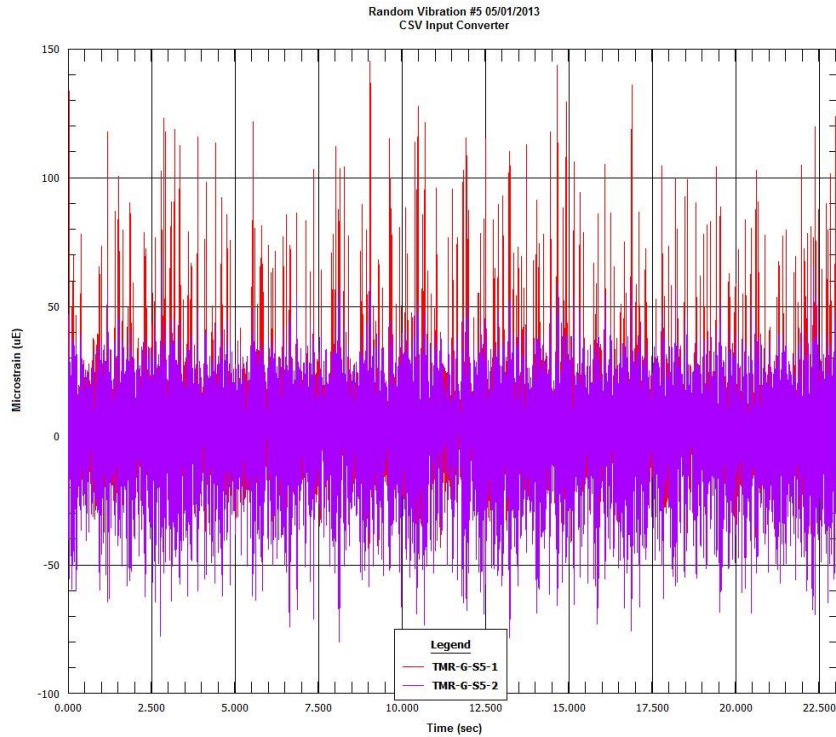


Figure 71. Vibration Test #5. Top-middle rod, Span 5. Micro-strain v. time.

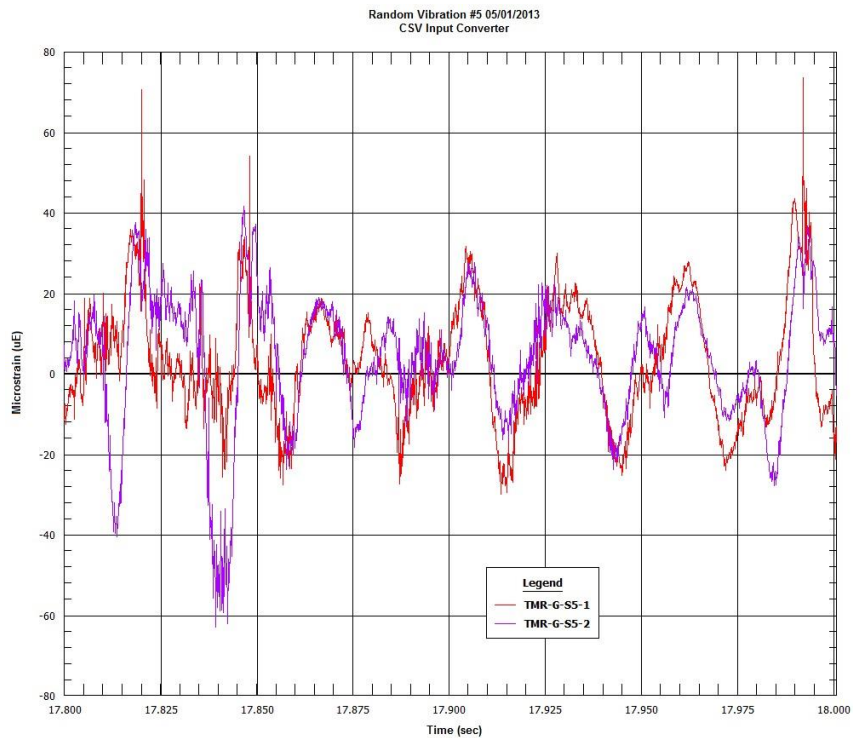


Figure 72. Vibration Test #5. Top-middle Rod, Span 5. Micro-strain v. time. Expanded time scale 17.8 to 18 seconds.

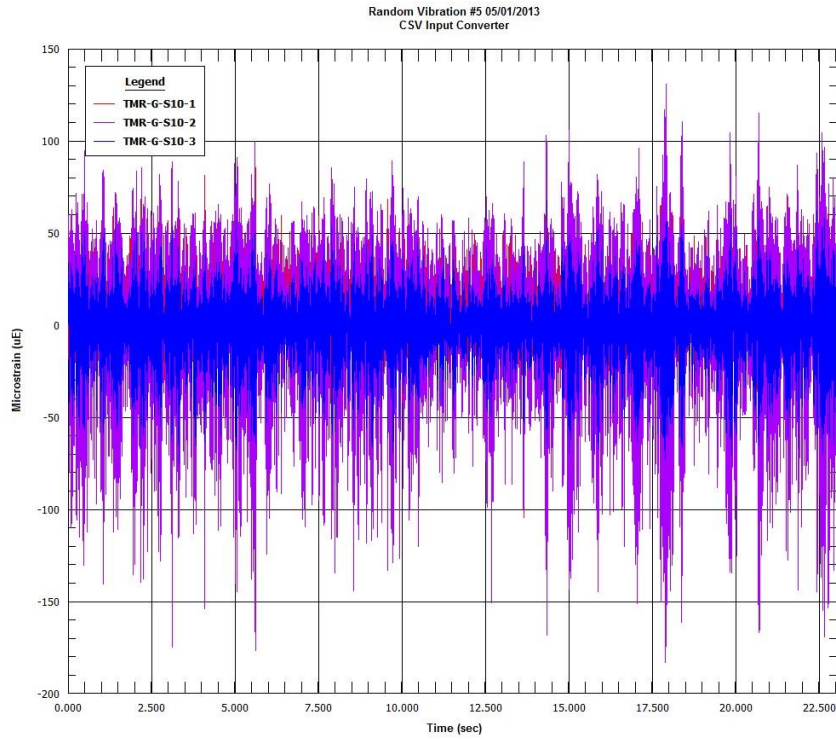


Figure 73. Vibration Test #5. Top-middle Rod, Span 10. Micro-strain v. time.

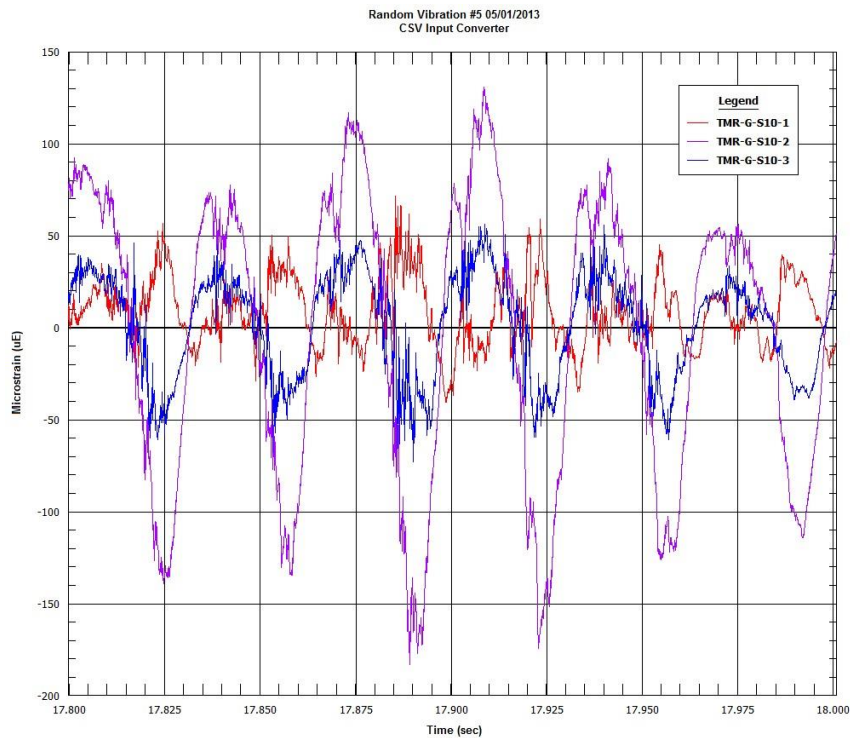


Figure 74. Vibration Test #5. Top-middle Rod, Span 10. Micro-strain v. time. Expanded time scale 17.8 to 18 seconds.

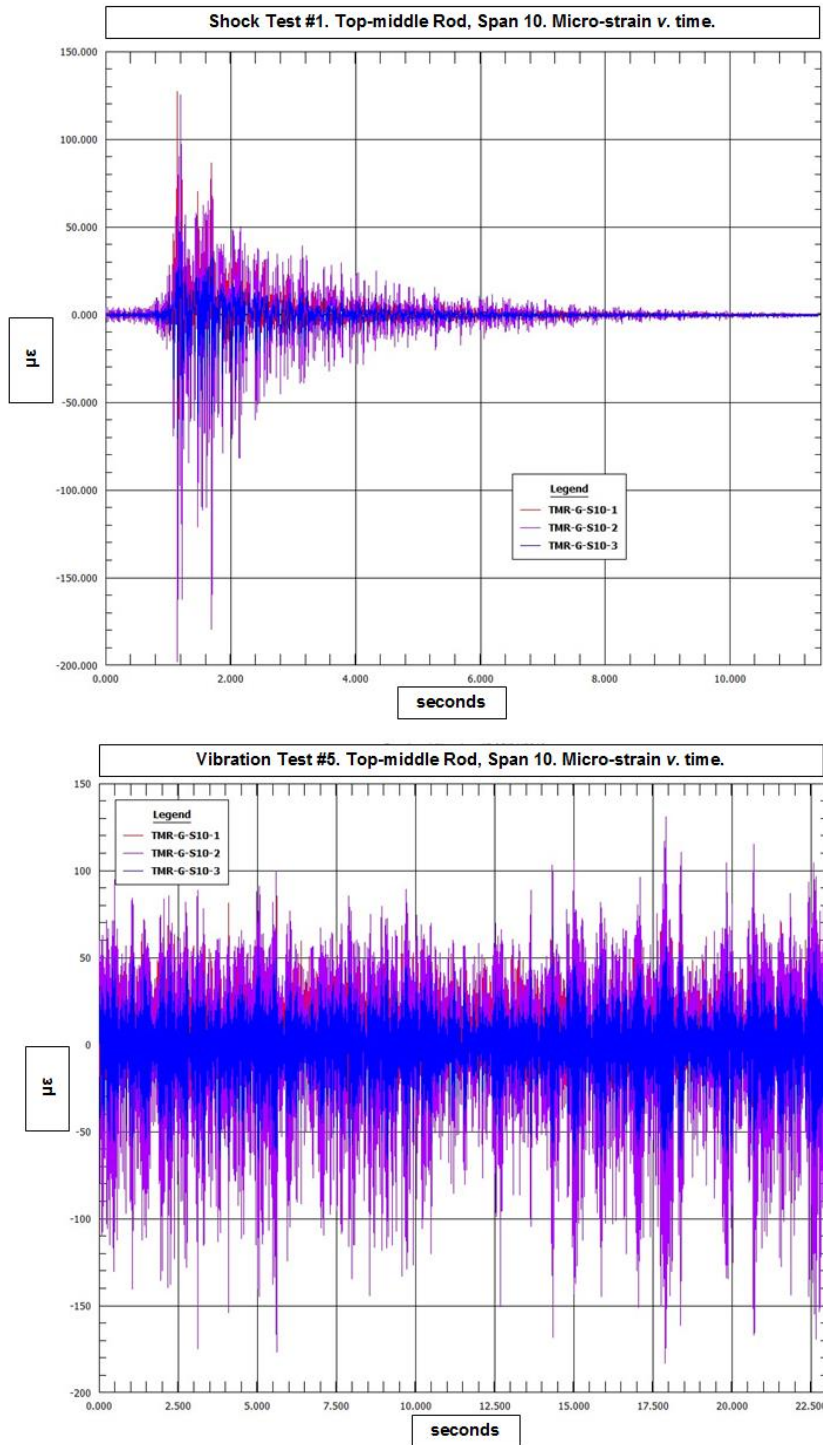


Figure 75. Comparison of Top-middle Rod, Span 10  $\mu\epsilon$  v. time for Shock Test #1 and Random Vibration Test #5.

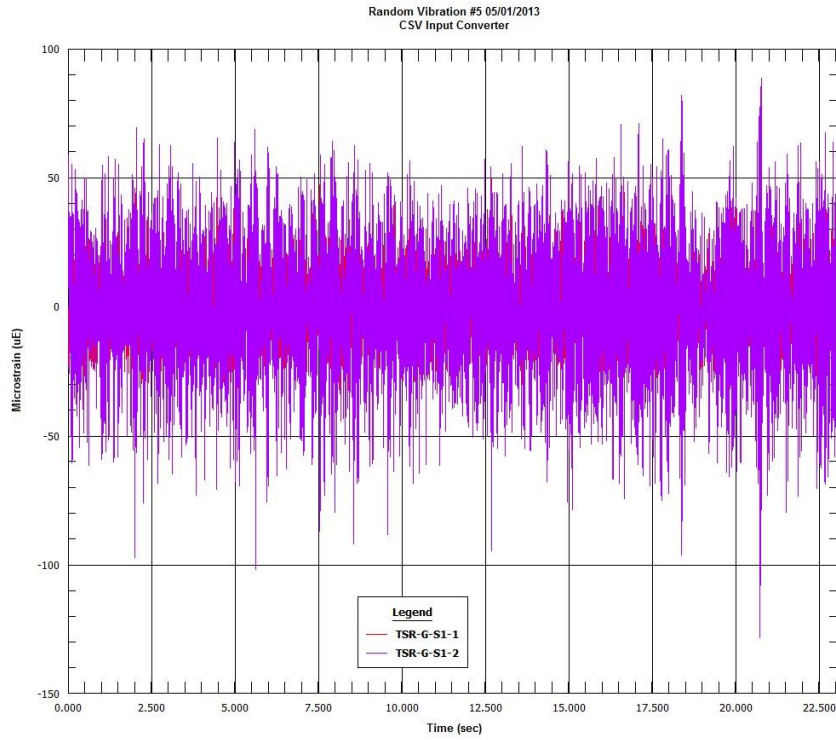


Figure 76. Vibration Test #5. Top-side Rod, Span 1. Micro-strain v. time.

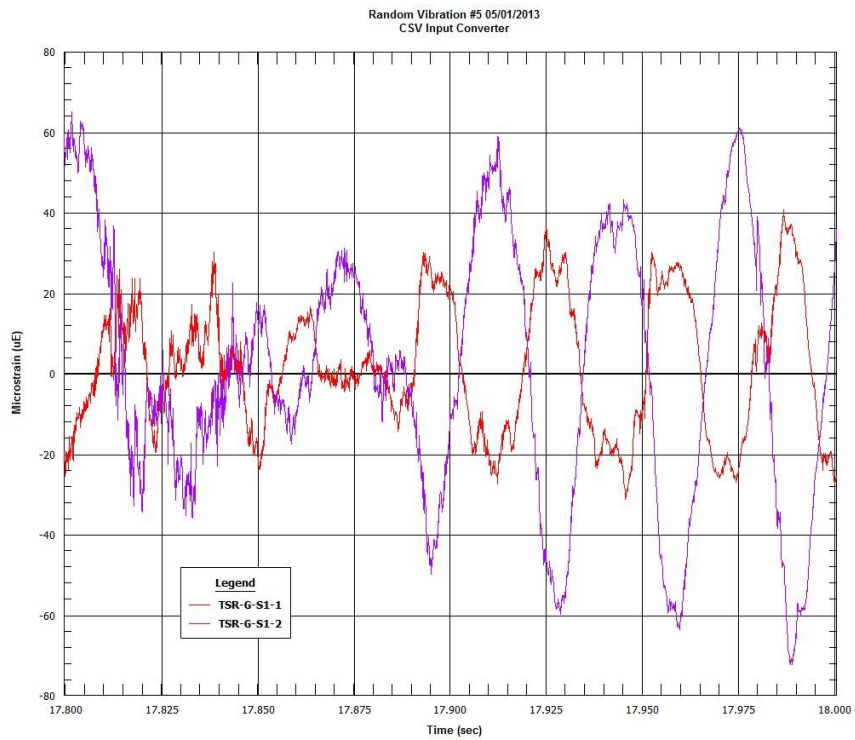


Figure 77. Vibration Test #5. Top-side Rod, Span 1. Micro-strain v. time. Expanded time scale 17.8 to 18 seconds.

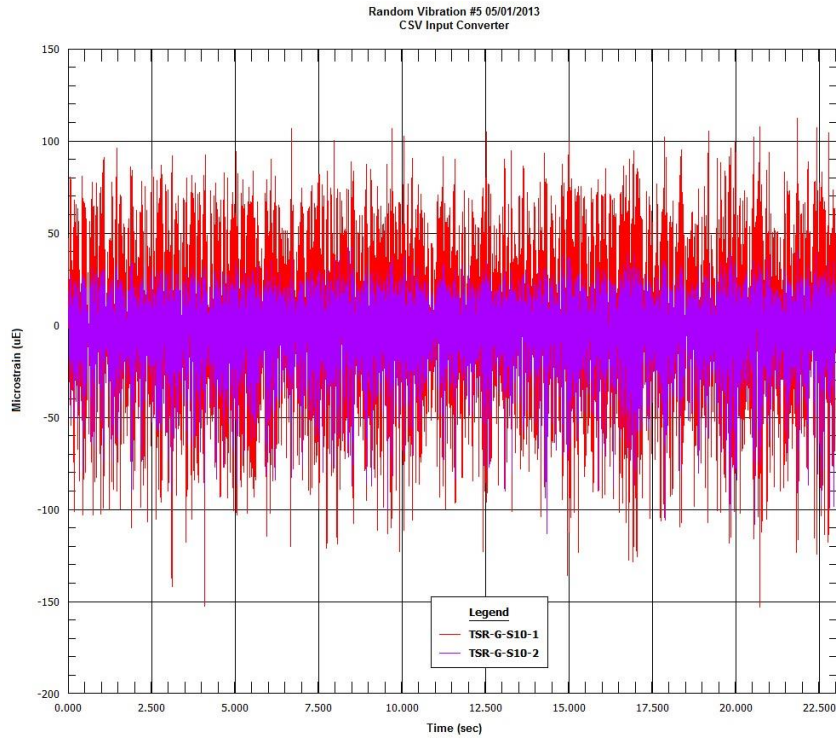


Figure 78. Vibration Test #5. Top-side Rod, Span 10. Micro-strain v. time.

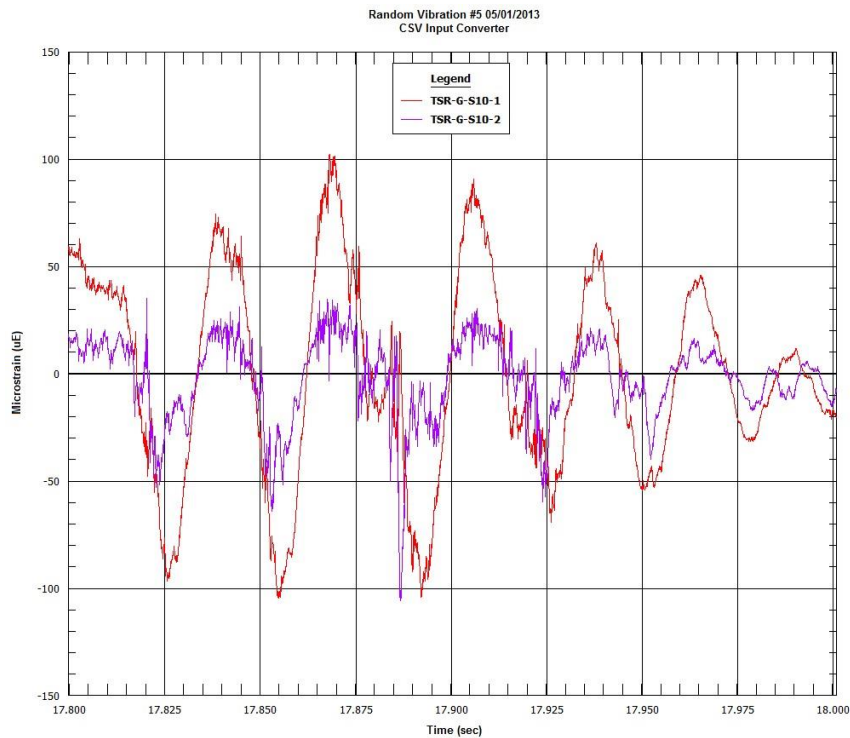


Figure 79. Vibration Test #5. Top-side Rod, Span 10. Micro-strain v. time. Expanded time scale 17.8 to 18 seconds.

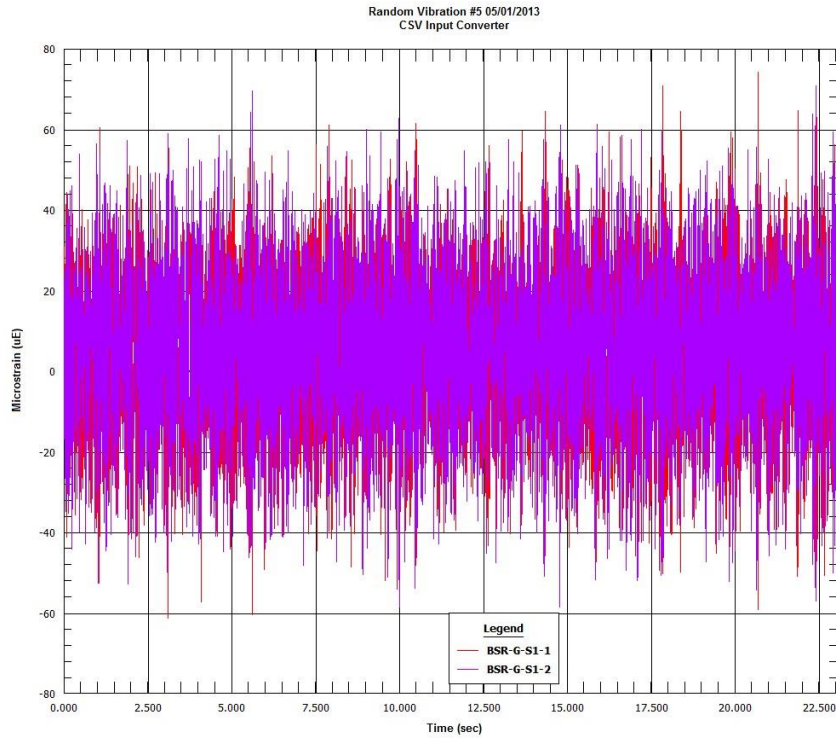


Figure 80. Vibration Test #5. Bottom-side Rod, Span 1. Micro-strain v. time.

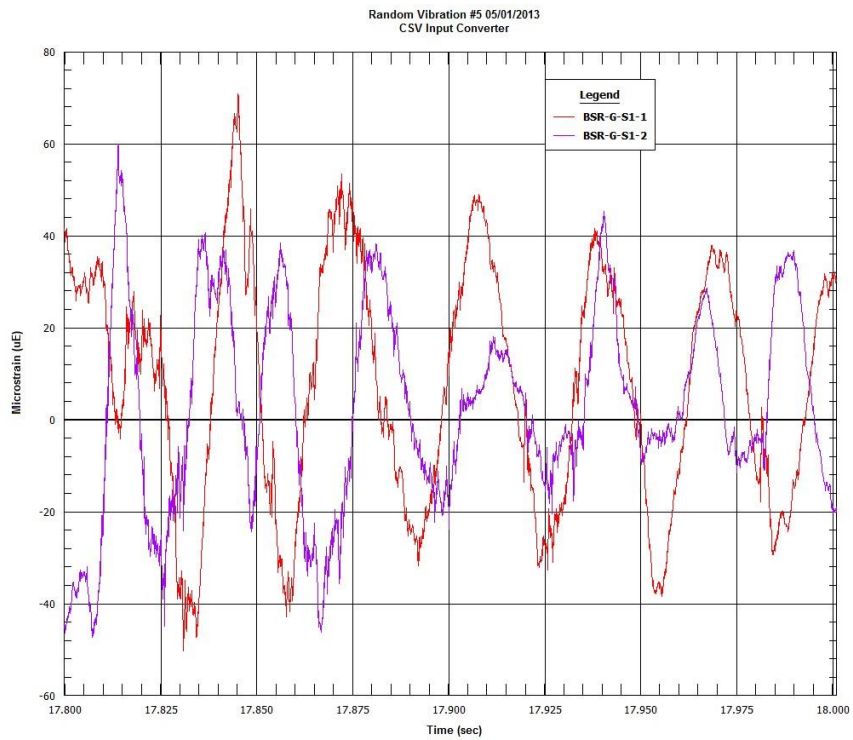


Figure 81. Vibration Test #5. Bottom-side Rod, Span 1. Micro-strain v. time. Expanded time scale 17.8 to 18 seconds.

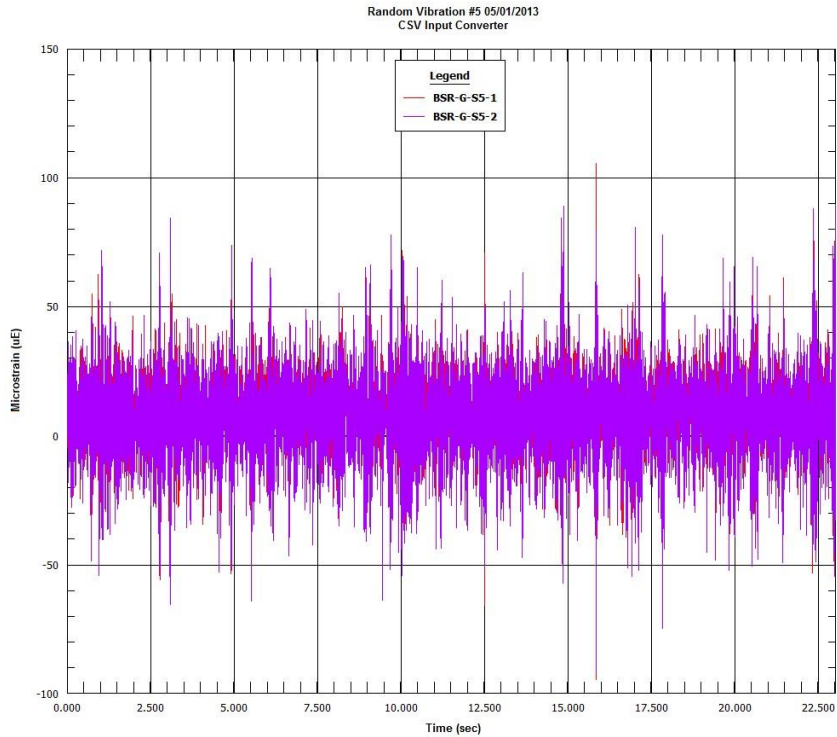


Figure 82. Vibration Test #5. Bottom-side Rod, Span 5. Micro-strain v. time.

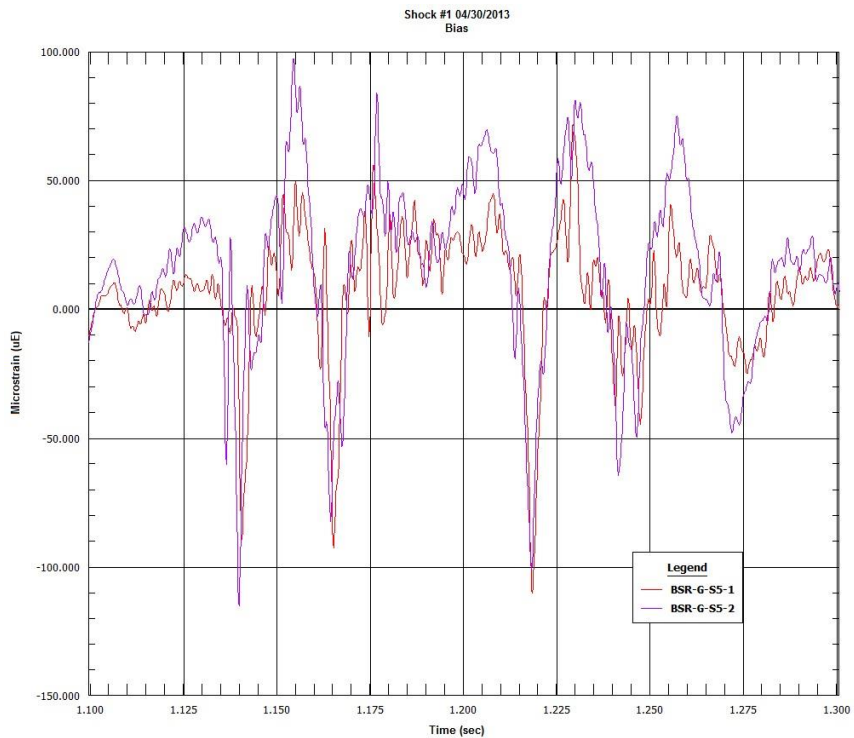


Figure 83. Vibration Test #5. Bottom-side Rod, Span 5. Micro-strain v. time. Expanded time scale 1.1 to 1.3 seconds.

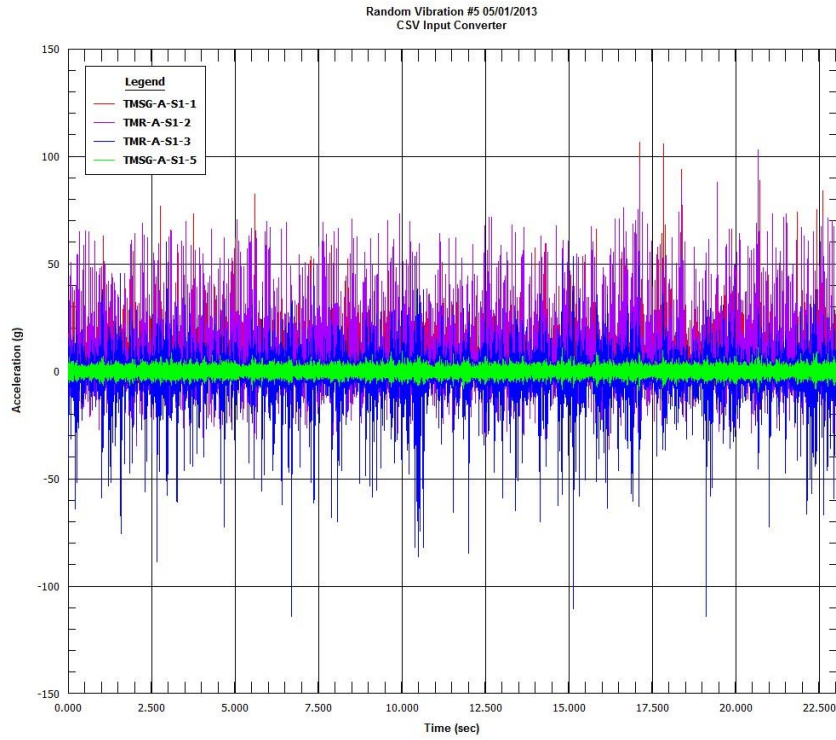


Figure 84. Vibration Test #5. Top-middle Spacer Grids and Rod, Span 1. Acceleration.

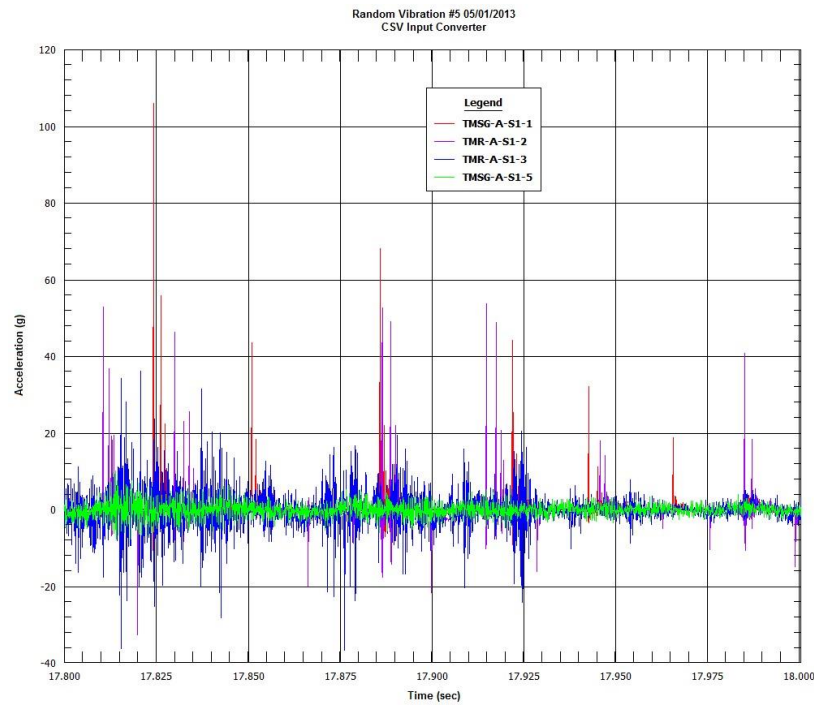


Figure 85. Vibration Test #5. Top-middle Spacer Grids and Rod, Span 1. Acceleration. Expanded time scale 17.8 to 18 seconds.

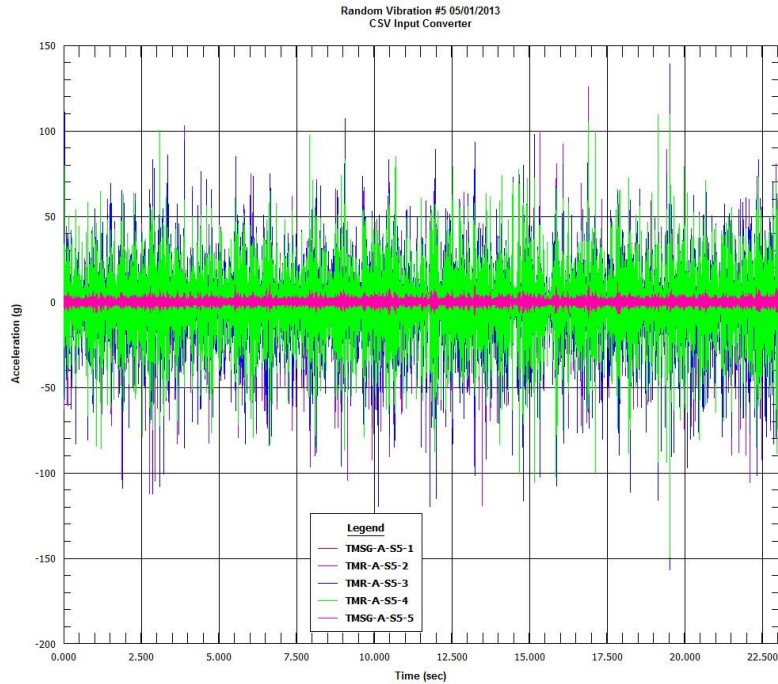


Figure 86. Vibration Test #5. Top-middle Spacer Grids and Rod, Span 5. Accelerations v. time.

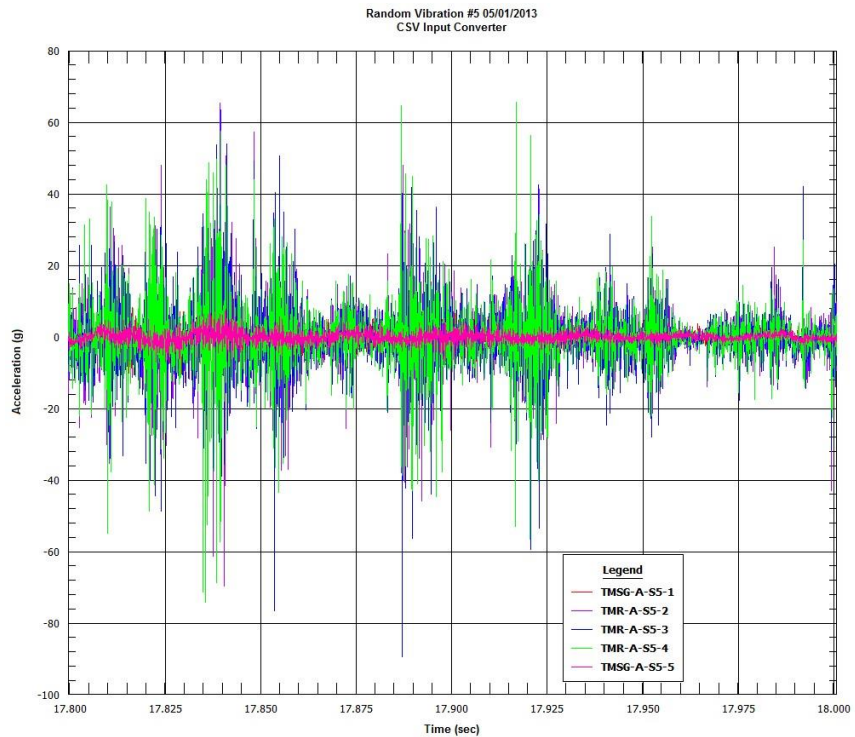


Figure 87. Vibration Test #5. Top-middle Spacer Grids and Rod, Span 5. Acceleration. Expanded time scale 17.8 to 18 seconds.

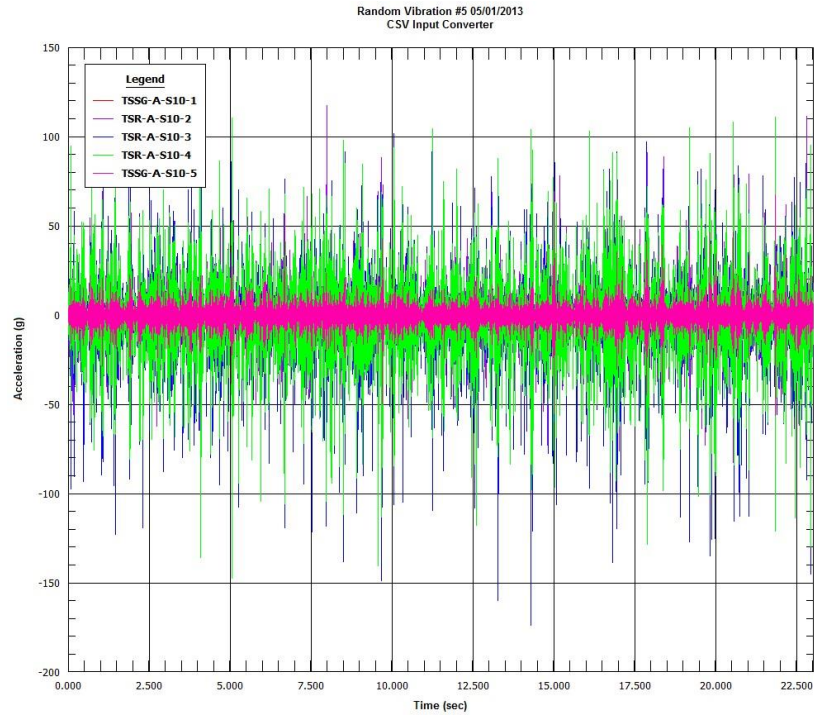


Figure 88. Vibration Test #5. Top-side Spacer Grids and Rod, Span 10. Accelerations v. time.

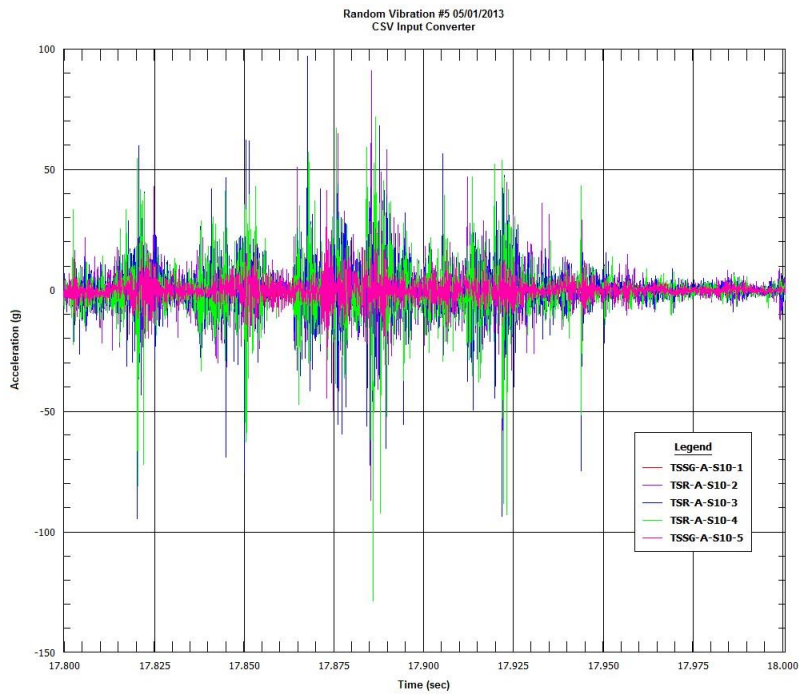


Figure 89. Vibration Test #5. Top-side Spacer Grids and Rod, Span 10. Acceleration. Expanded time scale 17.8 to 18 seconds.

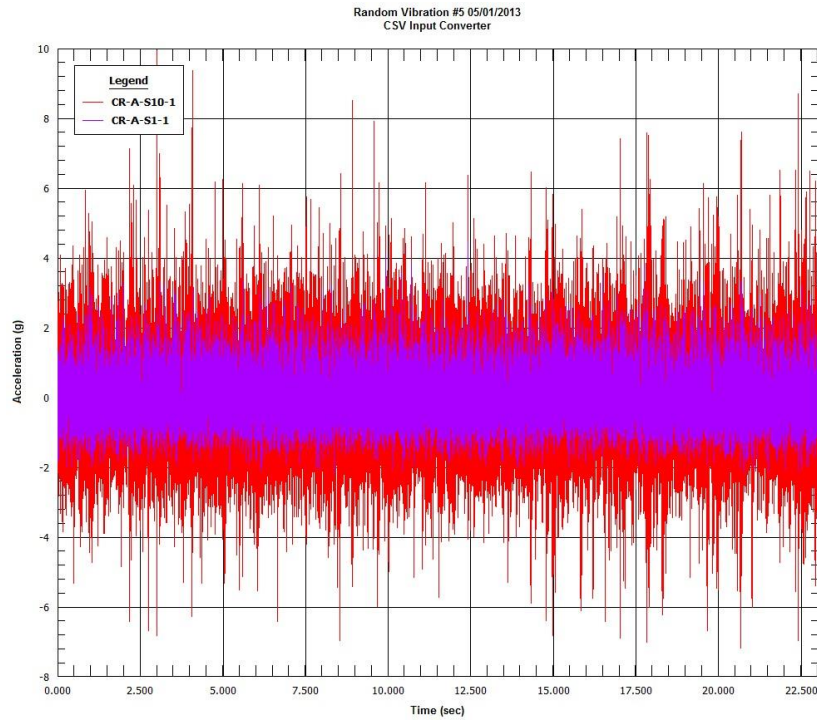


Figure 90. Vibration Test #5. Control Rod Acceleration v. time.

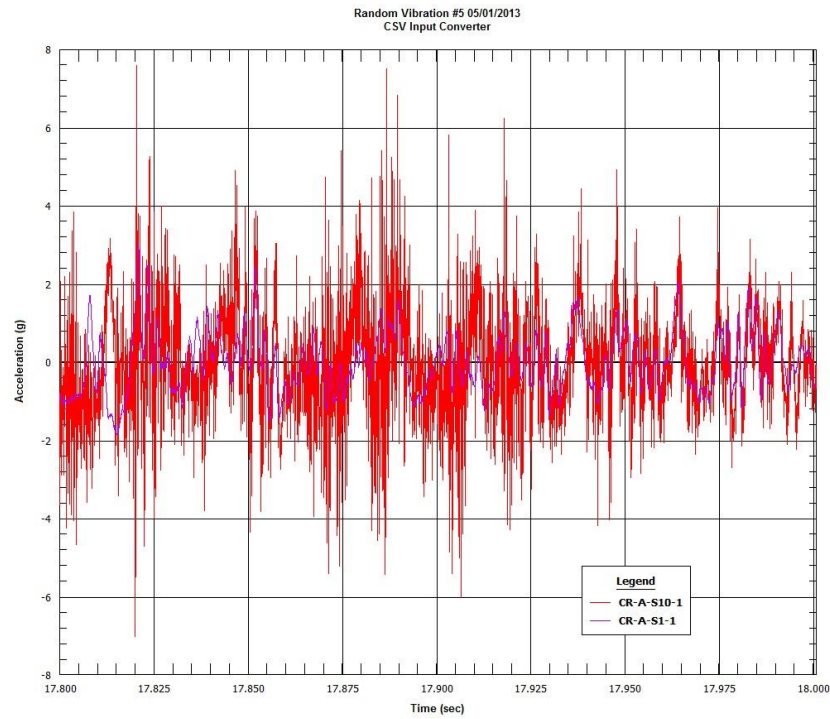


Figure 91. Vibration Test #5. Control Rod Acceleration v. time. Expanded time scale 17.8 to 18 seconds.

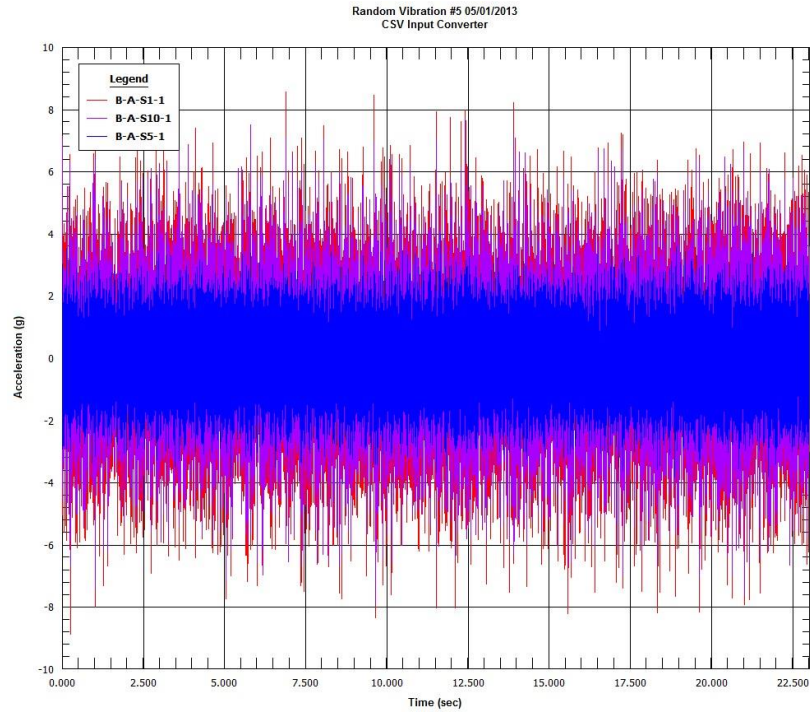


Figure 92. Vibration Test #5. Basket Accelerations v. time.

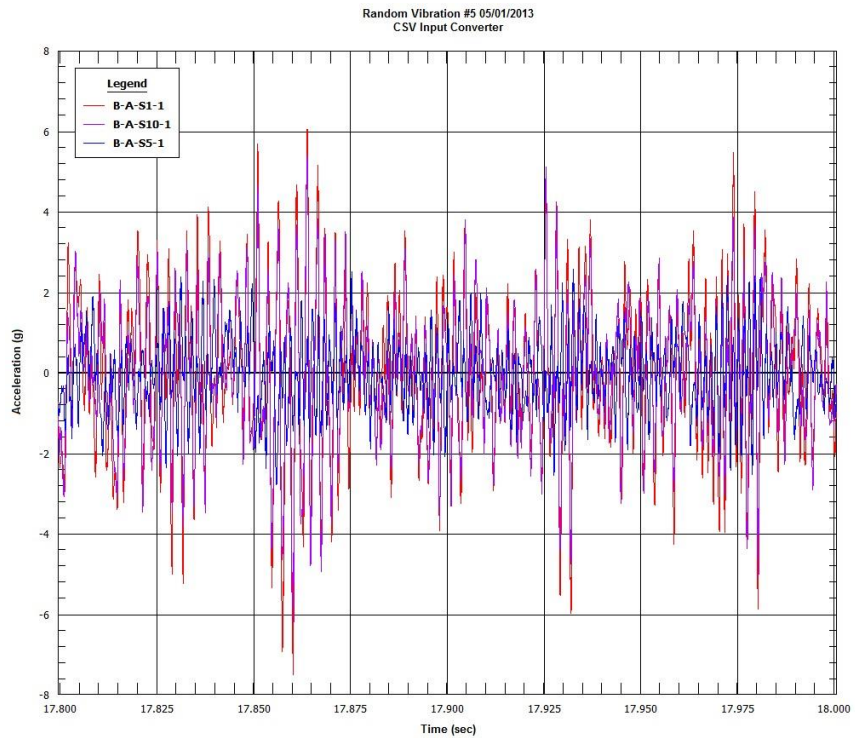


Figure 93. Vibration Test #5. Basket Accelerations v. time. Expanded time scale 17.8 to 18 seconds.

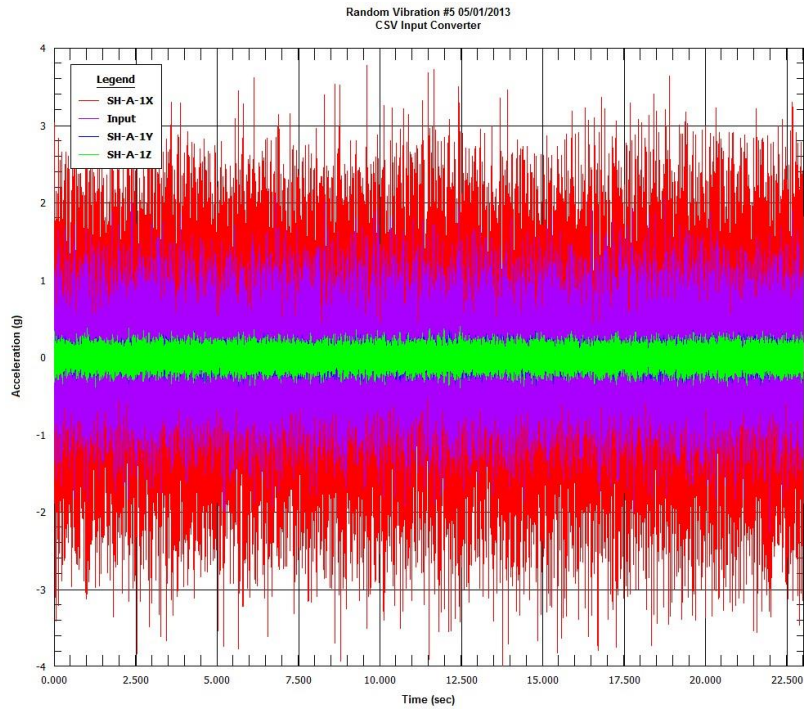


Figure 94. Vibration Test #5. Input (Control) Acceleration v. time and Triaxial Accelerations v. time on Basket Mounting Plate.

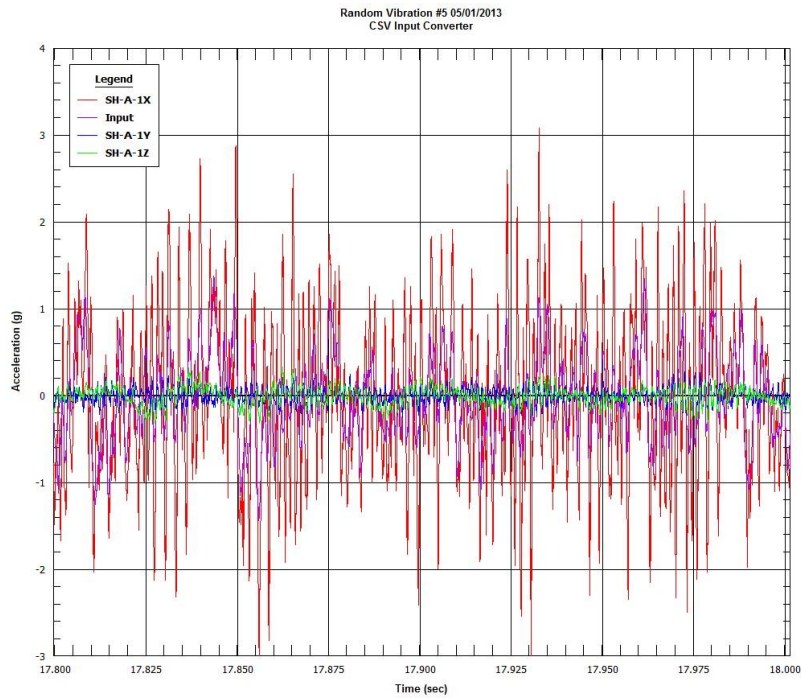


Figure 95. Vibration Test #5. Input (Control) Acceleration v. time and Triaxial Accelerations v. time on Basket Mounting Plate. Expanded time scale 17.8 to 18 seconds.

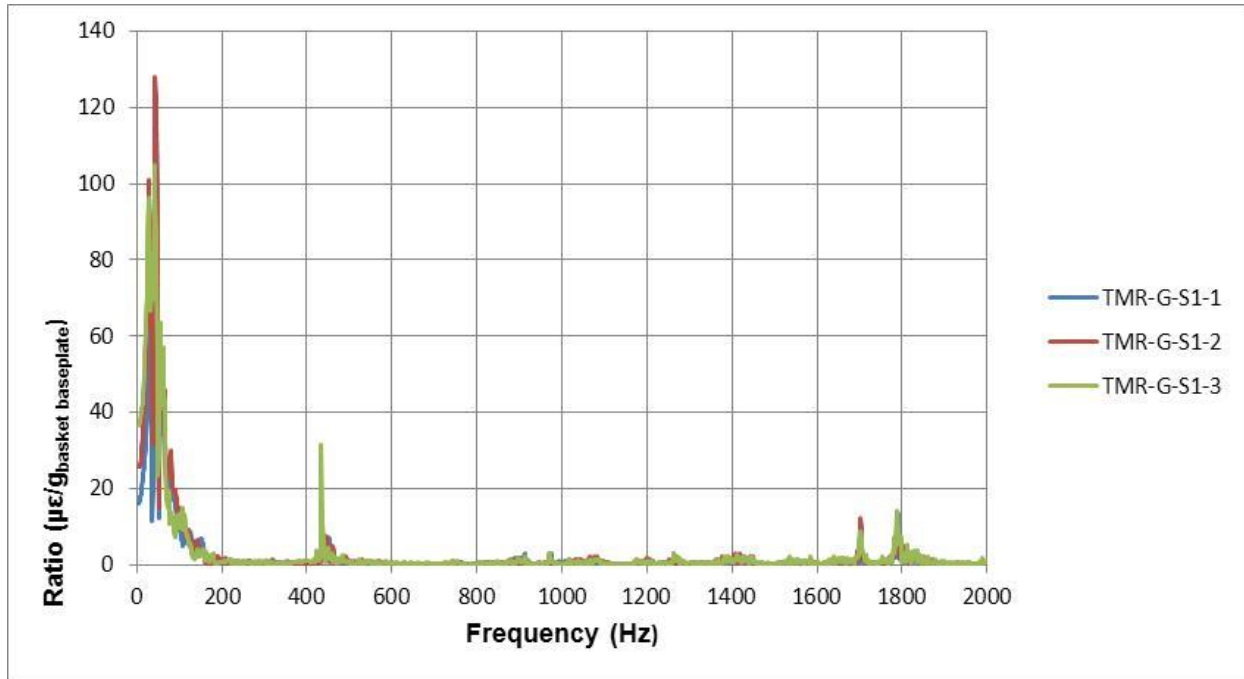


Figure 96. Vibration Test #5. Top-middle Rod, Span 1. Ratio of micro-strains to baseplate vertical acceleration (Channel 23) v. Hz.

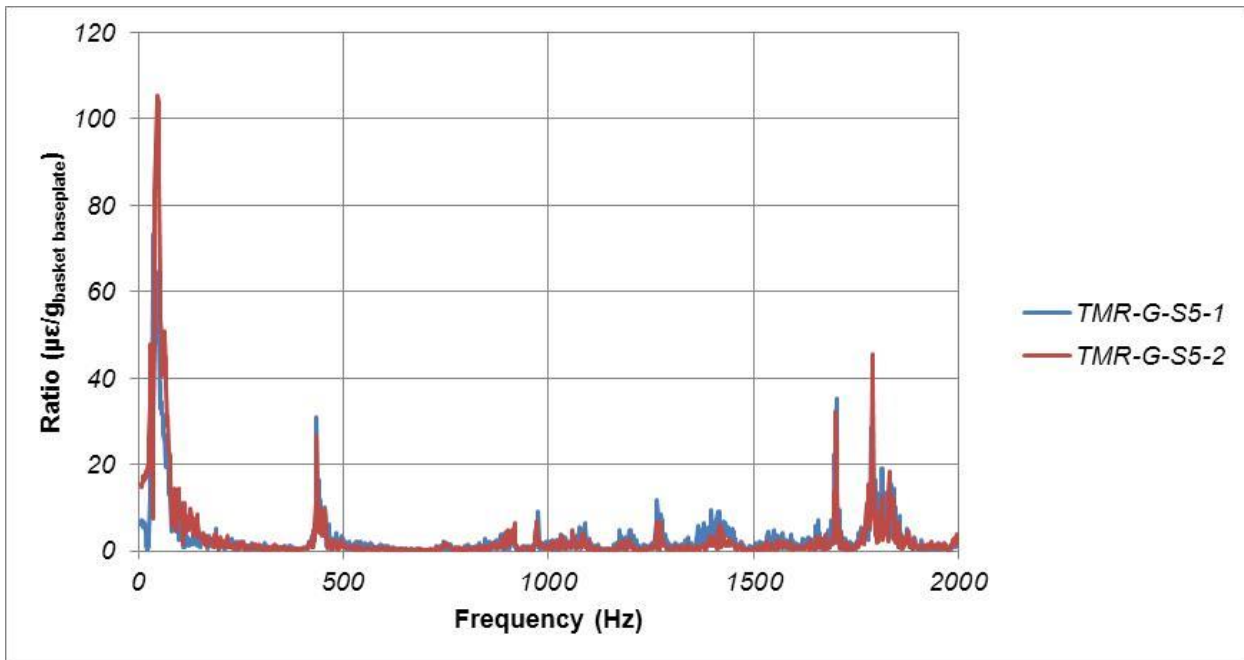


Figure 97. Vibration Test #5. Top-middle rod, Span 5. Ratio of micro-strain to baseplate vertical acceleration (Channel 23) v. Hz.

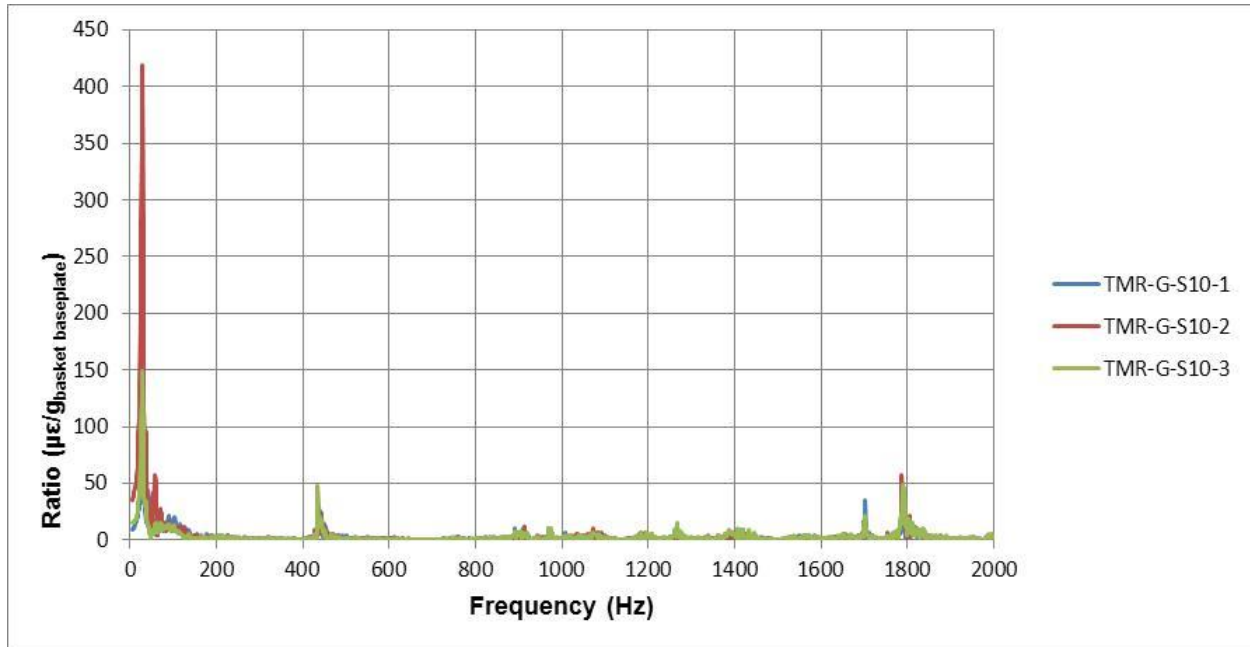


Figure 98. Vibration Test #5. Top-middle Rod, Span 10. Ratio of micro-strains to baseplate vertical acceleration (Channel 23) v. Hz.

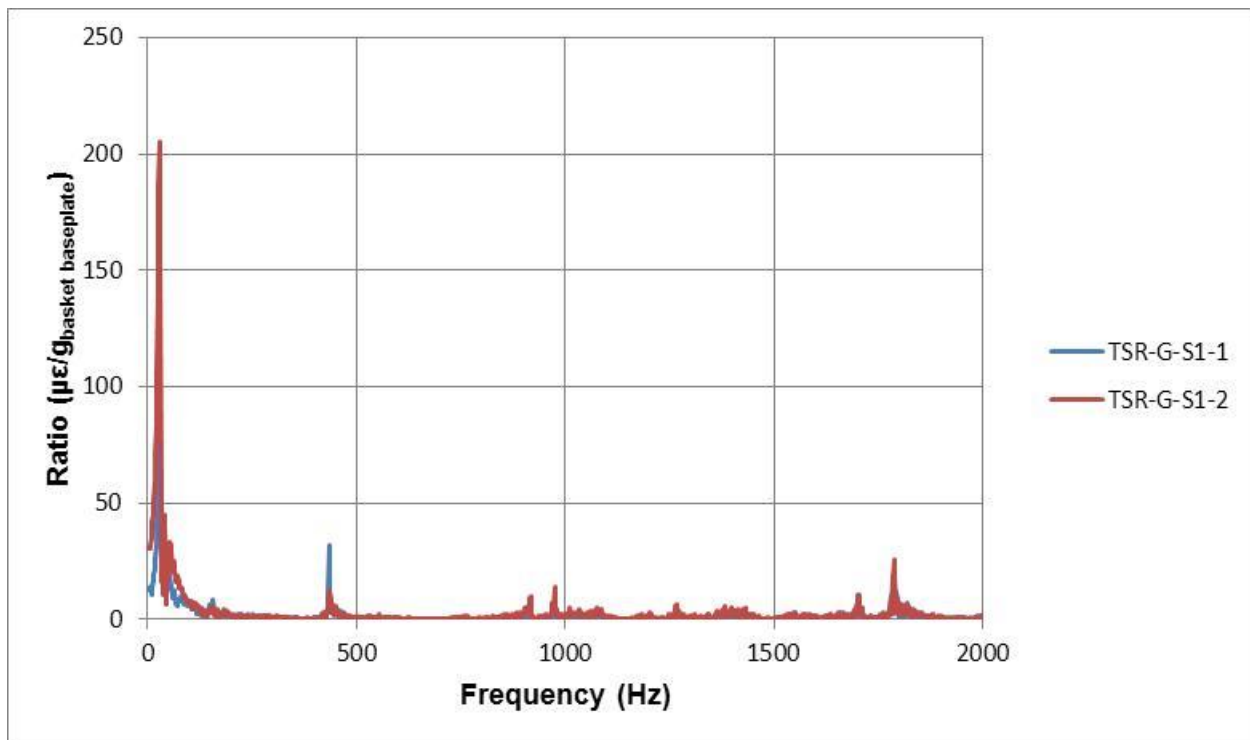


Figure 99. Vibration Test #5. Top-side Rod, Span 1. Ratio of micro-strains to baseplate vertical acceleration (Channel 23) v. Hz.

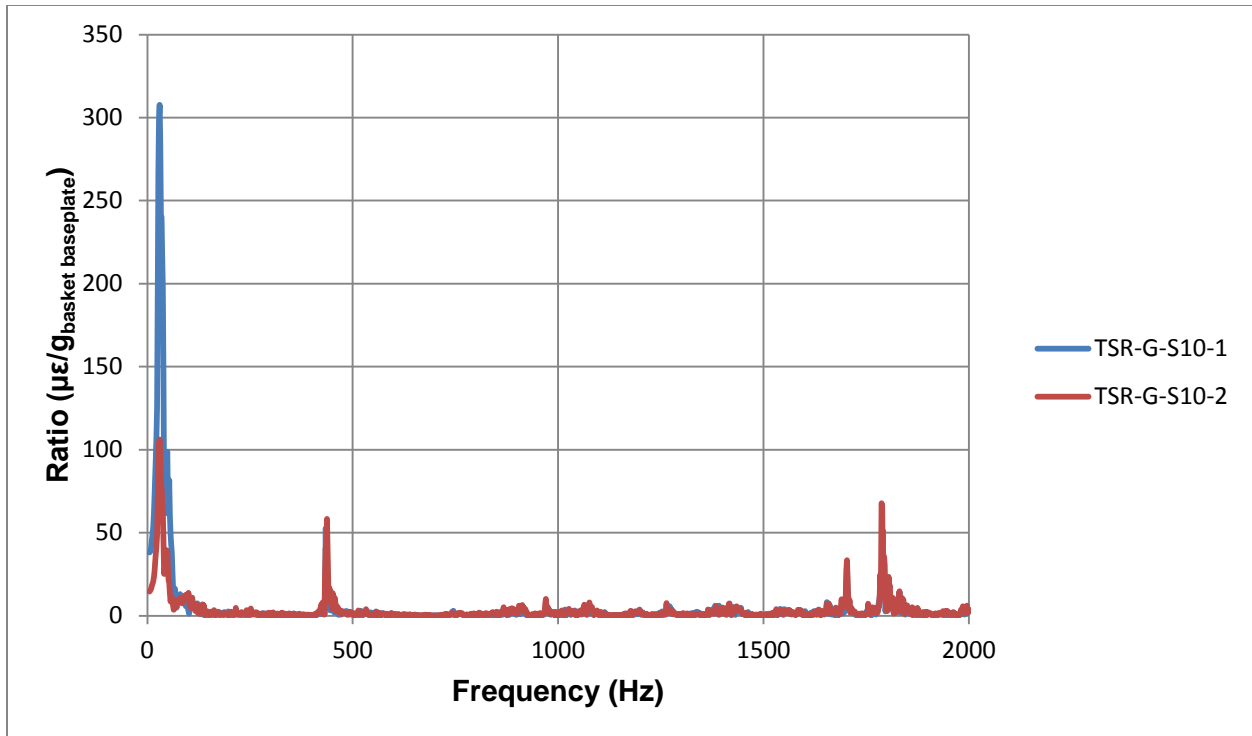


Figure 100. Vibration Test #5. Top-side Rod, Span 10. Ratio of micro-strains to baseplate vertical acceleration (Channel 23) v. Hz.

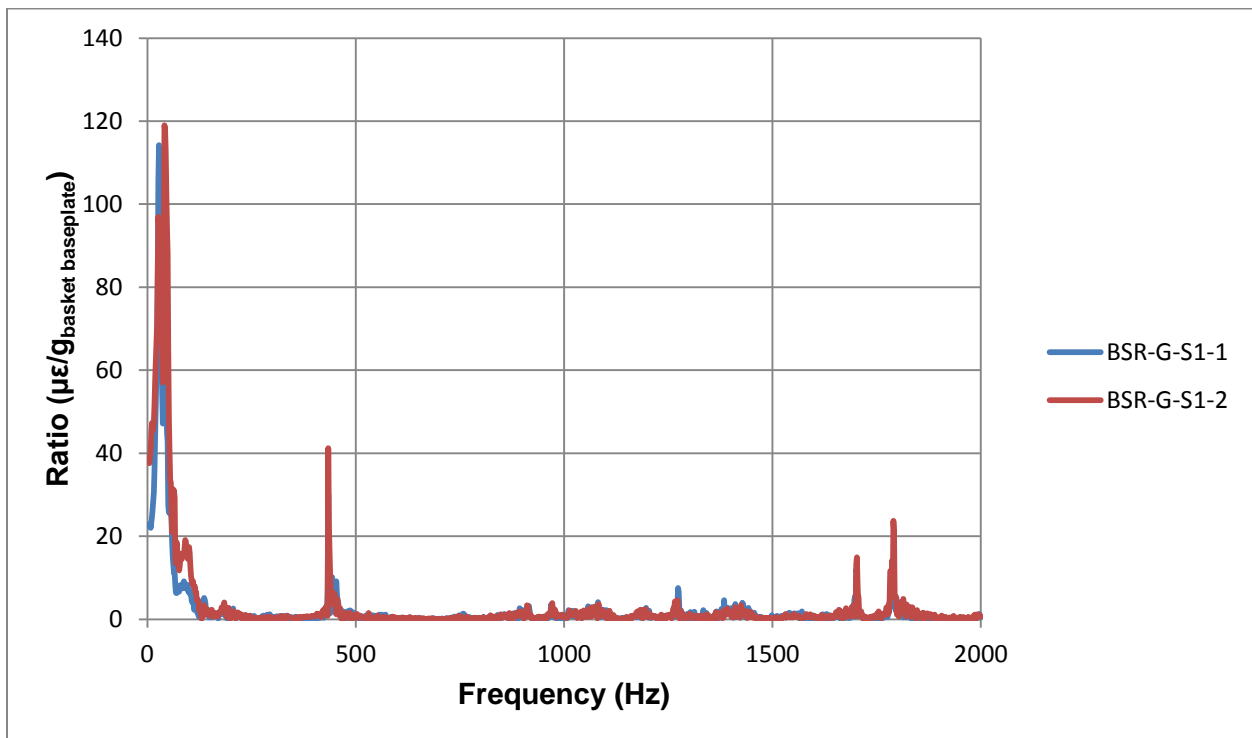


Figure 101. Vibration Test #5. Bottom-side Rod, Span 1. Ratio of micro-strains to baseplate vertical acceleration (Channel 23) v. Hz.

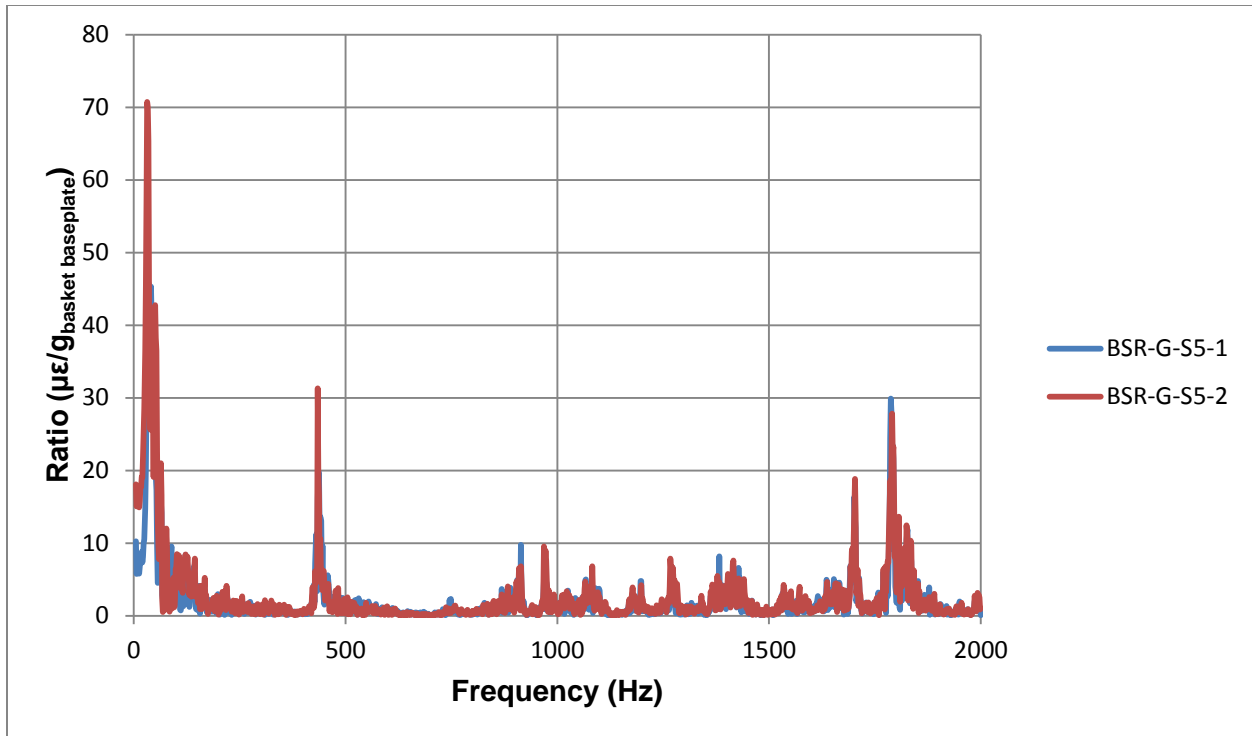


Figure 102. Vibration Test #5. Bottom-side Rod, Span 5. Ratio of micro-strains to baseplate vertical acceleration (Channel 23) v. Hz

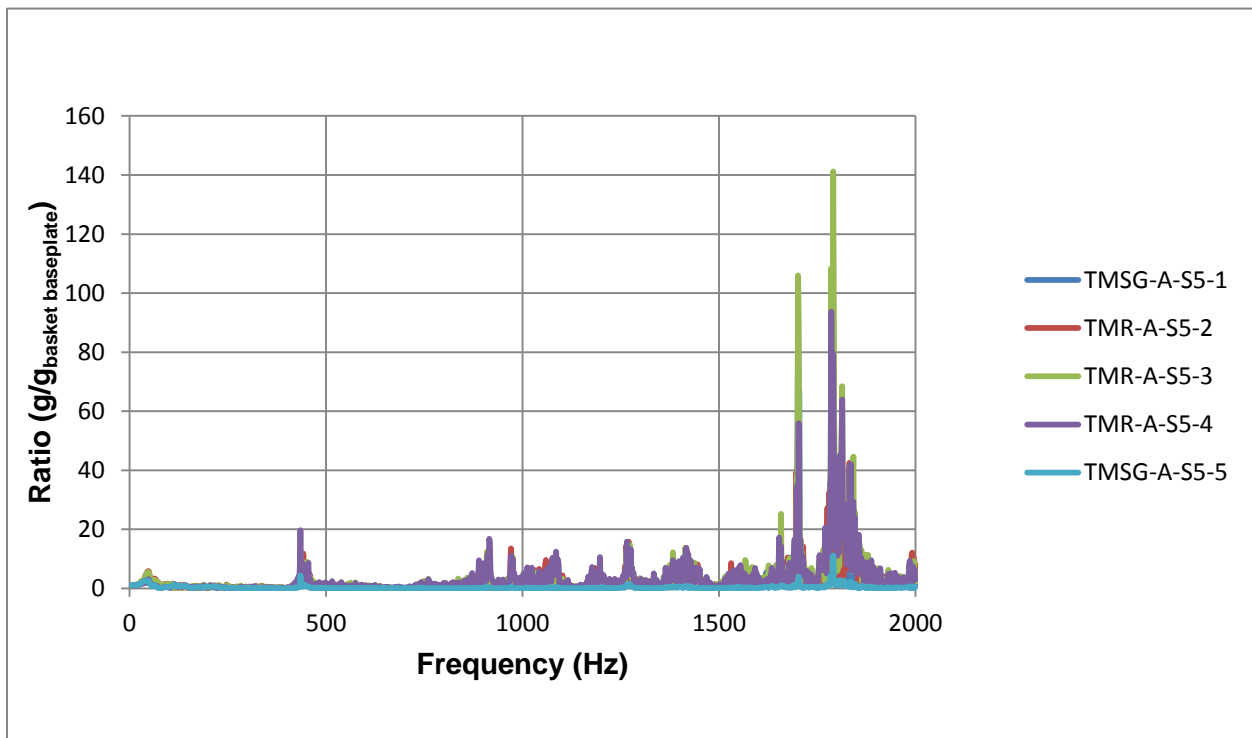


Figure 103. Vibration Test #5. Top-middle spacer grids and rod, Span 5. Ratio of assembly accelerations to baseplate vertical acceleration v. Hz.

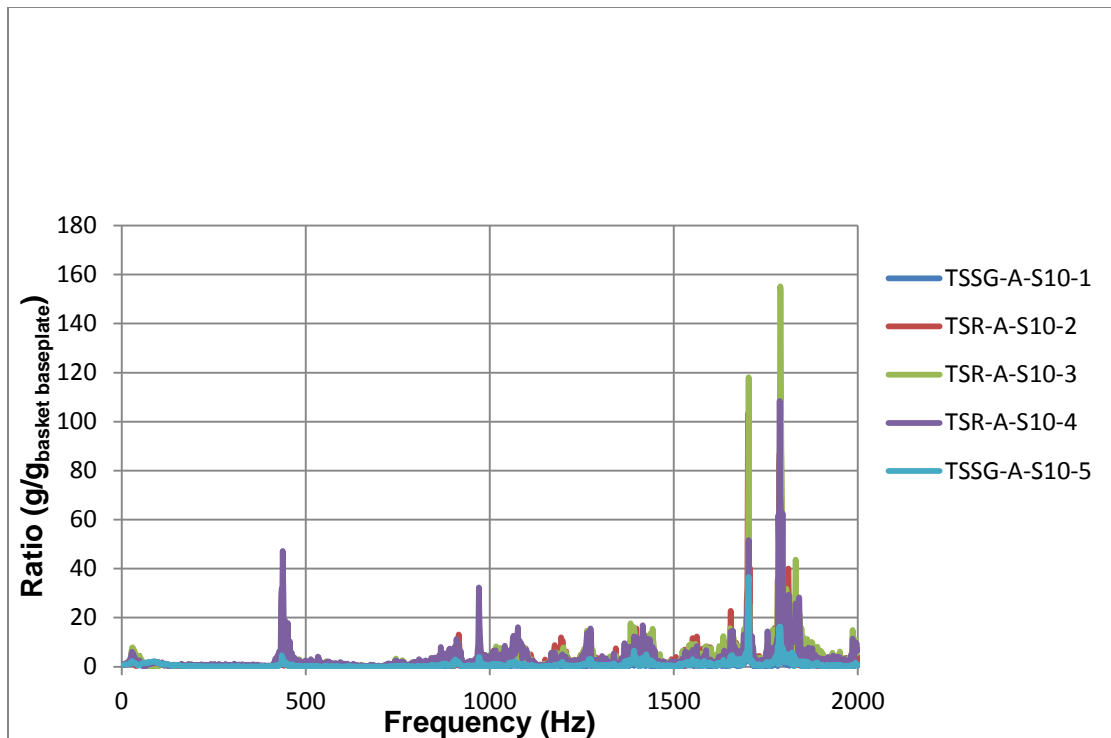


Figure 104. Vibration Test #5. Top-side spacer grids and rod, Span 10. Ratio of assembly accelerations to baseplate vertical acceleration v. Hz.

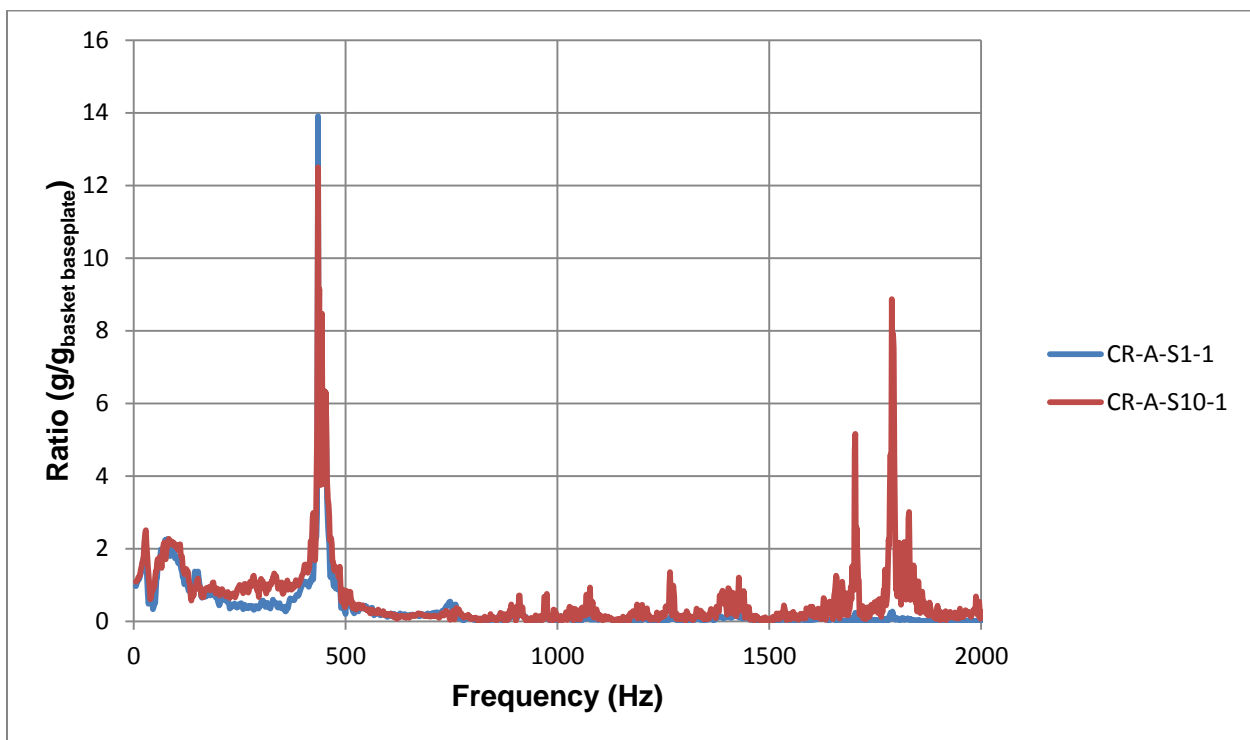


Figure 105. Vibration Test #5. Control rod. Ratio of control rod accelerations to baseplate vertical acceleration v. Hz.

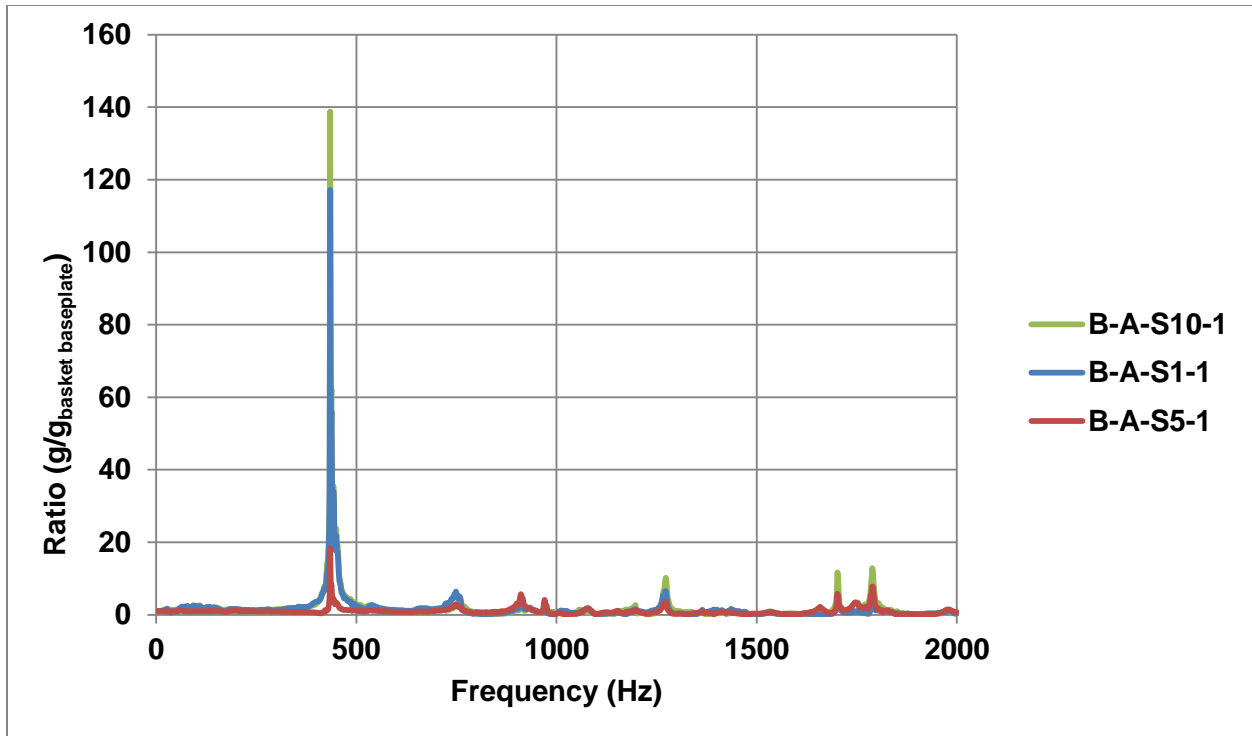


Figure 106. Vibration Test #5. Basket. Ratio of basket acceleration to baseplate vertical acceleration v. Hz.

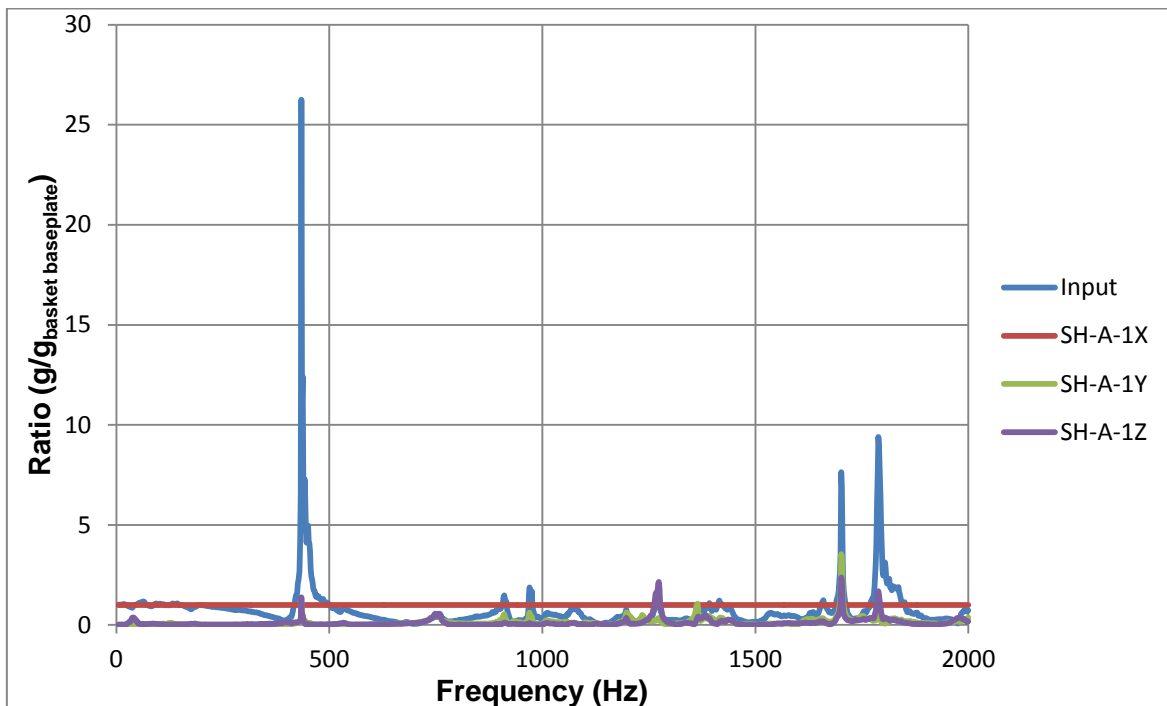


Figure 107. Vibration Test #5. Input (control) Accelerometer and Triaxial Basket Mounting Plate accelerometers. Ratio of accelerations to baseplate vertical acceleration (Channel 23) v. Hz.

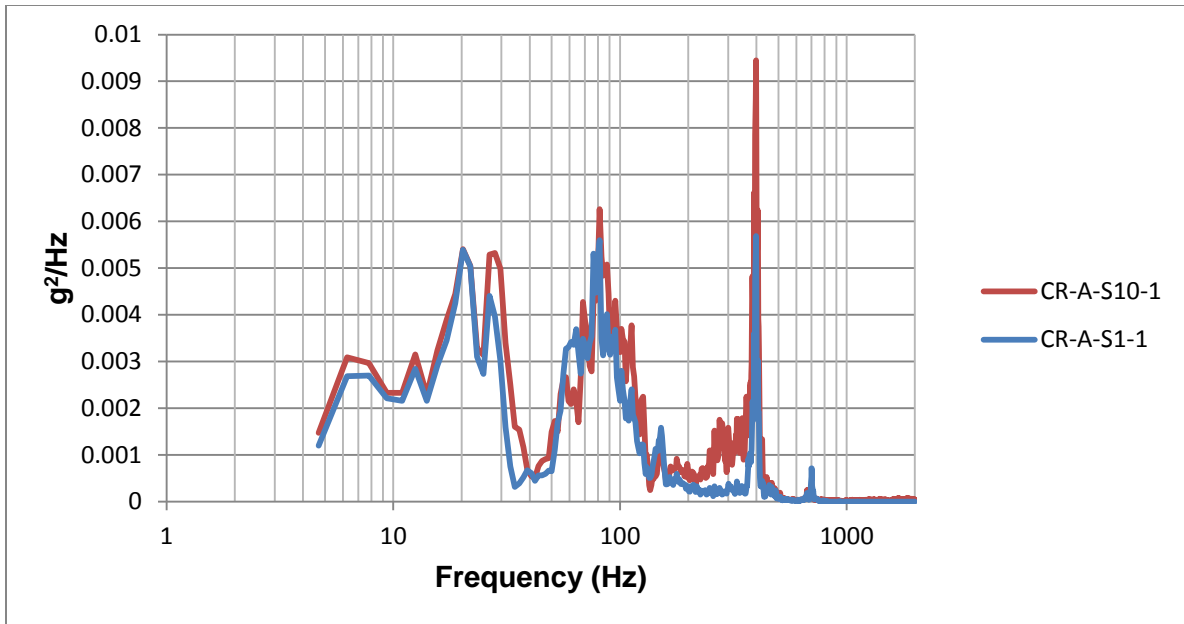


Figure 108. Vibration Test #5. Control Rod. Acceleration Power Spectral Density v. Hz.

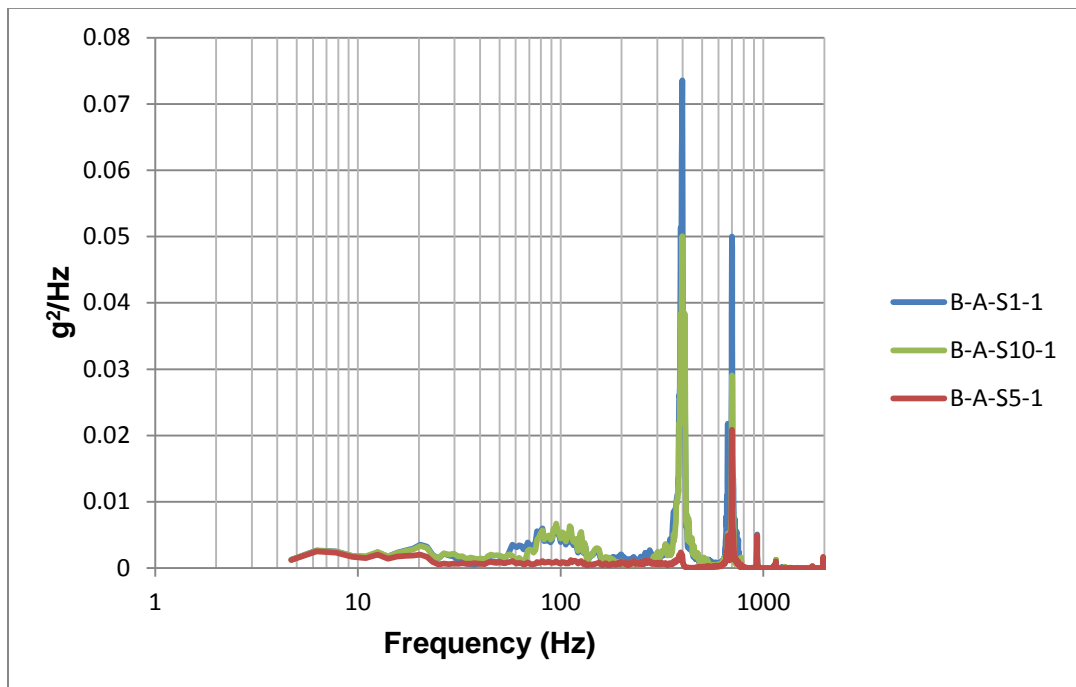


Figure 109. Vibration Test #5. Basket Acceleration Power Spectral Density v. Hz.

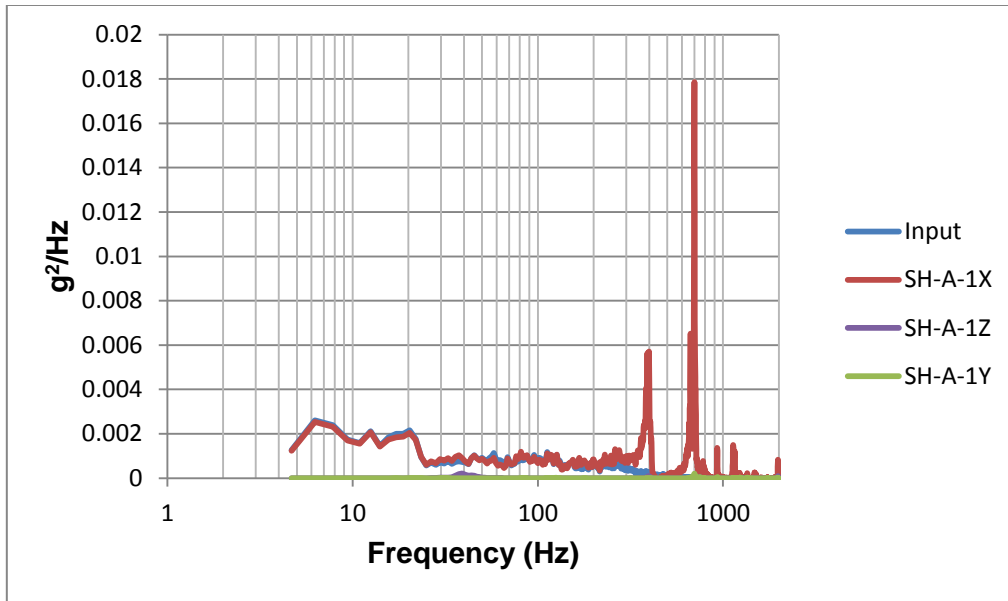


Figure 110. Vibration Test #5. Input (Control) and Triaxial Baseplate Acceleration Power Spectral Density v. Hz.

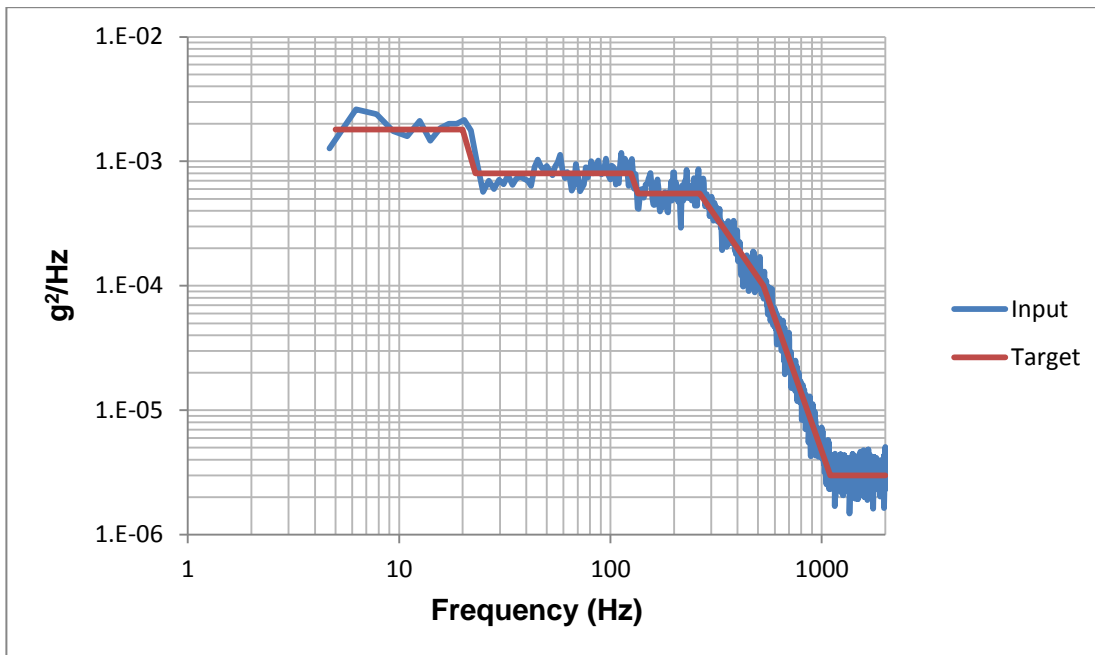


Figure 111. Vibration Test #5. Target Data Input to Shaker Control System v. Input (Control) (Channel 1) Acceleration Power Spectral Density v. Hz.

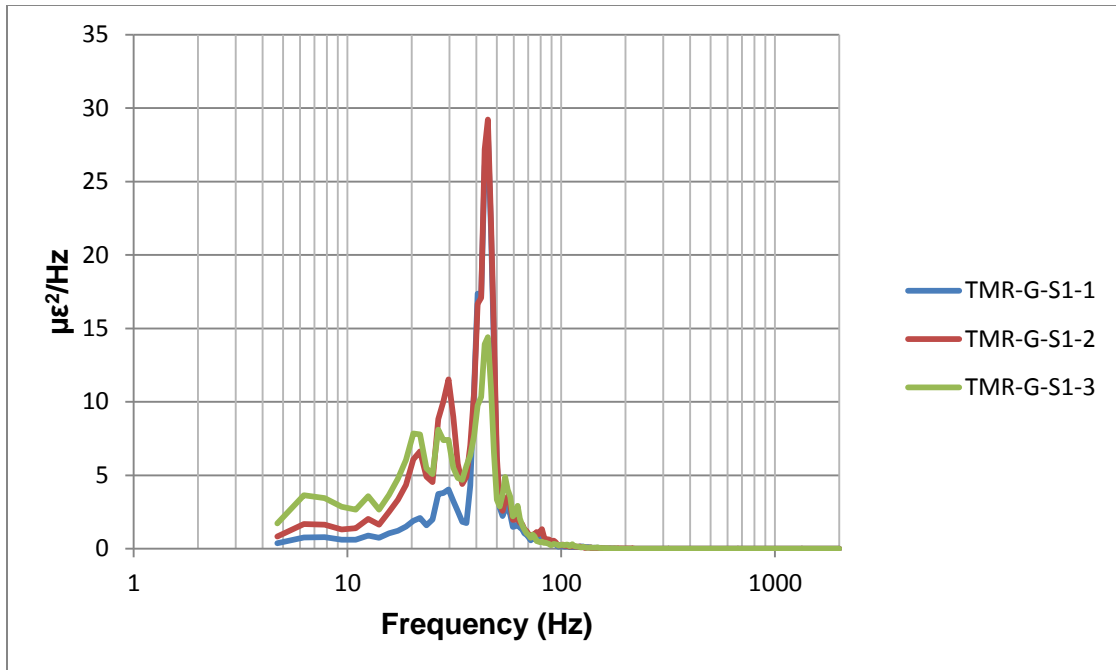


Figure 112. Vibration Test #5. Top-middle Rod, Span 1 Micro-strain Power Spectral Density v. Hz.

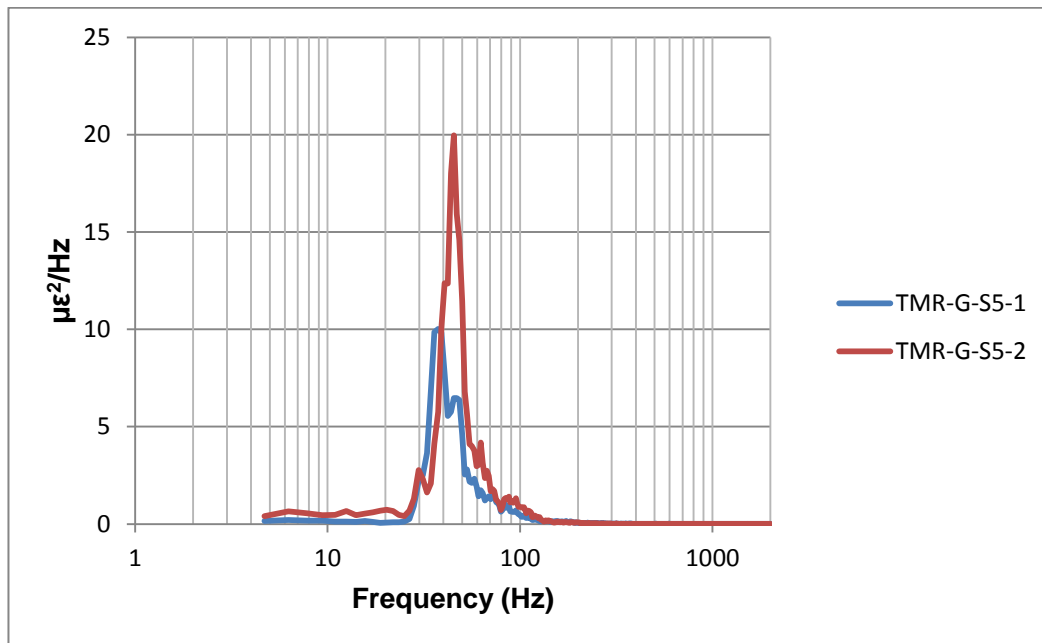


Figure 113. Vibration Test #5. Top-middle Rod, Span 5 Micro-strain Power Spectral Density v. Hz.

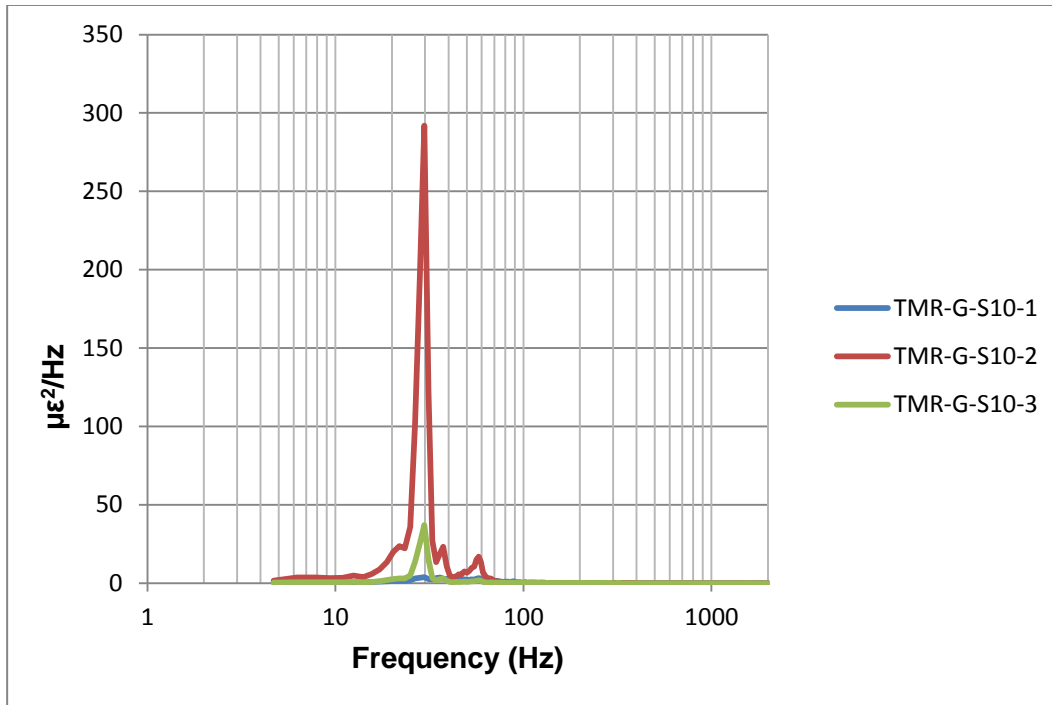


Figure 114. Vibration Test #5. Top-middle Rod, Span 10 Micro-strain Power Spectral Density v. Hz.

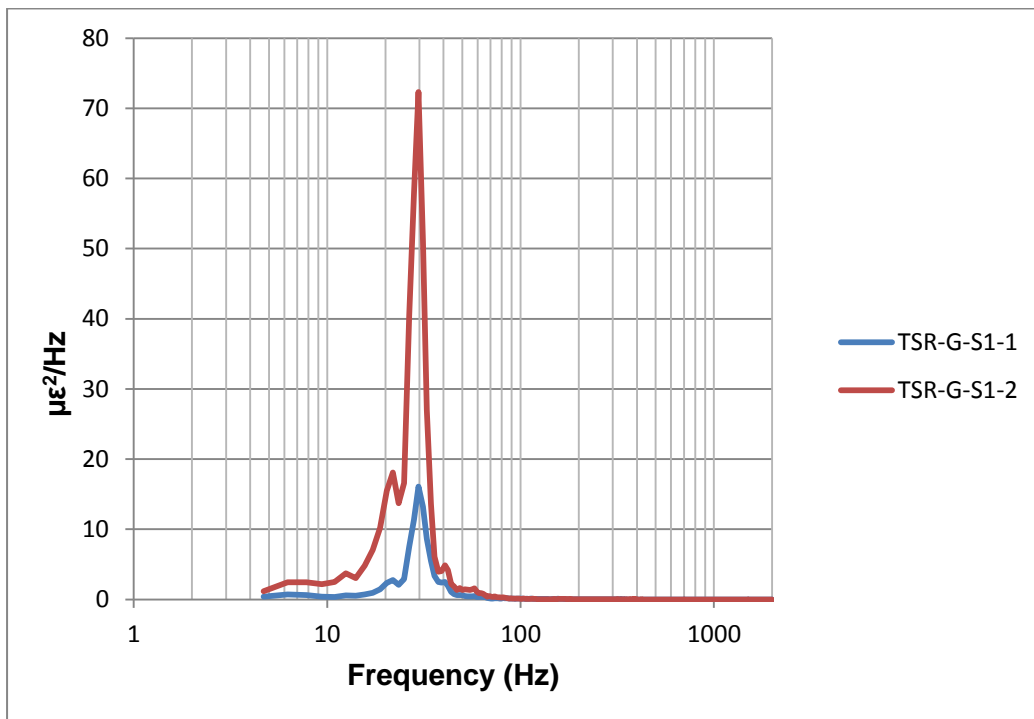


Figure 115. Vibration Test #5. Top-side Rod, Span 1 Micro-strain Power Spectral Density v. Hz.

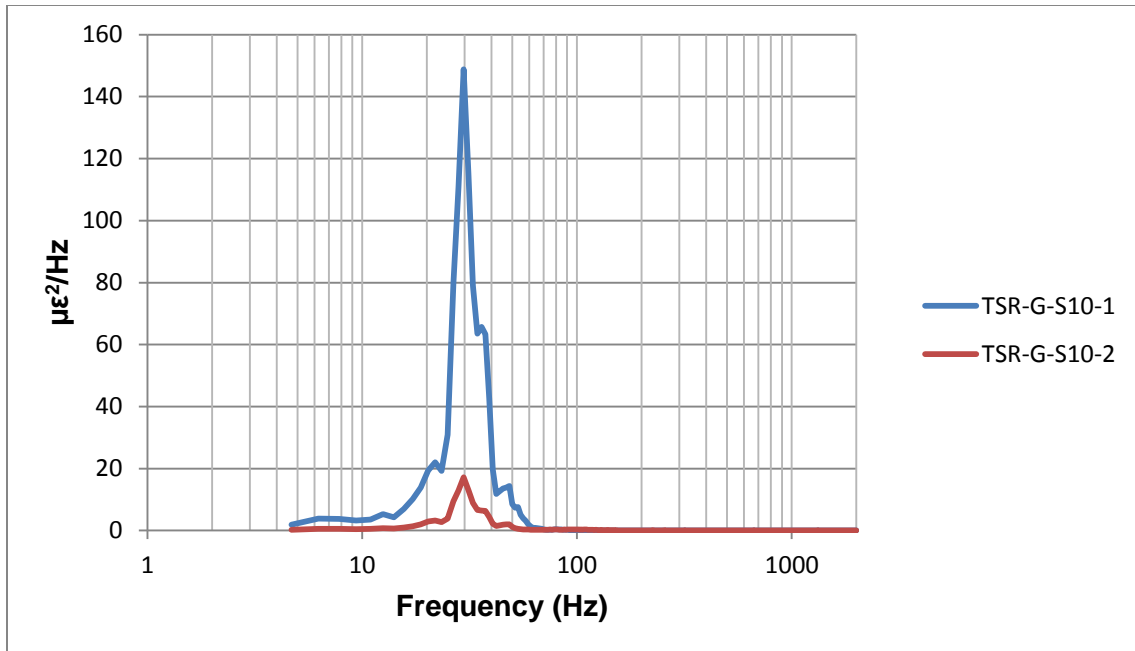


Figure 116. Vibration Test #5. Top-side Rod, Span 10 Micro-strain Power Spectral Density v. Hz.

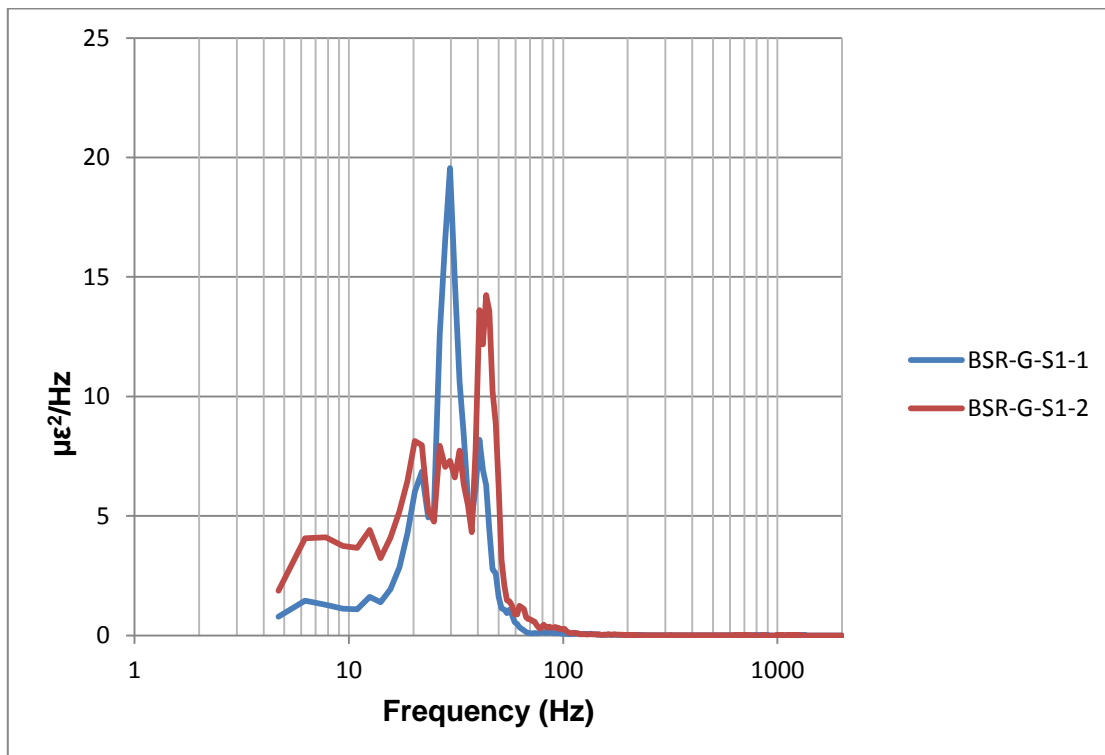


Figure 117. Vibration Test #5. Bottom-side Rod, Span 1 Micro-strain Power Spectral Density v. Hz.

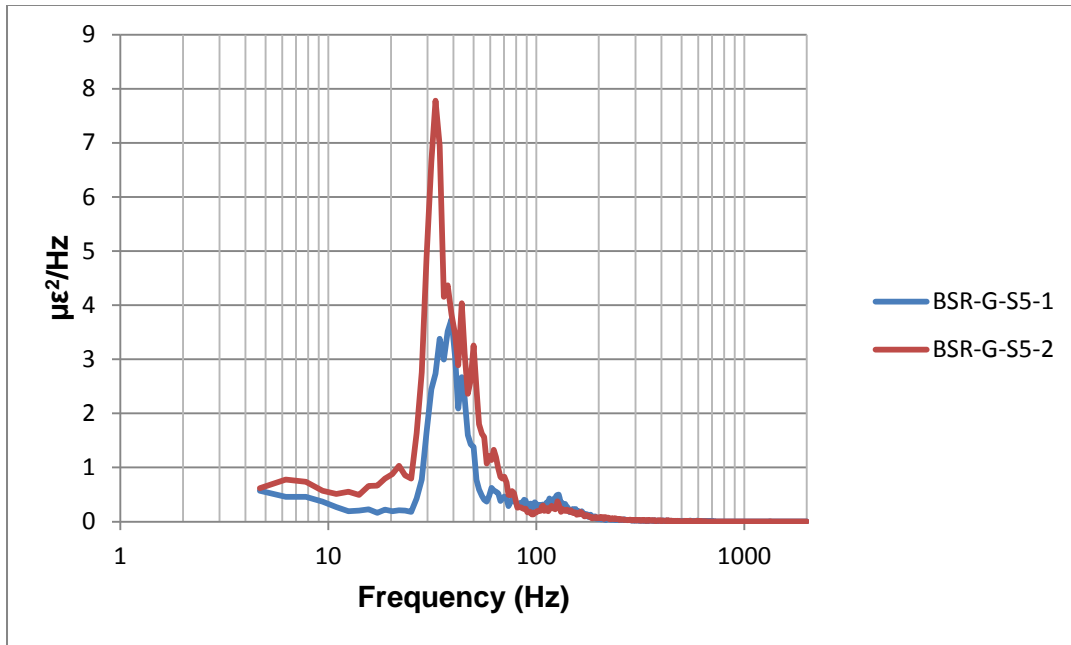


Figure 118. Vibration Test #5. Bottom-side Rod, Span 5 Micro-strain Power Spectral Density v. Hz.

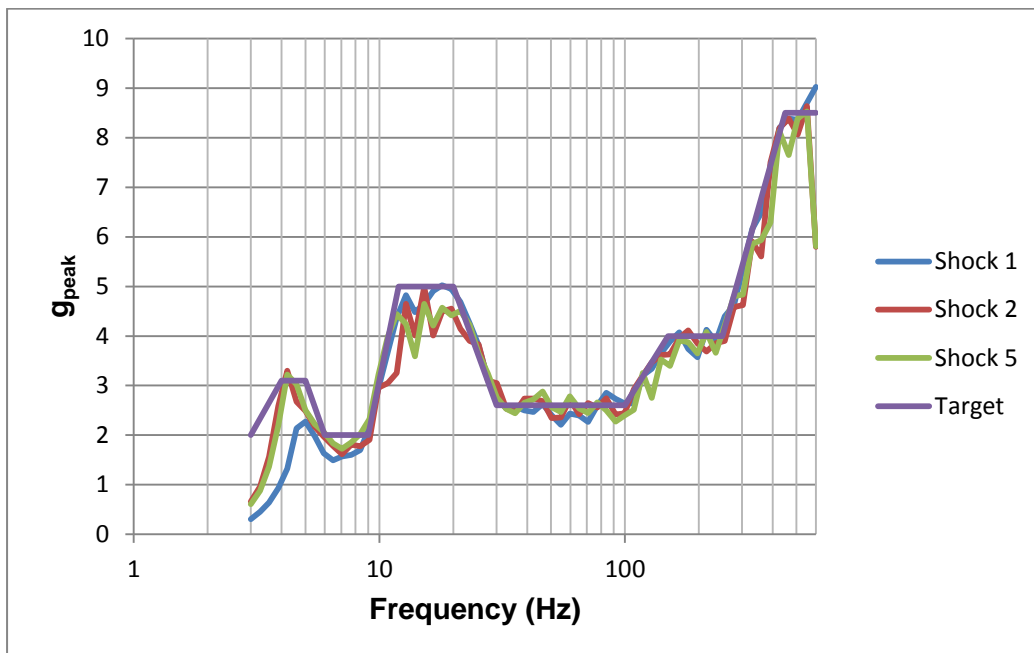


Figure 119. Target Data Input to Shaker Control System v. Peak Accelerations for Shock Tests #1, #2, and #5 v. Hz.

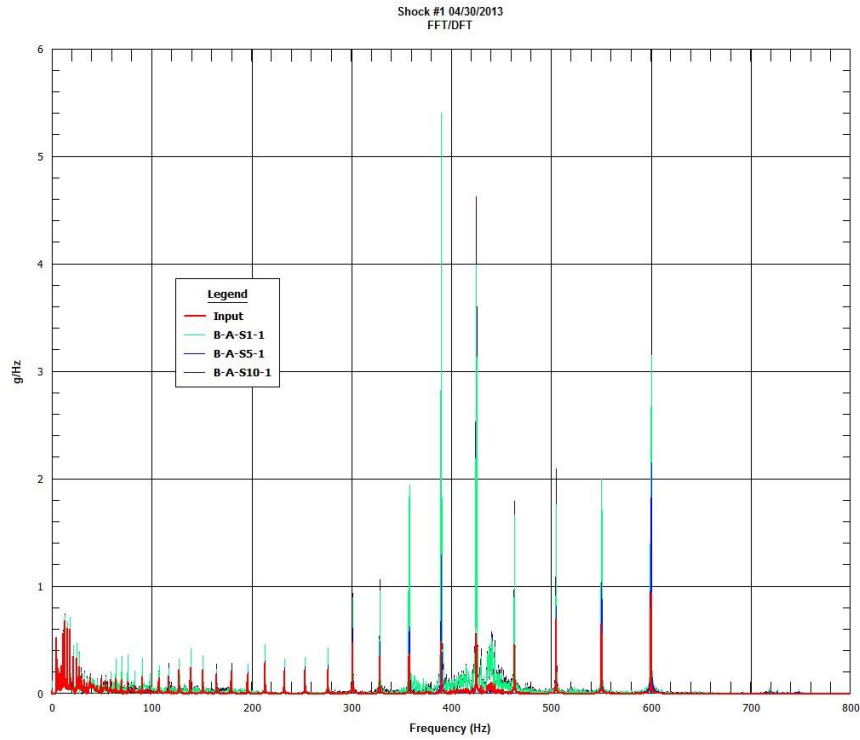


Figure 120. Shock Test #1. Input (Control, Channel 1) and Basket Accelerations Fast Fourier Transformation.

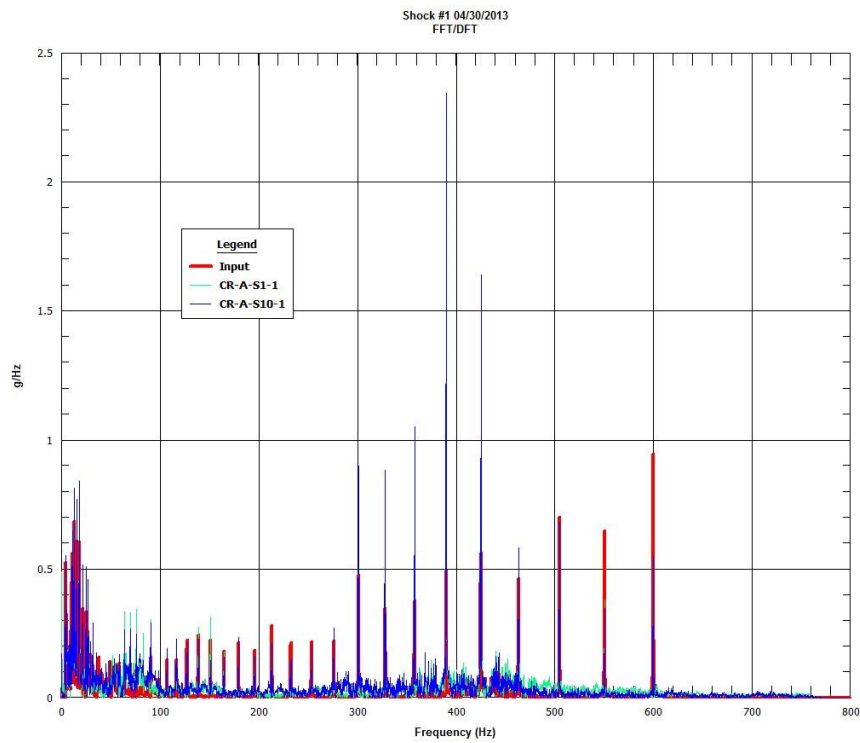


Figure 121. Shock Test #1. Input (Control, Channel 1) and Control Rod Accelerations Fast Fourier Transformation.

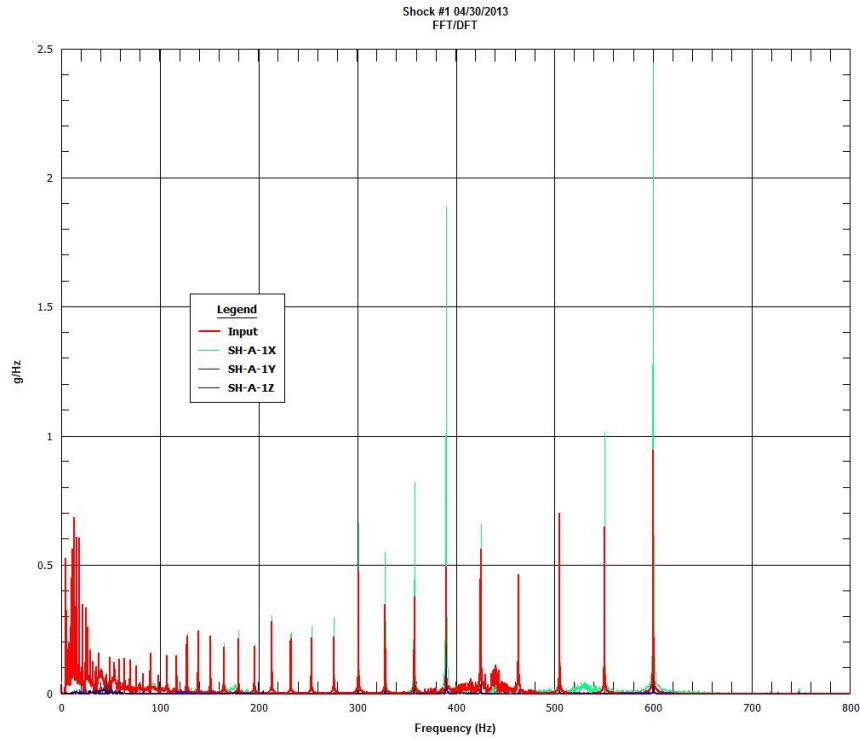


Figure 122. Shock Test #1. Input (Control, Channel 1) and Baseplate Triaxial Accelerations Fast Fourier Transformation.

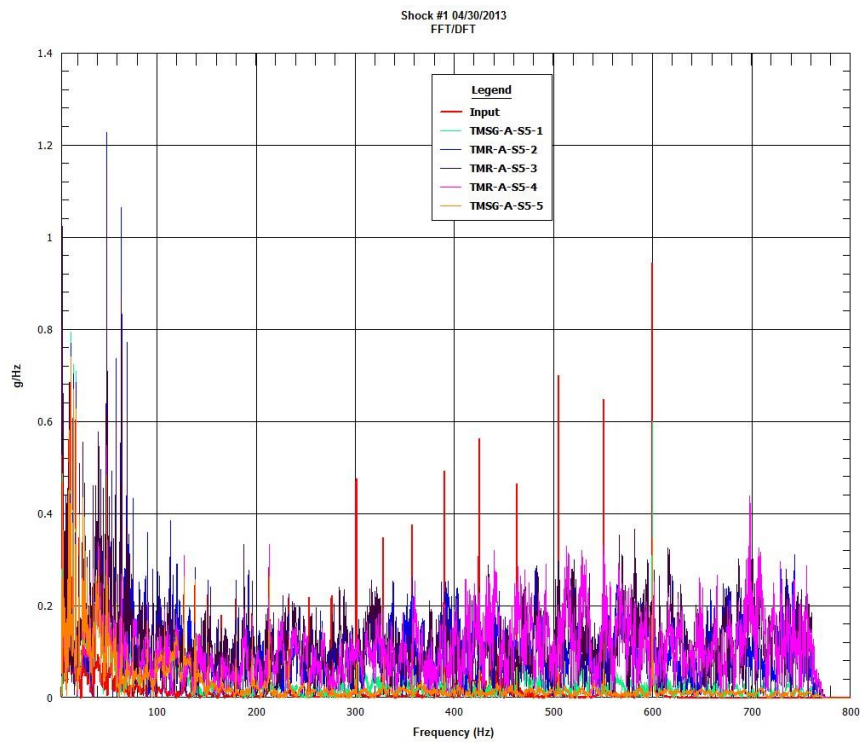


Figure 123. Shock Test #1. Input (Control, Channel 1) and Top-middle Spacer Grids and Rod, Span 5 Accelerations Fast Fourier Transformation.

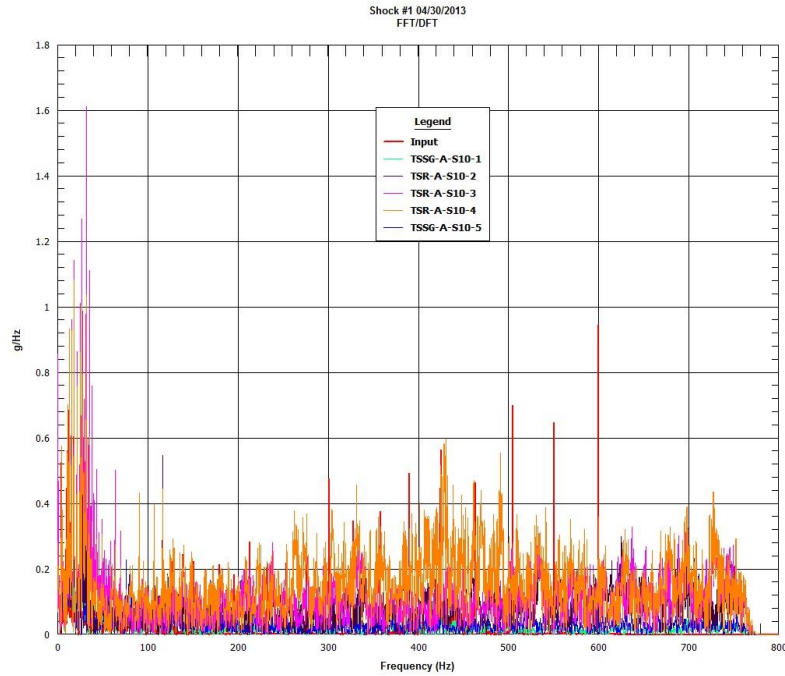


Figure 124. Shock Test #1. Input (Control, Channel 1) and Top-side Spacer Grids and Rod, Span 10 Accelerations Fast Fourier Transformation.

NOTE: The rods responded to the input accelerations at all frequencies.

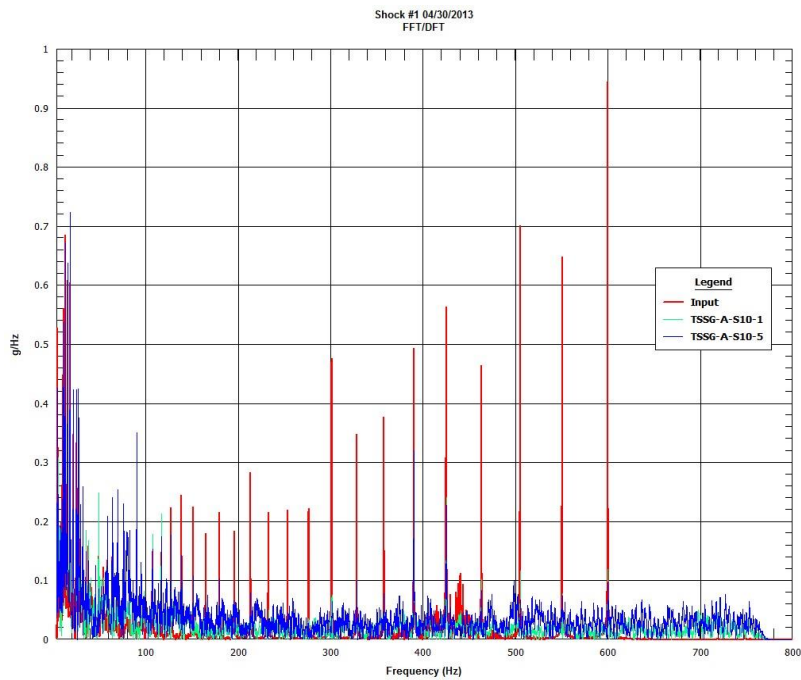


Figure 125. Shock Test #1. Input (Control, Channel 1) and Top-side Spacer Grids, Span 10 Accelerations Fast Fourier Transformation.

NOTE: The assembly spacer grids did not respond to the input accelerations beyond approximately 200Hz.

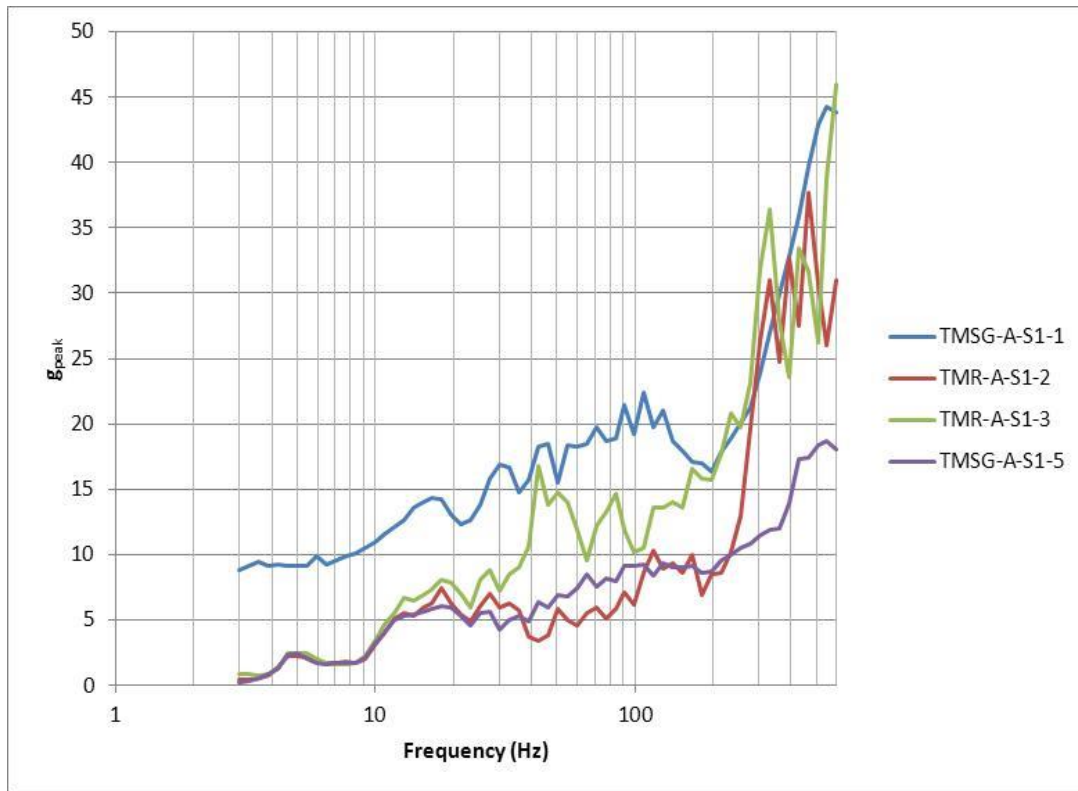


Figure 126. Shock Test #1 Shock Response Spectra. Top-middle Rod and Spacer Grids, Span 1, Accelerometers.

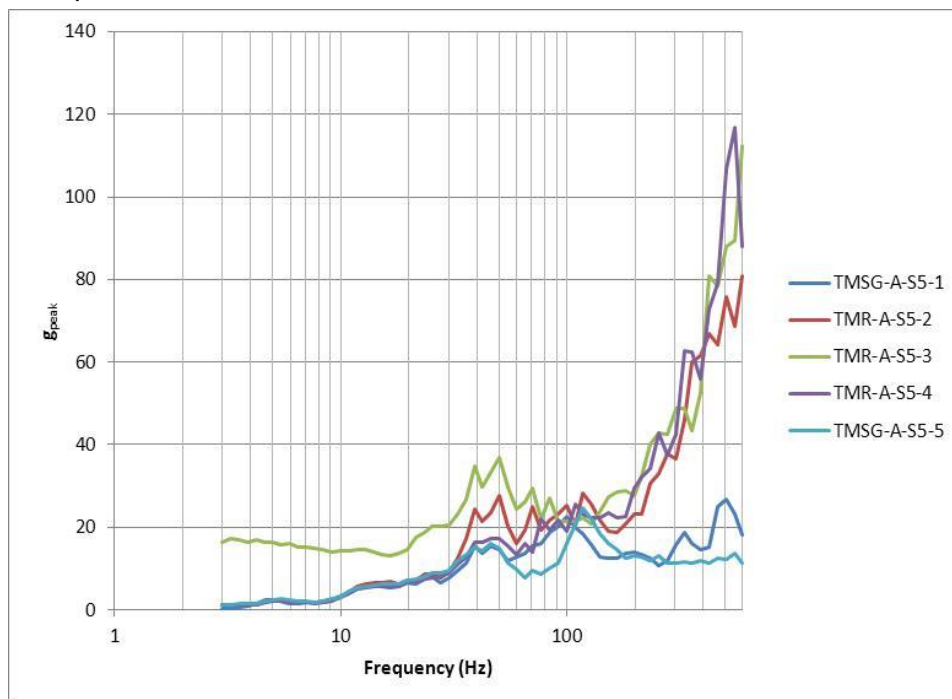


Figure 127. Shock Test #1 Shock Response Spectra Top-middle Rod and Spacer Grids, Span 5, Accelerometers.

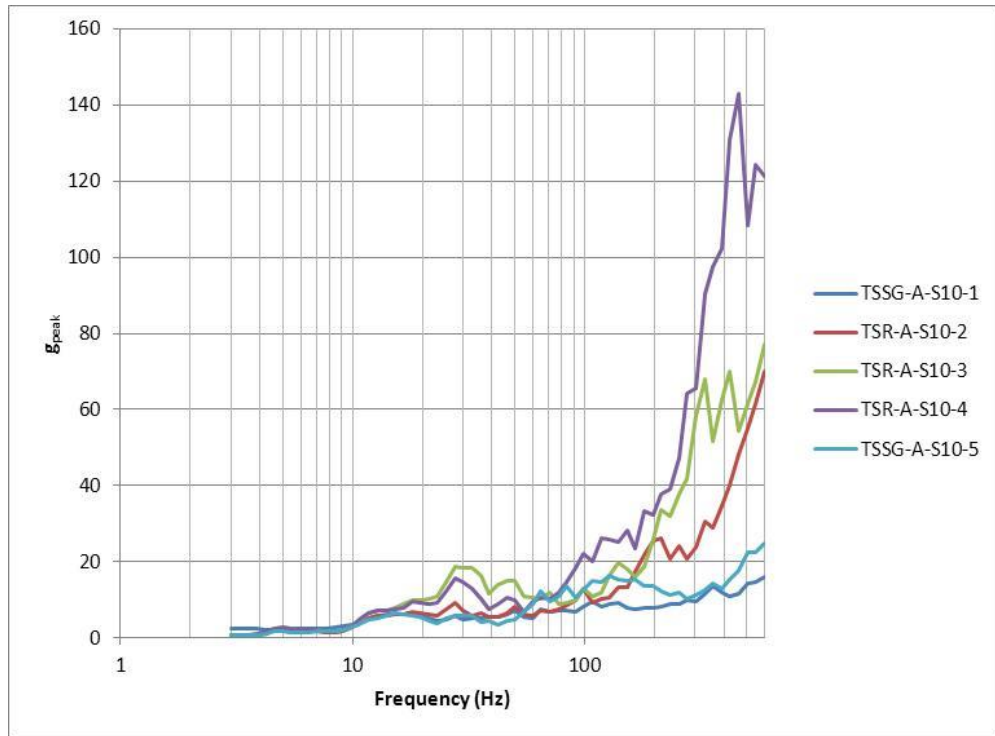


Figure 128. Shock Test #1 Shock Response Spectra Top-side Rod and Spacer Grids, Span 10, Accelerometers.

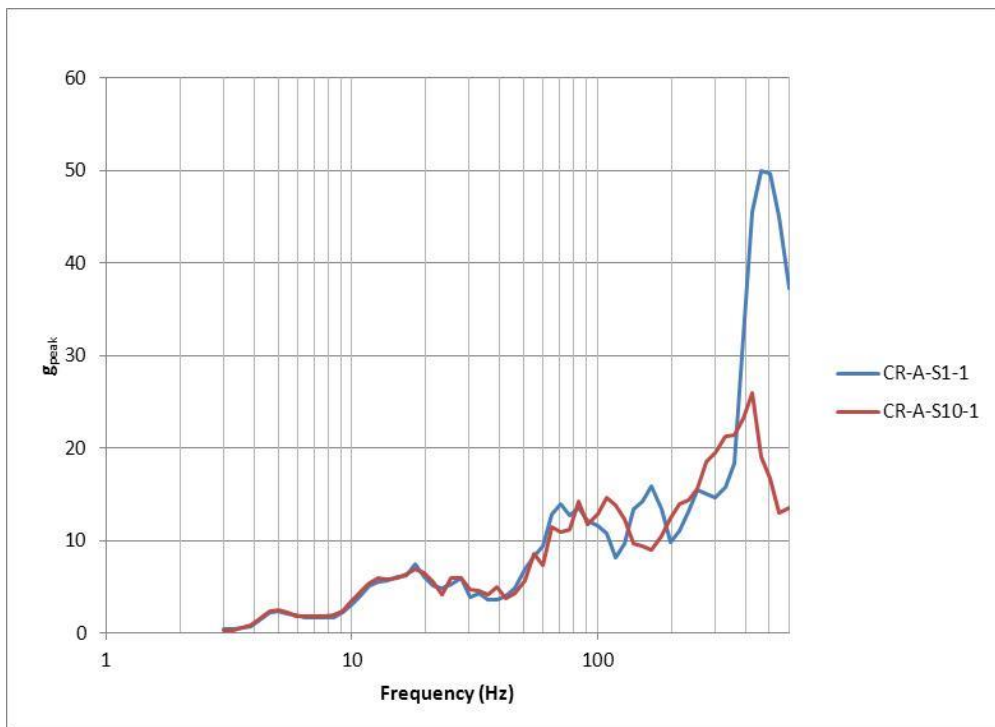


Figure 129. Shock Test #1 Shock Response Spectra Control Rod Accelerometers.

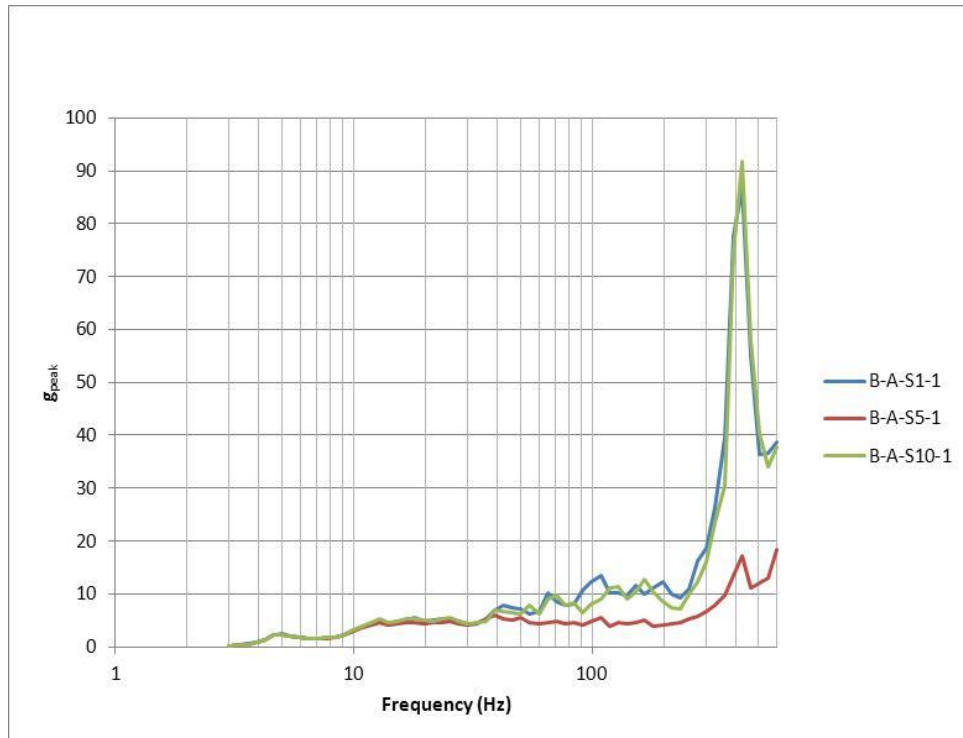


Figure 130. Shock Test #1 Shock Response Spectra Basket Accelerometers.

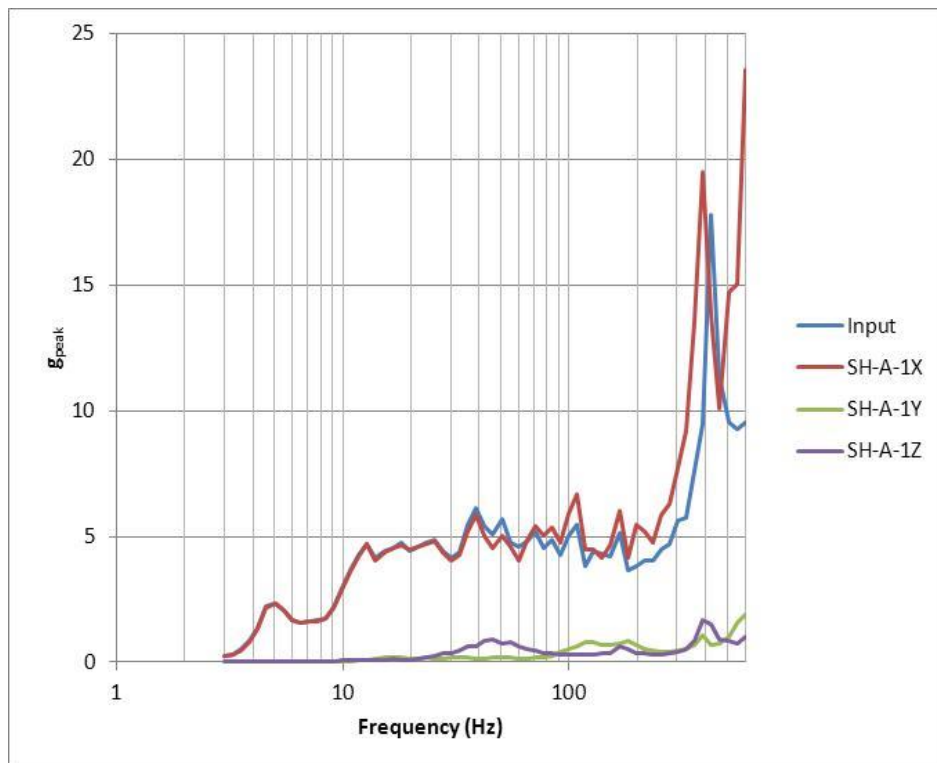


Figure 131. Shock Test #1 Shock Response Spectra INPUT/CONTROL and Triaxial Baseplate Accelerometers.

#### 4.4.6 Post-test Examination of Zircaloy Rods and Spacer Grids

After the tests were completed the basket was disassembled and the top-middle Zircaloy-4 rod was pulled a few inches in order to examine the region under the spacer grids to determine if the spacer-grid springs caused wear or damage to the rods. The tops of the spacer grids on the assembly were also examined to determine if there was damage possibly due to the assembly impacting the inner side of the basket top plate during the vibration/shock tests. Figures 132 – 135 illustrate the results of this examination.

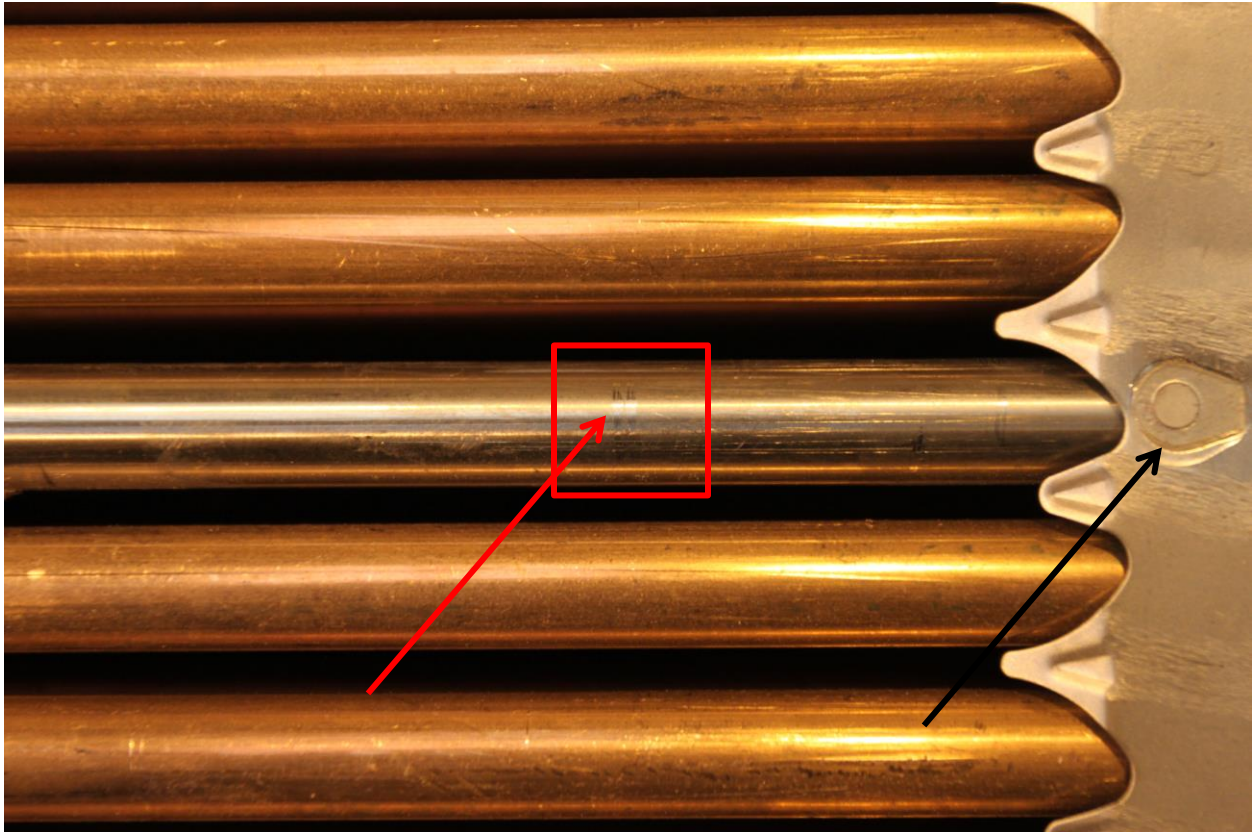


Figure 132. The bottom of the top-middle Zircaloy-4 rod at the bottom end of the assembly.

NOTE: The red box brackets the region of the rod that was within the spacer grid (partially shown on the right). The red arrow points to two regions of circumferential wear on the rod presumably caused by the spacer-grid springs during testing. The estimated depth of the wear is approximately 0.001 inch (0.025mm).

The black arrow shows deformation of the adhesive used to attach the accelerometer on the spacer grid. Upon disassembly of the basket this accelerometer was noted to have been detached from the spacer grid. The deformation is presumably due to impact of the accelerometer / assembly on the inner side of the top basket plate during testing (see Figure 135).

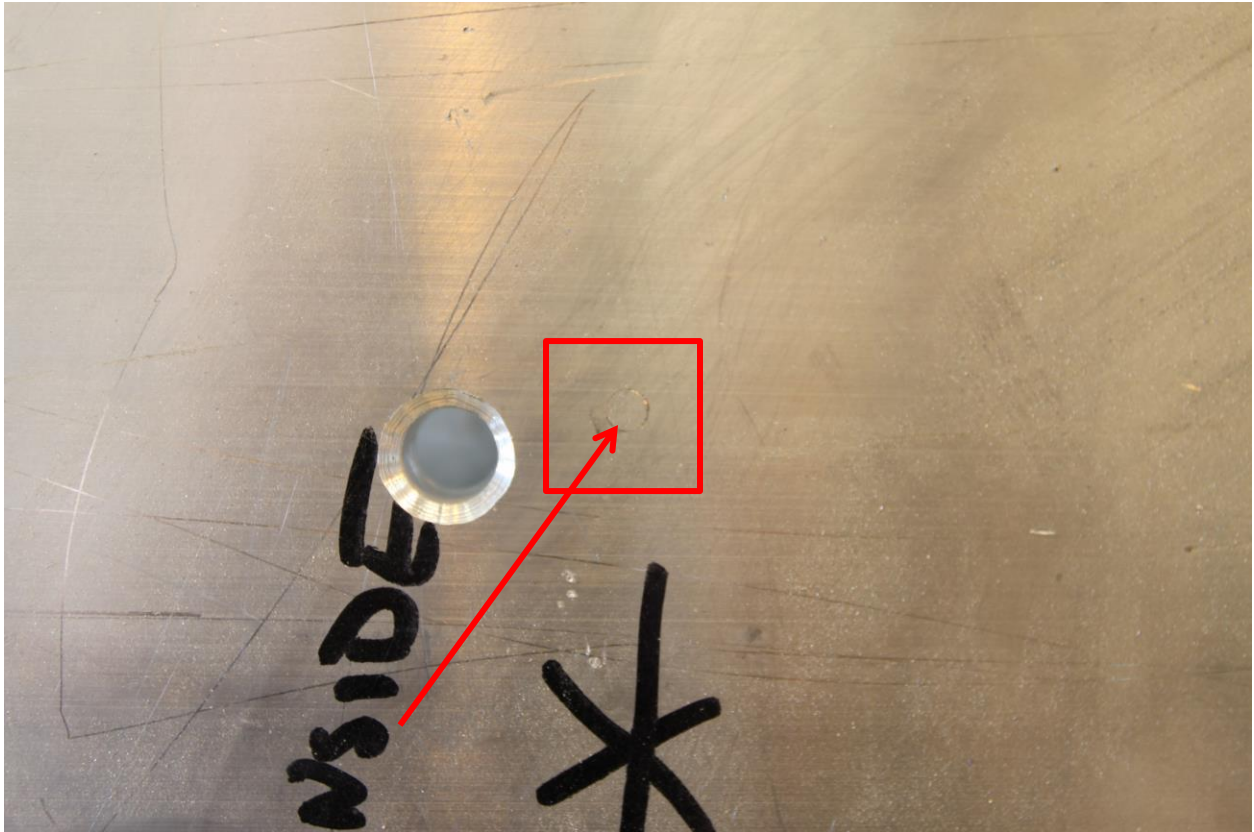


Figure 133. The inner side of the top basket plate.

NOTE: The red box brackets the region (red arrow) of the plate that was impacted by the accelerometer attached to the assembly spacer grid (see Figure 132).

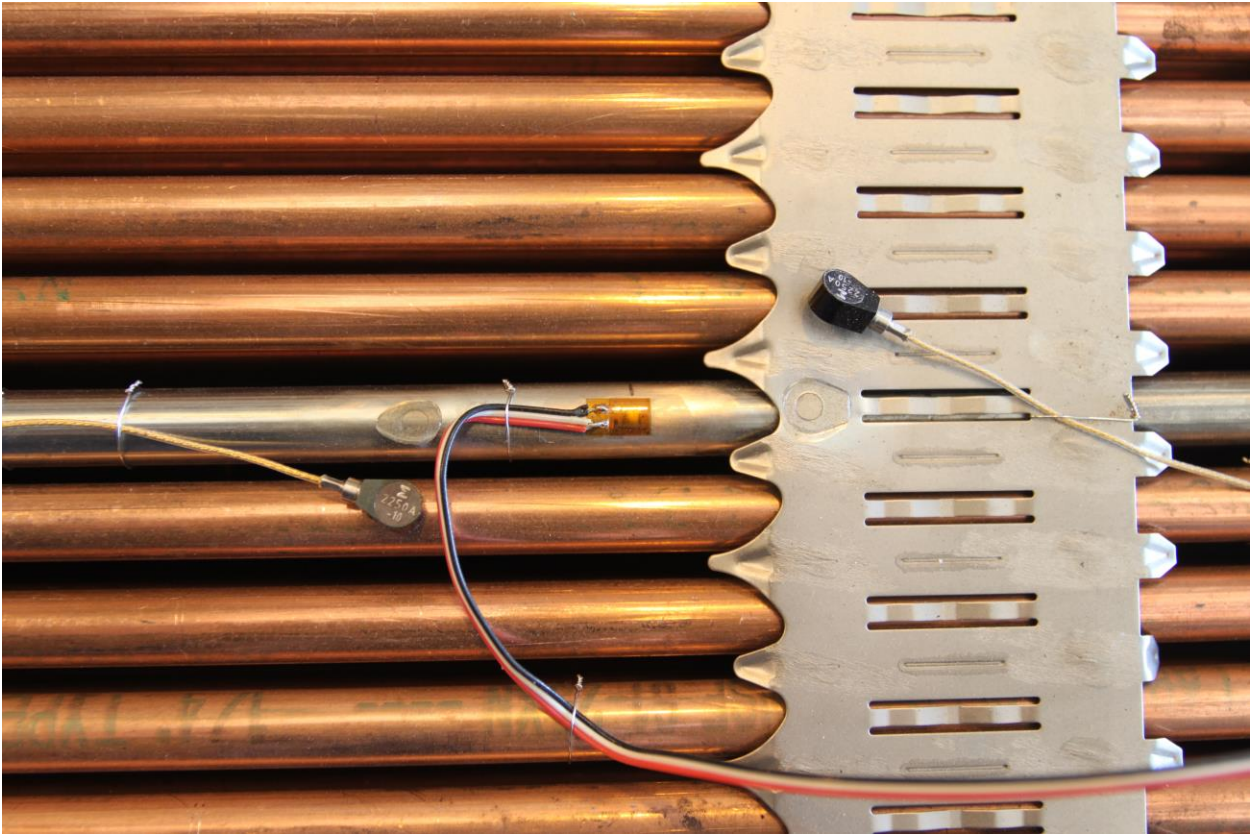


Figure 134. The top of the assembly, bottom end, showing top-middle Zircaloy-4 rod and adjacent spacer grid.

NOTE: The two accelerometers are detached presumably due to impact with the inner side of the basket top plate. Notice also the deformation of the adhesive used to attach the accelerometers on the rod and spacer grid due to this impact. The strain gauge and the region of the rod to its right are shown in Figure 135.

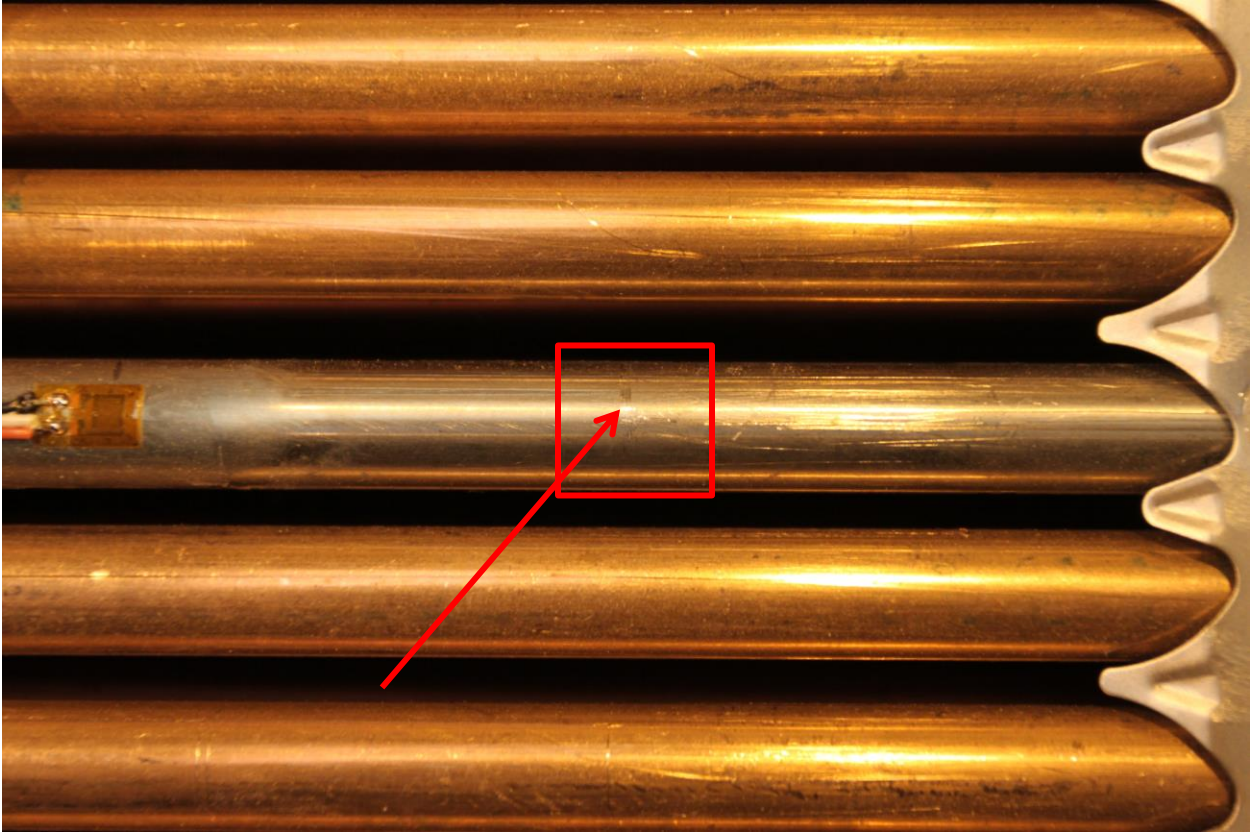


Figure 135. The top of the top-middle Zircaloy-4 rod at the bottom end of the assembly (with strain gauge attached). The box brackets the region of the rod that was within the spacer grid (partially shown on the right). The arrow points to a region of circumferential wear on the rod presumably caused by the spacer-grid springs during testing. The estimated depth of the wear is approximately 0.001 inch (0.025mm).

## 5. CONCLUSIONS AND RECOMMENDATIONS

A series of shaker tests of a surrogate PWR fuel assembly in a basket subjected to shock and vibration loading conditions closely matching those expected to occur during normal conditions of truck transport was conducted to measure the strains and accelerations on the rods and test unit.

The strains measured on the rods were very small, ranging from 35 to 213  $\mu\text{in./in.}$  ( $\mu\text{m/m}$ ). These strains are so low relative to the elastic limit of unirradiated and irradiated Zircaloy-4 that failure of the rods during NCT seems unlikely due to a strain-, or stress-, or fracture mechanics-based failure mode.

The shaker loadings applied to the test unit were based on shock and vibrations measured on casks during actual transport by truck. As most UNF will be transported by rail, the shaker tests should be repeated using data obtained from an appropriate rail transport data set.

The shaker tests simulated the configuration of an assembly in a basket within an actual cask on a truck trailer being transported on typical highways with the shaker simulating the truck trailer. The basket/assembly test unit was not within a cask when on the shaker. Tests should be conducted using actual truck casks and baskets, but preferably a rail cask, using the assembly used in the shaker tests, or an assembly with a full complement of zirconium alloy rods to measure the strains on those rods under more realistic conditions. Interactions with industry to procure a cask that could be used to perform such tests should be pursued.

The 1-ft (0.3-m) free drop of a cask containing an instrumented assembly should be performed to fully assess the response of fuel rods to all loadings defined for normal conditions of transport [1].

The data from the shaker tests provide information on the strains applied to fuel rods during normal conditions of truck transport. More data must be generated on high-burnup, long-term, aged Zircaloy to further assess the affect these strains have on UNF. The UFD Storage & Transportation Experimental activities to generate material property data should be continued to obtain the required data.



Figure 136. Observers of the assembly shaker tests, April 30, 2013.  
Left to right: Harold Adkins, PNNL; Sylvia Saltzstein, SNL; Brady Hanson, PNNL; and Ken Sorenson, Greg Koenig, Robert Wauneka, Paul McConnell, John Bignell, SNL.

## 6. REFERENCES

- [1] Code of Federal Regulations, Title 10, Part 71, “Packaging and Transportation of Radioactive Material”.
- [2] “Regulations for the Safe Transport of Radioactive Material,” Specific Safety Requirements No. SSR-6, International Atomic Energy Agency, 2012.
- [3] Standard Review Plan for Transportation Packages for Radioactive Material, NUREG-1609, US Nuclear Regulatory Commission.
- [4a] Magnuson, Cliff F., “Shock and Vibration Environments for Large Shipping Container During Truck Transport (Part II),” SAND78-0337 and NRC NUREG/CR-0128, May 1978.
- [4b] Magnuson, Cliff F., “Shock and Vibration Environments for Large Shipping Container During Truck Transport (Part I),” SAND77-1110, September 1977.
- [5] Magnuson, C.F., “Shock Environments for Large Transport Containers During Rail-Coupling Operations,” Sandia National Laboratories, Albuquerque, NM, SAND79-2168, NUREG/CR-1277, June 1980.
- [6] Nicholas Klymyshyn, Scott Sanborn, Harold Adkins, and Brady Hanson, “Fuel Assembly Shaker Test Simulation,” FCRD-UFD-2013-000168, Pacific Northwest National Laboratory, May 30, 2013.
- [7] Nicholas Klymyshyn, “Shaker Table Modeling Progress Report,” #UFDCST-120927-1, Pacific Northwest National Laboratory, September 2012.
- [8] Ken Geelhood and Carl Beyer, “Used Nuclear Fuel Loading and Structural Performance Under Normal Conditions of Transport – Supporting Material Properties and Modeling Inputs,” Pacific Northwest National Laboratory, US Department of Energy Used Fuel Disposition Campaign Report FCRD-UFD-2013-000123, March 16, 2013.
- [9] Rashid, Y.R., R.O. Montgomery, W.F. Lyons, “Fracture Toughness Data for Zirconium Alloys – Application to Spent Fuel Cladding in Dry Storage,” Electric Power Research Institute Technical Progress Report 1001281, January 2001.
- [10] FITNET Annex A, “Stress intensity factor (SIF) solutions,” [ocw.unican.es/enseñanzas-tecnicas/.../otros.../soluciones\\_fit\\_fitnet .pdf](http://ocw.unican.es/enseñanzas-tecnicas/.../otros.../soluciones_fit_fitnet.pdf), May 2006.
- [11] Y. Dai, M. Rodig and J. Altes, “Calculation of the Stress Intensity Factor for a Partial Circumferentially Cracked Tube Loaded in Bending by Using the Shell Line-Spring Model,” *Fatigue Fract. Engng Mater. Struct.*, Vol. 14, No. 1, pp. 11-23, 1991.

## 7. BIBLIOGRAPHY RELATED TO ASSEMBLY SHAKER TEST

“Draft American National Standard Design Basis for Resistance to Shock and Vibration of Radioactive Material Packages Greater than One Ton in Truck Transport,” American National Standards Institute, Inc. N14.23, May 1980.

Frank Wille, Viktor Ballheimer, Annette Rolle, Bernhard Droste, “Mechanical Behaviour of High Burn-Up SNF under Normal and Accident Transport Conditions – Present Approaches and Perspectives,” Bundesanstalt für Materialforschung und –prüfung White Paper, date unknown.

R.E. Glass and K.W. Gwinn, “Design Basis for Resistance to Shock and Vibration,” SAND89-0937C, date unknown.

Joe Rashid and Albert Machiels, “Simulation of Spent Fuel PWR Assembly Behavior under Normal Conditions of Transport,” IAEA International Conference on Spent Fuel Management, Vienna May 29 – June 4 2010 [ANATECH/EPRI .ppt presentation].

K.W. Gwinn, R.E. Glass, L.E. Romesberg, “Test Specification for TRUPACT-I Vibration Assessment,” SAND85-1369, February 1986.

Wayne Tustin, “What is the meaning of PSD in  $g^2/Hz$  units?,” VMEbus Systems, December 2005.

Cliff F. Magnuson, “Shock and Vibration Environments for Large Shipping Container during Truck Transport (Part I),” SAND77-1110, September 1977.

Cliff F. Magnuson, “Shock and Vibration Environments for Large Shipping Container during Truck Transport (Part II),” SAND78-0337 and NRC NUREG/CR-0128, May 1978.

K.W. Gwinn, R.E. Glass, K.R. Edwards, “Over-the-Road Tests of Nuclear Materials Package Response to Normal Environments,” SAND91-0079 and SAND91-2709C, December 1991.

Mark J. Suryan, “Final Report – Roadway Vibration Test of MOX Fresh Fuel Package,” Dynamark Engineering Inc. Certificate No. 0303-1013, August 2003 [test report to PACTEC].

Konrad Linnemann, “Remarks by GNS and BAM to SNL draft of ‘Test for Determining Loads on Spent Fuel under Normal Conditions of Transport’,” Bundesanstalt für Materialforschung und –prüfung letter to Ken Sorenson, March 2012.

Andreas Apel, Viktor Ballheimer, Christian Kuschke, Sven Schubert, Frank Wille, “Approach for the Use of Acceleration Values for Packages of Radioactive Material under Routine Conditions of Transport,” Proceedings of the 9<sup>th</sup> International Conference on the Radioactive Materials Transport and Storage, London, May 2012.

B.P. Dalziel, M.A. Elbestawi, J.W. Forest, “CANDU Irradiated Fuel Transportation: The Shock and Vibration Program,” Ontario Hydro report for Research Agreement No. 2715/R1/CF, date unknown.

Joseph Y. R. Rashid and Albert J. Machiels, “A Methodology for the Evaluation of Fuel Rod Failures under Transportation Accidents,” PATRAM 2004, date unknown.

Brian J. Koeppe, Harold Adkins Jr., David T. Tang, “Spent Nuclear Fuel Structural Response When Subjected to an Impact Accident,” source unknown, date unknown.

Gordon S. Bjorkman, “The Buckling of Fuel Rods in Transportation Casks under Hypothetical Accident Conditions,” PATRAM, date unknown.

J.T. Foley, “Transportation Shock and Vibration Descriptions for Package Designers,” Sandia Laboratories SC-M-72 0076, July 1972.

Clifford F. Magnuson, Leonidas T. Wilson, “Shock and Vibrations Environments for Large Shipping Containers on Rail Cars and Trucks,” SAND76-0427 and NRC NUREG766510, July 1977.

N. Igata and K. Domoto, "Fracture Stress and Elastic Modulus of Uranium Dioxide Including Excess Oxygen," *Journal of Nuclear Materials*, **45** (1972/73) 317-322, August 1972.

V. Ballheimer, F. Wille and B. Droste, "Mechanical safety analysis for high burn-up spent fuel assemblies under accident transport conditions," from *Packaging, Transport, Storage & Security of Radioactive Material*, Number 4, date unknown.

S. Uchikawa, H. Kishita, H. Ide, M. Owaki, K. Ohira, "Transportation Activities for BWR Fuels at NFI [Nuclear Fuel Industries, LTD.]," *Proceedings of Global 2009*, Paris, September 2009.

Thomas L. Sanders, Kevin D. Seager, Yusef R. Rashid, Peter R. Barrett, Anthony P. Malinauskas, Robert E. Einziger, Hans Jordan, Thomas A. Duffey, Stephen H. Sutherland, Philip C. Reardon, "A Method for Determining the Spent-Fuel Contribution to Transport Cask Containment Requirements," SAND90-2406, November 1992.

C. Brown, J. Guttman, C. Beyer, D. Lanning, "Maximum Cladding Stresses for Bounding PWR Fuel Rods during Short Term Operations for Dry Cask Storage," source unknown, September 2004.

Jy-An John Wang, Hong Wang, Yong Yan, Rob Howard, Bruce Bevard, "High Burn-up Spent Fuel Vibration Integrity Study Progress Letter Report (Out-of-cell fatigue testing development - Task 2.1)," ORNL/TM- 2010/288, January 2011.

Maurice Dallongeville, Aravinda Zeachandirin, Laurent Milet, "Simplified Approach to Study Fuel Rod Rupture Risks by Bending or Euler Buckling," *Proceedings of the 9th International Conference on the Radioactive Materials Transport and Storage*, London, May 2012.

David Olney and Brian Link, "Shock and vibration Measurement Using Variable Capacitance," *Endevco Technical Paper 296*, date unknown.

W. Koch, H. Lödging, W. Dunkhorst, Fraunhofer ITEM, Hannover, F. Lange, Meerbusch, "Integrity testing of fuel element mock-ups," source unknown, date unknown.

Elbestawi, M.A., Lau, D.F., "Irradiated Fuel Shock and Vibration Environment during Off-Site Transportation," *Ontario Hydro Research Report No. 83-482-K*, December 1983.

Forest, J.W., "Irradiated Fuel Transportation Shock and Vibration Program – Phase 2 Summary," *Ontario Hydro Research Division Report No. 85-190-K*, August 1985.

M. K. C de Baca and J. S. Cap, "Recommended Vibration and Shock Transportation Test Specifications for the Reactor Fuel Assembly," *SNL letter report March 2012*.

Nicholas Klymyshyn, "Shaker Table Modeling Progress Report," *PNNL Progress Report #UFDCST-120927-1*, September 2012.

Forest, J.W., "Irradiated Fuel Transportation Shock and Vibration Rail and Truck Field Tests," *Ontario Hydro Research Report No. 79-149-K*, March 1979.

Forest, J.W., "Impact and Fatigue Strength of Irradiated CANDU Fuel Bundles," *Ontario Hydro Research Report No. 80-321-K*, August 1980.

Forest, J.W., "Irradiated Fuel Transportation Shock and Vibration Study – Phase 1 Summary Report," *Ontario Hydro Research Division Report No. 82-60-K*, May 1982.

Dokainish, M.A., Elbestawi, M.A., "Random Response of a Tractor-Semitrailer System Carrying, an Irradiated Nuclear Fuel Shipping Flask," *Ontario Hydro Research Report No. 80-209-K*, June 1980.

Elbestawi, M.A., Dokainish, M.A., "Dynamic Response of a Railcar Carrying an Irradiated Nuclear Fuel Shipping Flask Subjected to Periodic and Stochastic Rail Excitation," *Ontario Hydro Research Report No. 80-190-K*, May 1980.

Elbestawi, M.A., Dokainish, M.A., "Dynamic Response of a Railcar Carrying an Irradiated Nuclear Fuel Shipping Flask," Ontario Hydro Research Report No. 80-53-K, March 1980.

Foley JT and MB Gens, "Environment Experienced by Cargo during Normal Rail and Truck Transport: Complete Data," Sandia Report No. SC-M-71-0241, 1971.

Foley J.T., "I. Techniques for Measuring Transportation and Handling Environments and II. Available Literature and How It May Help Package Designers," Sandia Report No. SC-M-70-266, 1970.

Foley J.T., "Normal and Abnormal Environments Experienced by Cargo on a Flatbed Truck," Sandia Report No. SC-DR-67-3003, 1968.

Foley J.T., "The Environment Experienced by Cargo on a Flatbed Tractor - Trailer Combination (Environmental Operations Analysis Study)," Sandia Report No. SC-RR-66-677, 1966.

Mortley, J. L., "Joint Army/AEC/Sandia Test of Truck Transport Environment, December 7-17, 1964 (Test No. T-10767)," Sandia Corporation Report SC-DR-65-278, August 1965.

Otts, J. V., "Impedance Measurement of a Flatbed Truck," Sandia Corporation Test Report No. T-10768, March 31, 1965.

Otts, J. V., "Force-Controlled Vibration Testing," Sandia Corporation Report SC-TM-31, February 1965.

Foley, J. T., "Transportation Shock and Vibration Descriptions for Package Designers, SC-M-72 0067, Sandia Laboratories, Albuquerque, April 1972.



# **APPENDIX A**

## **SUPPLEMENTAL FIGURES**



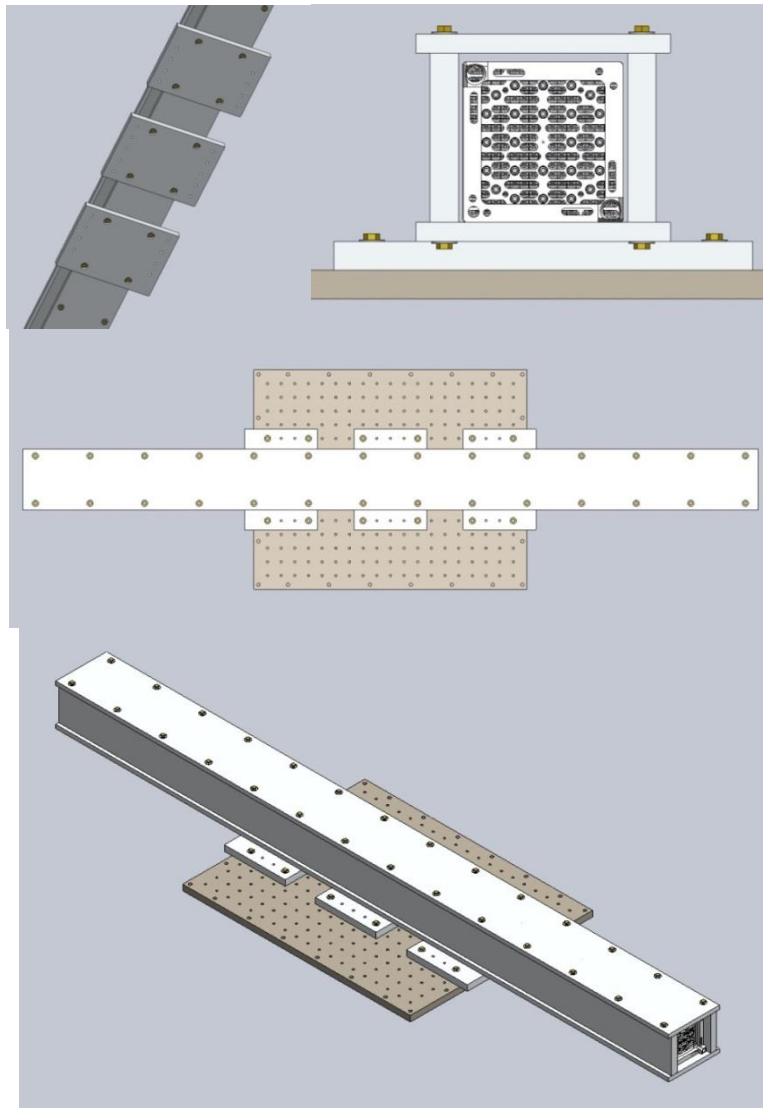


Figure A-1. Bottom, isometric, side, and top views of basket mounting plate.

NOTE: The shaker was mounted with an expander head onto which the basket mounting plates were bolted.

The expander head was 60 inches  $\times$  48 inches (152.4 cm  $\times$  121.9 cm).<sup>19</sup>

---

19. Calculations were made to determine the deflection at the ends of the basket as the basket was not supported by the shaker expander head for its full length. The basket is approximately 13-feet long and the expander head is 5-feet long, so the basket was unsupported for approximately four feet at each end. The calculations assumed that the assembly was within the basket. The natural frequency and modes of a beam were used in the calculation. The deflections calculated at the end of the basket were calculated to be only 0.003 in. (0.076 mm).

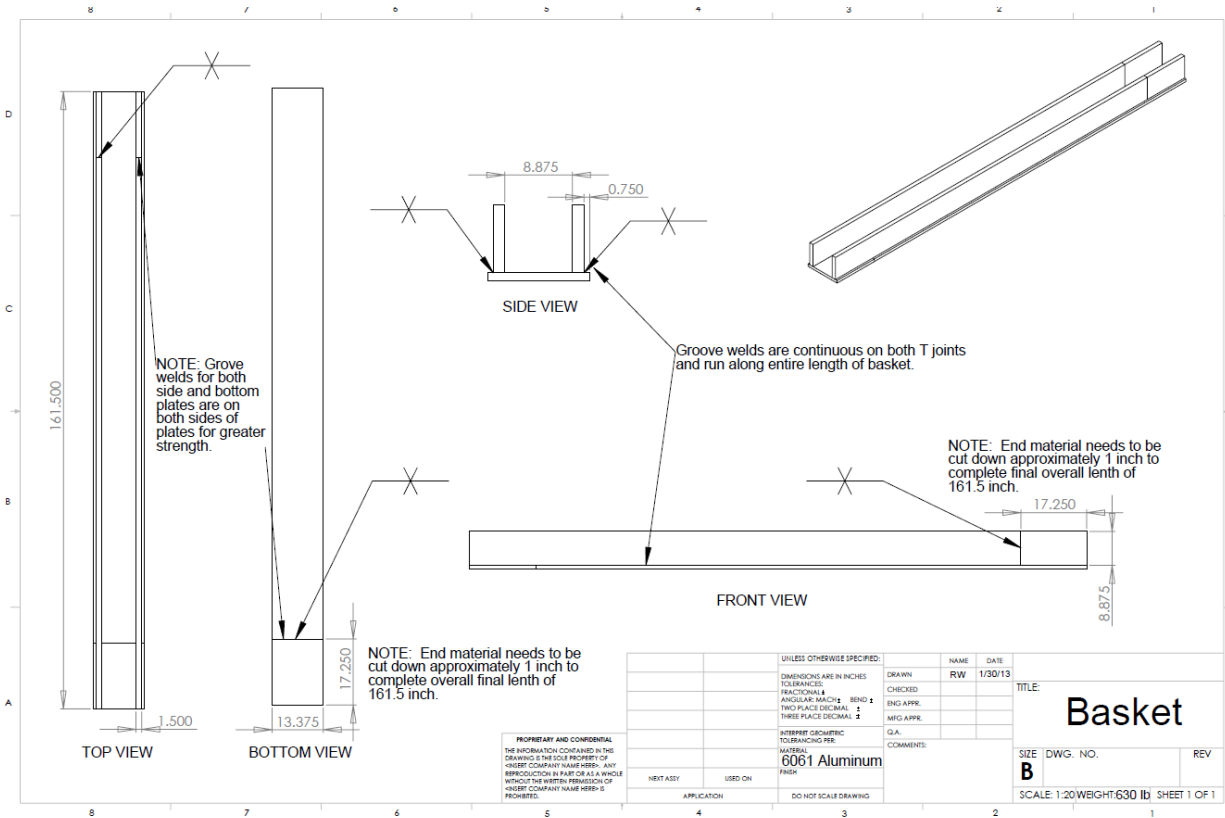


Figure A-2. Basket for shaker test.  
 NOTE: Assembly was placed within the basket which was bolted onto the shaker. The sides of the basket were bolted to the top and bottom sections rather than welded.

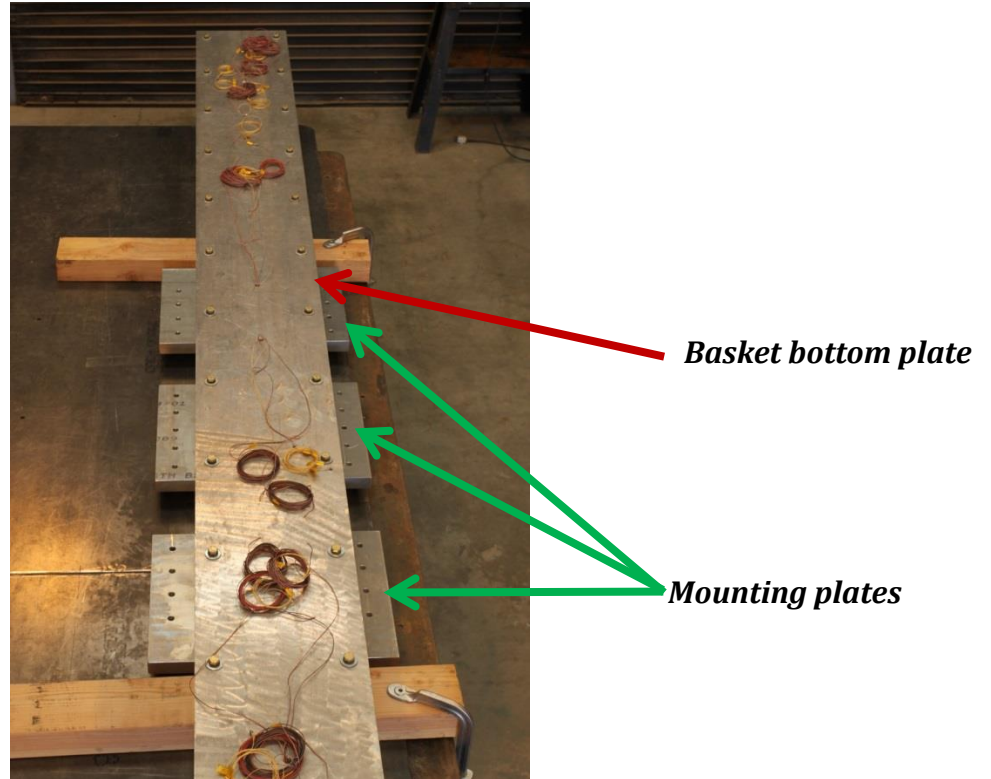


Figure A-3. Bottom plate of basket showing mounting plates.



Figure A-4. Assembly within basket.  
NOTE: Wires are shown leading from instrumentation on assembly through holes in top of basket.

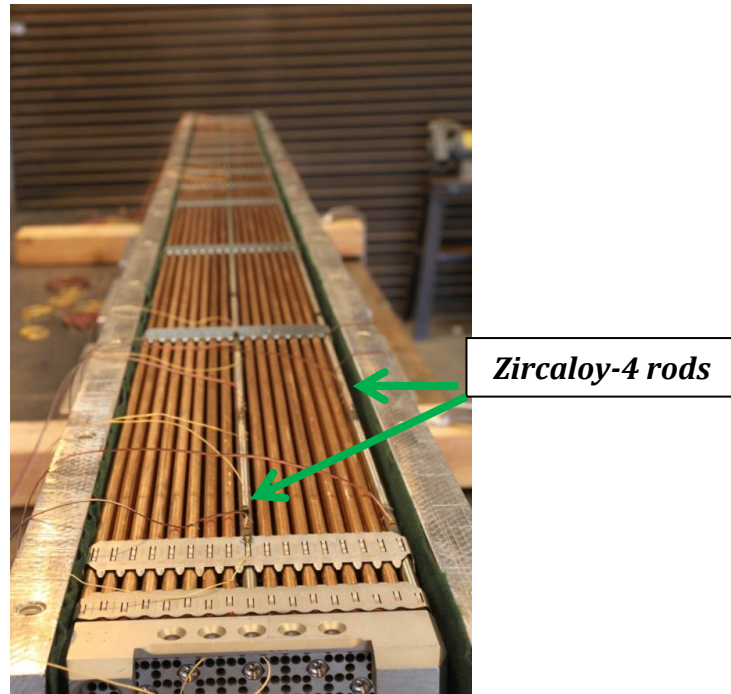


Figure A-5. Assembly in the basket.  
NOTE: Instrumentation can be seen on top-middle Zircaloy-4 rod and top-side rod on right.

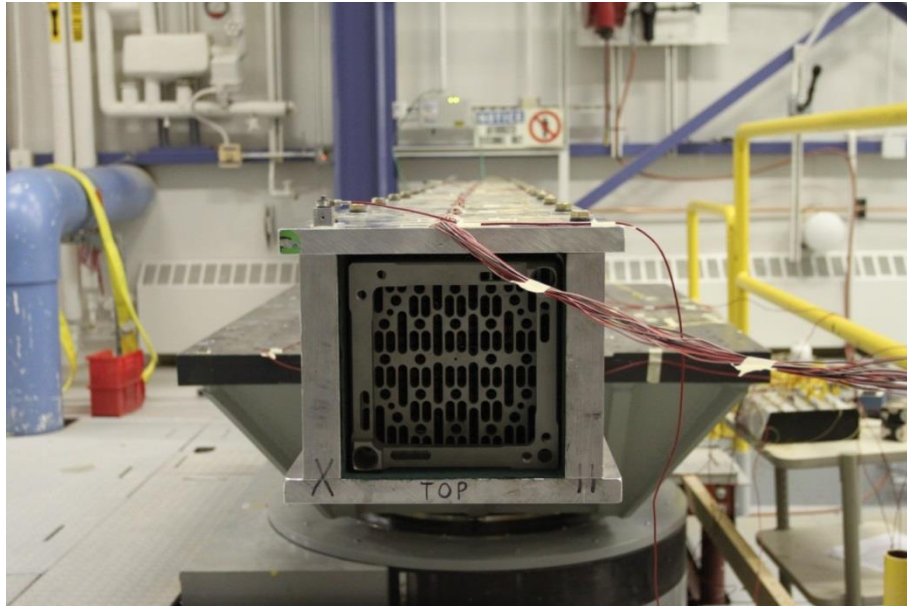


Figure A-6. End view of basket/assembly on shaker.  
NOTE: "TOP" on the basket indicates the top nozzle end of the assembly. There was a 0.45 in. (11.4 mm) gap between the top of the assembly and the inside of the basket and a 0.225 in. (5.7 mm) gap along the sides of the assembly.

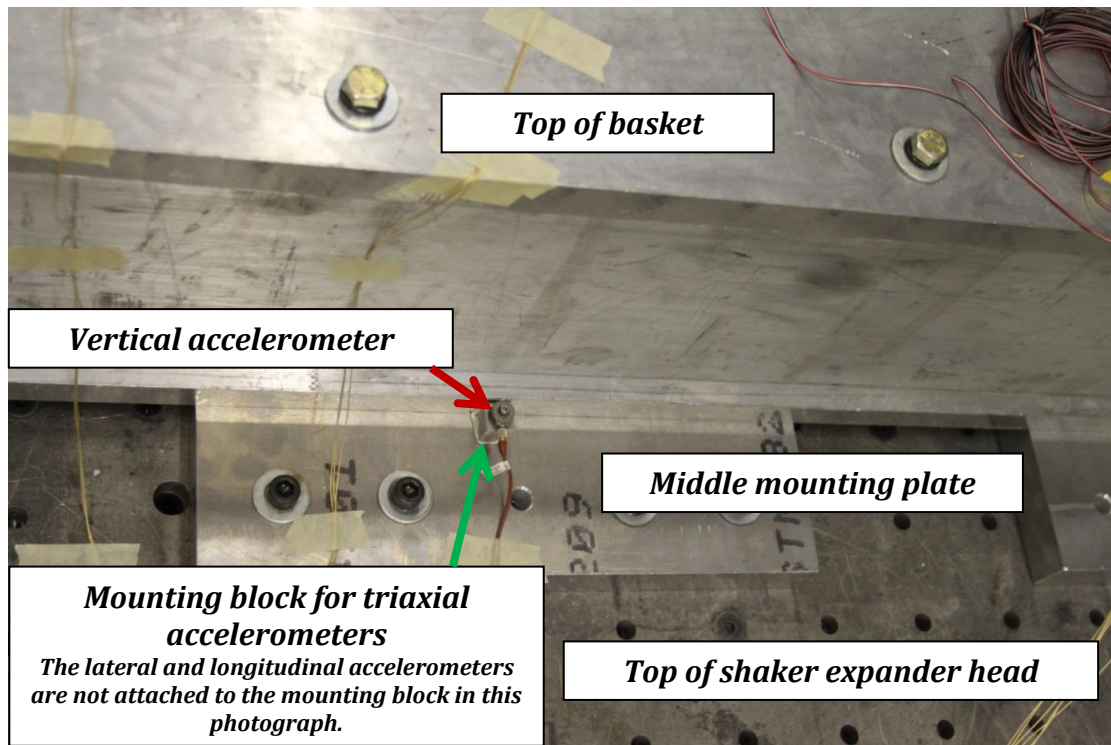


Figure A-7. Position of triaxial accelerometers mounting block on middle basket mounting plate.

NOTE: Only the vertical accelerometer is attached to the mounting block in this photograph.

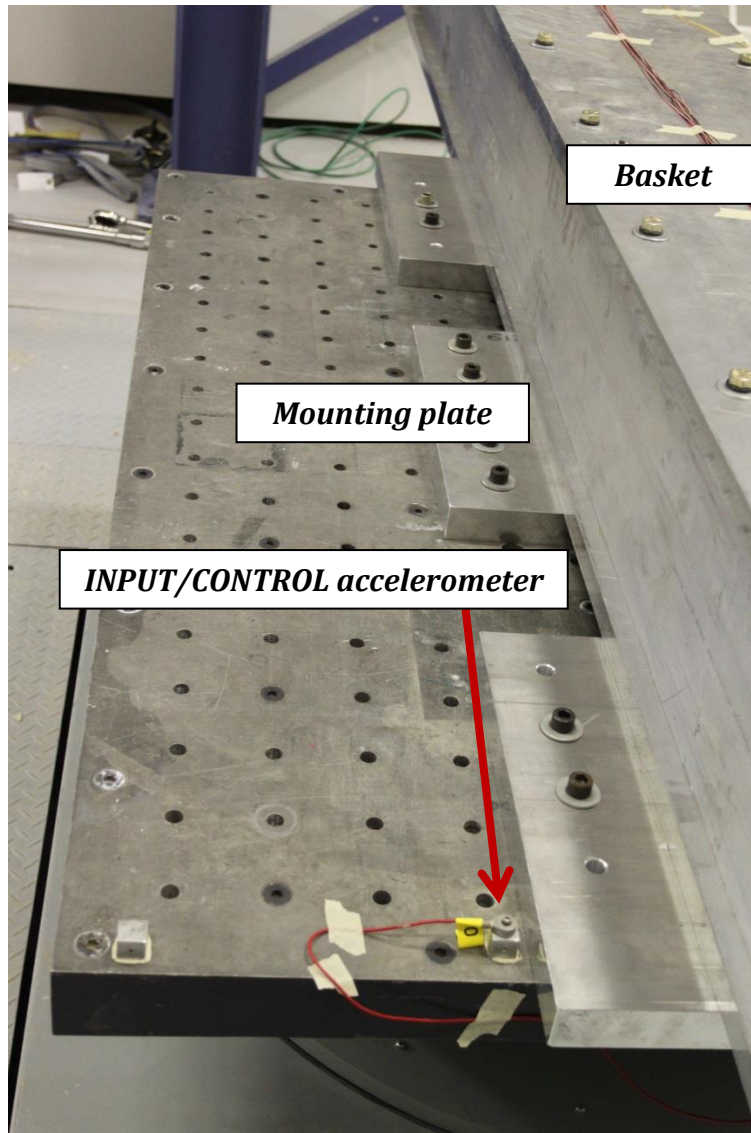


Figure A-8. Location of INPUT/CONTROL accelerometer on shaker.

**VISHAY**  
**PRECISION**  
**GROUP**

**MEME**® Strain Gages  
 and Instrumentation

**Micro-Measurements**

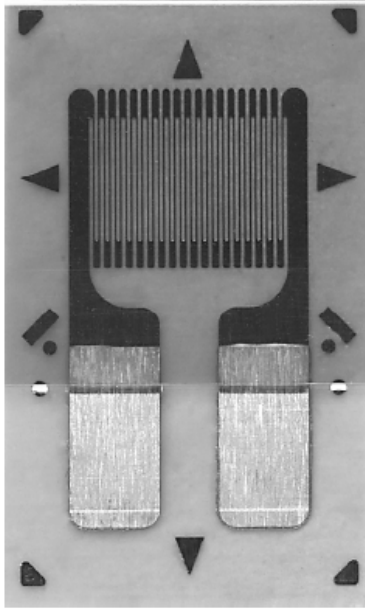
GAGE PATTERN DATA					
			<b>GAGE DESIGNATION</b>	<b>RESISTANCE (OHMS)</b>	<b>OPTIONS AVAILABLE</b>
			See Note 1		See Note 2
			CEA-XX-062UW-120 CEA-XX-062UW-350	120 ± 0.3% 350 ± 0.3%	<b>P2</b> <b>P2</b>
<b>DESCRIPTION</b>					
General-purpose gage. Exposed solder tab area is 0.07 x 0.04 in [1.8 x 1.0 mm].					
<b>GAGE DIMENSIONS</b>					
		Legend: ES = Each Section S = Section (S1 = Sec 1)		CP = Complete Pattern M = Matrix	
				inch	millimeter
<b>Gage Length</b>	<b>Overall Length</b>	<b>Grid Width</b>	<b>Overall Width</b>	<b>Matrix Length</b>	<b>Matrix Width</b>
0.062	0.220	0.120	0.120	0.31	0.19
1.57	5.59	3.05	3.05	7.9	4.8
<b>GAGE SERIES DATA</b>					
See Gage Series data sheet for complete specifications.					
<b>Series</b>	<b>Description</b>		<b>Strain Range</b>	<b>Temperature Range</b>	
CEA	Universal general-purpose strain gages.		±3%	-100° to +350°F [-75° to +175°C]	

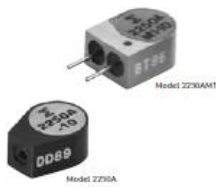
Figure A-9. Micro-Measurements Strain Gauge Data Sheet.<sup>2021</sup>

20. The resolution of these strain gauges is approximately 0.5 με (personal communication, Vishay Precision Group - Micro-Measurements Strain Gauges and Instrumentation technical representative, June 3, 2013).
21. The strain gauges (0.120 in. [3 mm] wide) were centered on the top of the rods, but straddled the rod circumference. A calculation was made to determine the strains measured at each side of the strain gauges relative to that measured at the top of the rod. The result was that the strains measured at the edges were 0.95 of that measured at the center line of the gauges (top of the rods). The strain data collected by the data acquisition system was an average of the strains across the width of the gauges.

## Model 2250A / AM1 -10 Isotron<sup>®</sup> accelerometer

### Features

- **NEW!** 2250A-10-R and 2250AM1-10-R are available as replacement sensors
- Low impedance output
- Adhesive mounting
- Lightweight (0.4 gm)
- Wide bandwidth, high S/N
- Flexible cable

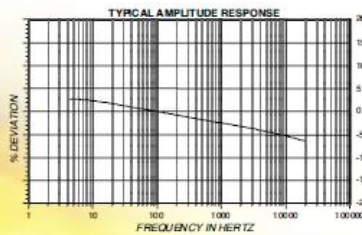
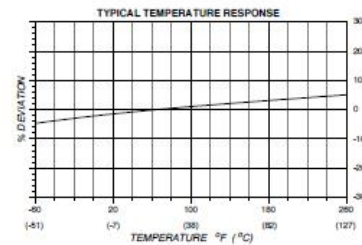
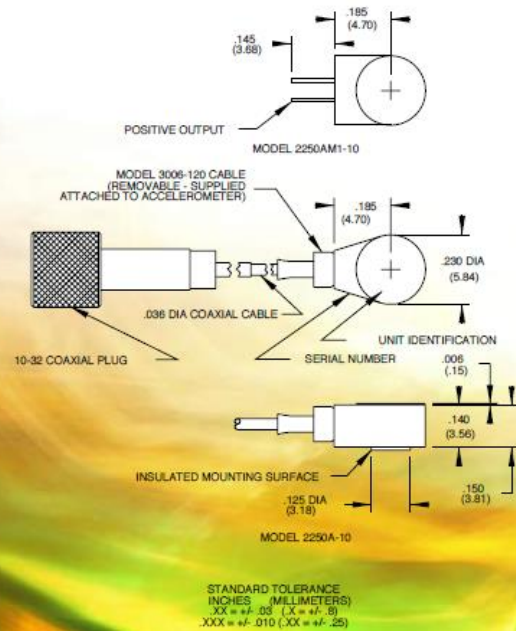


### Description

The Endevco<sup>®</sup> model's 2250A/AM1 are extremely small, adhesive mounting piezoelectric accelerometers with integral electronics, designed specifically for measuring vibration on mini-structures and small objects. These accelerometers offer high resonance frequency and wide bandwidth, their lightweight (0.4 gm) effectively eliminates mass loading effects. A field-replaceable miniature cable is supplied with the 2250A-10, and small gage, lightweight hook-up wires are supplied with the 2250AM1-10.

Models 2250A/AM1 feature Endevco's Piezite<sup>®</sup> type P-8 crystal element, operating in annular shear mode, which exhibits excellent output sensitivity stability over time. These accelerometers incorporate an internal hybrid signal conditioner in a two-wire system, which transmits its low impedance voltage output through the same cable that supplies the constant current power. Signal ground is isolated from the mounting surface by a ceramic mounting base. A tool is included in the package to ensure proper removal of the accelerometer from its mounting surface.

Endevco signal conditioner Models 4414B, 133, 2792B, 2793, 2775B or Oasis 2000 computer-controlled system are recommended for use with these accelerometers.



**MEGGITT**  
 smart engineering for  
 extreme environments

Figure A-10. Model 2250A/AM1-10 Accelerometer Data Sheet.

# Model 2250A / AM1 -10 Isotron<sup>®</sup> accelerometer

Endevco

## Specifications

The following performance specifications conform to ISA-RP-37.2 (1964) and are typical values, referenced at +75°F [+24°C] and 100 Hz, unless otherwise noted. Calibration data, traceable to National Institute of Standards and Technology (NIST), is supplied.

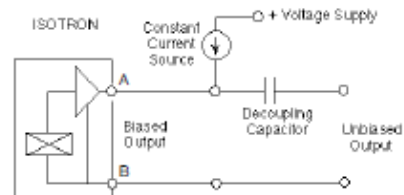
Dynamic characteristics	Units	
Range	g	±500
Voltage sensitivity ±5%	mV/g	10
Frequency response		See typical amplitude response
Resonance frequency	kHz	80
Amplitude response ±1dB	Hz	2 to 15 000
Temperature response		See typical curve
Transverse sensitivity	%	≤ 5
Amplitude linearity [4]	%	1 to 500 g
Output characteristics		
Output polarity		Acceleration directed into the base of unit produces positive output
Compliance voltage	Vdc	18 to 24
Supply current	mA	2 to 20
DC output bias voltage	Vdc	6.5 to 12.5
Output impedance	Ω	≤ 100
Residual noise 2 Hz to 25 kHz, broadband	equiv. g rms	0.0015
Grounding		Signal ground connected to case but isolated from mounting surface
Environmental characteristics		
Temperature range		-67°F to +257°F [-55°C to +125°C]
Humidity		Epoxy sealed, non-hermetic
Sinusoidal vibration limit	g pk	1000
Shock limit	g pk	2000
Base strain sensitivity	equiv. g pk/μ strain	0.0004
Thermal transient sensitivity	equiv. g pk/F° [1/°C]	0.1 [0.18]
Electromagnetic sensitivity	equiv. g rms/gauss	0.0001
Physical characteristics		
Dimensions		See outline drawing
Weight	gm (oz)	0.4 [0.01]
Case material		Anodized aluminum alloy case, beryllium copper lid, alumina mounting surface
Connector		<b>2250A-10:</b> 1.2 UNM threads. Recommended connector torque, 0.8 lbf-in [0.09 Nm] or finger tight using wrench. <b>2250AM1-10:</b> Solder terminal, "+" denoted by red dot. Flat surface provided for adhesive mounting
Mounting [1]		
Calibration		
Supplied:		
Sensitivity	mV/g	
Maximum transverse sensitivity	%	
Frequency response	dB	20 Hz to 15 kHz 15 kHz to 50 kHz

## Accessories

Product	Description	A-10/AM1-10	A-10-R/AM1-10-R
2211a	Accel. removal tool & connectivity wrench for 2250A-10	Included	Optional
25385	Accel. removal tool & connectivity wrench for 2250AM1-10	Included	Optional
300A-120 (I OR)	Cable assembly for 2250A-10	Included	Optional
302A-120	Cable assembly for 2250AM1-10	Included	Optional
32279	Mounting wax	Included	Optional

## Notes:

- Adhesives such as petro-wax, hot-melt glue, and cyanoacrylate epoxy (super glue) may be used to mount the accelerometer temporarily to the test structure. An adhesive mounting kit (P/N 31849) is available as an option from Endevco. To remove an epoxy-mounted accelerometer, first soften the epoxy with an appropriate solvent and then twist the unit off with the supplied removal wrench.
- Maintain high levels of precision and accuracy using Endevco's factory calibration services. Call Endevco's inside sales force at 1-800-982-6732 for recommended intervals, pricing and turn-around time for these services as well as for quotations on our standard products.



Continued product improvement necessitates that Endevco reserve the right to modify these specifications without notice. Endevco maintains a program of constant surveillance over all products to ensure a high level of reliability. This program includes attention to reliability factors during product design, the support of stringent Quality Control requirements, and compulsory corrective action procedures. These measures, together with conservative specifications, have made the name Endevco synonymous with reliability.

© ENDEVCO CORPORATION. ALL RIGHTS RESERVED. 30700 RANCHO VEJO ROAD, SAN JUAN CAPISTRANO, CA 92675 USA  
 (800) 982-6732 • (949) 453-8181 fax (949) 641-7231 • www.endevco.com • Email: applications@endevco.com

0607

**MEGGITT**  
 smart engineering for  
 extreme environments

Figure A-11 shows the dimensions of the NAC-LWT PWR basket simulated for the shaker test. The NAC basket is a series of cylindrical disks with a square section cutout for the assembly. The test basket constructed for the test is rectangular with internal dimensions the same as the NAC basket cutout.

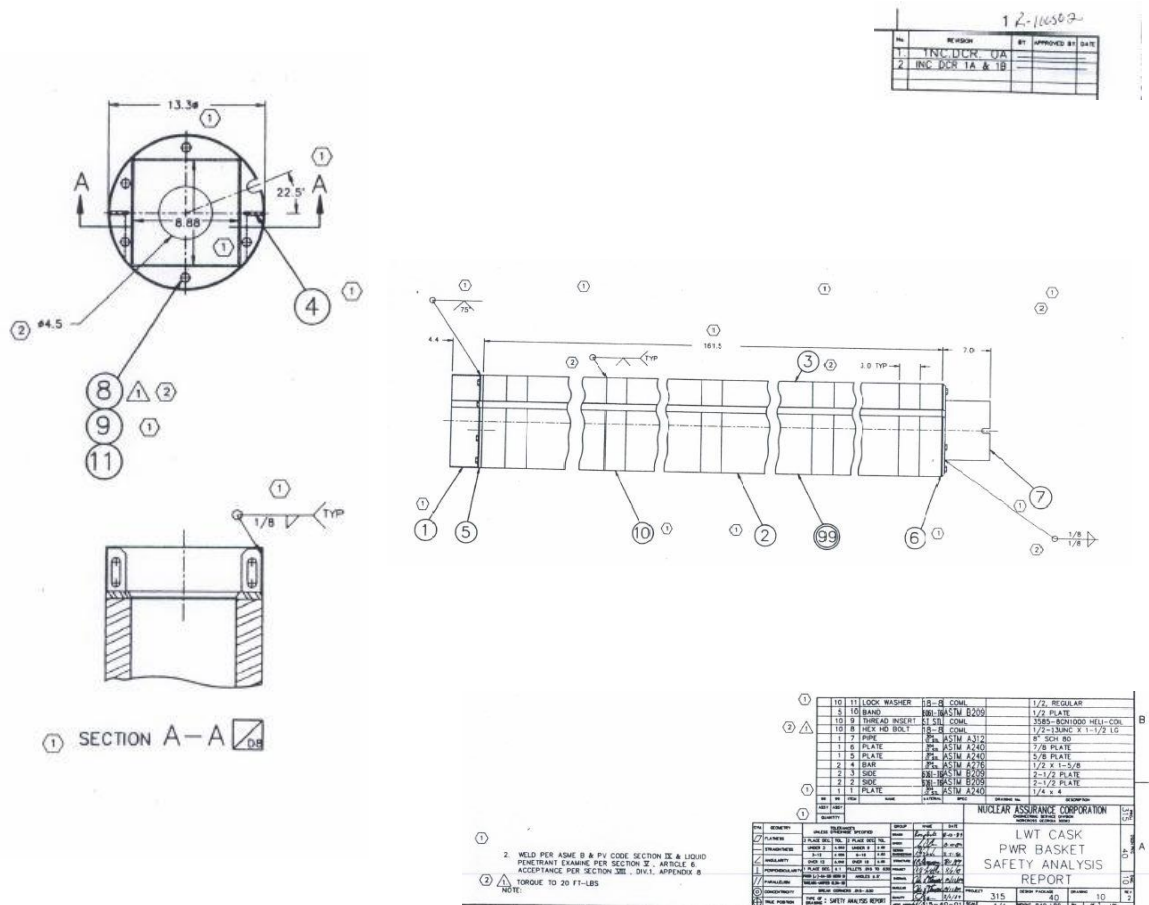


Figure A-11. Dimensions of the NAC-LWT PWR basket simulated to contain the assembly on the shaker.

Source: *Safety Analysis Report for the NAC-LWT, Revision 27, June 1999, Docket No. 9925 T-88004.*